Developing ozone-tolerant rice (*Oryza sativa* L.) through marker-assisted breeding for enhancing food security in air-polluted environments

Doctoral Dissertation

Submitted By

Muhammad Shahedul Alam

Giessen, 2025

Justus Liebig University, Giessen
Faculty 09 - Agricultural Sciences, Nutritional Sciences, and Environmental Management
Institute of Agronomy and Plant Breeding Ⅰ
Department of Agronomy and Crop Physiology

Developing ozone-tolerant rice (*Oryza sativa* L.) through marker-assisted breeding for enhancing food security in air-polluted environments

Inaugural Dissertation

Submitted in fulfillment of the requirements for the degree Doctor of Agricultural Sciences
(Dr. agr.)
to the
Faculty of Agricultural Sciences, Nutritional Sciences and Environmental Management

Submitted by
Muhammad Shahedul Alam

Giessen, 2025

Prepared with the permission of the

Faculty of Agricultural Sciences, Nutritional Sciences and Environmental Management,

Justus Liebig University, Giessen

Examination committee:

Head of the Examination Committee:	Prof. Dr. Jakob Santner
1st Examiner (Supervisor):	Prof. Dr. Michael Frei
2nd Examiner (Co-Supervisor):	Prof. Dr. Rod Snowdon
3rd Examiner:	Prof. Dr. John Clifton-Brown
4th Examiner:	Prof. Dr. Sarah Schießl-Weidenweber

Eidesstaatliche Erklärung

Erklärung gemäß der Promotionsordnung des Fachbereichs 09 vom 07. Juli 2004 § 17 (2)

„Ich erkläre: Ich habe die vorgelegte Dissertation selbständig und ohne unerlaubte fremde Hilfe und nur mit den Hilfen angefertigt, die ich in der Dissertation angegeben habe. Alle Textstellen, die wörtlich oder sinngemäß aus veröffentlichten Schriften entnommen sind, und alle Angaben, die auf mündlichen Auskünften beruhen, sind als solche kenntlich gemacht.
Bei den von mir durchgeführten und in der Dissertation erwähnten Untersuchungen habe ich die Grundsätze guter wissenschaftlicher Praxis, wie sie in der „Satzung der Justus-Liebig-Universität Gießen zur Sicherung guter wissenschaftlicher Praxis“ niedergelegt sind, eingehalten.“

Giessen, _____ _____

Muhammad Shahedul Alam

Publication Declaration

Certain sections of this thesis have already been published, while others are in the process of being prepared for publication in peer-reviewed journals. These published and forthcoming articles contribute to the dissemination of the research findings and reinforce the scientific rigor of this thesis.

Published papers:

Alam, M. S., Maina, A. W., Feng, Y., Wu, L.-B., & Frei, M. (2022). Interactive effects of tropospheric ozone and blast disease (*Magnaporthe oryzae*) on different rice genotypes. *Environmental Science and Pollution Research*, 29, 48893–48907. https://doi.org/10.1007/s11356-022-19282-z

Dedication

This thesis is dedicated to my **parents** and my wife, **Shathi**.

I solemnly dedicate this thesis to the martyrs and the wounded who selflessly sacrificed their lives in the pursuit of a just, democratic, and inclusive Bangladesh. This vision remains a distant dream. Yet, their unwavering courage has granted us the hope of a brighter future, especially on the historic day of **July 36** (August 5), 2024.

Words fall short of expressing my profound respect for the innocent children whose lives were lost in this heartbreaking event. In particular, I pay tribute to the three iconic heroes of July 36—**Abu Sayed**, **Mir Mugdho**, and **Shaikh Ashabul Yamin** —whose bravery and sacrifice will forever be etched in our memories.

Acknowledgments

It has been an incredible journey since I arrived in Germany in 2017. I shared a common dream with my PhD supervisor, **Prof. Dr. Michael Frei**, to develop ozone-tolerant rice for high-risk regions where ozone is a hidden threat to food security. Although I was only a Master's student at that time, I began working alongside **Dr. Md Ashrafuzzaman** in the greenhouse at the University of Bonn, pursuing this challenging goal parallel to my Master's coursework. Breeding rice for ozone tolerance was a significant challenge, but in 2019, **Prof. Frei** gave me the opportunity to work under his supervision, trusting me with this ambitious project. I am deeply grateful to him for his unwavering trust and belief in my potential. From the very beginning, I promised myself that I would breed ozone-tolerant rice—not merely conduct research for a doctoral degree. Today, I am proud that ozone-tolerant rice is on its way to becoming a reality.

I would like to express my heartfelt gratitude to my dear friend **Dr. Dereje Tamiru Demie**, who provided unwavering support during the initial phases of my breeding activities. When I was away from Germany, my plants began dying due to unfavorable soil conditions. Despite having backup plants, Dereje did everything he could to protect them, knowing that losing those plants would jeopardize my PhD journey. I also sincerely thank the greenhouse staff at the University of Bonn for their continuous support—I never received a “No” from any of my wonderful colleagues there. I sincerely thank **Dr. Michael Schneider** for his invaluable assistance in analyzing the GBS data, which was instrumental in developing KASP markers.

After moving from Bonn to Giessen, I was fortunate to have **Prof. Dr. Rod Snowdon** as a co-supervisor. His insightful suggestions, particularly on background selection, were invaluable. I thank **Dr. Eva Herzog** for her valuable suggestions on marker frequency in background genotyping. I am grateful to my friend **Dr. Frederike Zeibig**, who supported me immensely during the transition between universities. I also fondly remember **Dr. Yanru Feng**, a close colleague and family friend, for standing by me throughout my research journey.

I thank **Prof. Dr. Dr. Hans-Werner Koyro**, **Dr. Benjamin Wittkop**, and **Dr. Marzieh Shafiee-Hajiabad** for helping me manage the greenhouse space at the University of Giessen. Handling such a large number of breeding lines would have been impossible without their support. My heartfelt thanks go to all the greenhouse colleagues and the Weilburger Grenze field research station team. I am incredibly grateful to **Dr. Linbo Wu** for his immense support in facilitating

my work. His insightful guidance and special tips have always been immensely helpful. Words cannot express my gratitude to **Dr. Yavar Vaziritabar**, whose help with logistics and unconditional support during greenhouse experiments made all the difference. I sincerely thank my friend, **Ambika Pandey**, for taking care of my plants and for her unwavering support as one of my best friends since 2017. I also express my deep gratitude to **Sumitra Pantha** for her invaluable assistance—not only in my breeding activities but also for standing by my family during challenging times.

I would like to express my deepest gratitude to **Erika Schick**, **Liane Renno**, **Lea Schmitt**, and **Denise Schudt** for their tireless help in processing harvested samples. Without their assistance, the task would have been never-ending. Special thanks to **Christine Kessler-Turturici** for always greeting me with a smile, even during her busiest times—she truly made things easier with her positive attitude. The research group is fortunate to have someone like her.

I would also like to acknowledge the students who worked with me on their Bachelor's or Master's theses. I am incredibly grateful to **Dr. Sawitree Autarmat**, who spent a year with me as a PhD exchange student from Thailand. **Minh Khue Do** from Vietnam deserves special mention for his significant contributions—after me, he played the most crucial role in this work. **Aleena Ittapad Baburajan** and **Aishwarya Karki** from India were instrumental in completing the third experiment, and without their hard work, it would not have been possible. I also thank **Marc Hartung** from Germany and **Osimahon Blessing Omo** from Nigeria for their hard work during the greenhouse experiments. I am grateful to **Dr. Andriele Wairich** and **Dr. Johanna Krippner** for caring for Aleena, Aish, and Minh in my absence and to **Rigyan Gupta** from Bangladesh for managing the field trial.

Finally, I want to express my deepest gratitude to my family—my wife, **Shathi**, and our two sons, **Saad** and **Shaheer**. Breeding experiments often required me to spend long hours in the greenhouse, leaving little time for my family. Shathi never complained; instead, she would bring me food at the greenhouse, knowing I had been working without eating. Even during my most stressful moments, when I was not my best self, they accepted it without question. I am truly blessed to have such a supportive family. As a Bengali folk song beautifully says, "তুমি জানো নারে প্রিয়, তুমি মোর জীবনের সাধনা" – "You don't know, my beloved, you are the yearning of my life!"

List of Contents

Abbreviations

AEZ - Agro-Ecological Zone

AFLP - Amplified Fragment Length Polymorphism

ANOVA - Analysis of Variance

AOT - Accumulated Ozone over Threshold

ARI1 - Anthocyanin Reflectance Index 1

BBS - Blast Severity Score

BINA - Bangladesh Institute of Nuclear Agriculture

BRRI - Bangladesh Rice Research Institute

CSSL - Chromosome Segment Substitution Line

DAI - Days after Inoculation

DAO - Days after Ozone

DAT - Days after Transplanting

DMSO - Dimethyl Sulfoxide

DNA - Deoxyribonucleic Acid

DTF - Days to Flowering

DTM - Days to Maturity

EDU - Ethylenediurea

ETR - Electron Transport Rate

FGN - Filled Grain Number

GFP - Green Fluorescent Protein

gsw - Stomatal Conductance

GY - Grain Yield

HI - Harvest Index

HR - Hypersensitive Response

IGP - Indo-Gangetic Plain

IPCC - Intergovernmental Panel on Climate Change

IRRI - International Rice Research Institute

JA - Jasmonic Acid

KASP - Kompetitive Allele Specific PCR

LBS - Leaf Bronzing Score

Lic2 - Lichtenthaler Index 2

MAS - Marker-Assisted Selection

MDA - Malondialdehyde

NBI - Nitrogen Balance Index

NDVI - Normalized Difference Vegetation Index

NUE - Nitrogen Use Efficiency

PCA - Principal Component Analysis

PCD - Programmed Cell Death

PCR - Polymerase Chain Reaction

PH - Plant Height

PhiPS2 - Quantum Efficiency of Photosystem II

PM - Particulate Matter

PN - Panicle Number

PRI - Photochemical Reflectance Index

QTL - Quantitative Trait Loci

RAPD - Random Amplified Polymorphic DNA

RFLP - Restriction Fragment Length Polymorphism

RNA - Ribonucleic Acid

ROS - Reactive Oxygen Species

RYL - Relative Yield Loss

SA - Salicylic Acid

SB - Straw Biomass

SNP - Single Nucleotide Polymorphism

SSR - Simple Sequence Repeat

TCA - Tricarboxylic Acid Cycle

TGW - Thousand Grain Weight

TN - Tiller Number

UFGN - Unfilled Grain Number

UGW - Unfilled Grain Weight

USDA - United States Department of Agriculture

UTR - Untranslated Region

WMO - World Meteorological Organization

List of Tables

List of Figures

List of Appendices

List of Supplementary Tables

List of Supplementary Figures

Summary

Environmental stressors, particularly tropospheric ozone (O_3), which significantly reduces crop yields, are increasingly threatening global food security. Rice (*Oryza sativa* L.), a staple food for more than half of the world's population, is highly vulnerable to ozone stress. Chronic exposure to ozone results in reduced photosynthesis, accelerated senescence, and significant yield losses. This study aimed to develop ozone-tolerant rice varieties through marker-assisted breeding, focusing on two quantitative trait loci (QTLs), *OzT8* and *OzT9*, known for conferring ozone tolerance.

The research was conducted in four phases. The first phase investigated the interactive effects of ozone stress and blast disease (*Magnaporthe oryzae*) on different rice genotypes under controlled greenhouse conditions. Physiological measurements—including spectral reflectance indices, gas exchange parameters, biochemical analysis, and yield data—revealed that ozone exposure reduced blast disease severity. However, blast infection did not significantly affect the sensitivity of rice to ozone. While breeding for ozone tolerance had long been hindered by concerns about potential trade-offs with disease resistance, this study provided confidence that breeding for both traits is feasible.

In the second phase, marker-assisted backcross breeding was employed to introgress *OzT8* and *OzT9* from the donor parent Kasalath into two ozone-sensitive Bangladeshi rice varieties, BRRI dhan28 and Binadhan-11. Successive generations of genotypic and phenotypic selection resulted in the development of breeding lines homozygous for the tolerant alleles. Subsequently, 77 breeding lines harboring *OzT8* and/or *OzT9* were evaluated in a greenhouse experiment. These lines were assessed for key physiological traits—such as stomatal conductance, chlorophyll fluorescence, nitrogen balance index—and agronomic traits, including grain yield and biomass accumulation. Several lines demonstrated enhanced ozone tolerance, improved photosynthetic efficiency, reduced lipid peroxidation, and superior yield performance compared to their parental lines.

In the third and fourth phases, comprehensive greenhouse and field trials were conducted to confirm the performance of the selected breeding lines. Physiological traits (e.g., nitrogen balance index, stomatal conductance, chlorophyll fluorescence) and agronomic traits (e.g., grain yield, harvest index) were thoroughly analyzed. Results validated the superior

performance of breeding lines containing both *OzT8* and *OzT9*, with several lines showing significant yield improvements under ozone stress conditions.

This study highlights the potential of marker-assisted breeding in developing ozone-tolerant rice varieties, offering a promising solution to mitigate ozone-induced yield losses and improve rice production in air-polluted regions. It concludes with a recommendation for multi-location trials to validate the stability of ozone tolerance across diverse environments and to explore the integration of additional QTLs for greater genetic diversity and broader adaptation.

Zusammenfassung

Umweltstressoren wie troposphärisches Ozon (O_3), das die Ernteerträge von Nutzpflanzen erheblich verringert, bedrohen zunehmend die globale Ernährungssicherheit. Reis (*Oryza sativa* L.), ein Grundnahrungsmittel für mehr als die Hälfte der Weltbevölkerung, ist sehr anfällig für Ozonstress. Eine chronische Exposition gegenüber Ozon führt zu einer verringerten Photosynthese, beschleunigter Seneszenz und erheblichen Ertragseinbußen. Ziel dieser Studie war es, durch markergestützte Züchtung ozontolerante Reissorten zu entwickeln, wobei der Schwerpunkt auf zwei quantitativen Trait-Loci (QTLs), *OzT8* und *OzT9*, lag, von denen bekannt ist, dass sie Ozontoleranz verleihen.

Die Forschung wurde in vier Phasen durchgeführt. In der ersten Phase wurden die interaktiven Auswirkungen von Ozonstress und der Pilzkrankheit Rice Blast (*Magnaporthe oryzae*) auf verschiedene Reisgenotypen unter kontrollierten Gewächshausbedingungen untersucht. Physiologische Messungen - einschließlich spektraler Reflexionsindizes, Gasaustauschparameter, biochemischer Analysen und Ertragsdaten - ergaben, dass die Ozonbelastung den Schweregrad der Pilzerkrankung reduzierte. Die Infektion mit der Rice Blast hatte jedoch keinen signifikanten Einfluss auf die Empfindlichkeit von Reis gegenüber Ozon. Während die Züchtung auf Ozontoleranz lange Zeit durch Bedenken hinsichtlich möglicher Kompromisse mit der Krankheitsresistenz behindert wurde, zeigte diese Studie, dass die Züchtung auf beide Eigenschaften möglich ist.

In der zweiten Phase wurde die markergestützte Rückkreuzung eingesetzt, um *OzT*8 und *OzT9* aus dem Spenderelternteil Kasalath in zwei ozonempfindliche Reissorten aus Bangladesch, BRRI dhan28 und Binadhan-11, einzubringen. Die aufeinander folgenden Generationen genotypischer und phänotypischer Selektion führten zur Entwicklung von Zuchtlinien, die homozygot für die toleranten Allele sind. Anschließend wurden 77 Zuchtlinien mit *OzT8* und/oder *OzT9* in einem Gewächshausversuch untersucht. Diese Linien wurden im Hinblick auf wichtige physiologische Merkmale - wie stomatäre Leitfähigkeit, Chlorophyllfluoreszenz und Stickstoffbilanzindex - und agronomische Merkmale, einschließlich Kornertrag und Biomasseakkumulation, bewertet. Mehrere Linien zeigten eine erhöhte Ozontoleranz, eine verbesserte photosynthetische Effizienz, eine geringere Lipidperoxidation und eine bessere Ertragsleistung als ihre Elternlinien.

In der dritten und vierten Phase wurden umfassende Gewächshaus- und Feldversuche durchgeführt, um die Leistung der ausgewählten Zuchtlinien zu bestätigen. Physiologische Merkmale (z. B. Stickstoffbilanzindex, stomatäre Leitfähigkeit, Chlorophyllfluoreszenz) und agronomische Merkmale (z. B. Kornertrag, Ernteschlüssel) wurden gründlich analysiert. Die Ergebnisse bestätigten die überlegene Leistung von Zuchtlinien, die sowohl *OzT8* als auch *OzT9* enthalten, wobei mehrere Linien unter Ozonstressbedingungen deutliche Ertragssteigerungen aufwiesen.

Diese Studie unterstreicht das Potenzial der markergestützten Züchtung bei der Entwicklung ozontoleranter Reissorten, die eine vielversprechende Lösung zur Abschwächung ozonbedingter Ertragsverluste und zur Verbesserung der Reiserzeugung in luftverschmutzten Regionen darstellt. Sie schließt mit der Empfehlung, Versuche an mehreren Standorten durchzuführen, um die Stabilität der Ozontoleranz in verschiedenen Umgebungen zu validieren und die Integration zusätzlicher QTLs für eine größere genetische Vielfalt und eine breitere Anpassung zu untersuchen.

1 Introduction

Global food security faces mounting challenges due to environmental stressors threatening crop productivity. Among these, air pollution, particularly tropospheric ozone (O_3), has emerged as a significant factor adversely affecting agricultural yields worldwide (Agathokleous et al., 2023). Rapid industrialization, urbanization, and fossil fuel combustion have exacerbated the levels of ground-level ozone, leading to widespread reductions in crop yield and quality (Manisalidis et al., 2020; Das et al., 2021). Tropospheric ozone is a potent phytotoxin that disrupts plant physiological functions, including photosynthesis, stomatal regulation, and oxidative stress responses, resulting in significant declines in agricultural output (Emberson et al., 2018; Li et al., 2023). This issue is particularly pronounced in Asia, where rice production is a crucial component of food security and is increasingly threatened by rising ozone concentrations (Z. Feng et al., 2022).

Rice is a fundamental staple crop that sustains more than half of the global population, particularly in Asia, where it constitutes a major component of daily caloric intake (Sharif et al., 2014). However, the increasing prevalence of abiotic stresses, such as ozone pollution, has put immense pressure on rice production systems, necessitating urgent interventions to sustain and enhance yield stability (Mills et al., 2018b). Chronic exposure to elevated ozone levels has been shown to reduce rice yields by interfering with carbon assimilation, accelerating senescence, and causing oxidative damage to plant tissues (Z. Feng et al., 2022). In highly polluted regions such as China, India, and Bangladesh, rice yield losses attributable to ozone pollution range between 7.5% and 12.5%, highlighting the urgency of addressing this environmental stressor (Mills et al., 2018b; Frei et al., 2024).

The mechanisms underlying ozone-induced damage in plants are well-documented. Ozone enters plant leaves primarily through stomatal pores and rapidly decomposes into reactive oxygen species (ROS) in the apoplast, triggering oxidative stress and cellular damage (Kangasjärvi et al., 2005; Tamaoki, 2008). The resulting physiological disruptions include lipid peroxidation, chlorophyll degradation, reduced photosynthesis, protein oxidation, and DNA damage, all contributing to decreased crop productivity (Mills et al., 2018a, 2018b). Ozone-induced stress also affects light-harvesting efficiency and carboxylation capacity by inhibiting

the activity of ribulose-1,5-bisphosphate carboxylase/oxygenase (Rubisco), further exacerbating yield losses (Fiscus et al., 2005; Feng et al., 2008). Notably, the effects of ozone pollution on crop production extend beyond yield reduction to include compromised grain quality, increased spikelet sterility, and reduced biomass accumulation (Frei, 2015; Mills et al., 2018a, 2018b).

The economic and social consequences of ozone-induced yield losses are substantial. Reduced agricultural yields contribute to global food shortages, rising food prices, and increased economic vulnerability for smallholder farmers, particularly in developing countries with limited access to pollution mitigation technologies (Miao et al., 2016; Kang et al., 2023). Addressing the challenges of tropospheric ozone pollution requires a multifaceted approach that includes stricter air quality regulations, adopting resilient crop varieties through plant breeding, and sustainable agricultural practices (Agathokleous et al., 2023; Frei et al., 2024). A critical aspect of this strategy is the development of ozone-tolerant rice varieties through marker-assisted breeding, which offers a promising solution for enhancing crop resilience in polluted environments (Frei, 2015).

Efforts to develop ozone-tolerant rice varieties have gained momentum in recent years, leveraging advanced breeding techniques to identify and integrate ozone tolerance-related quantitative trait loci (QTLs) into elite cultivars (Tsukahara et al., 2013, 2015; Frei, 2015). Several QTLs, including *OzT8* and *OzT9*, have been identified as key genetic determinants of ozone tolerance in rice, conferring improved physiological and biochemical responses to ozone stress (Chen et al., 2011). Studies utilizing marker-assisted selection (MAS) have demonstrated that breeding lines incorporating these QTLs exhibit enhanced biomass production, lower spikelet sterility, and improved grain quality under ozone stress conditions (Y. Wang et al., 2014b; Jing et al., 2016).

Despite these advances, the development of ozone-tolerant rice varieties presents particular challenges, including potential trade-offs with other agronomic traits and biotic stress resistance. For instance, interactions between ozone tolerance and rice blast disease resistance remain poorly understood, raising concerns about whether selecting for ozone tolerance could inadvertently affect susceptibility to blast (Kangasjärvi et al., 2005; Singh et al.,

2020). Moreover, while antiozonants such as ethylenediurea (EDU) have shown promise in protecting crops from ozone damage, their large-scale application is hindered by regulatory constraints and potential environmental risks (Gupta et al., 2018; Frei et al., 2024). Consequently, a comprehensive breeding strategy integrating genetic, physiological, and agronomic approaches is necessary to ensure the successful development of resilient rice cultivars (Agathokleous et al., 2023).

In light of these considerations, this thesis aims to investigate the potential of marker-assisted breeding for developing ozone-tolerant rice varieties, focusing on evaluating the physiological, biochemical, and yield-related responses of breeding lines containing ozone tolerance QTLs. The research objectives include (1) assessing the interactive effects of ozone stress and blast disease on different rice genotypes, (2) evaluating the performance of breeding lines containing *OzT8* and *OzT9* under controlled ozone stress conditions, and (3) conducting comprehensive greenhouse and field trials to identify the most suitable ozone-tolerant rice varieties for deployment in high-risk agricultural regions.

2 Literature Review

2.1 The growing challenge of air pollution on crop production

Air pollution poses an increasingly significant threat to global crop production, with far-reaching consequences on global food security and agricultural sustainability. The impact of air pollution on crop yields is highly complex, as it is closely linked to climate change, presenting a multifaceted challenge for modern agriculture (Agathokleous et al., 2023). As industrialization and urbanization continue to expand at an unprecedented rate, releasing pollutants, such as tropospheric or ground-level ozone (O_3), nitrogen oxides (NO_x), sulfur dioxide (SO_2), and particulate matter (PM), into the atmosphere has intensified to alarming levels (Manisalidis et al., 2020). These pollutants, often invisible to the naked eye, can have profound and detrimental effects on crop growth, yield, and quality, affecting the entire agricultural ecosystem (Das et al., 2021; Z. Feng et al., 2022).

Tropospheric ozone, in particular, is a potent phytotoxin capable of causing extensive damage to plant tissues and interfering with photosynthesis. This interference reduces crop productivity and can manifest as visible leaf damage (Emberson et al., 2018). Chronic exposure to elevated ozone levels has been shown to reduce yields of staple crops like wheat, rice, and soybeans by interfering with carbon assimilation and accelerating senescence. The impact of ozone pollution is particularly concerning, as it can affect crops over large geographical areas, potentially leading to widespread reductions in agricultural output (Li et al., 2023).

Air pollution significantly reduces agricultural yields, leading to substantial economic losses for farmers, disruptions in global food markets, and rising food prices (Miao et al., 2016; Dong & Wang, 2023). It is further worsened by climate change, with elevated carbon dioxide levels and shifting weather patterns exacerbating crop stress (Agathokleous et al., 2023). Smallholder farmers in developing regions, who rely on traditional practices and lack access to pollution mitigation technologies, are disproportionately affected, leaving them vulnerable to these challenges (Kang et al, 2023; Li et al., 2024; Frei et al., 2024). Addressing this multifaceted issue requires urgent interdisciplinary research to assess long-term impacts alongside integrated strategies such as stricter air quality regulations, the adoption of resilient crop varieties through plant breeding, and sustainable agricultural practices. Collaborative global efforts are essential to mitigate emissions, enhance agricultural resilience, and develop

pollution-tolerant crops (Agathokleous et al., 2023; Frei et al., 2024). Failure to act could severely compromise food security, mainly as the population grows and demand for agricultural products rises.

2.2 Formation and global distribution of tropospheric ozone

Ozone is distributed across two main layers of the Earth's atmosphere: the stratosphere and the troposphere. The majority, about 90%, is found in the stratosphere, between 10 and 17 km above the Earth's surface, extending up to approximately 50 km. This region is commonly known as the ozone layer; the remaining ozone is located in the lower atmosphere (0–10 km), known as tropospheric or ground-level ozone, which has distinct properties and impacts compared to stratospheric ozone (Ainsworth et al., 2012; WMO, 2014; P. Li et al., 2017; Mills et al., 2018b). Unlike stratospheric ozone, often referred to as "good ozone" for its role in forming the protective ozone layer that shields Earth's biota from harmful ultraviolet radiation, tropospheric ozone, commonly termed "bad ozone," acts as a greenhouse gas contributing to direct radiative forcing (0.35–0.37 W m^{-2}) and serves as a detrimental pollutant with significant adverse impacts on human health, vegetation, and ecosystems (Agathokleous et al., 2015; Monks et al., 2015; Chang et al., 2017; Gaudel et al., 2018). While approximately 10% of tropospheric ozone originates from stratospheric influx (Stevenson et al., 2006), the majority is formed through complex photochemical reactions involving ozone precursor gases such as nitrogen oxides (NO_x = NO + NO_2), volatile organic compounds (VOCs), carbon monoxide (CO), and methane (CH_4) (Ainsworth et al., 2012; Simpson et al., 2014). The rise in tropospheric ozone concentration since the industrial era is primarily attributed to anthropogenic activities, including energy production, transportation, fossil fuel combustion, industrialization, urbanization, deforestation, and population growth (Cho et al., 2011; IPCC, 2014; Brauer et al., 2016). These activities release ozone precursor gases into the atmosphere, triggering photochemical reactions that generate this secondary pollutant (Akimoto, 2003; Yamaji et al., 2006).

Ozone pollution has been recognized as a significant environmental issue since the mid-20th century, initially identified in North America during the 1950s and later in Europe and Japan by the 1970s, with adverse effects subsequently reported in urban and industrial regions globally (Haagen-Smit, 1952; Fowler et al., 2008). The emissions of synthetic chlorofluorocarbons have contributed to stratospheric ozone depletion. In contrast,

tropospheric ozone concentrations have been influenced by emissions of precursor gases such as nitrogen oxides (NOx) and volatile organic compounds (VOCs). Effective control measures in North America and Western Europe have reduced peak ozone levels (Ainsworth, 2017). Still, emissions in rapidly developing regions of Asia continue to rise, surpassing global mitigation efforts (Ashmore, 2005). The damaging effects of tropospheric ozone on crops were first observed in the USA during the 1940s and linked to photochemical reactions involving NOx and organic trace gases in sunlight (Middleton et al., 1950; Haagen-Smit & Fox, 1954). Reports of ozone-induced damage to vegetation emerged in other regions, including Europe and Japan, by the 1970s (The Royal Society, 2008). Despite curbing emissions of precursor gases in highly developed regions since the 1990s, global background tropospheric ozone concentrations continue to rise, driven by emissions in densely populated, economically developing areas, particularly in Asia. This trend is expected to persist, with extreme regional peaks projected through the 21st century, even as mitigation policies are gradually implemented (The Royal Society, 2008; IPCC, 2014).

Ozone is a dynamic and short-lived air pollutant, and its concentrations vary significantly across regions, influenced by factors such as temperature, sunlight, and human activities. In temperate regions with pronounced seasonality, ozone levels range from approximately 20 ppb in parts of Australia and South America to 55–60 ppb in regions such as Asia, Europe, and North America, with concentrations typically higher in the Northern Hemisphere (Monks et al., 2015; Ainsworth, 2017). Hot and sunny weather significantly accelerates ozone formation, resulting in peak concentrations during summer afternoons, with extreme episodic levels reaching 200–400 ppb in urban areas and during heat waves, far surpassing the damage threshold of 40 ppb that adversely affects plants (Jain et al., 2005; Tiwari et al., 2008; Fowler et al., 2008). Asia, marked as an ozone hotspot, faces severe pollution scenarios, especially in developing countries, driven by rapid economic and population growth, increased precursor gas emissions, and insufficient air quality regulations (Brauer et al., 2016; Mills et al., 2018b). Between 1990 and 2013, global population-weighted ozone concentrations increased by 8.9%, with the highest rises observed in Bangladesh, India, and Pakistan (ca. 20%) compared to the global average (ca. 9%) (Brauer et al., 2016). China, the largest emitter of ozone precursor gases (NOx) in Asia, experienced an increasing trend in various ozone metrics between 2013 and 2017 (Feng et al., 2015; Zeng et al., 2019). Despite efforts in developed countries to control ozone through air quality regulations, current tropospheric ozone

concentrations continue to pose a significant threat to crops and vegetation globally, with metrics such as AOT40 and flux-based indices widely used for risk assessment, particularly in highly polluted regions (Mills et al., 2011; Agathokleous et al., 2018). As ozone levels are expected to rise further, particularly in Asia, its impact on vegetation and ecosystems will remain a pressing environmental concern.

2.3 Impact of tropospheric ozone on plants

Ozone significantly impacts plant physiology, affecting both natural ecosystems and agricultural production systems (Weigel et al., 2015). As a molecule of three oxygen atoms, ozone is a potent oxidizing agent. It enters plant leaves primarily through open stomata during gas exchange and rapidly decomposes into reactive oxygen species (ROS) in the humid apoplastic environment, causing oxidative stress (Kangasjärvi et al., 2005; Tamaoki, 2008; Mills et al., 2018b). The effects of ozone on crops can be categorized into acute and chronic, depending on the duration and concentration of exposure. Acute effects occur at high concentrations (typically >150 ppb) over a short duration, while chronic effects result from prolonged exposure to lower concentrations (<150 ppb) (Frei, 2015). Both scenarios lead to the generation of ROS, such as singlet oxygen ($^1O_2$), hydrogen peroxide (H_2O_2), superoxide radicals (O_2^-), and hydroxyl radicals (•OH), which cause oxidative damage, disrupt cellular processes, and trigger programmed cell death, often resulting in visible necrotic symptoms on leaves (Kangasjärvi et al., 2005; Ainsworth, 2017). These physiological disruptions include lipid peroxidation, chlorophyll degradation, reduced photosynthesis, protein oxidation, and damage to nucleic acids, all of which adversely affect crop yield and quality (Mills et al., 2018a). Ozone-induced stress also affects the photosynthetic machinery, reducing light-harvesting efficiency and carboxylation efficiency due to the loss of ribulose 1,5-bisphosphate carboxylase/oxygenase (Rubisco) activity. Declines in photosynthetic electron transport and stomatal conductance further exacerbate the reduction in carbon assimilation, with significant impacts on crop productivity (Calatayud & Barreno, 2001; Fiscus et al., 2005). Studies have shown that elevated ozone concentrations degrade chlorophyll and carotenoids, decreasing pigment concentrations and reducing photosynthetic capacity (Feng et al., 2008; Yuan et al., 2016; P. Li et al., 2017). Non-destructive spectral reflectance methods have corroborated these findings, indicating greater resilience in ozone-tolerant genotypes compared to sensitive ones (Ashrafuzzaman et al., 2017; Begum et al., 2020).

The potential global risks of increasing surface ozone exposure by 2030 were assessed based on two trajectories of ozone pollution outlined in the Intergovernmental Panel on Climate Change Special Report on Emissions Scenarios (IPCC SRES): the A2 scenario, representing a high-emissions trajectory and the B1 scenario, representing a lower-emissions trajectory. Under these scenarios, total global agricultural losses are projected to reach $17–35 billion annually under the A2 scenario, reflecting an increase of $6–17 billion compared to the year 2000. In contrast, the B1 scenario projects annual agricultural losses of $12–21 billion, corresponding to an increase of $1–3 billion from 2000 levels (Avnery et al., 2011). Major crops such as soybeans, wheat, rice, and maize exhibit varying sensitivities to ozone, with yield reductions of approximately 13%, 7%, 5%, and 6%, respectively. This translates to significant threats to food security, especially in regions like East Asia, where annual crop production losses are valued at $63 billion (Mills et al., 2018b; Z. Feng et al., 2022). China exhibits the highest relative yield losses among major crops, with reductions of 33% for wheat, 23% for rice, and 9% for maize, as illustrated in Figure 1 (Z. Feng et al., 2022). The heterogeneous ozone distribution across regions and seasons further complicates its impacts on agriculture, with the highest yield losses observed for soybean in the Americas, wheat in India and China, and rice in South and Southeast Asia (Mills et al., 2018a, 2018b).

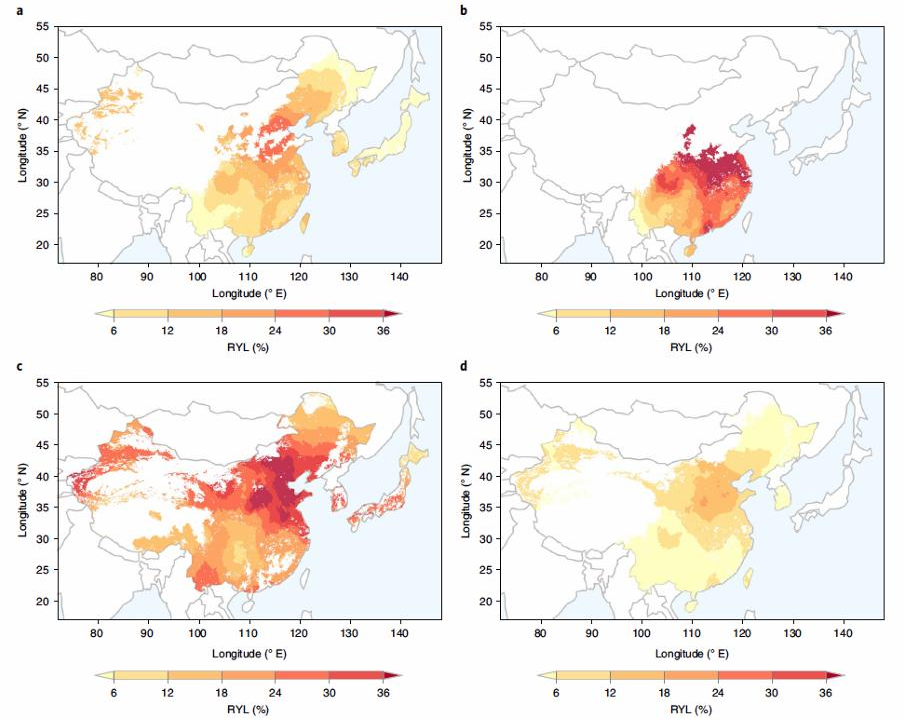

Figure 1 Relative yield losses (RYLs) for different crops calculated from Asian-specific exposure-RY relationships and the AOT40 values across China, Japan, and South Korea. a-d,

RYL(%) of inbred rice (a), hybrid rice (b), wheat (c), and maize (d) in Asia. Results were derived from the AOT average across the last three years (China, 2017-2019; Japan, 2015-2017; and South Korea, 2016-2018). This figure was adapted from Z. Feng et al. (2022).

Moreover, ozone-induced stress affects not only crop yield but also quality. Ozone exposure has been linked to increased protein concentrations in grains due to growth dilution effects but reduces starch content, which is critical for crop quality (Wang & Frei, 2011; Zheng et al., 2013). For instance, in rice, elevated ozone exacerbates grain chalkiness, diminishing consumer acceptance, and increases lignin and phenolics in straw, reducing its utility as livestock feed (Frei et al., 2011; Y. Wang et al., 2014a; Frei, 2015).

2.4 Plant tolerance mechanisms in response to ozone stress

Plant tolerance to ozone stress involves a complex interplay of physiological adaptations, biochemical defenses, and molecular responses (Guo et al., 2024; Nowroz et al., 2024). To cope with elevated ozone levels, plants employ a combination of stress avoidance and defense strategies, which are critical for mitigating damage and maintaining cellular and metabolic functions. Stress avoidance involves controlling ozone entry into the leaf, while defense mechanisms focus on detoxifying ozone within plant tissues (Frei, 2015).

A key avoidance mechanism is stomatal closure, controlled by guard cells that regulate the stomatal aperture. This serves as the first line of defense against ozone (Ainsworth, 2017). Elevated ozone levels reduce stomatal conductance (gsw) by increasing substomatal CO_2 concentration (Ci) and may impair stomatal responsiveness to environmental cues over time (Paoletti & Grulke, 2005). Cultivars with faster stomatal dynamics are better equipped to manage gas exchange under ozone stress (Paoletti & Grulke, 2010). In Arabidopsis thaliana, stomatal conductance plays a critical role in determining ozone sensitivity, with the *SLOW ANION CHANNEL ASSOCIATED 1 (SLAC1)* protein being essential for ozone-induced stomatal closure. SLAC1 mediates anion efflux and cell membrane depolarization, which regulate potassium efflux through K+ channels, aided by OST1 protein kinase phosphorylation (Vahisalu et al., 2008, 2010). Additionally, GUARD CELL HYDROGEN PEROXIDE-RESISTANT1 (GHR1) is implicated in stomatal responses to ozone-induced reactive oxygen species (ROS) (Sierla et al., 2018). Stomatal movements also influence gas exchange, photosynthetic efficiency, and plant sensitivity to ozone. The transcription factors GOLDEN 2-LIKE1 (GLK1)

and GOLDEN 2-LIKE2 (GLK2) regulate genes related to stomatal activity, and manipulating these factors can improve ozone tolerance (Nagatoshi et al., 2016). Environmental factors like light, temperature, and humidity affect ozone uptake through stomata, impacting grain yield (Mills et al., 2011; Pleijel et al., 2000). Despite progress, ozone defense mechanisms remain species-specific, and experimental results often vary, necessitating further research.

The detoxification of ozone or ozone-derived reactive oxygen species (ROS) in the apoplast serves as a critical second line of defense following ozone entry into the leaf through the stomata (Kangasjärvi et al., 2005; Frei, 2015). Among the various enzymatic and non-enzymatic antioxidants involved, apoplastic ascorbate (AsA) plays a particularly significant role in ozone defense due to its high concentration and its distribution across different cellular compartments (Luwe et al., 1993; Conklin & Barth, 2004; Baier et al., 2005; Yendrek et al., 2015). Studies have shown that apoplastic ascorbate can detoxify 30–50% of the ozone that enters leaves across different plant species (Moldau et al., 1997; Turcsányi et al., 2000). AsA can neutralize oxidative stress by donating electrons, and mutants with reduced AsA levels (e.g., vtc mutants) exhibit higher ozone sensitivity (Conklin et al., 1996, 1997, 2000). Apoplastic AsA levels are particularly significant for detoxification, as seen in winter wheat and other species (Feng et al., 2010a). The enzyme ascorbate oxidase (AO) regulates the redox state of apoplastic AsA, with overexpression increasing foliar injury under ozone stress (Sanmartin et al., 2003).

Ozone exposure triggers visible leaf symptoms, such as pale green or yellow lesions along veins, resembling pathogen-induced programmed cell death (PCD). Ozone may mimic pathogen elicitors, inducing hypersensitive response (HR)-like cell death, dependent on specific gene expression programs (McDowell & Dangl, 2000; Rao & Davis, 2001). Ozone also induces pathogenesis-related (PR) proteins, as seen in tobacco, where genes like β-1,3-glucanase and chitinase are rapidly expressed under ozone stress (Ernst et al., 1992). Salicylic acid (SA), a key player in pathogen defense, is transiently elevated in response to ozone, along with increased activity of phenylalanine ammonia-lyase (PAL) (Yalpani et al., 1994; Ogawa et al., 2005). In rice, visible ozone damage is quantified using leaf bronzing scores (LBS), and QTLs on chromosomes 3 and 9 have been linked to this trait (Frei et al., 2008). Furthermore, the *OsORAP1* gene in rice has been identified as a candidate for ozone tolerance. Knockout of this gene in the susceptible type resulted in enhanced tolerance to ozone stress, as evidenced by reduced leaf damage (Ueda et al., 2015b).

Anthocyanins and proanthocyanidins (PAs) contribute to ozone resistance by accumulating in response to stress, mediated by WRKY transcription factors such as *McWRKY71* (Zhang et al., 2022). Studies in soybeans have identified multiple QTLs related to foliar injury, highlighting genetic diversity in ozone tolerance (Burton et al., 2016).

Interestingly, plants also exhibit hormetic responses to ozone, where low levels of exposure can stimulate growth and defense mechanisms. This non-linear response suggests that plants have evolved to tolerate and even benefit from mild oxidative stress (Agathokleous et al., 2019a, 2019b). Plant hormones like SA, ethylene (ET), and jasmonic acid (JA) also influence ozone responses by modulating cell death and defense signaling pathways. Interactions between these pathways can mitigate oxidative bursts and HR cell death, highlighting the complexity of ozone-induced defense mechanisms (Rao et al., 2000). Reduced biomass and yield under ozone stress have been linked to specific genetic loci, such as *APO1* on chromosome 6A in rice, offering potential targets for breeding ozone-tolerant crops (Tsukahara et al., 2013, 2015).

2.5 The vital role of rice in global food security

Rice (*Oryza sativa* L.), a member of the Poaceae family, is one of the most important staple crops worldwide, particularly in Asia, where it is the most widely grown and consumed food crop (Zhao et al., 1998; Londo et al., 2006; McCouch et al., 2016). As a diploid species (n=12) and primarily self-pollinated, rice belongs to the genus *Oryza*, which encompasses a diverse range of cultivated and wild species. Among these, *Oryza sativa*, commonly known as Asian rice, and *Oryza glaberrima*, or African rice, are the two main cultivated species. While *O. sativa* is predominantly cultivated across Asia, *O. glaberrima* is grown in specific regions of Africa. The genus *Oryza* also includes several wild relatives such as *O. rufipogon*, *O. nivara*, and *O. barthii*, which have played pivotal roles in the domestication and evolution of cultivated rice (Londo et al., 2006).

The domestication of rice has occurred independently in different regions. Asian rice (*O. sativa*) was domesticated approximately 10,000 years ago from its wild ancestor, *Oryza rufipogon*, in southern China, particularly near the Pearl River basin (X. Huang et al., 2012). This domestication process resulted in two major subspecies: *O. sativa spp. japonica*, characterized by its short, sticky grains, and *O. sativa spp. indica*, known for its long, non-sticky grains. *O. sativa spp. japonica* was the first to be domesticated in southern China, while

O. sativa spp. indica emerged later in South and Southeast Asia through hybridization between japonica and wild relatives, making it genetically intermediate between cultivated and wild rice (X. Huang et al., 2012). In contrast, African rice (*O. glaberrima*) was domesticated more recently, around 3,000 years ago, from its wild ancestor *O. barthii* in the Niger River region of Africa. Despite its localized cultivation, *O. glaberrima* remains significant due to its unique genetic traits, including resistance to certain pests, diseases, and abiotic stresses (Kovach et al., 2007; X. Huang et al., 2012; M. Wang et al., 2014). Today, rice is cultivated on every continent except Antarctica (Dachler, 2023) and is grown in over 110 countries (Sharif et al., 2014).

Rice plants undergo three main growth phases: vegetative, reproductive, and ripening, involving processes such as plant height increase, tillering, flowering, and grain maturation (Fageria, 2007). Growth duration varies by variety and environment, with long-duration cultivars showing higher acetylene-reducing activity at heading than short-duration varieties (Ladha et al., 1986). In Asia, long-duration cultivars are used for single-rice crops, while shorter-duration ones suit early- and late-rice systems (S. Zhang et al., 2014). Temperature and day length significantly influence phenology, with rising temperatures generally shortening growth phases, although day length offsets some temperature effects on vegetative growth (Zhang et al., 2013; S. Zhang et al., 2014). Some rice-growing countries have adopted three distinct rice-growing seasons based on growth duration. In Bangladesh, rice cultivation is organized into three main seasons: Boro (January-May), the most productive and irrigated dry winter season; Aus (May-August), a primarily rainfed pre-monsoon season; and Aman (August-December), a monsoon-dependent season benefiting from abundant rainfall (Gaihre et al., 2015; Hossen et al., 2012).

Rice is a carbohydrate-rich crop comprising 80% of its weight as carbohydrates, is a staple food providing essential nutrition to over half of the global population and contributing to more than one-fifth of the world's caloric intake (Sharif et al., 2014; Mohidem et al., 2022). While white rice remains the most widely consumed form, brown rice offers superior nutritional benefits. Brown rice is particularly rich in lipids, vitamins (E, B5, and thiamine), minerals (calcium, folate, and iron), dietary fiber, and bioactive compounds such as phytic acid, phenols, sterols, flavonoids, and oryzanol, which exhibit antioxidant properties and potential health benefits (Mir et al., 2016; Zhao et al., 2020; Mohidem et al., 2022). Moreover, significant intra-varietal differences in nutrient composition have been documented, with

variations of up to 9 g protein, 5.65 mg iron, 3.34 mg zinc, 1.6 mg thiamin, 0.392 mg riboflavin, and 7.2 mg niacin per 100 g of unpolished rice (Kennedy & Burlingame, 2003), highlighting its potential as a nutritionally diverse food source. Due to poverty, many individuals rely on rice as their primary source of daily calories, as they lack the financial means to afford a more diverse range of foods (Dachler, 2023).

In the 2022/2023 marketing year, global rice production reached 516.73 million metric tons (Figure 2). In comparison, production increased to 522.65 million metric tons in the 2023/2024 marketing year. Rice is the third most important grain crop globally, following maize, which ranks first, and wheat, which ranks second. In the 2023/2024 marketing year, maize production reached 1.23 billion metric tons, while wheat production totaled 791.24 million metric tons (USDA, 2024). According to the USDA, China remains the largest rice producer for the 2023/2024 season, contributing 28% of global production with 144.62 million metric tons. India follows closely, accounting for 26% with a total output of 137.83 million metric tons. Bangladesh ranks third, producing 37 million metric tons and representing 7% of global production, while Indonesia takes fourth place with 6% and a total production of 33.02 million metric tons (USDA, 2024).

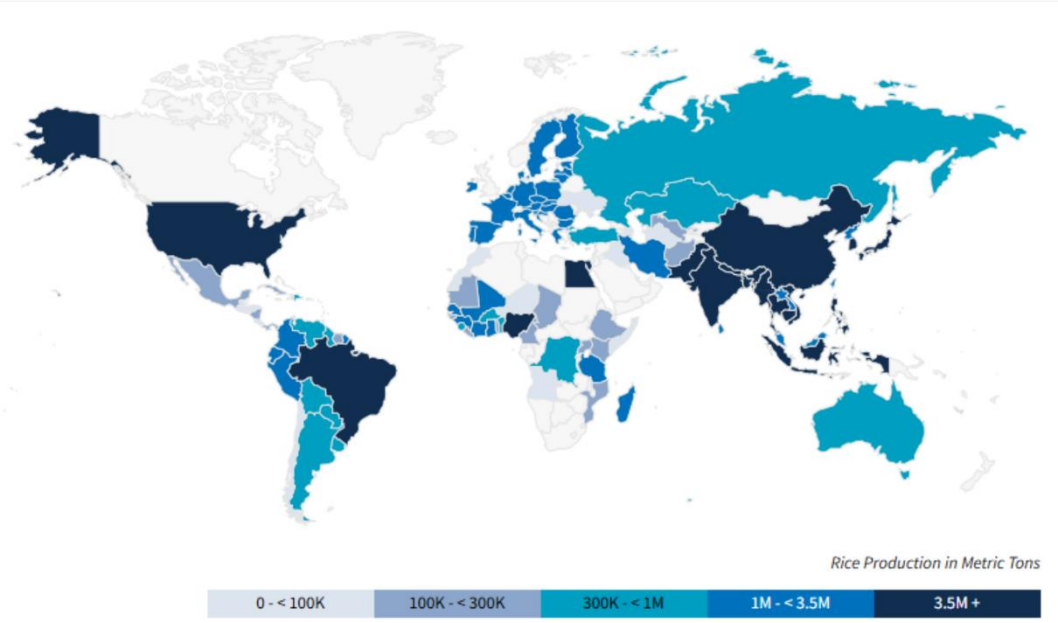

Figure 2 Global rice production map for the 2023/2024 marketing year. This map illustrates the distribution of rice production worldwide, with production levels categorized by metric tons. Darker shades represent higher production volumes, with the leading producers predominantly located in Asia. This figure was adapted from USDA (2024).

2.6 The role of tropospheric ozone in reducing rice productivity across Asia

Rice production in Asia is increasingly threatened by a combination of abiotic and biotic stresses, which significantly reduce yield and quality (Tan et al., 2018; Mahmood-Ur-Rahman et al., 2019; Sarma et al., 2023). Tropospheric ozone (O_3) pollution has emerged as a critical concern, causing substantial yield reductions across Asia. Elevated O_3 levels negatively affect rice physiology, including photosynthesis, biomass accumulation, and grain quality (Shang et al., 2024). China, India, Bangladesh, and Indonesia, the world's leading rice-growing regions, are among the countries most at risk of ozone-induced rice yield losses. Studies utilizing the latest ozone-flux-based crop yield response models and current ozone pollution data estimate yield losses in these regions to range between 7.5% and 12.5% of total rice production (Figure 3) (Mills et al., 2018b). However, many farmers in Asia remain unaware of the specific impacts of ozone pollution on crop yields, as its effects are often not visibly apparent, making it challenging to link yield losses directly to ozone exposure (Rai & Agrawal, 2012; Z. Feng et al., 2022). Additionally, interactions between ozone pollution and other environmental factors, such as climate change, can obscure the direct impacts of ozone, complicating the issue further (Du et al., 2024). While ozone concentrations have been declining or stabilizing in Europe and North America, they are rising steadily in Asia (Feng et al., 2021). Research suggests that a 1% increase in tropospheric ozone concentration can lead to a 2.3% decrease in rice productivity (Mahmood et al., 2020).

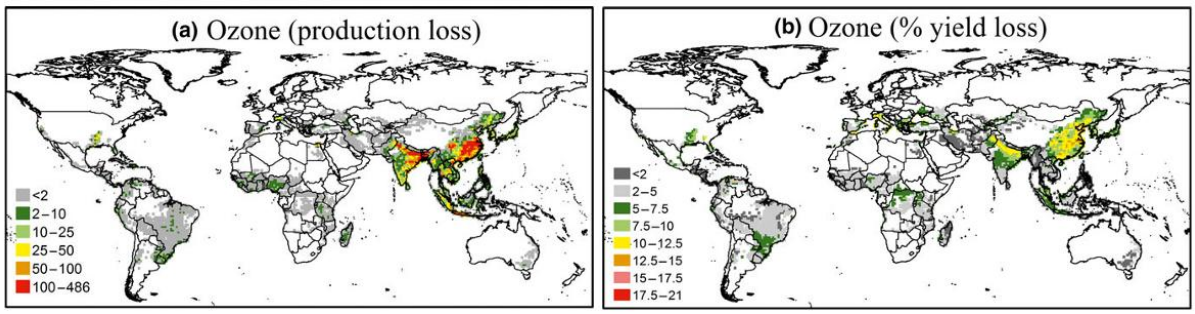

Figure 3 Global impacts of ozone stress on rice production are shown for 1 × 1° grid squares where the average rice production exceeds 500 tons (0.0005 Tg). (a) Illustrates the reduction in rice production caused by ozone stress, expressed in thousand tons (0.001 Tg) per grid square. (b) Depicts the average percentage yield loss due to ozone stress during the period 2010–2012. This figure was adapted from Mills et al. (2018b).

Historical data indicate that global ozone concentrations reached approximately 50 ppb by 2000, with levels between 31–50 ppb causing an estimated 18% reduction in rice yields and an additional 10% loss at 51–75 ppb (Feng & Kobayashi, 2009). Regionally, ozone pollution is responsible for over 10% of global rice yield losses (Ainsworth, 2008; Van Dingenen et al., 2009), with specific impacts of 20% in East Asia (Chen et al., 2011) and 15% in India (Debaje, 2014; Mills et al., 2018b). Controlled experiments further emphasize the detrimental effects of ozone, showing yield reductions of up to 50% compared to controls due to impaired yield-contributing components, such as reduced spikelet number, lower grain mass, higher spikelet sterility, and fewer tillers (Akhtar et al., 2010; Frei et al., 2012; Yamaguchi et al., 2014).

East Asia is identified as a hotspot for ozone pollution, with significant increases in concentrations over recent decades (Chang et al., 2017; Z. Feng et al., 2022). In eastern China, ozone levels rose by an average of 1.45 ppb per year between 2015 and 2022, with heatwaves during the summer months (June–July–August) accelerating the increase to 4.74 ppb per year in Maximum Daily 8-hour Average (MDA8) ozone concentrations (Wang et al., 2023). The COVID-19 pandemic led to a temporary reduction in industrial and vehicular emissions, resulting in slightly lower ozone levels in 2020, yet concentrations rebounded as activities resumed (Chen et al., 2023).

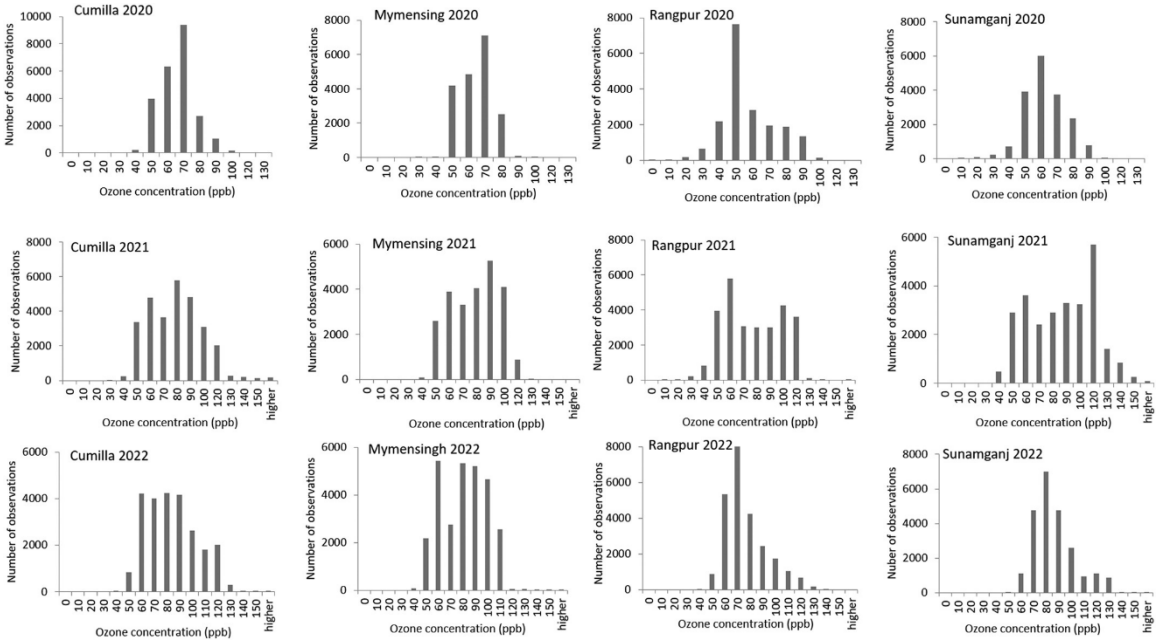

Figure 4 Ozone concentrations across four experimental locations during the Boro rice growing seasons (2020–2022). Each data point represents an ozone measurement recorded

at 3-minute intervals between 09:00 and 17:00 h using a handheld mobile ozone monitor positioned adjacent to the experimental fields. This figure was adapted from Frei et al. (2024).

Similarly, India is witnessing rising tropospheric ozone levels, particularly in the Indo-Gangetic Plain (IGP), a critical rice-producing region. Ozone levels in the northeastern Gangetic Plain have increased by 6–7.2% per decade, aligning with rising emissions of ozone precursors like nitrogen oxides (NOx) and carbon monoxide (CO) due to growing coal and petroleum consumption (Lal et al., 2012).

Bangladesh has experienced the sharpest rise in near-surface ozone pollution among the ten most populous countries, with levels increasing by 20% from 59 ppb to 72 ppb between 1990 and 2013 (Brauer et al., 2016). This trend is driven by high population density, rapid economic growth, and emissions of ozone precursors (David et al., 2019). Favorable meteorological conditions, such as high temperatures and radiation from February to June, further promote ozone formation (Frei, 2015). Field experiments during three consecutive Boro seasons in Bangladesh revealed seasonal daytime ozone averages ranging from 59.4 ppb to 84.2 ppb (Figure 4), leading to an estimated 10.4% yield loss in rice (Frei et al., 2024). Ozone consistently exceeded 40 ppb—the damage threshold for crops—throughout the seasons. Cumilla recorded the highest levels, peaking at 190 ppb, while Rangpur reported the lowest. The temporary reduction in ozone concentrations during the 2020 COVID-19 lockdowns highlights the significant influence of human activities on pollution levels (Frei et al., 2024).

These findings underscore the urgent need to address tropospheric ozone pollution across Asia, as its rising concentrations threaten rice productivity and food security in the region. Implementing effective mitigation strategies, including reducing emissions of ozone precursors and enhancing farmer awareness of ozone's impacts, is critical to safeguarding rice production.

2.7 Ensuring food security across Asia in the face of ozone pollution

A multi-faceted approach is necessary to ensure food security across Asia in the face of ozone pollution. This includes implementing stricter air pollution regulations to reduce ozone precursor emissions, applying ozone protectants during critical plant growth stages, and developing ozone-tolerant crop varieties (Agathokleous et al., 2023; Dewan et al., 2024; Frei et al., 2024).

Implementing stricter air pollution regulations to reduce ozone precursor emissions across Asia represents a critical long-term strategy for improving air quality and mitigating the impacts of climate change. This strategy addresses the root cause of the problem by targeting the sources of ozone precursors, thereby creating a more favorable environment for crop growth. Implementing effective emission control measures requires collaboration between agricultural stakeholders, policymakers, and industry. Research indicates that reducing emissions of key ozone precursors—namely nitrogen oxides (NOx), volatile organic compounds (VOCs), and carbon monoxide (CO)—yields significant benefits, including enhanced air quality and reduced adverse health outcomes (Tagaris et al., 2010; Fann et al., 2018). Notably, East Asia, particularly China, has experienced the most rapid growth in ozone precursor emissions in recent years (Cooper et al., 2010). These emissions not only degrade local air quality but also contribute to elevated ozone levels in western North America through long-range atmospheric transport (West et al., 2009a, 2009b; Cooper et al., 2010).

Addressing these challenges requires coordinated emission control efforts at both local and regional scales. For example, studies demonstrate that reducing emissions of NOx, xylene, and ≥C3 alkenes in the Beijing-Tianjin-Hebei region, as well as in neighboring provinces, significantly decreases the frequency of ozone-exceedance days (Wang et al., 2021). However, the effectiveness of emission reductions varies depending on the geographic region and the specific pollutants targeted. For instance, reductions in NOx emissions in tropical and Southern Hemisphere regions have a more pronounced impact on increasing methane levels and long-term surface ozone per unit of emissions reduced compared to reductions in temperate regions of the Northern Hemisphere (West et al., 2009a, 2009b). Furthermore, the radiative forcing associated with short-lived air pollutants is influenced by the location and source type of precursor emissions, underscoring the need for geographically targeted interventions (Unger et al., 2008).

Policymakers designing effective control strategies must therefore account for several critical factors, including regional variations in emission sources, the cost-effectiveness of specific mitigation measures, and the potential impacts of climate change on ozone formation and removal processes. While stringent regulations on ozone precursor emissions generally yield positive outcomes, a holistic approach addressing multiple pollutants and incorporating both local and regional emission sources is likely to achieve the most substantial improvements in air quality (Amann & Lutz, 2000; Xing et al., 2019). This comprehensive strategy is essential

for advancing sustainable environmental management and public health objectives across Asia.

Further, Antiozonants have been explored as a potential solution to mitigate ozone-induced crop yield loss, with ethylenediurea (EDU) emerging as the most extensively studied and long-established chemical compound for this purpose . EDU, chemically known as N-[2-(2-oxo-1 imidazolidinyl)ethyl]-N'-phenylurea, was first introduced by Carnahan et al. in 1978 and successfully used to protect bean plants from ozone-induced visible leaf injury. Since then, numerous studies have confirmed the efficacy of EDU in providing protection against ozone in various plant species, particularly in sensitive genotypes (Feng et al., 2010b; Manning et al., 2011). EDU applications are primarily conducted through spraying and soil drenching, although stem injections have also been reported in certain cases (Paoletti et al., 2007; Manning et al., 2011). EDU treatment has been shown to mitigate ozone-induced crop damage by reducing lipid peroxidation, increasing chlorophyll content, and enhancing antioxidant activities (Gupta et al., 2018; Singh et al., 2018). Additionally, EDU application significantly enhances photosynthesis-related traits, biomass production, and yield components in crops exposed to elevated ozone levels, further demonstrating its efficacy in protecting plants and improving overall crop productivity under ozone stress (Agathokleous, 2017; Ashrafuzzaman et al., 2017; Shang et al., 2022). Interestingly, while EDU offers protection against ozone damage, its effectiveness may vary depending on the ozone concentration and crop variety. For instance, EDU could provide only 31% protection in rice under high ozone pollution (Shang et al., 2022). Similarly, EDU provided incomplete protection in some varieties of wheat, as evidenced by the low abundance of many primary metabolism-related proteins (Gupta et al., 2018). Additionally, phenyl urea (PU) has shown promise in mitigating crop ozone stress (Chaudhary & Rathore, 2020). Catechin, a compound found in tea leaves, has also demonstrated potential as an ozone protectant for rice, helping maintain chlorophyll content and antioxidant systems (Kittipornkul et al., 2020).

The effectiveness of antiozonants, such as EDU, has been clearly demonstrated in experiments, highlighting their potential to improve crop yields under current air pollution levels. However, several limitations must be addressed before considering large-scale application: (i) EDU is not yet commercially available; (ii) its repeated application is labor-intensive, posing practical challenges; and (iii) its ecotoxicological impacts and potential

effects on human health have not been thoroughly studied, making it difficult to justify widespread use in food production systems (Frei et al., 2024).

The development of ozone-tolerant crop varieties has been extensively discussed as a potential strategy to mitigate the adverse effects of rising tropospheric ozone concentrations on agricultural productivity. The cultivation and breeding of ozone-tolerant varieties offer a viable short- to mid-term solution for sustaining and potentially enhancing crop yields under elevated ozone levels (Frei et al., 2024). Numerous studies have documented genotypic variation in the responses of crop species to high ozone exposure, including wheat (Biswas et al., 2008), soybean (Burkey & Carter, 2009), and rice (Sawada & Kohno, 2009). This genotypic variability serves as a fundamental prerequisite for the implementation of adaptive breeding programs (Mills et al., 2018b; Agathokleous et al., 2023).

Notably, some research suggests that modern crop varieties may exhibit greater sensitivity to ozone stress compared to older varieties or landraces. For example, Hansen et al. (2019) observed that a landrace wheat variety demonstrated a higher degree of phenotypic plasticity under varying environmental conditions, including ozone stress, compared to modern cultivars. Moreover, the identification of quantitative trait loci (QTL) and candidate genes associated with ozone tolerance in major crops provides critical resources for breeding programs aimed at enhancing resilience to ozone stress (Frei, 2015; Mills et al., 2018b; Agathokleous et al., 2023).

2.8 Progress in developing ozone-tolerant rice varieties

Large-scale rice breeding programs for tolerance to ozone are missing, although some studies reported possible quantitative trait loci (QTL) and candidate genes. A single locus on chromosome 6A was identified associated with the ozone-induced yield loss in rice based on the Sasanishiki/Habataki chromosome segment substitution lines, and the *ABERRANT PANICLE ORGANIZATION 1 (APO1)* was suggested a potential candidate gene (Tsukahara et al., 2013, 2015). Using a population of backcross inbred lines derived from a cross between Nipponbare (ozone-sensitive) and Kasalath (ozone-tolerant), several quantitative trait loci (QTLs) associated with ozone tolerance were identified. Two of these QTLs were validated through chromosome segment substitution lines (CSSLs) and subjected to further investigation: *OzT8*, located on chromosome 8, which influenced biomass under ozone stress,

and *OzT9*, located on chromosome 9, which affected leaf symptom development. Subsequent physiological analyses utilized CSSLs carrying the tolerant Kasalath alleles within the genetic background of Nipponbare: SL46 (*OzT8*) and SL41 (*OzT9*) (Y. Wang et al., 2014b). *OzT8* was associated with the capacity to sustain high photosynthetic rates despite ozone-induced stomatal closure (Chen et al., 2011).

To elucidate the physiological mechanisms and identify candidate genes underlying *OzT9*, transcriptome analysis was performed. This analysis revealed a highly ozone-responsive putative ascorbate oxidase gene (*Os09g036590*) localized near the *OzT9* QTL (Frei et al., 2010). Functional characterization using reverse genetic approaches, including knockout and overexpression studies, confirmed the gene's role in oxidative stress response and ozone-induced leaf symptom formation (Ueda et al., 2015b). Subcellular localization studies employing GFP-fusion proteins demonstrated its apoplastic localization (Ueda et al., 2015b). However, heterologous expression in *Arabidopsis thaliana* indicated that the encoded protein did not exhibit ascorbate oxidase activity. Instead, the protein was classified as part of a novel clade within the ascorbate oxidase family, lacking ascorbate oxidation capability. Consequently, the gene was renamed *OZONE RESPONSIVE APOPLASTIC PROTEIN1 (OsORAP1)* (Ueda et al., 2015b). Further studies indicated that *OsORAP1* mediates ozone-induced cell death, potentially through interactions with plant hormones such as salicylic acid and jasmonic acid. Sequence polymorphisms in the promoter and 5'-UTR regions between Nipponbare and Kasalath were identified and hypothesized to contribute to differential ozone-induced expression in sensitive versus tolerant genotypes (Ueda et al., 2015b).

Marker-assisted selection was employed to develop QTL pyramiding lines containing chromosomal segments from Kasalath at both *OzT8* and *OzT9* loci within the Nipponbare genetic background. Season-long field experiments in ozone-enriched environments in China revealed that these pyramiding lines outperformed Nipponbare in several yield components, including biomass and spikelet sterility. They also surpassed lines carrying single QTLs (Y. Wang et al., 2014b). Furthermore, one pyramiding line (L81) exhibited enhanced resistance to ozone-induced grain quality deterioration compared to Nipponbare (Jing et al., 2016). The SL41 line carrying *OzT9* demonstrated improved straw quality under high ozone conditions relative to Nipponbare, a trait of particular significance in regions like Bangladesh, where rice straw serves as a critical feed source for ruminant herbivores (Frei et al., 2011).

These findings highlight the utility of incorporating ozone-tolerance QTLs, such as *OzT8* and *OzT9*, to improve yield and quality traits under ozone stress in Nipponbare-derived genetic backgrounds. These findings highlight the potential for developing ozone-tolerant rice varieties by integrating ozone-tolerance QTLs into rice cultivars grown in regions affected by elevated ozone concentrations. Advanced molecular breeding techniques, particularly marker-assisted selection (MAS), offer a promising approach, as MAS provides a substantial improvement over traditional, time-intensive breeding methods such as pedigree selection (Collard & Mackill, 2008; Frei, 2015).

2.9 Possible synergies or trades off in ozone-tolerant rice breeding

Crops are subject to various abiotic and biotic stresses under field conditions, which significantly impact yield and sustainability (Chojak-Koźniewska et al., 2018; Cohen & Leac, 2019). Among these, increasing tropospheric ozone concentrations and blast disease caused by the filamentous ascomycete fungus *Magnaporthe oryzae* represent two coinciding stresses that severely affect rice (*Oryza sativa* L.) yields worldwide (Singh et al., 2020; Ashrafuzzaman et al., 2021).

Rice blast disease, a major constraint in rice production, thrives under specific climate conditions characterized by high relative humidity (>90%) and temperatures ranging from 24 to 30 °C, which can trigger epidemic outbreaks (Hensawang et al., 2017). The fungus *M. oryzae* infects rice plants at all developmental stages, causing leaf, node, neck, and panicle blast. Infection begins with the attachment of a three-celled conidium to the rice leaf cuticle, and within 4 to 5 days, necrotrophic lesions develop, enabling profuse sporulation and rapid disease spread to neighboring plants (Wilson & Talbot 2009; Boddy, 2016). Under favorable conditions, blast disease can lead to catastrophic yield losses ranging from 60% to 100%, particularly in rice-growing regions of Asia and Africa, posing a significant threat to global food security (Kihoro et al., 2013). The annual global rice yield loss due to the blast is equivalent to the amount needed to feed 60 million people (Pennisi, 2010).

The co-occurrence of blast disease in regions with elevated ambient ozone levels suggests potential interactions between these stresses in field-grown rice. However, little is known about whether these interactions result in synergies or trade-offs in tolerance or resistance to these stress factors. A potential shared mechanism underlying the impacts of both stresses

is programmed cell death (PCD), a common plant response to both ozone stress and pathogen attack (Heath, 2000; Kangasjärvi et al., 2005).

Unlike biotic stresses, plants have not co-evolved with high tropospheric ozone concentrations, making it unlikely that they possess specific ozone receptors. Instead, plants respond to ozone exposure through an apoplastic oxidative burst, which mimics the response to pathogen attack (Kangasjärvi et al., 2005). This oxidative burst triggers signaling cascades that induce PCD, leading to the formation of necrotic lesions on plant leaves (Kangasjärvi et al., 2005). While disease resistance mechanisms rely on PCD to confine pathogens and limit their spread within plant tissues (Apel & Hirt, 2004), tolerance to ozone stress requires the suppression of PCD caused by ozone-derived reactive oxygen species (ROS) in the apoplast (Ueda et al., 2015b).

Understanding potential synergies or trade-offs between ozone tolerance and blast resistance is, therefore, critical for developing rice varieties that can withstand these dual stresses.

2.10 Marker-assisted breeding for stress tolerance rice

Marker-assisted breeding (MAS) leverages DNA markers as indirect selection tools in breeding programs, offering significant advantages over conventional breeding methods. This approach is particularly beneficial for traits that are challenging to select phenotypically, reducing the breeding cycle by 3–6 years and delivering substantial economic benefits (Collard & Mackill, 2008; Alpuerto et al., 2009; Hospital, 2009). For example, MAS in rice breeding for salinity and phosphorus-deficiency tolerance is projected to generate $50–$900 million in incremental economic benefits over 25 years (Alpuerto et al., 2009).

Single nucleotide polymorphisms (SNPs) are highly valued in MAS due to their low cost, accuracy, and reproducibility. The Kompetitive Allele Specific PCR (KASP) assay is a popular SNP genotyping technology offering flexible design and high-throughput capabilities (Dipta et al., 2024). SNPs are widely used in germplasm identification, quality control, linkage mapping, and development of trait-specific markers (Dipta et al., 2024; He et al., 2014). Other marker types, such as restriction fragment length polymorphisms (RFLPs), random amplified polymorphic DNA (RAPD), amplified fragment length polymorphisms (AFLPs), and simple sequence repeats (SSRs), also play roles in MAS (Nadeem et al., 2018). Advances in sequencing

technologies have further popularized genetic or functional markers derived directly from genes (Varshney, 2010).

MAS has been particularly effective in developing stress-tolerant rice varieties for traits such as drought tolerance, disease resistance, insect resistance, and submergence tolerance. However, its success depends on the specific stress factor and the characteristics of associated quantitative trait loci (QTLs) (Shinada et al., 2014; Mehta et al., 2019). For example, the *Saltol* QTL has been widely used for salinity tolerance. Researchers transferred *Saltol* from FL478 to Pusa Basmati 1509, producing near-isogenic lines (NILs) with 96.67–98.57% recurrent parent genome recovery. These NILs demonstrated higher yields, improved salinity tolerance, and retained desirable grain quality (Yadav et al., 2020). Similarly, *Saltol* was introgressed into the popular rice variety ADT 43, resulting in salt-tolerant lines with high yield and favorable cooking quality (Geetha et al., 2017). Other studies have reported the successful development of salinity-tolerant lines through backcrossing, pyramiding, and controlled stress evaluations (Huyen et al., 2012; Ali et al., 2013). MAS has also contributed significantly to drought-tolerant rice breeding through the pyramiding of large-effect QTLs for grain yield under drought conditions into mega-varieties. This approach has facilitated the development of commercially viable drought-tolerant cultivars (Swamy & Kumar, 2013; Chengqi et al., 2023).

Despite its success, MAS faces challenges in certain contexts. For example, breeding for iron toxicity tolerance in West Africa has been limited due to the small effects and wide confidence intervals of relevant QTLs (Sikirou et al., 2015). Similarly, the pyramiding of QTLs for cold tolerance at the fertilization stage shows potential but requires further refinement (Shinada et al., 2014). In crops with complex genomes, such as sugarcane, the application of MAS is hindered by genetic complexity and polyploidy (Sandhu et al., 2022). Additionally, many markers published in research fail to translate into practical applications due to logistical and genetic constraints (Xu & Crouch, 2008).

To fully realize the potential of MAS, its implementation must be integrated with high-throughput phenotyping, genotyping, and advanced computational tools. This holistic approach will address existing challenges and enhance the efficiency of breeding programs, enabling the development of robust, stress-tolerant crop varieties (Hasan, 2021; Sandhu et al., 2022).

2.11 Research objectives

This thesis addresses three main objectives, focusing on marker-assisted breeding for ozone-tolerant rice. Four experiments were conducted to investigate specific research questions to achieve these objectives.

We aimed to ensure that the breeding efforts for ozone tolerance did not inadvertently compromise disease resistance, as maintaining resistance to plant pathogens is a critical trait in crop improvement. Therefore, it was essential to establish at least a neutral relationship between ozone tolerance and disease resistance to justify the selection of ozone tolerance in breeding programs. We conducted the first experiment to investigate this relationship to assess potential trade-offs or correlations between these traits.

Experiment 1 : Interactive effects of tropospheric ozone and blast disease (*Magnaporthe oryzae*) on different rice genotypes

This study aimed at evaluating different rice genotypes under the combined treatment of ozone and blast stress. Our specific research questions were

1.1 Does ozone exposure affect the plants' responses to blast disease and vice versa?

1.2 Are ozone and blast tolerance correlated in different rice genotypes, either positively or negatively?

Marker-assisted breeding was employed to incorporate the ozone-tolerant QTLs *OzT8* and *OzT9* into two popular ozone-sensitive rice varieties. The resulting breeding lines were evaluated across three experiments to assess their performance.

Experiment 2: Assessing ozone tolerance in rice (*Oryza sativa* L.) breeding lines containing ozone tolerance QTLs *OzT8* and *OzT9*

This preliminary screening experiment was conducted with the following objectives:

2.1 To assess the physiological and biochemical responses of rice breeding lines containing *OzT8* and/or *OzT9* under ozone stress.

2.2 To evaluate the yield performance of the breeding lines under ozone stress conditions.

2.3 To identify and select ozone-tolerant lines for further advancement and detailed investigation.

Experiment 3 + 4: Comprehensive evaluation of ozone-tolerant rice (*Oryza sativa* L.) breeding lines through physiological and agronomic trait analysis

The most suitable ozone-tolerant line was selected through a comprehensive greenhouse experiment and a subsequent field experiment. The specific objectives of the study were:

3.1 To identify the rice breeding lines most tolerant to ozone stress, based on physiological and yield parameters, through a greenhouse experiment.

3.2 To evaluate the suitability of these breeding lines under field conditions.

3 Materials and Methods

3.1 Experiment 1: Interactive effects of tropospheric ozone and blast disease (*Magnaporthe oryzae*) on different rice genotypes

3.1.1 Plant materials and growth conditions

The experiment was conducted in a climate-controlled greenhouse from September 2020 to February 2021. Nine different rice genotypes were used in this experiment: (i) Nipponbare, an ozone sensitive Japanese *Japonica* rice variety (Jing et al., 2016) (ii) BRRI dhan28, an ozone sensitive and popular Bangladeshi *Indica* rice variety (Ashrafuzzaman et al., 2018) (iii) Binadhan-11, an ozone sensitive and Bangladeshi modern *Indica* rice variety (Ashrafuzzaman et al., 2018) (iv) IR64, an ozone sensitive (Ashrafuzzaman et al., 2018) and one of the world's most widely grown *Indica* rice varieties, also known as blast resistant (Sallaud et al., 2003) (v) Kasalath, a Bangladeshi *Aus* landrace which is the donor for ozone tolerant quantitative trait loci (Frei et al., 2008, 2010) (vi) L81, an ozone tolerant genotype carrying introgressions of two ozone tolerant quantitative trait loci from Kasalath in the background of Nipponbare (Y. Wang et al., 2014b) (vii) CO39, a blast-susceptible *Indica* rice genotype (Telebanco-Yanoria et al., 2011) (viii) Koshihikari, a blast-susceptible short-grain rice *Japonica* cultivar (Kobayashi et al., 2018) (ix) Kitaake, a model *Japonica* rice cultivar (G. Li et al., 2017). These seeds were collected from the plants grown in a greenhouse of University of Bonn, Germany and had no stress exposure.

Seeds were germinated at 30 °C in deionized water in the dark for three days (Ashrafuzzaman et al., 2018). The seedlings were then transferred to a mesh floating on solutions containing one-fourth strength Yoshida nutrient solution (pH 5.5) and placed under natural light in the greenhouse for seven days (Yoshida et al., 1976). The pH was adjusted to 5.5.

A total of one hundred forty-four pots were filled with local clay-silt luvisol soil with 16% clay, 77% silt, 7% sand, 1.2% organic carbon and pH 6.5 (Ueda et al., 2015a, Ashrafuzzaman et al., 2017). To ensure balanced nutrition, "NovaTec classic 12-8-16" (12% N, 8% P2O5, 16% K2O) was applied initially at the rate of 0.8 g/pot. The same fertilizer dose was applied at the reproductive stage. For blast inoculation, two 10-day-old seedlings of each genotype were sown in a 10-cm diameter pot. The pots were placed in trays filled with water from transplanting throughout the growing season. Supplementary lighting was provided in the greenhouse from 7 a.m. to 6 p.m. to ensure a minimum photosynthetic photon flux density

(PPFD) of 300 µmol m^{-2} s^{-1}. The minimum temperature of the greenhouse was set to 28/22 °C (day/night), and the average humidity was 53% (Ashrafuzzaman et al., 2018).

Four different treatments with four replicates were implemented: (a) control, (b) blast, (c) ozone, and (d) ozone & blast. In total, eight open-top chambers (length 1m, width 1m, height 1m) were used for control (4 chambers) and ozone fumigation (4 chambers). In each chamber, there were two trays, and each tray accommodated nine pots of different genotypes (two plants per pot). Plants from one tray were infected with the blast in each chamber, while the other was treated as control (without ozone) or only ozone stress.

3.1.2 Growth of fungal pathogen, inoculum preparation and inoculation of rice plants

Magnaporthe oryzae isolate Li1497 (1328) was used for blast inoculation. Isolate Li1497 was grown on potato dextrose agar (PDA) for seven days and then sub-cultured on rice leaf agar (50 g fresh rice leaves, 15 g agar, 10 g soluble starch, 2 g yeast extract in 1000ml water). The cultures were incubated under UV light (16/8 h day/night) at 25° C for 14 days to induce sporulation. Conidia of *M. oryzae* were harvested by scraping off the mycelia using tap water with a drop of Tween 20 and 0.4% gelatin and then strained through a double layer of cheesecloth. Rice plants at the three-leaf stage (twenty-four days old seedlings) were inoculated by spraying with conidial suspensions (10^5 conidia/ml) using a hand sprayer, which is optimal for visible disease reactions (Li et al., 2014; H. Zhang et al., 2014; Deng et al., 2016; Chen et al., 2019; Chakraborty et al., 2020; Norvienyeku et al., 2021). The inoculated plants were kept in a dark, moist incubation chamber at 25° C and >95% RH for 24 h, and were subsequently taken back to the greenhouse. The other non-inoculated plants were also kept in the dark, moist chamber to ensure the same growth condition.

3.1.3 Ozone treatment

Plants were exposed to an ozone treatment from 14 DAT (Days after transplanting) to 137 DAT (until the end of growth season) in open top chambers (OTC) (Ueda et al., 2015a). A custom-made ozone generator (UB 01; Gemke Technik GmbH, Ennepetal, Germany) was used to ensure an ozone concentration of 100 ppb for 7 hours (9:00-16:00h) every day. As input, dried air passing through silica gels was used, and the generated ozone was first percolated through water to remove reactive gases other than ozone. Then ozone-enriched air was blown into the chambers and evenly distributed via perforated plastic pipes running above

the plant canopy. The ozone output was regulated by an ozone monitor (K100 W; Dr. A. Kuntze GmbH, Meerbusch, Germany) and detected by an ozone sensor (GE 760 ozone; Dr. A. Kuntze GmbH, Meerbusch, Germany) placed inside the fumigation chambers. Besides, the ozone concentrations were continuously monitored in the different chambers with an independent handheld ozone monitor (series 500; Aeroqual Ltd. Auckland, New Zealand) at five minutes intervals. The average recorded ozone concentration was 103 ± 12 ppb (average ± standard error) in the ozone treatment, whereas the average concentration in control conditions was 22 ± 6 ppb. Control plants were exposed to ambient ozone concentrations, but in the control conditions, the ambient ozone concentrations were maintained below the damage threshold level (40 ppb) (Ashrafuzzaman et al., 2018). Ozone fumigation was continued for 123 days until all genotypes reached maturity.

3.1.4 Assessment of leaf blast severity

Visual leaf blast symptoms were quantified as blast severity score (BSS) using a scoring scale ranging from 0 to 9 (Hensawang et al., 2017), which was assessed 10, 20, and 60 DAI (days after inoculation). Score classification of rice blast disease and disease severity level was as follows: no lesion observed (Score 0, Severity 0%), small brown specks of pin-point size, or larger brown specks without a sporulating center (Score 1, Severity 1%), small roundish to slightly elongated, necrotic gray spots, about 1-2 mm in diameter, with a distinct brown margin (Score 3, Severity 5%), necrotic gray spots about 1-2 mm, with a brown margin, typical blast lesions infecting 4-10% of the leaf area (Score 5, Severity 25%), necrotic gray lesion about 2-5 mm, with a yellow margin, typical blast lesions infecting 26-50% of the leaf area (Score 7, Severity 50%), the lesion expands more than 75% leaf area affected (Score 9, Severity 75%) (Hensawang et al., 2017).

3.1.5 Evaluation of ozone-induced leaf symptoms

Visible leaf symptoms of ozone stress as leaf bronzing score (LBS) were assigned at 10, 20, and 60 DAO / DAI (days after ozone/days after inoculation) to two fully expanded leaves of each plant as previously described (Frei et al., 2008, Ueda et al., 2015a). The score ranged from 0 (no ozone-induced symptoms) to 10 (the whole leaf severely damaged).

3.1.6 Spectral reflectance and stomatal conductance

Spectral reflectance measurements were taken using a Polypen RP410 instrument (Photon Systems Instruments, Drasov, Czech Republic) three times at 10, 20, and 60 DAO. Three points were measured from the second youngest fully expanded leaf of each plant, and the average of the three points was calculated. The following indices were determined: normalized difference vegetation index (NDVI) = $(R_{780} – R_{630}) / (R_{780} + R_{630})$ (Rouse et al., 1973); photochemical reflectance index (PRI) = $(R_{528} - R_{567}) / (R_{528} + R_{567})$ (Gamon et al., 1992); Lichtenthaler index 2 (Lic2) = R_{440} / R_{690} (Lichtenthaler et al., 1996, 2005); and anthocyanin reflectance index 1 (ARI1) = $1/R_{550} – 1/R_{700}$ (Gitelson et al., 2001). Vegetation indices were selected based on significant differences between treatments and relatedness with ozone stress. Stomatal conductance measurements were performed at 20 DAO using a leaf porometer (Model SC1, Decagon Devices, Pullman, WA). Two points were measured from each plant's second-youngest fully expanded leaf, and the average of the two points was calculated.

3.1.7 Biomass and yield

Plants were harvested when all genotypes had reached maturity. During harvesting, plant height, tiller number, and panicle numbers were measured. Harvested plants were dried in the oven at 50 °C for 72h, and other agronomic characteristics such as single plant weight, filled grain number, hundred kernel weight, grain yield, straw biomass, and harvest index were measured.

3.1.8 Lipid peroxidation analysis

To evaluate the lipid peroxidation in different genotypes, malondialdehyde (MDA) content in the shoot was quantified from each treatment at 20 DAO. The samples were collected between 10:00 h and 12:00 h, immediately frozen in liquid nitrogen, and stored at -80^{o} C until further analysis. The amount of MDA was measured as described previously (Hodges et al., 1999; Höller et al., 2014). Extraction was performed from approximately 100 mg of ground tissues with 1.5 mL of 0.1% (w/v) Trichloroacetic acid (TCA). After ultrasonication for 5 minutes, samples were centrifuged at 4^{o} C, and 14,000 g for 15 min, and the supernatants were divided into two aliquots of 500 µL into 14 ml falcon-tube. These aliquots of the same extract were mixed with reaction solution I (background reference) that contained 0.01%

(w/v) 2,6-di-tert-butyl-4-methylphenol (BHT) dissolved in 20% TCA (w/v), and reaction solution II additionally containing 0.65% 2-thiobarbituricacid (TBA), respectively. The mixture was then heated to 95^{o} C for 30 min, and the absorbance was measured at 440, 532, and 600 nm. Blank samples were also prepared with 0.1% (w/v) TCA solution instead of sample supernatant, and the absorbance was subtracted from each sample value.

3.1.9 Statistical analysis

Analysis of variance (ANOVA) was performed by mixed model three-way ANOVA using the program R (R for Windows 3.5.1), packages nlme, and emmeans (R Core Team, 2018). Ozone, blast, genotype, and their interactions were considered fixed effects, while chamber as a random effect. The mean comparison was performed by Tukey's test for posthoc adjustment and P values less than 0.05 were considered as significant. Vegetation indices at 20 DAO, LBS at 20 DAO, BSS at 20 DAO, stomatal conductance at 20 DAO, MDA at 20 DAO, panicle number, filled grain number, straw biomass, and grain yield was used for the Pearson correlation matrix analysis.

3.2 Breeding scheme and line development

The marker-assisted backcross breeding program was developed to introgress previously characterized ozone tolerance QTLs, *OzT8* and *OzT9*, from the donor parent Kasalath (Frei et al., 2008; 2010) into two recipient parents: (i) BRRI dhan28, a popular but ozone-sensitive Bangladeshi Indica rice variety (Ashrafuzzaman et al., 2018), and (ii) Binadhan-11, a modern Bangladeshi Indica rice variety also sensitive to ozone (Ashrafuzzaman et al., 2018). Two parallel breeding schemes were implemented to develop the desired lines: (A) BRRI dhan28 × Kasalath and (B) Binadhan-11 × Kasalath. The breeding process, illustrated in Figure 5, began with initial crosses producing F_1 progeny, followed by backcrossing to the respective recipient parents to generate BC_1F_1 progeny. Genotyping of the BC_1F_1 lines was then performed to identify individuals carrying Kasalath introgressions at the *OzT8* and *OzT9* loci.

As an initial step in genotyping to identify polymorphic SNPs across the genome, all three parental lines were subjected to genotyping-by-sequencing (GBS) in collaboration with the Japan International Research Center for Agricultural Sciences (JIRCAS), Japan. Suitable SNP markers were subsequently converted into KASP (Kompetitive Allele Specific PCR) markers (Table 1) following LGC Genomics' KASP assay design guidelines. Genotyping was performed using the commercial services provided by LGC Genomics (Middlesex, UK). The RFLP marker interval reported by Frei et al. (2008) was defined as the target region, encompassing 1.17 Mb (9.63–10.80 Mb on chromosome 9) in the *OzT9* region and 1.07 Mb (23.11–24.18 Mb on chromosome 8) in the *OzT8* region.

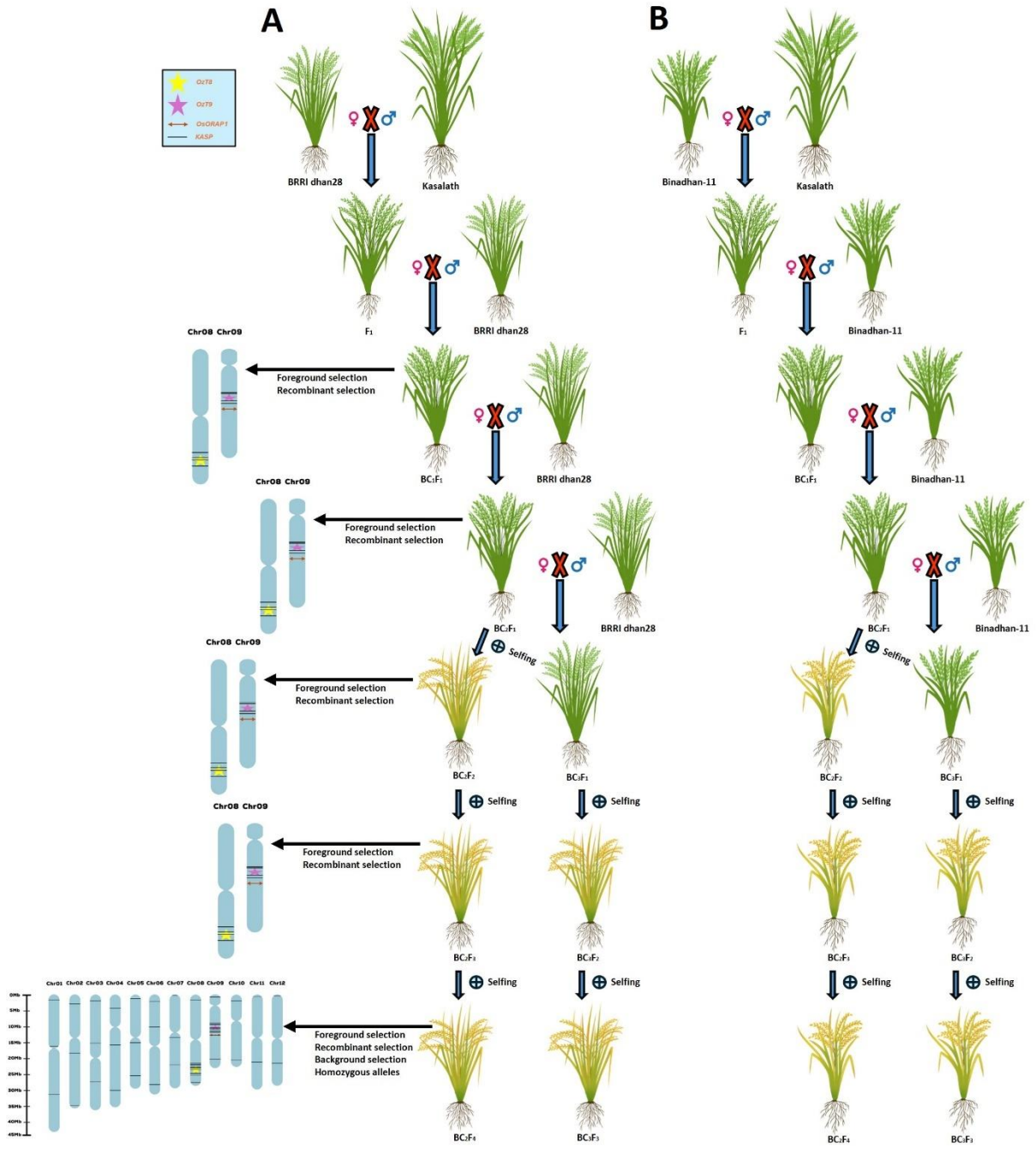

Figure 5 Schematic representation of the backcross breeding scheme for the introgression of ozone tolerance QTLs (*OzT8* and *OzT9*) into rice cultivars. (A) Cross between BRRI dhan28 (recurrent parent) and Kasalath (donor parent), followed by backcrossing and selection for desired loci using marker-assisted selection (MAS). (B) Cross between Binadhan-11 (recurrent parent) and Kasalath (donor parent), with subsequent backcrossing and selection. The selection process integrates both phenotyping and genotyping. Foreground and recombinant selection were performed from BC_1F_1 to BC_2F_4 and BC_3F_3 progeny to identify favorable allelic combinations on chromosomes 8 and 9. Background selection was conducted on BC_2F_4 and

BC_3F_3 progeny to evaluate the recovery of the recurrent parent's genetic background. Self-pollination in advanced backcross generations ensured the fixation of homozygous alleles for the target loci. Chromosome diagrams highlight the positions of KASP markers.

In the case of *OzT9*, previously published work (Ueda et al., 2015b; Ashrafuzzaman et al., 2020) strongly suggests that polymorphisms in the *OsORAP1* (RAP ID Os09g0365900 or MSU ID LOC_Os09g20090) gene are associated with this QTL. From the GBS, developing KASP markers explicitly in this gene was impossible. Therefore, PCR was carried out during each genotyping session to amplify the *OsORAP1* gene using primers specifically designed for the ozone-sensitive and ozone-tolerant alleles (Ashrafuzzaman et al., 2020). The PCR mixture consisted of 10 µl GoTaq Green Master Mix (Promega, Mannheim, Germany), 0.4 µl of each 10 µM primer, 1 µl DMSO, 6.2 µl water, and 2 µl of the extracted DNA sample. The PCR thermal cycling conditions were as follows: initial denaturation at 94 °C for 5 min, followed by 35 cycles of denaturation at 94 °C for 45 s, annealing at a primer set-specific temperature for 45 s, and extension at 72 °C for 2 min. A final extension step at 72 °C for 10 min concluded the amplification process. The tolerant *OsORAP1* allele was detected using the forward primer 5'-GCCTTCCTCCTTGTGGTCG-3' and the reverse primer 5'-GAGGGAACGTCCCACTGTTG-3', with an annealing temperature of 57°C. The sensitive *OsORAP1* allele was identified using the forward primer 5'-CGTGTAGATCCTCGTACCAATGTACC-3' and the reverse primer 5'-TCCGGGTGCGACACGTTG-3', with an annealing temperature of 58°C.

The first round of genotyping, encompassing foreground selection and recombinant selection, was conducted on 218 BC_1F_1 lines to identify those with Kasalath introgressions at *OzT8* and *OzT9*. Of these lines, 135 were derived from the cross (A) BRRI dhan28 × Kasalath, and 83 were derived from (B) Binadhan-11 × Kasalath. Foreground selection for each QTL was performed utilizing one KASP marker at the left border and another at the right border. Furthermore, two KASP markers, situated approximately one Mb away from the left and right borders, were employed for recombinant selection (Table 1). This genotyping procedure successfully identified lines carrying heterozygous tolerant alleles at the QTL positions, with or without recombination.

Table 1 Kompetitive Allele-Specific PCR (KASP) markers used for foreground, recombinant, and background selection.

SNP ID	Sequence	Position	Purpose
RIOZ_101	AAGTCCATGATACCATGCAGAGGCTTGTATAGTGAGAGTTAAGTCGTGAT[**C/G**]GAACAAGGAC TACCTGGGCCCTTGGAGTTTGCTGTGCGGCCTTCTTTGAA	Chr1:1574479	Background selection
RIOZ_102	TTTTCGCTGAAGCATCACTTGCATCCTAAAAAAAATTAAAGTACCTGGGC[**G/A**]GCAAAGGCTGG GAGTGACGGCGAGTCAAGGATGTCGGTCGCTGGCAGAGG	Chr1:16348756	Background selection
RIOZ_103	ACCCGAATCACGAGGGCAGTTAAACGAAGGTGTCCAGCTGATTGTTGAGT[**C/T**]TCATGAACACA TGAGATCGCACAAGGCCCAAGAACTCCACGTCAGGAGAA	Chr1:31792507	Background selection
RIOZ_104	tccttgaagacatatgtcatcggctagggtcatcactggacagtctggtg[**g/a**]ccgattgtggttcaatccaggcacgatttgc agaaatccaagctttaatc	Chr2:2472513	Background selection
RIOZ_105	TGAGCCCAGAGATCTGGGCGACGTTGACTCCTGTCACGGCCGATCCCTGC[**C/A**]TGTTGCTGGTG TTTCCAGCCATGTGAAGGCCGGAGAAGAAGAAGTCTTCC	Chr2:17165627	Background selection
RIOZ_106	ACTGGAGGCCCAACCTGTATTATGGGATGAGATCCCAAATGCAAAAATCA[**C/T**]ACAAGTTTGTC ATGATTTTGTCGTAAGATCTGTCCTTTTACGAGTGGAAA	Chr2:35090950	Background selection
RIOZ_107	GAAAGCTGGTCTCCATACTTGATCCTTTGCAAACAAAACTAGAGGTAACC[**A/G**]TTGTGTTTTTAT CCTTACTTTTCTAAATCTTTTTTCTGTCTTTGATGGTT	Chr3:1856562	Background selection
RIOZ_108	GCTGCAAATCTCCACCTATGGAAGTAATGCCAGAAGATGGTTTTACCATC[**T/C**]CTGGCTTAGCCT CTAGTTCTAAATCAAAATTATTAGCATTCAAATTATCC	Chr3:15217206	Background selection
RIOZ_109	AGAGCAATCGAAATGGCAGGGCAAGAAGGCCACGCCATGAAGGACAAGTT[**C/A**]GACAGGGGC ATTGGATTTAAGGCCGCGGCCACCGCTGCGCATCATCCGGA	Chr3:27956992	Background selection

RIOZ_110	GAGCCCATGTTTACCACAACCTATCAAGTGAAGGCAATTATGAGTCAAAT[**C/T**]GATAAAGCCTC ACTCGAGacaagagcttgaagctatgatgcatcaatctt	Chr4:4054239	Background selection
RIOZ_111	TAGCAAGACCAAAGTCGGCAAGTTTCACAGATCCATTCCTATGCACCAGT[**A/G**]TATTGCCACACT TCACATCCCTACAAGAATTTTGAACATTGAAGTACATG	Chr4:16023012	Background selection
RIOZ_112	AAAGAATGATGTGGATCGTCGTTTCAAATTCTCGAGTGTAAAAGGACAGG[**C/A**]CGAGTGGTTAT CAATAATTAATTAGTGTAACCCTAAACCAAATGAAATGA	Chr4:30123004	Background selection
RIOZ_113	AACATGCCGTGCCCATGCTTGCCATGCTTGAACTTGCCATGGTGGCCGTG[**C/T**]TTGCCATGCTTG AACTTGCCGCCGTGGTGACCGCCGTAGCCATGGCCGTA	Chr5:1000902	Background selection
RIOZ_114	ccttaatatgaccaatcacattacaacgatgttcagggctatatttctcc[**c/a**]cacacttgaagcaaaggccctaagcacacct atagtatttcagctatcta	Chr5:14280112	Background selection
RIOZ_115	AGAGATACTATGCTTTTGTGTGAACATGCAGGTTATCCTGTGTTCTTCTT[**C/T**]GCCACTCGAGAA TATTTACTCAGAGGTTTGTTTCTCACCTAATTGATTTT	Chr5:25256654	Background selection
RIOZ_116	GGAATAAGTGTTTTTGATTAAGAATGTAATGAATCCACATCATATATTTT[**T/C**]ACACATAAAAGA GCCAGAGTAACAATATACAATTTCGGCACCTGTTCTGT	Chr6:2028173	Background selection
RIOZ_117	ataccctgaggggttcagatcatcgaatcttagcgccaacacagccatg[**a/c**]tagtttacgaagccagaggatgcgaagcc tactcgccaggagatctcgtc	Chr6:10801446	Background selection
RIOZ_118	GTGAGCCCGGGACCCAGAACAAGACCGGGTCCGAGGCATACCTTAGGCTA[**C/T**]ATTCTTAAGAT ATAGATTTTATCCACTAAACCTAAGGTCAGGATGGAAAT	Chr6:27039570	Background selection
RIOZ_119	TCTGTACGATTGGCAACTAGAATCTTGTACAGATCTACGGGGATACTGGC[**C/A**]GATCACAAAAA CATATTGTTGGGGTTCCTGTCATCTTAGTTTGTGCCAAG	Chr7:372129	Background selection

RIOZ_120	CAGAGATGACACAGTGCTGTGACACAGTACTGAAGCTAAATCGGAGATGC[**C/T**]ATAGTCCTGTG ACGTTGGATAAATCTCAACCATCCAATGCGCAGCAAACG	Chr7:13268038	Background selection
RIOZ_121	TTAGTACTGATCTGATAACTGAACTGTCAGAGAAACAGTAGAAGAGATAA[**A/C**]GCAACGACAG TTTCAGTTCCAGTTTCAGCTTTAATTTCCTCCATAATTTC	Chr7:22303126	Background selection
RIOZ_122	TTTTAGCTCAGATATACATTTGCGTGCTCGCTCAAAGAGATGTTTAGTGG[**T/C**]TGGGAGTTGTTT TGATTGAGATATGGCAGTTAATTTTCCCAGATCTGAGT	Chr8:1525984	Background selection
RIOZ_123	TAATAAAGTCTTCACATACTTTCTTGGACTGCCACAAATGTTGGATGCTC[**G/C**]CCGGAGACACCT AGTTGGCTAGGAGGATGACCTCCAAGATTATCAGCTCA	Chr8:21943017	Background selection
RIOZ_124	tgctattgtacttgctctcaGTGGTGGCTGCAACGCAGACAGASGGGCTA[**A/C**]YTTTCGCCGCGAAATT GTACTGCTACTACTGCTATCTTTGTGGTGGTTGA	Chr8:22179503	Background selection
RIOZ_125	AGGAGGACGAATGCTCTTGGTGTCAATCTCAAGTGCTCAAGGATGAATCT[**C/T**]GAACCTCACTT GCTTTTCAATCTAACTCAATCCAACTCAAAAGATTCACT	Chr8:22885079	Recombinant selection
RIOZ_126	ATATAGATCATTTTATCTTTCTCTTAATTTGCCTCTGACYTTTAGAATGA[**C/G**]AGTTGTTTTGGGAY GGAGGTCGTAGTATGTAACAACGGTATACTCCACGG	Chr8:23360411	Foreground selection
RIOZ_127	atttaatgcaaagattgtaatacttctccactaagttaggttgttgggcc[**c/t**]atgtggtaacccctttatggtataaaaggaggt mcaggcctacttagggag	Chr8:23538390	Recombinant selection
RIOZ_128	TCAATTTACAAATATTAGTTATCTACAAGCTTCCATTGCACACAAAGACA[**A/G**]GATAGCTTGGGG GAGAACTTGTGAAGTAATGGGTTCAATCCTTAGCCACG	Chr8:23845725	Foreground selection
RIOZ_129	CAGTATCAATAATGCATGCCAATGTTTAAGTGAAAAGATCTTTTATTTCC[**G/T**]CTGCGTTCGTTGT GTGGTGTATACCCCTACATGATAGTGGGGGAGTACTA	Chr8:24878875	Recombinant selection

RIOZ_130	GCCCGTAAAATATACTACTAATATGGGCTCATGGGCTGGTTGCTTCCAAT[**C/A**]TCTTTCGGTAGC CATAACACTGGGCCGCACCCTATGGGCCGATTCATGGG	Chr8:25434293	Background selection
RIOZ_131	TGGAAACACGGCTAGTTGAGTCAGAAAATGTCTGCATGATTGATCGCGTC[**A/G**]TTGCGTCCGAT CCATTGCCGGAATAACAACGACCACGACTTACATCTATC	Chr8:27449978	Background selection
RIOZ_132	tttttagtctcggtttataagcgtaacaggattagatgatctttattccc[**g/a**]gttggggttaccaaccgggactaaagatcaca ccaaccgagagtaaagat	Chr9:714308	Background selection
RIOZ_133	ATCTATCCAACAGCTTGTAACTTGGCAATGAATCTGGTAACAAGCTTGTA[**G/C**]CATCCAGCACAA AAAATGATTGGCTAACACAGATCTTGACTCAAAATGGA	Chr9:8995601	Background selection
RIOZ_134	tgcaagcgatcagaacAAACAATGGAGAATTCGTGGAGAGGCTGATCGTC[**G/A**]GTCTCTGTCTCGTC CTAATAGCGCASGAGGAGGATTCGCTTCTgtaacga	Chr9:9346103	Recombinant selection
RIOZ_135	CTACTAGATGAATTTGAGGACTGCAGTGAGGCCGGATCTCAAAGGGGCAG[**T/C**]TCCTGGATTGC AAAGGTTCGTCACAATCCTTTGAAAAGGGGTAACCCCCA	Chr9:9682191	Foreground selection
RIOZ_136	gatctcaggcaatggtgtggttctgaatgccctgctcgttccgatctctc[**g/a**]tgcgtgcaagcgatcaaaaccggggaagca gacagaagcagcacaggcta	Chr9:10282788	Recombinant selection
RIOZ_137	GGTTTATATATATTTATGATTATACTTTTGTATCACATACCCTCTTCGAT[**C/T**]CAAAATATAAGATT GTTTAGCATATAGATCTTTTCATTCTAAAATATAGG	Chr9:10364620	Recombinant selection
RIOZ_138	AACGCGGTATGCAAAGTTCCYRACCGTACCGATACCGTTTYCGYAAAACt[**a/t**]atataataataatattt ttaCTGATGTTACCGTTTTCAAAATTTAGTTTT	Chr9:10499193	Foreground selection
RIOZ_139	GATATCCATGGAGGGCGGTGACTCCGGGTTTTTCAGGTTTTCGGCAGCGG[**C/T**]GCCGGTGCCAR TGCCTGCACACCAGGCACGGAGGGCGCTATCAGATCTAC	Chr9:11247783	Recombinant selection

RIOZ_140	TAGTAGGGCACCAGCTGTTGAGGTTCAGGTCTCCTGCTTCTGCTGCTTTC[**A/G**]TGCAGCCTTTGG ACCGTCAACATGCTGGGCTGTACGTTCAGTAAAGTAGG	Chr9:11838697	Background selection
RIOZ_141	AAGAGATCTCTCCTTCAAAATAGTACTAATAATCCATATCTTGATTAGAT[**C/G**]ACTCGGTCCACG GAGTGTACTAGGAGAATCAGAAGCGCCGTAGCGACTGT	Chr9:12077825	Background selection
RIOZ_142	TTTTCAACGTGAGAGATTCTTCCAGATCTTTCTTTCTTCTTCCTTAGGAG[**T/C**]AGTGATCCAAGAT GATTGATTATTACGGCACGATATCAATCAATCATGCA	Chr9:20212811	Background selection
RIOZ_143	CAAAATTTTTAGGGCGATGCTCCGGTGCAATATACTTGAAGTATTCTACT[**C/T**]CGAGTAGAATTA ATCTGGATCGTTTATTTTAAAGGGTATGTAAGTAATCT	Chr10:1666053	Background selection
RIOZ_144	CACGTTCGAAACAATCGCAAGATTGGCAAGTAAACTCTCCTGCTTGCTTG[**C/T**]TCACAACCACAT CAGATCATTGATCAATGTTTCATCAGCTCATCACTTCT	Chr10:20377057	Background selection
RIOZ_145	gtcagttgcaggatcaaactgactggcacgcccgcatctcatcaacctttg[**g/a**]gacctgcattggagctaagcagatctccca gaccagtgtgtcatattttt	Chr11:509659	Background selection
RIOZ_146	GAAGAGGAAATAACAAAAGCAATTAGTCCACTTGTTGAAAAGTACTTTCC[**A/G**]AAGGAATCTTC TTCGGTATATAAGGTAACTTTCTGGCCTAATTTCTATGT	Chr11:21190408	Background selection
RIOZ_147	tcctgtgcaggtccaaaagttgttgagatgmgggcgtgccagtcagtttg[**a/g**]tcctgcaactgacaagatatgcaaatagt agatcaaacagccgatcggct	Chr12:239773	Background selection
RIOZ_148	GGCCTCTGAACTCGAGGAGTTCAGATCTTGTGCTCACGAGAGGTGGCAGC[**G/A**]ACTGCATCCA AAGGGGAAGGGGGAGAAGAATCTGTCATGTAGCTATGGTA	Chr12:21834365	Background selection

To restore the recipient's parental background, the desired BC_1F_1 lines were backcrossed again to produce BC_2F_1 progeny. A second round of genotyping was conducted on 1,034 BC_2F_1 lines using markers previously developed for identifying Kasalath segments at QTL positions. Of these 1,034 BC_2F_1 lines, 551 were derived from the cross (A) BRRI dhan28 × Kasalath, and 483 from (B) Binadhan-11 × Kasalath. These lines were further screened for the desired phenotype, applying criteria such as plant architecture resembling the respective recipient parent (height, erect leaves, and large panicles), low sterility, grain size, shape, and color (as Kasalath has a red grain pericarp), and reduced or no awns (Kasalath typically has pronounced awns). This genotyping procedure successfully identified lines carrying either a single QTL, *OzT8* or *OzT9*, or both (*OzT8* + *OzT9*) QTLs with heterozygous tolerant alleles at the respective positions, with or without recombination. Subsequently, a few selected lines underwent an additional backcross to develop the BC_3F_1 progeny. For the third backcross, plants were chosen based on genotyping results from the second round and phenotypic characteristics observed up to the flowering stage.

To advance and generate homozygous lines, 50 BC_2F_1 lines from cross A and 40 BC_2F_1 lines from cross B were selected. From each line, 48 seedlings were planted to grow BC_2F_2 plants and advance to BC_2F_3 generation. Simultaneously, 167 BC_3F_1 lines (100 from cross A and 67 from cross B) were planted for advancement. During these stages, phenotyping was performed based on previously established criteria. Subsequently, 2,300 BC_2F_2 lines (1,378 from cross A and 922 from cross B) and 46 BC_3F_1 lines (25 from cross A and 21 from cross B) were genotyped using markers developed earlier (Table 1).

This genotyping procedure successfully identified lines carrying homozygous tolerant alleles at most of the targeted QTL positions. Following genotyping and phenotyping, 44 BC_2F_2 breeding lines from cross A and 30 BC_2F_2 lines from cross B were selected. From each line, 48 seedlings were planted to grow BC_2F_3 plants. Additionally, 10 BC_3F_1 lines (five from cross A and five from cross B) were selected for further advancement. From each of these lines, 48 seedlings were planted to grow BC_3F_2 plants, which were subsequently advanced to the BC_3F_3 generation. Phenotyping was performed based on previously established criteria. Following this, genetic markers (Table 1) that had been previously developed were used for genotyping a total of 2,200 BC_2F_3 lines (1,189 from cross A and 1,011 from cross B) and 96 BC_3F_2 lines (54 from cross A and 42 from cross B). This genotyping procedure again successfully identified lines carrying homozygous tolerant alleles at the QTL positions. In parallel, initial screening

experiments for ozone tolerance were conducted using the selected BC_2F_2 progeny (Supplementary Table 1).

Based on the genotypic data and initial screening experiments, 10 lines from cross A (eight from BC_2F_3 and two from BC_3F_2) and nine lines from cross B (seven from BC_2F_3 and two from BC_3F_2) were selected for the final experiment (Supplementary Table 2,3). As part of the genotyping process, 41 KASP markers (Table 1) were developed (Hospital & Charcosset, 1997), including four markers previously utilized outside the QTL regions. These markers were designed to target all chromosomes for comprehensive background selection. Additional plants from the selected lines were cultivated independently for further analysis. The selected lines were genotyped using the 41 KASP markers to characterize the background genome. Concurrently, two additional KASP markers for *OzT9* and one for *OzT8* were developed to facilitate recombinant selection within the QTL regions (Table 1). Foreground selection was subsequently reconfirmed using seven markers, four of which had been employed in the earlier stages of the genotyping process. The background genome recovery in the breeding lines was determined using the following formula (Singh et al., 2018):

Genome Recovery (%) = (Number of markers matching the recurrent parent /
Total number of markers tested) × 100

This formula calculates the percentage of the recurrent parent's genome in the breeding lines.

3.3 Experiment 2: Assessing ozone tolerance in rice (*Oryza sativa* L.) breeding lines containing ozone tolerance QTLs *OzT8* and *OzT9*

3.3.1 Plant materials and growth conditions

The experiment was conducted in a climate-controlled greenhouse at the University of Giessen, 35392, Giessen, Germany, between September 2022 and February 2023. A total of seventy-seven (77) rice lines were evaluated in this study. These included: (i) Kasalath, a Bangladeshi aus landrace known as a donor for ozone-tolerant quantitative trait loci (Frei et al., 2008, 2010); (ii) BRRI dhan28, a popular Bangladeshi indica rice variety that is ozone-sensitive (Ashrafuzzaman et al., 2018); (iii) Binadhan-11, a modern Bangladeshi indica rice variety also classified as ozone-sensitive (Ashrafuzzaman et al., 2018); (iv) Forty-four (44) BC_2F_3 breeding lines derived from the BRRI dhan28 × Kasalath cross; and (v) Thirty (30) BC_2F_3 breeding lines derived from the Binadhan-11 × Kasalath cross (Supplementary Table 1).

Seed germination was carried out in Petri dishes containing deionized water at 30°C in complete darkness for two days, following the protocol described by Ashrafuzzaman et al. (2018). By the end of this period, more than 80% of the seeds from each genotype had successfully germinated. The germinated seeds were subsequently transferred to the greenhouse. Petri dishes containing the seeds were replenished with one-fourth strength Yoshida nutrient solution (pH 5.5) and exposed to natural light in the greenhouse for six days (Yoshida et al., 1976).

The experimental setup in the greenhouse included 40 quick pots (Herrman Meyer KG, Art.-Nr.: 741239) arranged in trays (H. Nitsch & Sohn GmbH & Co. KG, Art. Nr.: 481091). Each tray contained 24 spaces, each with a volume of 400 cm^3. The artificial soil mixture used in the pots consisted of a 3:1 ratio of Hawita F.-E. Typ N (Hawita Gruppe GmbH, catalog number: 0104006) and Profile Porous Ceramic (PPC) Greens Grade (TURF Handels GmbH, catalog number: Profile Sport). Osmocote Exact 3-4 M fertilizer (Herrman Meyer KG, catalog number: 81416) was incorporated into the soil mixture at a rate of 4 g/L.

Seven-day-old seedlings were transplanted into the quick pots in a semi-randomized block design experiment. Four open-top chambers (1.625 m in height) were constructed to maintain a uniform microclimate. Two chambers were designated for ozone treatment, while the remaining two were control chambers. Three seedlings of the same genotype were transplanted within each chamber, with 10 trays, accommodating 231 plants per chamber.

The plants were irrigated twice weekly to ensure adequate water availability in each tray. Beginning two weeks after transplanting, 50 mL of a 15 g/L Peter Excel fertilizer solution was applied fortnightly to each tray until the plants reached maturity. Supplementary lighting was provided in the greenhouse from 7:30 a.m. to 4:30 p.m., ensuring a minimum photosynthetic photon flux density (PPFD) of 400 µmol m^{-2} s^{-1}. The greenhouse maintained an average temperature of 26/21°C (day/night) and an average relative humidity of 73%.

3.3.2 Ozone treatment and monitoring

At 32 days after transplanting (DAT), fully established plants in both ozone chambers were subjected to ozone treatment until 148 DAT, near the end of the growing season. The ozone treatment was applied daily at a target concentration of 85–90 parts per billion (ppb) for 7 hours each day (9:00–16:00). Ozone was generated using the Ozone-Generator AQUARIZON 1.0 (INNOTEC High Engineering GmbH, Panoramastr. 5, D-76327 Pfinztal, Germany). The generated ozone was blown via a fan connected to a central pipe, which distributed the gas through perforated plastic pipes positioned above both ozone chambers.

Ozone levels were monitored in real-time using an ozone gas analyzer (Anseros ozone gas analyzer mp, Anseros Klaus Nonnenmacher GmbH, Tübingen, Germany). Additionally, the concentrations in the chambers were continuously measured at 3-minute intervals with an independent handheld ozone monitor (Series 500; Aeroqual Ltd., Auckland, New Zealand). The mean ozone concentration recorded in the ozone chamber was 91 ± 18 ppb (standard deviation), whereas the control chamber maintained a mean concentration of 27 ± 7 ppb (standard deviation). Control plants were exposed to ambient ozone concentrations, consistently maintained below the threshold level for damage (40 ppb).

3.3.3 Assessment of ozone-induced leaf symptoms

Visible symptoms of ozone stress, assessed as the leaf bronzing score (LBS), were recorded on the second fully expanded leaves of each plant at 3, 24, 38, 80, and 109 days after ozone (DAO) exposure, following the methodologies described by Frei et al. (2008) and Ueda et al. (2015a). The LBS scale ranged from 0, indicating no visible ozone-induced symptoms, to 10, representing severe damage across the entire leaf surface.

3.3.4 Vegetation indices

Measurements of the normalized difference vegetation index (NDVI) and Lichtenthaler index 2 (Lic2) were conducted at 3, 24, 38, 80, and 109 days after ozone (DAO) exposure, using a Polypen RP410 instrument (Photon Systems Instruments, Drásov, Czech Republic). The NDVI was calculated using the formula NDVI = $(R_{780} – R_{630})/(R_{780} + R_{630})$ (Rouse et al., 1973), where R_{780} and R_{630} represent reflectance at wavelengths of 780 nm and 630 nm, respectively. Similarly, Lic2 was determined as Lic2 = R_{440}/R_{690} (Lichtenthaler et al., 1996, 2005), with R_{440} and R_{690} denoting reflectance at 440 nm and 690 nm, respectively. Before measurements, the instrument was calibrated using the Spectral Reflection Standard. Data were collected from the second youngest fully developed leaf.

3.3.5 Nitrogen balance index (NBI)

The DUALEX leaf clip meter (ForceA, Orsay, France) was employed to measure the Nitrogen Balance Index (NBI), a reliable indicator of plant nitrogen status. Data were collected from the second youngest fully expanded leaf at 3, 24, 38, 80, and 109 DAO. The NBI, which represents the ratio of leaf chlorophyll to flavonoids, integrates these two parameters into a more precise measurement. This index serves as a robust indicator of plant nitrogen status and is directly correlated with the mass nitrogen content of the plant. Furthermore, the NBI demonstrates reduced sensitivity to environmental variations compared to chlorophyll measurements alone, enhancing its reliability under diverse conditions.

3.3.6 Gas exchange and chlorophyll fluorescence measurement

A LI-600 Porometer/Fluorometer (LI-COR, Inc., Lincoln, Nebraska, USA) was employed to measure stomatal conductance, the quantum efficiency of photosystem II (PhiPS2), and the electron transport rate (ETR) simultaneously. The quantum efficiency of photosystem II (PhiPS2) was calculated using the formula PhiPS2 = (Fm’ - Fs)/Fm’, where Fm’ represents the maximum fluorescence under actinic light, and Fs indicates the steady-state terminal fluorescence. Data were collected from the second youngest fully expanded leaf at five time points corresponding to different stages of ozone exposure: 3, 24, 38, 80, and 109 DAO. These time points collectively spanned all the growth stages of the plants.

For additional measurements, twelve breeding lines (six from BRRI dhan28 background and six from Binadhan-11 background), along with the parental lines (BRRI dhan28, Binadhan-11, and Kasalath), were selected to evaluate net carbon assimilation rate (A), intercellular CO_2 concentration (Ci), and transpiration rate (E). These parameters were measured using a LI-6800 Photosynthetic Gas Exchange System (LI-COR, Inc., Lincoln, Nebraska, USA) at 116 DAO. Measurements were conducted on the second youngest fully expanded leaf between 9:00 a.m. and 4:00 p.m. under controlled conditions: a constant photosynthetic photon flux density of 400 µmol photons m^{-2} s^{-1}, a CO_2 reference concentration of 400 ppm, a leaf temperature of 22°C, a relative humidity of 60%, and a flow rate of 300 µmol s^{-1}.

3.3.7 Lipid peroxidation analysis

To assess lipid peroxidation in different genotypes, shoots' malondialdehyde (MDA) content was quantified for each treatment at 50 DAO, following the procedure outlined in Section 3.1.8.

3.3.8 Yield and biomass assessment

Plants were harvested at physiological maturity specific to each genotype. During harvest, plant height and panicle number were recorded. Subsequently, the harvested plants were dried in an oven at 50 °C for 72 hours. Additional agronomic traits, including the number of filled grains, grain yield, and straw biomass, were measured to assess overall performance.

3.3.9 Statistical analysis

For the variance analysis (ANOVA), the experimental data were subjected to a mixed model analysis utilizing the package lme4 in R. Ozone treatment, genotype, and their interaction were designated as fixed effects. In contrast, block and chamber were designated as random effects. The Dunnett test was performed to compare the breeding lines with their corresponding recipient parents to assess differences further. P-values less than 0.05, 0.01, and 0.001 were considered statistically significant. For the Dunnett test, relative values (calculated as the ratio of measurements under ozone stress conditions to those under control conditions) were utilized. Microsoft Excel was used to generate graphical representations, incorporating both relative and absolute values.

3.4 Experiment 3 + 4: Comprehensive evaluation of ozone-tolerant rice (*Oryza sativa* L.) breeding lines through physiological and agronomic trait analysis

Experiment 3

3.4.1 Plant materials and experimental conditions

A total of 22 rice lines were selected for this study, including three parental lines: the donor parent Kasalath and the recipient parents BRRI dhan28 and Binadhan-11. Based on genotypic data and preliminary screening results, 19 lines were further chosen for detailed experimentation. These comprised 10 lines derived from the BRRI dhan28 × Kasalath cross (eight BC_2F_4 and two BC_3F_3) and 9 from the Binadhan-11 × Kasalath cross (seven BC_2F_4 and two BC_3F_3). Detailed information is provided in Supplementary Table 2, 3.

The experiment was conducted between April 2023 and October 2023 in a climate-controlled greenhouse at the University of Giessen's research station (Weilburger Grenze 25, 35398, Gießen).

The seeds were germinated under dark conditions for 48 hours in deionized water at 30°C using Petri dishes, following the protocol described by Ashrafuzzaman et al. (2018). During this period, an average germination rate exceeding 80% was observed across all genotypes used in the experiment. Following germination, the Petri dishes were transferred to a greenhouse environment, where the deionized water was replaced with a one-fourth-strength Yoshida nutrient solution adjusted to a pH of 5.5, as Yoshida et al. (1976) described. For the cultivation of rice plants, the universal substrate Hawita F.-E. Type N (Hawita Gruppe GmbH, Catalogue No. 0104006) was utilized. This substrate was mixed with Profile Porous Ceramic (PPC) Greens Grade (TURF Handels GmbH, Catalogue No. Profile Sport) in a 3:1 ratio. Additionally, Osmocote Exact 3–4M (Herrman Meyer KG, Catalogue No. 81416) was incorporated at a concentration of 4 g per liter of substrate to ensure the provision of essential nutrients.

The experiment was conducted using a semi-randomized block design. Eight open-top chambers measuring 1.625 m height were constructed to provide a controlled microclimate. Four chambers were allocated for ozone treatment, while the remaining four served as controls. A total of 576 1-liter pots (H. Nitsch & Sohn GmbH & Co. KG, Art. No.: 502210) were used, each filled with the previously prepared plant substrate and placed in planting trays (Hermann Meyer KG, Art. No.: 749651). The pots were arranged in the greenhouse, each chamber containing six planting trays, accommodating 88 plants (4 plants from each

genotype) per chamber. The planting trays maintained saturated soil conditions, ensuring consistent moisture levels throughout the experiment.

Nine-day-old seedlings were transplanted into plant pots filled with substrate. Irrigation was carried out twice weekly to maintain adequate moisture levels in each planting tray. Fourteen days after transplantation, the initial fertilizer application was conducted using a 50 mL solution of Peters Excel fertilizer at a concentration of 15 g/L, which was applied to each planting tray. This fertilization process was repeated at two-week intervals until the plants reached maturity. The greenhouse environment was supplemented with artificial lighting from 7:30 AM to 4:30 PM to achieve a minimum photosynthetic photon flux density (PPFD) of 400 µmol m^{-2} s^{-1}. The average day/night temperatures within the greenhouse were recorded at 30.09°C/20.95°C, respectively, while the average day/night relative humidity levels were 61.85% and 85.55%, respectively.

3.4.2 Ozone exposure and monitoring

At 30 days after transplanting (DAT), the fully established plants were subjected to ozone fumigation in all ozone chambers, continuing until 153 DAT. The target ozone concentration was maintained at 100–110 parts per billion (ppb) for 7 hours daily (9:00–16:00). The procedure is detailed in Section 3.3.2 above. The average recorded ozone concentration in the treatment chambers was 107.20 ± 19.52 ppb, while the control chamber had an average concentration of 48.62 ± 12.51 ppb. Control plants were exposed to ambient ozone concentrations, which exceeded the plant-damaging threshold of 40 ppb due to the greenhouse's proximity to an adjacent highway.

3.4.3 Physiological traits

Following the procedures described in Sections 3.3.4 and 3.3.5, measurements of the normalized difference vegetation index (NDVI), Lichtenthaler index 2 (Lic2), and the Nitrogen balance index (NBI) were conducted on the second youngest fully expanded leaf at 16, 33, 60, and 75 days after ozone (DAO) exposure.

A LI-600 Porometer/Fluorometer (LI-COR, USA) was used to measure stomatal conductance, the quantum efficiency of photosystem II (PhiPS2), and electron transport rate (ETR) simultaneously. Measurements were taken from the second youngest fully expanded leaf at

five ozone exposure stages: 16, 33, 60, and 75 days after ozone (DAO) exposure, covering all plant growth stages.

Additionally, net carbon assimilation rate (A), intercellular CO_2 concentration (Ci), and transpiration rate (E) were assessed at 65 DAO using a LI-6800 Photosynthetic Gas Exchange System. Measurements were conducted on the second youngest fully expanded leaf under controlled conditions: 400 µmol photons m^{-2} s^{-1} photon flux density, 400 ppm CO_2, 22°C leaf temperature, 60% relative humidity, and 300 µmol s^{-1} flow rate.

3.4.4 Agro-morphological traits

Visible ozone stress symptoms, quantified as the leaf bronzing score (LBS), were recorded on the second fully expanded leaves at 16, 33, 60, and 75 DAO using the method of Alam et al. (2022). The LBS scale ranged from 0 (no symptoms) to 10 (severe damage). Flowering time (days to flowering) was recorded throughout the experiment, using the germination date as a reference, when 50% flowering was visible for each genotype.

Plants were harvested at maturity for biomass and yield component analysis. Plant height and panicle number were recorded, and samples were oven-dried at 50° C for 72 hours. Agronomic traits were measured, including filled grain number, thousand-grain weight (based on 100 randomly selected grains), unfilled grain number, grain yield, straw biomass, and harvest index. The harvest index was expressed as the percentage of filled grain weight to total biomass. A seed counter (Contador, Pfeuffer GmbH, Germany) was used for grain quantification.

3.4.5 Statistical analysis

The experimental data were analyzed using analysis of variance (ANOVA) through a mixed model approach implemented with the lme4 package in R. Ozone treatment, genotype, and their interaction were treated as fixed effects. In contrast, block and chamber were treated as random effects. The Dunnett test was employed to compare the breeding lines with their recipient parents to assess differences further. Statistical significance was determined at $P < 0.05$, $P < 0.01$, and $P < 0.001$ thresholds. For the Dunnett test, relative values—calculated as the ratio of measurements under ozone stress conditions to those under control conditions—were used. Graphical representations, based on both relative and absolute values, were generated using Microsoft Excel. The principal component analysis (PCA) and Pearson

correlation matrix were analyzed using relative values calculated as the ratio of the trait value under the stress treatment to its value under the control. Additionally, data collected at various growth stages were averaged to compute relative values that reflect the overall responses of different genotypes throughout the growth period. Pearson's correlation was determined using the corrplot package in R. Principal Component Analysis (PCA) was performed in R using the FactoMineR package for analysis and the Factoextra package for visualization.

Experiment 4

3.4.6 Experimental site and plant materials

The experiment was conducted in Amtoli, Madokhola, Sreepur, Gazipur (latitude 24° 18' 36'' N, longitude 90° 44' 05'' E), located in the Madhupur Tract (Agro-Ecological Zone 28, AEZ-28). The study was carried out during the irrigated (Boro) season of 2024, which is characterized as the dry season, primarily reliant on irrigated water. During this season, rice crops are typically transplanted from December to early February and harvested between April and June.

The experiment included a total of 13 genotypes, comprising five breeding lines derived from the cross BRRI dhan28 × Kasalath, five breeding lines from the cross Binadhan-11 × Kasalath, and three parental lines: BRRI dhan28, Binadhan-11, and Kasalath.

3.4.7 Experimental design and field management

Field preparation, fertilizer application, and field management were conducted following the Bangladesh Rice Research Institute (BRRI) guidelines. The seeds were soaked in a water container for 24 hours. After soaking, the seeds were removed from the water, placed in gunny bags, and kept in a dark room to facilitate germination. Once germinated, the seedlings were pre-grown in nursery beds. Meanwhile, the experimental fields were ploughed using a tractor, followed by laddering to ensure proper soil leveling. Weeds and stubbles were manually removed during field preparation to optimize soil conditions.

Thirty-five-day-old seedlings were transplanted from the nursery beds into the prepared experimental fields. Uniform seedlings were transplanted at a spacing of 20 cm × 15 cm, with one seedling per hill. Fertilizers were applied at the following rates: urea (270 kg ha^{-1}) as a nitrogen source, triple superphosphate (115 kg ha^{-1}) for phosphorus, muriate of potash (150

kg ha^{-1}) for potassium, gypsum (75 kg ha^{-1}) for sulfur, zinc sulfate (6 kg ha^{-1}) for zinc, and boron (7 kg ha^{-1}) for boron. The fertilizer application schedule included an initial installment at 12 days after transplanting (DAT), consisting of one-third of the total urea and the full doses of all other fertilizers. The remaining urea was applied in two split doses as topdressing at 30 and 45 DAT. Pesticides were applied as needed to minimize insect and pest infestations. To maintain optimal field conditions, weeding was performed manually three times at intervals of 15, 30, and 45 DAT.

The experiment was designed as a split-plot arrangement with three replicates. The main plot treatment included exposure to EDU (Ethylenediurea) with two levels: with and without EDU. The subplots represented different genotypes. Each subplot measured 1.5 m^2 (1 m × 1.5 m) and included 33 randomly selected plants for yield estimation at harvest, while border plants were excluded from data collection.

3.4.8 Monitoring ambient ozone and application of EDU

Ambient ozone concentrations were monitored daily at the experimental sites from the day of transplanting to harvest. Measurements were taken between 9:00 AM and 5:00 PM (8 hours per day) at 3-minute intervals using a handheld ozone monitor equipped with a data logger (Series 500; Aeroqual Ltd., Auckland, New Zealand). The average ambient ozone concentration during this period was 88.99 ± 31.10 ppb.

Starting one week after transplanting and continuing until harvest, all plants in the experimental plots were treated weekly with a 300 ppm solution of ethylenediurea (EDU). The solution was applied using a backpack pesticide sprayer, ensuring that all leaves were saturated during each application. EDU, which is not commercially available, was obtained from Prof. William J. Manning of the Stockbridge School of Agriculture, University of Massachusetts (Manning et al., 2011). Fresh EDU solutions were prepared weekly at each experimental location. Plants in the control (non-EDU) treatment were sprayed with an equivalent volume of water to ensure consistency in application methods.

3.4.9 Yield data collection

Grain yield and straw yield data were collected following the harvest. The grains were separated manually through hand threshing and then sun-dried to reduce moisture content.

Similarly, the straw was sun-dried to ensure consistent drying. After drying, the weights of both grains and straw were recorded. The recorded data were subsequently converted to units of tons per hectare (t ha^{-1}). Additionally, the harvest index (HI) was calculated as a percentage to measure the partitioning efficiency of biomass into grains.

3.4.10 Analysis of breeding lines with the Dunnett test

The Dunnett test was used to compare the breeding lines against their recipient parents to identify significant differences. Statistical significance was evaluated at three thresholds: $P < 0.05$, $P < 0.01$, and $P < 0.001$. The test utilized relative values, expressed as the ratio of measurements under ambient ozone conditions to those under ethylenediurea (EDU) treated conditions. Additionally, graphical representations were prepared using relative and absolute values to visualize the results comprehensively. These visualizations were created using Microsoft Excel.

4 Results

4.1 Experiment 1: Interactive effects of tropospheric ozone and blast disease (*Magnaporthe oryzae*) on different rice genotypes

We investigated potential trade-offs or correlations between blast disease and ozone in a climate-controlled greenhouse at the University of Bonn, Germany, from September 2020 to February 2021, and we present the experimental results in this section.

4.1.1 Differential visual symptoms in response to ozone and blast inoculation

After blast inoculation and exposure to ozone, plants were repeatedly phenotyped using the visual scoring scale; LBS for ozone and BSS for the blast. Visual symptoms did not occur in control plants but were only seen in plants exposed to ozone, blast, or combined treatment. Blast inoculated plants showed a significant average decrease in BSS under ozone fumigation. In contrast, blast inoculation did not significantly affect leaf bronzing score to ozone in all three sampling dates (Table 2).

LBS and BSS exhibited highly significant genotypic differences. The most visible ozone damage was seen in CO39, followed by Binadhan-11, IR64, BRRI dhan28, Koshihikari, Nipponbare, Kitaake, and the least symptoms in Kasalath and L81 (Supplementary Table 4). BSS was highest in CO39, followed by Koshihikari, Nipponbare, BRRI dhan28, IR64, and Kasalath. No blast symptoms were observed in Binadhan-11 and Kitaake. Under combined ozone and blast treatment, CO39 and L81 showed a decreased BSS, whereas the BSS did not change for other genotypes (Supplementary Table 4). Overall, the visual symptom assessment demonstrated that ozone exposure rather reduced blast severity; in contrast, blast disease did not significantly affect ozone sensitivity.

4.1.2 Spectral reflectance indices

When averaged across all genotypes, a significant response of vegetation indices was seen due to ozone, blast, and ozone and blast treatment. Comparing treatment responses on the individual sampling days, significant effects of blast treatment occurred at 20 DAO for all the indices. In addition, a significant effect caused by blast on PRI and Lic2 was also seen on DAO 10. Blast by genotype interaction was primarily seen at 20 DAO. In contrast, vegetation indices significantly responded to ozone in all three sampling dates. In addition, significant ozone by

genotype interaction was observed. Significant interactions between ozone and blast and among ozone, blast, and genotype were seen at 10 and 20 DAO for all vegetation indices (Table 2). All the indices demonstrated highly significant genotypic differences.

Values for NDVI, a proxy for leaf greenness (chlorophyll content), were significantly lower in blast-infected plants than in the control at 20 DAO. Leaf greenness was significantly lower in ozone-affected plants than in the blast or control treatment on all three sampling days. Interestingly, double stress, i.e., ozone and blast, did not significantly reduce leaf greenness compared to ozone stress only (Table 2). Comparing individual genotypes at 20 DAO, leaf greenness was not affected in blast-exposed Binadhan-11 and Kitaake. However, all ozone-treated plants showed a significant decrease in leaf greenness compared to control except for highly ozone tolerant L81. For combined ozone and blast stress, none of the plants showed a significant change in leaf chlorophyll content compared to ozone stress only (Figure 6A).

PRI estimates the photosynthetic light use efficiency and showed significantly decreased values in blast-affected plants compared to control at 20 DAO. In all three sampling dates, ozone treatment induced a significant reduction in PRI compared to blast or control. No significant difference was observed between ozone and ozone and blast except for 10 DAO (Table 2). When comparing genotypes at 20 DAO, no significant differences were seen between ozone and ozone and blast. All the genotypes under ozone and ozone and blast treatments showed a significant reduction in PRI compared to control and blast, except for L81, which showed no significant differences between blast and ozone and blast treatment (Figure 6B).

Vegetation index Lic2 represents the carotenoid to chlorophyll pigment ratio, which tends to decrease under stress conditions. A significant decrease in Lic2 in ozone stress compared to control or blast was observed. At 60 DAO, Lic2 did not significantly change in the blast compared to the control, and no significant response in Lic2 was observed in the ozone and blast compared to ozone except for 10 DAO (Table 2). None of the genotypes showed significant responses to blast compared to control and to ozone compared to ozone and blast for Lic2 (Figure 6C). In contrast, we observed a significant decrease in Lic2 in ozone and ozone and blast compared to control or blast except for L81, which showed nonsignificant responses between blast and ozone (Figure 6C).

Table 2 Descriptive statistics and ANOVA of physiological data under stress and control conditions.

Traits	Date	LS means (Treatment)								ANOVA results (Pr > F)						
		Control		Blast		Ozone		Ozone & Blast								
		Mean	SD	Mean	SD	Mean	SD	Mean	SD	Bl	Oz	Ge	BlxGe	OzxGe	OzxBl	OzxBlxGe
LBS	10 DAO	n.d.	n.d.	n.d.	n.d.	5.28^{a}	1.83	5.38^{a}	1.96	n.d.	n.d.	<.0001	0.923	n.d.	n.d.	n.d.
	20 DAO	n.d.	n.d.	n.d.	n.d.	5.75^{a}	2.15	5.94^{a}	2.14	n.d.	n.d.	<.0001	0.634	n.d.	n.d.	n.d.
	60 DAO	n.d.	n.d.	n.d.	n.d.	5.42^{a}	1.81	5.51^{a}	1.91	n.d.	n.d.	<.0001	0.751	n.d.	n.d.	n.d.
BSS	10 DAO	n.d.	n.d.	1.67^{a}	1.88	n.d.	n.d.	1.44^{b}	1.63	n.d.	n.d.	<.0001	n.d.	<.0001	n.d.	n.d.
	20 DAO	n.d.	n.d.	2.44^{a}	2.54	n.d.	n.d.	1.89^{b}	1.87	n.d.	n.d.	<.0001	n.d.	<.0001	n.d.	n.d.
	60 DAO	n.d.	n.d.	2.44^{a}	2.54	n.d.	n.d.	1.89^{b}	1.87	n.d.	n.d.	<.0001	n.d.	<.0001	n.d.	n.d.
NDVI	10 DAO	0.52^{a}	0.05	0.50^{a}	0.09	0.36^{c}	0.10	0.41^{b}	0.09	0.0816	0.0047	<.0001	0.2447	<.0001	0.0001	0.0009
	20 DAO	0.58^{a}	0.06	0.42^{b}	0.16	0.36^{c}	0.13	0.35^{c}	0.13	<.0001	0.0001	<.0001	0.0001	<.0001	<.0001	0.0002
	60 DAO	0.72^{a}	0.03	0.72^{a}	0.03	0.58^{b}	0.09	0.57^{b}	0.10	0.3998	0.0001	<.0001	0.4164	<.0001	0.5561	0.3209
PRI	10 DAO	0.01^{a}	0.01	0.01^{a}	0.02	-0.03^{c}	0.03	-0.02^{b}	0.03	0.0369	0.0006	<.0001	0.1744	<.0001	<.0001	<.0001
	20 DAO	0.02^{a}	0.02	-0.02^{b}	0.04	-0.04^{c}	0.04	-0.04^{c}	0.04	<.0001	0.0001	<.0001	0.0001	<.0001	<.0001	<.0001
	60 DAO	0.04^{a}	0.01	0.03^{a}	0.01	-0.02^{b}	0.03	-0.02^{b}	0.03	0.9456	0.0001	<.0001	0.8430	<.0001	0.3986	0.6792
Lic2	10 DAO	0.64^{b}	0.08	0.68^{a}	0.10	0.52^{d}	0.10	0.60^{c}	0.11	<.0001	0.0432	<.0001	0.0080	<.0001	0.0041	0.0003
	20 DAO	0.74^{a}	0.11	0.64^{b}	0.16	0.55^{c}	0.14	0.55^{c}	0.14	<.0001	0.0010	<.0001	0.0136	<.0001	<.0001	<.0001
	60 DAO	0.92^{a}	0.04	0.91^{a}	0.05	0.68^{b}	0.13	0.65^{b}	0.14	0.0517	<.0001	<.0001	0.9211	<.0001	0.2596	0.3756
ARI1	10DAO	-0.24^{b}	0.18	-0.14^{b}	0.36	0.39^{a}	0.42	0.31^{a}	0.44	0.7216	0.0024	<.0001	0.2346	<.0001	0.0015	<.0001
	20 DAO	-0.26^{c}	0.27	0.22^{b}	0.61	0.53^{a}	0.59	0.61^{a}	0.59	<.0001	0.0001	<.0001	<.0001	<.0001	<.0001	<.0001
	60 DAO	-0.61^{b}	0.15	-0.61^{b}	0.16	0.36^{a}	0.80	0.25^{a}	0.65	0.0913	0.0001	<.0001	0.6156	<.0001	0.1479	0.5260
SC (mmol m^{-2} s^{-1})	20 DAO	418^{a}	20.88	332^{b}	15.72	265^{c}	9.73	261^{c}	10.07	<.0001	<.0001	<.0001	<.0001	<.0001	<.0001	<.0001
MDA (nmol g^{-1}) FW	20 DAO	8.61^{c}	0.86	10.27^{b}	1.67	13.08^{a}	2.05	12.74^{a}	1.78	0.0001	0.0002	<.0001	0.0443	<.0001	<.0001	0.0003

Note: Mean values of all genotypes are shown. Different superscript letters following mean values within one row indicate significant differences at $p < 0.05$ by Tukey's HSD test. LS, least square means; SD, standard deviation; Bl, blast; Oz, ozone; Ge, genotype; DAO, days after ozone; LBS, leaf bronzing score; BBS, blast severity score; n.d., not determined; NDVI, normalized difference vegetation index; PRI, photochemical reflectance index; Lic2, Lichtenthaler index 2; ARI1, anthocyanin reflectance index 1; SC, stomatal conductance (mmol m^{-2} s^{-1}); MDA, malondialdehyde (nmol g^{-1}); FW, fresh weight.

ARI1 represents anthocyanin level in plants and was significantly higher in the blast treatment compared to control at 20 DAO. In addition, ARI1 was higher in ozone and ozone and blast compared to control or blast, while no significant difference was seen between ozone and ozone and blast (Table 2). Ozone-tolerant genotype L81 did not show any significant variation for ARI1 among all treatments. The highest ARI1 was seen in CO39 under ozone stress (Figure 6D), which is highly susceptible to blast or ozone. However, there were no significant differences for ARI1 between control and blast and ozone and ozone and blast in any genotypes (Figure 6D).

In summary, vegetation indices were generally affected under ozone fumigation. On the other hand, in double stress, vegetation indices were not significantly different from those in ozone stress but rather worse than in the blast treatment. Moreover, prolonged ozone fumigation increased the adverse effect, whereas blast severity did not increase in plants after a certain period.

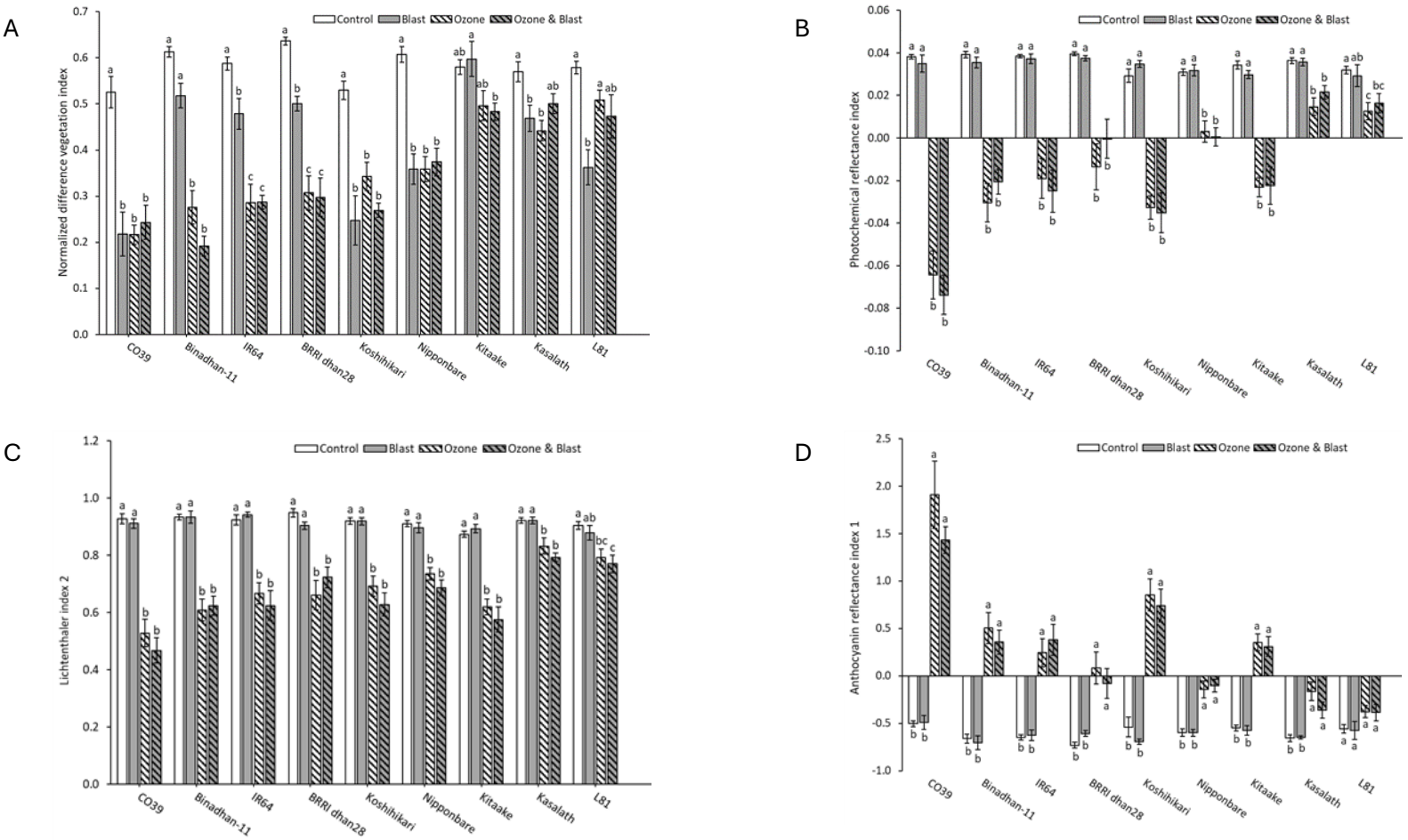

Figure 6 Vegetation indices at 20 DAO based on the reflectance spectra of nine rice genotypes exposed to ozone, blast, ozone and blast, or control conditions. Y-axis represents different indices and bars indicate the mean value ± standard errors (n = 8), X-axis represents different rice genotypes. Letters above the bars indicate pair-wise comparison ($P < 0.05$) within the genotype (mean values not sharing the same letter are significantly different).

4.1.3 Physiological characteristics

As a proxy for photosynthetic gas exchange, stomatal conductance was measured at 20 DAO. Individual and combined treatment effects and highly significant genotypic differences were seen. Compared to control, stomatal conductance was significantly lower in the blast, ozone, and ozone and blast. However, there was no significant difference between ozone and ozone and blast (Table 2). Significantly reduced stomatal conductance was observed in all the genotypes except for Kitaake and Kasalath in blast compared to control. Stomatal conductance was not lower in ozone and blast than in ozone, and in most cases, both were significantly lower than control or blast. Ozone-tolerant L81 showed a significant difference between control and other treatments, and Kasalath showed a significant difference between control and ozone and blast (Figure 7).

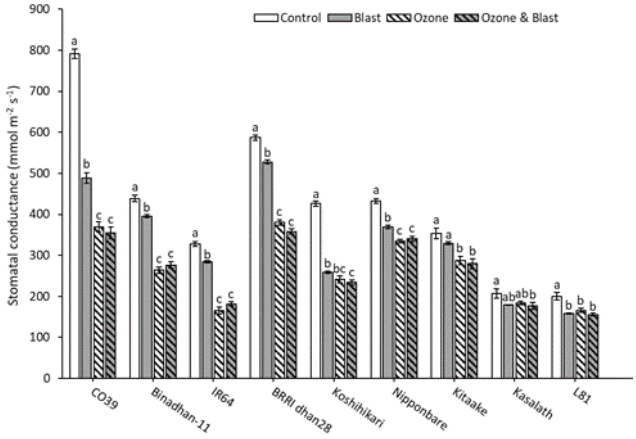

Figure 7 Stomatal conductance (mmol m^{-2} s^{-1}) at 20 DAO of nine rice genotypes exposed to ozone, blast, ozone and blast, or control conditions. Bars indicate the mean value ± standard errors (n = 8). Letters above the bars indicate pair-wise comparison ($P < 0.05$) within the genotype (mean values not sharing the same letter are significantly different).

MDA concentration was also measured from the plants harvested at 20 DAO to quantify lipid peroxidation as an indicator of oxidative stress. Averaged over all genotypes, significant increases of MDA occurred due to individual and combined stress treatments. Shoot MDA concentration was significantly higher in ozone than in control or blast, but there was no significant difference between ozone and ozone and blast. In addition, blast led to significantly higher MDA concentration than control (Table 2). Kasalath did not show any significant increase in lipid peroxidation in any of the treatments, while L81 showed significantly elevated MDA only in ozone and blast compared to control (Figure 8). Ozone and

blast susceptible CO39 and Koshihikari showed significantly higher MDA concentration in the blast, ozone, and ozone and blast compared to control. Other genotypes, i.e., Binadhan-11, IR64, BRRI dhan28, Nipponbare, and Kitaake, did not show significant differences in MDA concentration between control and blast. The same trend was observed for ozone and ozone and blast; however, ozone and ozone and blast showed significantly higher MDA than control or blast for those genotypes. Generally, our results suggested that ozone caused much higher oxidative stress than blast (Figure 8).

In summary, photosynthetic gas exchange and lipid peroxidation were significantly affected by individual or combined stress, but no escalation occurred due to combined ozone and blast treatment.

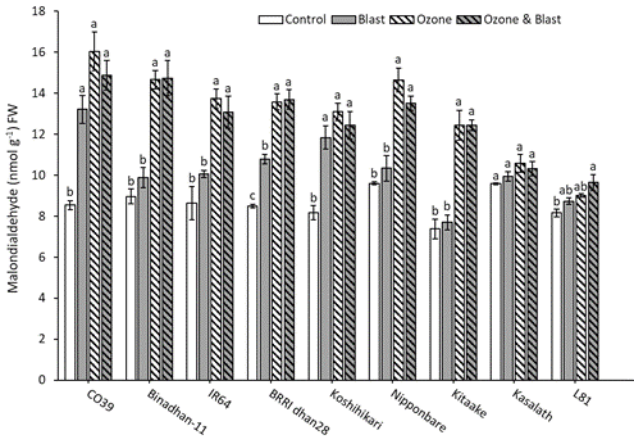

Figure 8 Malondialdehyde (MDA) concentrations at 20 DAO in leaves of nine rice genotypes exposed to ozone, blast, ozone and blast, or control conditions. Bars indicate mean value ± standard errors (n = 3), fresh weight (FW). Letters above the bars indicate pair-wise comparison ($P < 0.05$) within the genotype (mean values not sharing the same letter are significantly different).

4.1.4 Yield components

Several yield components were determined to reflect both straw and grain yields. Six yield components such as panicle number, single plant weight (g), filled grain number, grain yield (g), straw biomass (g), and harvest index showed significant treatment effects due to the decline in the ozone treatment (Table 3). In addition, four traits such as panicle number, filled grain number, grain yield (g), and harvest index showed a considerable blast effect (Table 3).

Table 3 Descriptive statistics and ANOVA results for phenotypic traits under stress and control conditions.

Traits	LS means (Treatment)								ANOVA results (Pr > F)						
	Control		Blast		Ozone		Ozone & Blast								
	Mean	SD	Mean	SD	Mean	SD	Mean	SD	Bl	Oz	Ge	BlxGe	OzxGe	OzxBl	OzxBlxGe
Plant height (cm)	81.17[a]	19.20	82.08[a]	20.07	73.42[b]	20.98	74.44[b]	21.53	0.3132	0.0032	<.0001	0.8742	0.1992	0.9539	0.8814
Tiller number	3.81[a]	1.26	3.47[ab]	1.13	3.36[ab]	0.93	3.17[b]	0.91	0.0287	0.0708	<.0001	0.9849	0.0036	0.5605	0.9801
Panicle number	3.44[a]	1.23	2.92[b]	1.11	2.64[b]	0.93	2.56[b]	0.88	0.0100	0.0242	<.0001	0.9554	0.0042	0.0592	0.9709
Single plant weight (g)	6.87[a]	3.48	6.36[a]	3.28	4.86[b]	3.12	4.88[b]	3.49	0.1197	<.0001	<.0001	0.8096	<.0001	0.0876	0.1387
Filled grain number	133[a]	82	110[b]	75	82[c]	67	79[c]	59	0.0001	0.0001	<.0001	0.2465	<.0001	0.0040	0.6046
Hundred kernel weight (g)	1.96[a]	0.19	1.97[a]	0.22	2.01[a]	0.20	1.99[a]	0.20	0.6419	0.1655	<.0001	0.7991	0.0014	0.5970	0.7856
Grain yield (g)	2.54[a]	1.37	2.09[b]	1.29	1.58[c]	1.11	1.49[c]	0.95	0.0001	0.0001	<.0001	0.2160	<.0001	0.0063	0.5559
Straw biomass (g)	4.33[a]	2.26	4.27[a]	2.14	3.29[b]	2.08	3.39[b]	2.60	0.8558	0.0003	<.0001	0.6109	0.0037	0.5399	0.1321
Harvest index	0.37[a]	0.07	0.32[b]	0.07	0.33[b]	0.07	0.32[b]	0.08	0.0028	0.2134	<.0001	0.6770	0.0774	0.0241	0.6064

Note: Mean values per individual plant of all genotypes are shown. SD, standard deviation; LS means, least square means; Bl, blast; Oz, ozone.

LS mean values not sharing the same superscript letter are differ significantly from each other at $P < 0.05$ by Tukey HSD post hoc comparison.

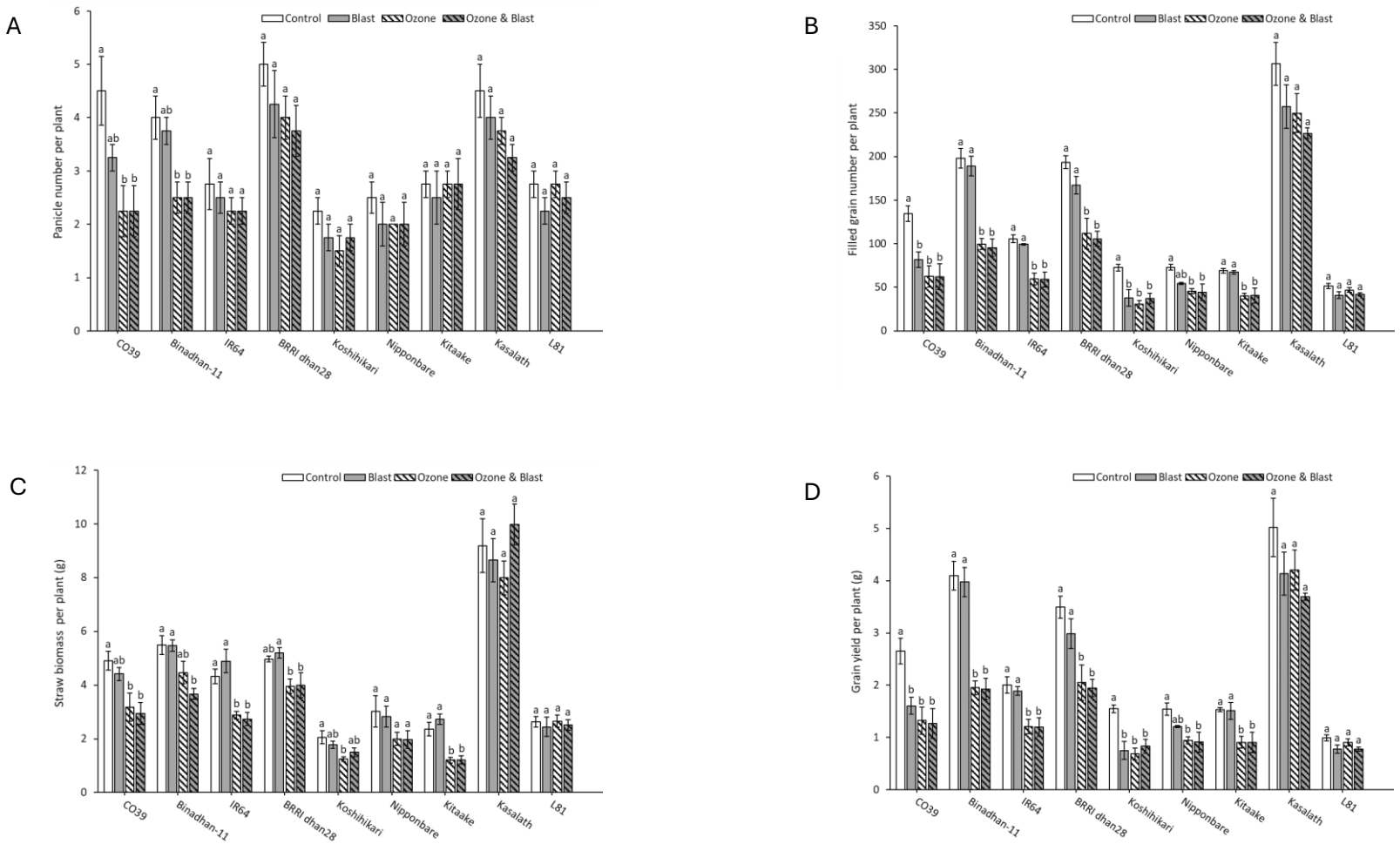

Figure 9 Yields and yield components of nine different rice genotypes exposed to four different treatments: ozone, blast, ozone and blast, or control conditions. Bars indicate mean value ± standard errors (n = 4). Letters above the bars indicate pair-wise comparison ($P < 0.05$) within the genotype (mean values not sharing the same letter are significantly different).

There was a significant interaction for ozone by genotype for all traits except for plant height, but no interaction was identified for a blast by genotype (Table 3). In addition, ozone by blast interaction was observed only for filled grain number, grain yield, and harvest index, but no interaction was seen for ozone, blast, and genotype (Table 3). Compared to the control, the average grain yield loss due to blast, ozone, and ozone and blast across all genotypes was around 17%, 37%, and 41%, respectively. However, the difference in yield loss between ozone and blast and ozone was statistically insignificant (P = 0.6568). Compared to the blast treatment and control, significant straw biomass reduction was observed in ozone and ozone and blast treatment (Table 3).

All the harvest fractions exhibited highly significant genotypic differences (Table 3). Panicle number per plant was significantly reduced in CO39 and Binadhan-11 for ozone and ozone and blast compared to control; while other genotypes did not show any significant responses (Figure 9A). The filled grain number was not significantly affected in the ozone tolerant genotypes Kasalath and L81 due to ozone or blast or ozone and blast (Figure 9B). In contrast, a significant reduction in filled grain number was observed in CO39 and Koshihikari due to blast, ozone, and ozone and blast (Figure 9B). Straw biomass was significantly reduced in most genotypes in ozone and ozone and blast compared to control, except for Nipponbare, L81, and Kasalath, which did not show a significant reduction (Figure 9C). There was no escalation due to combined ozone and blast treatment compared to ozone in any genotype (Figure 9C). Compared to control, a significant grain yield loss due to blast was seen only in CO39 and Koshihikari (Figure 9D). However, most genotypes, except Kasalath and L81, showed a significantly reduced yield in ozone and ozone and blast-affected plants compared to control or blast. The combined ozone and blast treatment did not exacerbate yield loss in any genotype compared to individual ozone or blast treatment (Figure 9D).

In conclusion, yield components were highly affected, mainly due to the negative effects of ozone on the filled grain number (Table 3).

4.1.5 Correlations between traits

We conducted a correlation analysis (Figure 10) to analyze how different traits were interrelated within the three stress treatments (ozone, blast, and ozone and blast). For this analysis, we used relative values (value in the stress treatment/value in the control). The strongest correlations were seen in auto-correlated traits, i.e., between different vegetation

indices or between different yield components. BSS showed a strong correlation with almost all of the traits within the blast treatment, and LBS in ozone treatment also significantly correlated with most of the traits. However, no significant correlation was observed for BSS within ozone and blast treatment, where LBS was significantly associated with most other traits (Figure 10C). Notably, grain yield was significantly correlated with most traits when plants were exposed to individual treatment, i.e., ozone or blast. In the combined ozone and blast treatment, the strongest correlation was identified between grain yield and LBS rather than BSS (Figure 10C). These data demonstrated that in combined ozone and blast treatment, ozone was the dominating stress for plants compared to blast.

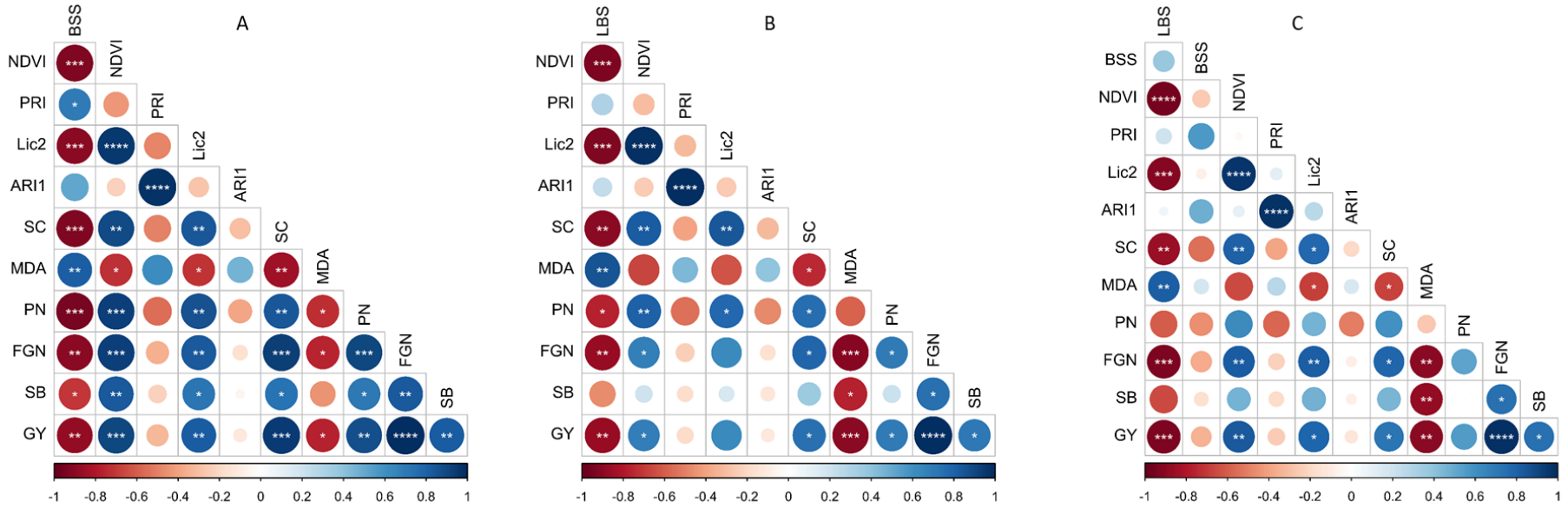

Figure 10 Pearson correlation matrix for phenotypic traits of rice genotypes exposed to blast (**A**), ozone (**B**), and ozone and blast (**C**). Asterisk indicates statistically significant correlation at *p < 0.05; ** p < 0.01; p < 0.001; ***; p < 0.0001****. BBS, blast severity score; LBS, leaf bronzing score; NDVI, normalized difference vegetation index; PRI, photochemical reflectance index; Lic2, Lichtenthaler index 2; ARI1, anthocyanin reflectance index 1; SC, stomatal conductance (mmol m^{-2} s^{-1}); MDA malondialdehyde (nmol g^{-1}); FW, fresh weight; PN, panicle number; FGN, filled grain number; SB, straw biomass (g); GY, grain yield (g). Relative values (ratio of value for plants grown under stress conditions relative to the control condition) were used except for BSS and LBS (n = 9).

4.2 Background genome recovery in breeding lines

In parallel with the first experiment, which focused on identifying potential trade-offs or correlations between blast disease and ozone, we continued breeding ozone-tolerant rice. We implemented a marker-assisted backcross breeding strategy to ensure that the breeding lines retained most of the genome from the recipient parent (BRRI dhan28 or Binadhan-11), with the targeted locus inherited from the donor parent. In this section, we discuss the genome recovery status of the breeding lines.

To evaluate the recovery of the recurrent parent genome in breeding lines derived from the cross BRRI dhan28 × Kasalath, 41 Kompetitive Allele-Specific PCR (KASP) markers were utilized for background genotyping. The analysis revealed an average genome recovery of 87.07% among the breeding lines originating from BRRI dhan28. Within this group, the genotype MFOL-2236 exhibited a genome recovery rate of 82.93%, whereas MFOL-233 demonstrated a higher recovery rate of 92.68% (Figure 11, 12A; Supplementary Table 3).

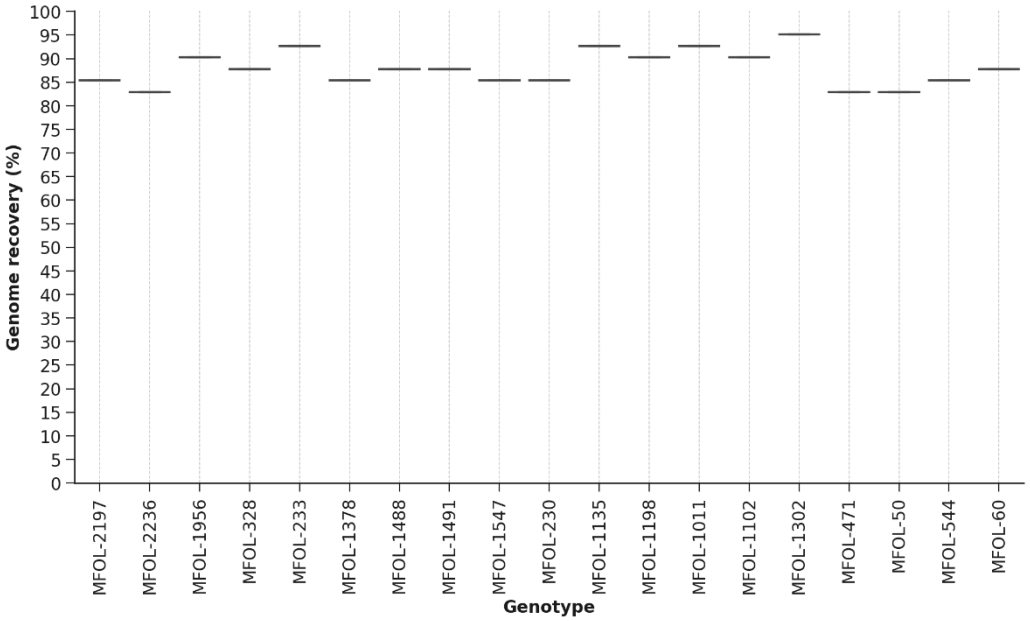

Figure 11 Comparison of genome recovery percentage across different breeding lines originated from the cross BRRI dhan28 × Kasalath and Binadhan-11 × Kasalath.

Similarly, breeding lines derived from the cross Binadhan-11 × Kasalath exhibited an average genome recovery of 88.89%. The recovery rates ranged from 82.93% (observed in MFOL-471 and MFOL-50) to 95.12% (observed in MFOL-1302) (Figure 11, 12B; Supplementary Table 3).

This variation indicates differential recovery rates across genotypes, with certain lines achieving closer proximity to the recurrent parent genome.

These results highlight the efficiency of the background selection process in facilitating substantial recovery of the recurrent parent genome. Furthermore, the findings underscore the utility of KASP markers in background genotyping for marker-assisted backcrossing, demonstrating their effectiveness in accelerating the development of improved breeding lines.

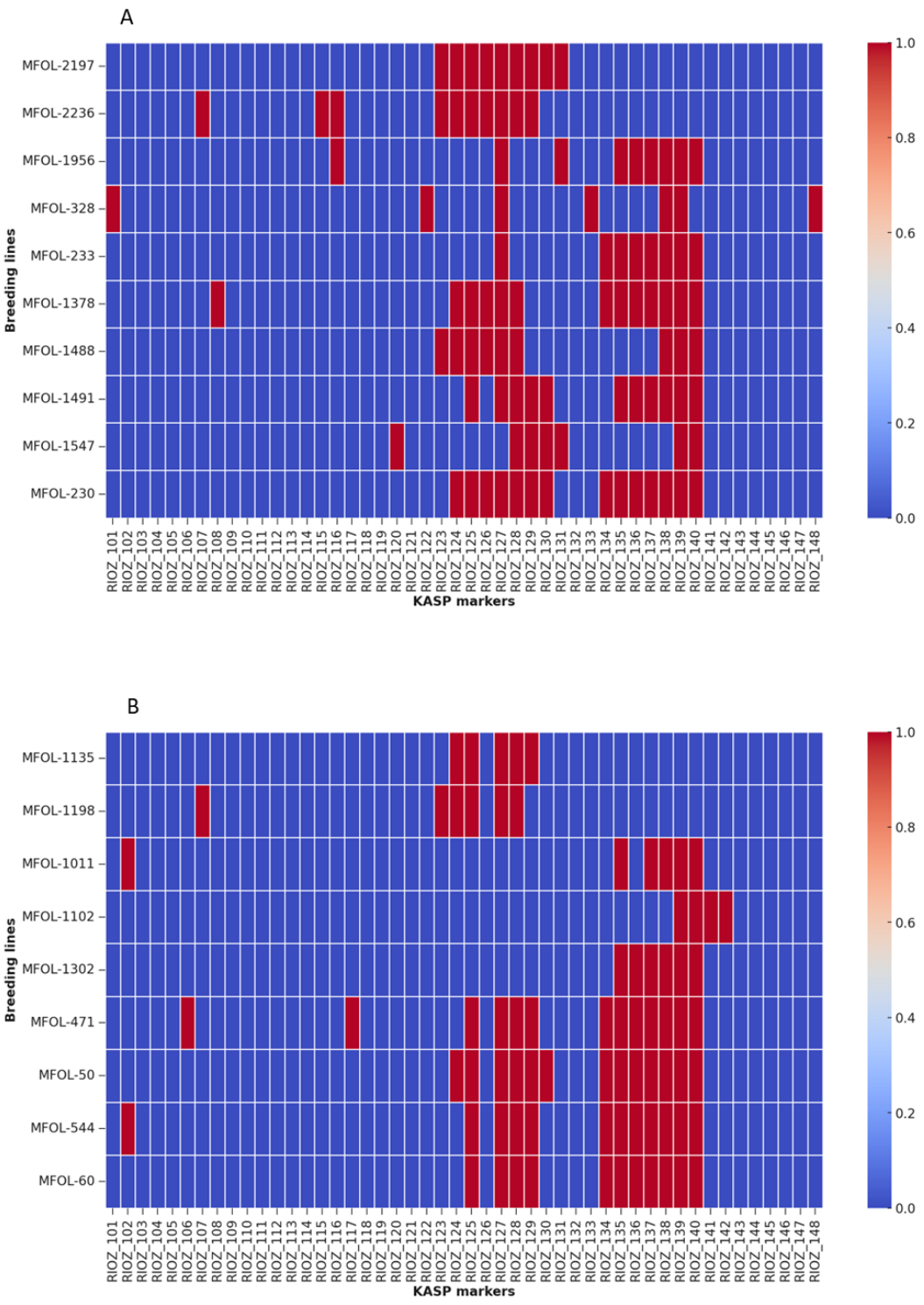

Figure 12 Heatmap illustrating the genome recovery variation in different breeding lines derived from the crosses: (A) BRRI dhan28 × Kasalath, compared against the recipient parent BRRI dhan28, and (B) Binadhan-11 × Kasalath, compared against Binadhan-11. The analysis is based on KASP markers, where blue represents alleles identical to the recipient parent (BRRI dhan28 or Binadhan-11), and red indicates allelic variations corresponding to the donor parent (Kasalath).

4.3 Experiment 2: Assessing ozone tolerance in rice (*Oryza sativa* L.) breeding lines containing ozone tolerance QTLs *OzT8* and *OzT9*

In this section, we present the results of our experiment conducted in a climate-controlled greenhouse at the University of Giessen, Germany, from September 2022 to February 2023. We screened breeding lines for enhanced physiological and agronomic performance under ozone stress conditions.

4.3.1 Physiological and biochemical responses of breeding lines to ozone stress

The physiological and biochemical characteristics of rice breeding lines developed from the crosses between BRRI dhan28 × Kasalath and Binadhan 11 × Kasalath were repeatedly assessed under both controlled conditions and ozone stress treatments. A summary of the results, including descriptive statistics and the outcomes of the ANOVA, is presented in Tables 4 and 5, respectively.

Breeding lines from BRRI Dhan28 X Kasalath cross

Visual symptoms were absent in the control plants but were observed exclusively in plants subjected to ozone treatment. Initially, ozone exposure did not significantly influence the Leaf Bronzing Score (LBS). However, by 80 DAO and 109 DAO, a significant difference in LBS was detected between the ozone-treated plants and the control group (Table 4). Across all measurement dates, LBS demonstrated highly significant genotypic differences and significant interactions between genotype and ozone treatment (Table 4).

Under ozone stress, vegetation indices representing plant foliar pigments, specifically chlorophyll (NDVI) and the chlorophyll-to-carotenoid ratio (Lic2), exhibited significant reductions compared to control conditions at multiple time points (Table 4). At 3 DAO, the treatment effect was minimal; however, substantial reductions in NDVI were observed at 24 DAO, where ozone stress significantly decreased NDVI values compared to the control group (Table 4). Similarly, at 80 DAO, a significant decline in NDVI was noted in ozone-stressed plants compared to the control (Table 4). Significant reductions in Lic2 were detected at 80 and 109 DAO. Genotypic effects were significant across all time intervals for both indices, underscoring inherent genetic variability. Additionally, a significant treatment-by-genotype interaction was observed at later stages: NDVI at 38, 80, and 109 DAO, and Lic2 at 38 and 80 DAO, highlighting variability in the response to ozone stress among the evaluated breeding lines (Table 4).

The Nitrogen Balance Index (NBI), a reliable indicator of plant nitrogen status, exhibited consistently lower values under ozone stress, with significant genotypic effects observed across all measurement intervals. Notably, the interaction effects at later stages (38, 80, and 109 DAO) were highly significant, underscoring the detrimental impact of ozone on nitrogen metabolism, which varied depending on the genotype (Table 4).

A sharp decline in stomatal conductance (gsw) was observed under ozone treatment, particularly at 24 DAO, where the treatment effect was statistically significant. Notably, significant variation among genotypes was detected only at 80 DAO (Table 4). However, the genotype-by-treatment interaction was not statistically significant at any measurement time points. The quantum yield of photosystem II (PhiPS2), a critical indicator of photosynthetic efficiency representing the ratio of electrons transported through PSII to the number of photons absorbed by chlorophyll molecules in PSII, did not exhibit any significant treatment effects across the sampling dates. However, significant genotypic responses to ozone treatment were observed for PhiPS2 at 24 and 109 DAO (Table 4). Similarly, the electron transport rate (ETR), a key parameter reflecting the rate of electron flow through the photosynthetic electron transport chain, did not exhibit a significant response to ozone treatment. However, significant genotypic differences in ETR were observed at 24 DAO, 80 DAO, and 109 DAO (Table 4). No significant interaction between ozone treatment and genotype was detected in both PhiPS2 and ETR.

At 116 DAO, the net CO_2 assimilation rate (A), a critical physiological parameter indicative of photosynthetic capacity, quantifying the amount of CO_2 uptake through plant leaves, exhibited no significant response to treatment. Additionally, there were no significant genotypic effects or evidence of a significant ozone-by-genotype interaction (Table 4). Transpiration rate (E), a key physiological process involving water vapor loss from leaf surfaces to the atmosphere, exhibited no significant response to treatment. Highly significant genotypic transpiration rate (E) differences were recorded, but no significant interactions between ozone and genotype were detected (Table 4). Intercellular CO_2 concentration (Ci), representing the availability of CO_2 for photosynthesis within the plant, showed no significant treatment effect. However, significant genotypic differences in Ci were observed, while ozone-by-genotype interactions remained non-significant (Table 4).

Malondialdehyde (MDA) levels, a biochemical marker of oxidative stress, were significantly elevated under ozone stress at 50 DAO, indicating increased lipid peroxidation and cellular

damage caused by ozone exposure (Table 4). Across all genotypes, ozone treatment led to a significant increase in MDA concentrations, with shoot MDA levels consistently higher in ozone-treated plants than in control plants. Furthermore, MDA levels exhibited highly significant genotypic differences, underscoring variability in oxidative stress responses among genotypes. A significant interaction between ozone treatment and genotype was also detected (Table 4).

Table 4 Descriptive statistics and analysis of variance (ANOVA) for physiological and biochemical traits of breeding lines derived from the cross between BRRI dhan28 and Kasalath under ozone stress and control conditions.

Traits	Date	LS means (treatment)				ANOVA					
		Control		Ozone		Ozone-Treatment		Genotype		Interaction	
		Mean	SD	Mean	SD	Pr(>F)	F values	Pr(>F)	F values	Pr(>F)	F values
LBS	24 DAO	0	0	0.81	0.50	0.1458	18.39	**0.0034**	1.72	**0.0034**	1.72
	38 DAO	0	0	1.64	1.09	0.133	22.26	**<0.0000**	2.39	**<0.0000**	2.39
	80 DAO	0	0	3.46	0.79	**0.0102**	387.66	**<0.0001**	11.31	**<0.0001**	11.31
	109 DAO	0	0	4.40	1.00	**0.0098**	421.50	**<0.0001**	12.54	**<0.0001**	12.54
NDVI	3 DAO	0.64	0.04	0.64	0.03	**0.0059**	7.64	**<0.0001**	2.19	0.4617	1.01
	24 DAO	0.74	0.02	0.72	0.03	**<0.0001**	206.38	**0.0005**	1.93	0.5932	0.94
	38 DAO	0.66	0.01	0.63	0.02	0.0752	71.06	**<0.0001**	2.24	**0.0001**	2.05
	80 DAO	0.73	0.04	0.63	0.04	**0.0311**	418.74	**<0.0001**	4.13	**<0.0001**	4.40
	109 DAO	0.63	0.03	0.57	0.07	0.1163	29.31	**<0.0001**	4.43	**<0.0001**	3.75
Lic2	3 DAO	0.74	0.03	0.72	0.02	0.1339	6.00	**<0.0001**	2.45	0.7720	0.83
	24 DAO	0.93	0.07	0.89	0.06	0.2195	7.76	**0.0002**	2.04	0.1089	1.38
	38 DAO	0.73	0.03	0.70	0.04	0.1567	4.93	**<0.0001**	2.34	**0.0043**	1.70
	80 DAO	0.94	0.08	0.67	0.07	**0.02545**	625.01	**0.0013**	2.93	0.0615	1.76
	109 DAO	0.72	0.05	0.63	0.09	**<0.0001**	107.52	**<0.0001**	3.98	**<0.0001**	3.81
NBI	3 DAO	102.14	17.91	88.82	16.02	0.2178	7.88	**<0.0001**	5.85	0.2729	1.13
	24 DAO	133.02	32.50	107.38	28.66	0.1870	10.93	**<0.0001**	2.62	0.1427	1.24
	38 DAO	138.14	26.89	106.12	28.22	0.0728	75.82	**<0.0001**	3.41	**0.0016**	1.80
	80 DAO	109.40	29.19	70.66	23.61	0.0594	114.03	**<0.0001**	3.80	**0.0011**	2.98
	109 DAO	83.68	22.75	59.27	21.72	0.0783	65.44	**0.0119**	2.28	**<0.0001**	4.51
	3 DAO	0.54	0.16	0.15	0.13	0.1224	26.37	**<0.0001**	2.01	**0.0056**	1.66

gsw (mol m^{-2} s^{-1})	24 DAO	0.47	0.21	0.09	0.11	**0.0434**	213.67	0.2668	1.13	0.9133	0.72
	38 DAO	0.30	0.20	0.10	0.08	0.1860	11.06	0.4119	1.04	0.7543	0.84
	80 DAO	0.28	0.19	0.10	0.07	0.1453	18.52	**0.0340**	1.95	0.1638	1.42
	109 DAO	0.21	0.12	0.06	0.05	0.1860	11.06	0.4119	1.04	0.7543	0.84
PhiPS2	3 DAO	0.72	0.09	0.73	0.02	0.7419	0.18	0.3576	1.07	0.6711	0.89
	24 DAO	0.75	0.02	0.74	0.02	0.1453	18.52	**0.0340**	1.95	0.1638	1.42
	38 DAO	0.71	0.08	0.74	0.02	0.4403	1.46	0.0980	1.30	0.1217	1.27
	80 DAO	0.71	0.07	0.70	0.07	0.0605	110.17	0.1107	1.56	0.1926	1.36
	109 DAO	0.68	0.06	0.70	0.06	0.5457	0.75	**0.0057**	2.49	0.0920	1.62
ETR (µmol m^{-2} s^{-1})	3 DAO	24.79	8.82	24.67	8.64	0.7419	0.18	0.3576	1.07	0.6711	0.89
	24 DAO	15.81	6.84	14.07	6.78	0.1033	37.29	**<0.0001**	3.06	0.7891	0.82
	38 DAO	19.07	9.04	12.58	6.32	0.4404	1.46	0.0981	1.30	0.1218	1.27
	80 DAO	18.98	9.02	16.40	8.06	0.9249	0.01	**<0.0001**	3.08	0.0952	1.61
	109 DAO	19.45	10.04	13.66	6.10	0.5457	0.75	**0.0057**	2.49	0.0920	1.63
A (µmol m^{-2} s^{-1})	116 DAO	29.60	8.65	18.65	9.00	0.9612	0.00	0.9020	0.73	0.1736	1.21
E (mol m^{-2} s^{-1})	116 DAO	0.04	0.02	0.03	0.01	0.4873	1.08	**0.0010**	3.90	0.4204	1.03
Ci (µmol mol^{-1})	116 DAO	367.46	6.34	362.28	7.11	0.2483	5.92	**<0.0001**	2.78	0.2225	1.16
MDA (nmol g^{-1}) FW	50 DAO	13.58	2.47	20.24	4.00	**0.0354**	321.82	**<0.0001**	8.61	**<0.0001**	6.60

Note: Mean values of all genotypes are shown. LS, least square means; DAO, days after ozone; SD, standard deviation; LBS, leaf bronzing score; NDVI, normalized difference vegetation index; Lic2, Lichtenthaler index 2; NBI, nitrogen balance index; gsw, stomatal conductance(mol m^{-2} s^{-1}); PhiPS2, quantum efficiency of photosystem II; ETR, electron transport rate (µmol m^{-2} s^{-1}); A, CO_2 assimilation rate (µmol m^{-2} s^{-1}); E, transpiration rate (mol m^{-2} s^{-1}); Ci, intercellular CO_2 concentration (µmol mol^{-1}); MDA, malondialdehyde (nmol g^{-1}); FW, fresh weight.

Breeding lines from Binadhan-11 X Kasalath cross

A significant difference in LBS was observed between the ozone-treated plants and the control group at 80 DAO and 109 DAO. Furthermore, LBS exhibited highly significant genotypic variation across all measurement intervals and significant genotype × ozone treatment interactions (Table 5).

NDVI values exhibited significant reductions under ozone stress compared to the control at 24, 80, and 109 DAO. Genotypic variation and genotype × treatment interactions were significant across all time points, except at 3 DAO (Table 5). Similarly, Lic2 values showed significant decreases at later stages, particularly at 80 and 109 DAO under ozone stress. While significant genetic variation was evident across all time points, the genotype × treatment interaction effects became significant at 38, 80, and 109 DAO (Table 5).

NBI values were consistently lower under ozone stress; however, the effect was not statistically significant. Significant genotypic variation was observed across all measurement time points. Furthermore, the interaction effects between genotype and treatment were significant at 38, 80, and 109 DAO (Table 5).

Stomatal conductance (gsw) consistently decreased under ozone stress, although this reduction was not statistically significant. Significant genotypic variation was observed at 3, 24, and 38 DAO. However, the interaction between genotype and treatment was significant only at 3 DAO (Table 5). The PhiPS2 values remained consistent between control and ozone conditions, with no significant differences observed in treatment effects or interactions across all measured time points (Table 5). Similarly, ETR values did not exhibit significant treatment effects throughout the measurement period. However, genotypic differences were significant at 80 and 109 DAO, accompanied by significant interaction effects at 109 DAO (Table 5).

Net CO_2 assimilation rate (A), transpiration rate (E), and intercellular CO_2 concentration (Ci) were evaluated at 116 DAO. The analysis revealed no significant effects of treatment on these parameters (Table 5). However, highly significant genotypic differences were observed for both net CO_2 assimilation rate (A) and transpiration rate (E). No significant ozone-by-genotype interactions were detected for these parameters. In contrast, intercellular CO_2 concentration (Ci) exhibited neither significant genotypic differences nor significant interactions between ozone and genotype (Table 5).

Across all genotypes, ozone treatment resulted in a significant increase in MDA levels. Additionally, significant genotypic variation was observed. Furthermore, the interaction between treatment and genotype exhibited a statistically significant effect (Table 5).

In summary, the results reveal reductions in key physiological and biochemical traits of rice breeding lines containing ozone tolerance QTLs (*OzT8* and/or *OzT9*) derived from BRRI dhan28 or Binadhan-11 under ozone stress. Notable impacts were observed on traits such as leaf bronzing score, chlorophyll indices (NDVI, Lic2), and malondialdehyde (MDA) levels across measurement intervals, indicating decreased photosynthetic pigments and increased oxidative stress. While reductions in stomatal conductance and the Nitrogen balance index (NBI) were evident, these effects were not statistically significant, potentially due to variability within treatments and the limited number of experimental chambers per treatment. Photosynthetic efficiency (PhiPS2, ETR) and gas exchange parameters (A, E, Ci) exhibited minimal or non-significant responses to ozone stress, highlighting genotypic differences. Overall, breeding lines from both genetic backgrounds containing QTLs *OzT8* and/or *OzT9* demonstrated differential responses to ozone stress.

Table 5 Descriptive statistics and analysis of variance (ANOVA) for physiological and biochemical traits of breeding lines derived from the cross between Binadhan-11 and Kasalath under ozone stress and control conditions.

Traits	Date	LS means (treatment)				ANOVA					
		Control		Ozone		Ozone-Treatment		Genotype		Interaction	
		Mean	SD	Mean	SD	Pr(>F)	F values	Pr(>F)	F values	Pr(>F)	F values
LBS	24 DAO	0	0	1.10	0.86	0.1913	10.41	**0.0210**	1.63	**0.0210**	1.63
	38 DAO	0	0	2.24	1.52	0.1529	16.67	**0.0022**	1.96	**0.0022**	1.96
	80 DAO	0	0	3.98	0.97	**0.0111**	327.43	**<0.0001**	9.51	**<0.0001**	9.51
	109 DAO	0	0	4.81	1.22	**0.0089**	506.01	**<0.0001**	19.39	**<0.0001**	19.39
NDVI	3 DAO	0.64	0.03	0.63	0.03	0.2674	5.01	0.4968	0.98	0.3096	1.12
	24 DAO	0.73	0.03	0.70	0.04	**0.0297**	32.12	**0.0008**	2.10	**0.0389**	1.53
	38 DAO	0.65	0.01	0.62	0.03	0.134	21.90	**<0.0001**	2.85	**0.0259**	1.60
	80 DAO	0.74	0.02	0.62	0.06	**0.0407**	244.07	**<0.0001**	4.83	**0.0002**	3.28
	109 DAO	0.65	0.02	0.57	0.07	**0.0467**	184.89	**<0.0001**	6.45	**<0.0001**	6.74
Lic2	3 DAO	0.73	0.02	0.71	0.02	0.2448	6.11	**0.0011**	2.06	0.9743	0.56
	24 DAO	0.92	0.07	0.85	0.08	0.1940	10.11	**0.0038**	1.89	0.5560	0.94
	38 DAO	0.73	0.03	0.67	0.05	0.1826	11.63	**<0.0001**	3.38	**0.0542**	1.47
	80 DAO	0.95	0.07	0.64	0.08	**0.0218**	852.78	**0.0010**	2.89	**0.0040**	2.53
	109 DAO	0.75	0.04	0.61	0.09	**0.0347**	27.29	**<0.0001**	4.64	**0.0004**	3.12
NBI	3 DAO	107.71	24.88	110.92	20.13	0.3054	3.70	**<0.0001**	4.66	0.4905	0.99
	24 DAO	149.76	32.85	111,05	38,96	0.0557	130.05	**<0.0001**	3.11	0.4231	1.03
	38 DAO	144.14	33.23	99.82	29.86	0.0623	103.93	**<0.0001**	2.85	**0.0127**	1.71
	80 DAO	92.54	29.07	65.75	23.38	0.1353	21.48	**0.0017**	2.75	**0.0198**	2.07
	109 DAO	82.90	22.02	53.79	17.16	0.0718	77.89	**0.0008**	2.94	**<0.0001**	3.63
	3 DAO	0.50	0.22	0.13	0.13	0.2228	7.50	**<0.0001**	2.17	**0.0096**	1.75

gsw (mol m^{-2} s^{-1})	24 DAO	0.39	0.20	0.08	0.10	0.1228	26.21	**0.0205**	1.63	0.2498	1.17
	38 DAO	0.28	0.18	0.14	0.14	0.1060	35.38	**<0.0001**	2.39	0.1136	1.34
	80 DAO	0.21	0.14	0.16	0.12	0.4205	1.66	0.0799	1.65	0.2804	1.21
	109 DAO	0.20	0.10	0.10	0.07	0.0795	63.43	0.2239	1.29	0.2017	1.33
PhiPS2	3 DAO	0.73	0.03	0.72	0.03	0.4205	1.66	0.0799	1.65	0.2804	1.21
	24 DAO	0.74	0.06	0.74	0.02	0.0795	63.43	0.2240	1.29	0.2017	1.33
	38 DAO	0.71	0.08	0.74	0.01	0.2312	6.93	0.1582	1.27	0.0997	1.36
	80 DAO	0.71	0.07	0.71	0.06	0.3637	2.42	0.4884	0.99	0.4177	1.04
	109 DAO	0.69	0.08	0.69	0.07	0.4316	1.54	0.5691	0.94	0.5217	0.97
ETR (µmol m^{-2} s^{-1})	3 DAO	24.23	6.82	24.36	7.85	0.9551	0.01	0.1732	1.39	0.1943	1.35
	24 DAO	17.03	7.20	15.41	6.83	0.9425	0.01	0.4685	0.99	0.0917	1.60
	38 DAO	20.49	8.86	13.17	6.02	0.9624	0.00	0.5179	0.97	0.9824	0.53
	80 DAO	20.60	7.99	14.44	7.24	0.3180	3.36	**<0.0001**	2.19	0.9311	0.64
	109 DAO	21.43	7.43	14.52	5.81	0.1668	13.90	**<0.0001**	4.65	**0.0465**	1.81
A (µmol m^{-2} s^{-1})	116 DAO	30.18	8.28	17.59	7.21	0.1264	24.70	**<0.0001**	3.13	0.0938	1.37
E (mol m^{-2} s^{-1})	116 DAO	0.04	0.02	0.03	0.01	0.4076	1.80	**0.0109**	2.84	0.8681	0.45
Ci (µmol mol^{-1})	116 DAO	365.50	7.34	361.06	7.29	0.3067	3.66	0.0651	1.71	0.8256	0.63
MDA (nmol g^{-1}) FW	50 DAO	11.97	2.33	18.18	4.00	**0.0324**	383.93	**<0.0001**	12.72	**<0.0001**	8.79

Note: Mean values of all genotypes are shown. LS, least square means; DAO, days after ozone; SD, standard deviation; LBS, leaf bronzing score; NDVI, normalized difference vegetation index; Lic2, Lichtenthaler index 2; NBI, nitrogen balance index; gsw, stomatal conductance(mol m^{-2} s^{-1}); PhiPS2, quantum efficiency of photosystem II; ETR, electron transport rate (µmol m^{-2} s^{-1}); A, CO_2 assimilation rate (µmol m^{-2} s^{-1}); E, transpiration rate (mol m^{-2} s^{-1}); Ci, intercellular CO_2 concentration (µmol mol^{-1}); MDA, malondialdehyde (nmol g^{-1}); FW, fresh weight.

4.3.2 Selection of breeding lines based on leaf bronzing score, stomatal conductance, and morphological traits

To narrow down the breeding lines, we considered leaf bronzing score (LBS) (Figure 13A, 14A) and stomatal conductance (gsw) (Figure 13B, 14B) data at 38 DAO. Additionally, the plants were phenotyped, and those exhibiting morphological similarity to the recipient parents, BRRI dhan28 (Table 6) or Binadhan-11 (Table 7), were selected. Breeding lines with an erect structure, lower LBS and higher stomatal conductance than the recipient parents were identified for further investigation. Conversely, breeding lines that performed better in terms of LBS or gsw but exhibited a spreading growth habit, experienced lodging, or lacked morphological resemblance to the recipient parents were excluded from further investigation. Only selected lines were evaluated further for their physiological and agronomic performance.

Breeding lines from BRRI Dhan28 X Kasalath cross

Breeding lines of BRRI dhan28, including *OzT8*, MFOL-2109, MFOL-2197, and MFOL-2236, exhibited lower leaf damage symptoms, as indicated by leaf bronzing score (LBS), compared to their recipient parent BRRI dhan28 at 38 DAO (Figure 13A). These lines also demonstrated higher stomatal conductance (gsw) and exhibited morphological traits resembling BRRI dhan28 (Table 6, Figure 13B). A similar trend was observed in MFOL-1926, MFOL-1956, and MFOL-328, which contained *OzT9*, as well as in breeding lines containing both QTLs (*OzT8* + *OzT9*), including MFOL-1378, MFOL-1488, MFOL-1491, MFOL-1547, and MFOL-2388 (Table 6, Figure 13). Based on these favorable characteristics, these lines were selected for further investigation.

Table 6 Morphological characteristics of breeding lines derived from the BRRI dhan28 × Kasalath cross.

QTLs	Line	Type	Remarks
OzT8	MFOL-2149	Spreading	X
	MFOL-2218	Spreading	X
	MFOL-2248	Spreading	X
	MFOL-2163	Spreading	X
	MFOL-2109	Erect, similar to BRRI dhan28	Selected
	MFOL-2181	Spreading	X
	MFOL-2179	Spreading	X

	MFOL-2090	Spreading	X
	MFOL-2102	Spreading	X
	MFOL-2197	Moderately erect, close to BRRI dhan28	Selected
	MFOL-2204	Spreading	X
	MFOL-2236	Erect, similar to BRRI dhan28	Selected
OzT9	MFOL-2018	Spreading	X
	MFOL-1798	Spreading	X
	MFOL-1926	Moderately erect, close to BRRI dhan28	Selected
	MFOL-2026	Spreading	X
	MFOL-1925	Spreading	X
	MFOL-1973	Spreading	X
	MFOL-96-325	Spreading	X
	MFOL-1881	Spreading	X
	MFOL-1778	Spreading	X
	MFOL-1801	Spreading	X
	MFOL-117-331	Spreading	X
	MFOL-1928	Spreading	X
	MFOL-1857	Spreading	X
	MFOL-328	Moderately erect, close to BRRI dhan28	Selected
	MFOL-1956	Erect, close to BRRI dhan28	Selected
	MFOL-111-328	Spreading	X
	MFOL-1856	Spreading	X
	MFOL-1772	Spreading	X
	MFOL-1779	Spreading	X
	MFOL-1838	Spreading	X
OzT8 + OzT9	MFOL-1491	Erect, close to BRRI dhan28	Selected
	MFOL-2395	Spreading	X
	MFOL-2406	Spreading	X
	MFOL-1474	Spreading	X
	MFOL-2349	Spreading	X
	MFOL-1325	Spreading	X
	MFOL-1547	Erect, close to BRRI dhan28	Selected
	MFOL-2388	Moderately erect, close to BRRI dhan28	Selected
	MFOL-1378	Moderately erect, close to BRRI dhan28	Selected
	MFOL-1488	Moderately erect, close to BRRI dhan28	Selected
	MFOL-1720	Spreading	X
	MFOL-2301	Spreading	X

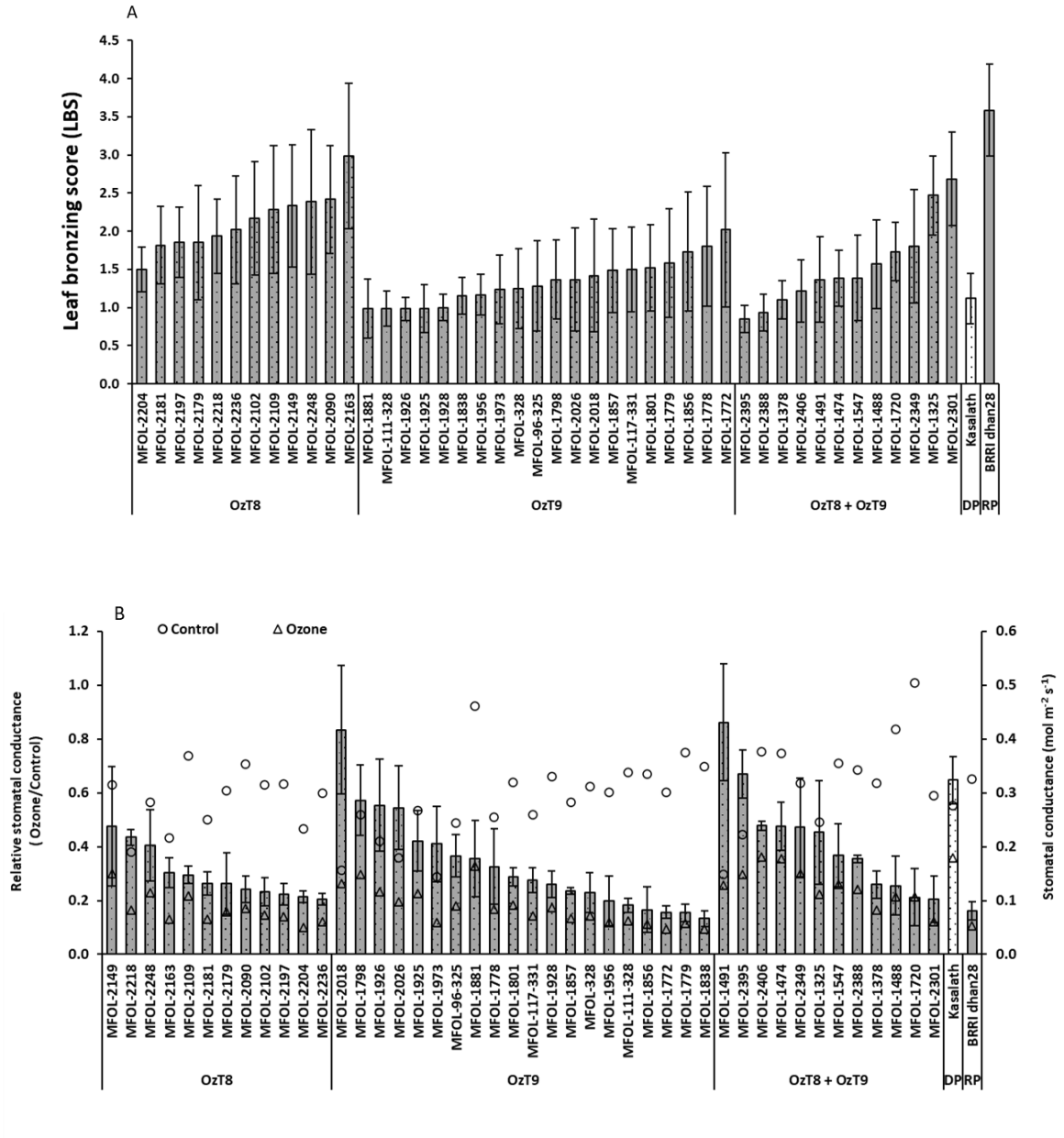

Figure 13 (A) Leaf bronzing scores of breeding lines derived from the cross BRRI dhan28 × Kasalath at 38 DAO. Bars represent mean values with standard errors (n = 3). (B) Relative stomatal conductance of the breeding lines (BRRI dhan28 × Kasalath). Bars represent mean relative values with standard errors (n = 3). Circular and triangular markers indicate absolute values under control and ozone treatments, respectively. DP refers to the donor parent (Kasalath), and RP refers to the recipient parent (BRRI dhan28).

Breeding lines from Binadhan-11 X Kasalath cross

When compared to their recipient parent, Binadhan-11, the breeding lines MFOL-1135, MFOL-1163, MFOL-1198, and MFOL-1281, containing the *OzT8* QTL, exhibited a lower leaf

bronzing score (LBS) (Figure 14A) and higher relative stomatal conductance (gsw) (Figure 14B) while maintaining a morphology similar to Binadhan-11 (Table 7). A similar trend was observed in the breeding lines MFOL-1001, MFOL-1011, MFOL-1031, MFOL-1102, and MFOL-1302, which carried the *OzT9* QTL, as well as in the lines with double QTLs (*OzT8* + *OzT9*), MFOL-471, MFOL-544, and MFOL-579 (Figure 14A, B and Table 7).

Table 7 Morphological characteristics of breeding lines derived from the Binadhan-11 × Kasalath cross.

QTL's	Line	Type	Remarks
OzT8	MFOL-1135	Erect, similar to Binadhan-11	Selected
	MFOL-1198	Erect, similar to Binadhan-11	Selected
	MFOL-1211	Spreading	X
	MFOL-1238	Spreading	X
	MFOL-1281	Moderately erect, close to Binadhan-11	Selected
	MFOL-1231	Erect, close to Binadhan-11	Selected
	MFOL-1163	Moderately erect, close to Binadhan-11	Selected
	MFOL-1216	Spreading	X
	MFOL-1263	Spreading	X
	MFOL-1133	Spreading	X
	MFOL-1170	Spreading	X
	MFOL-1259	Spreading	X
	MFOL-1121	Spreading	X
	MFOL-1154	Spreading	X
	MFOL-1131	Spreading	X
OzT9	MFOL-774	Spreading	X
	MFOL-1102	Erect, close to Binadhan-11	Selected
	MFOL-1011	Erect, close to Binadhan-11	Selected
	MFOL-1302	Erect, close to Binadhan-11	Selected
	MFOL-1001	Moderately erect, close to Binadhan-11	Selected
	MFOL-1031	Moderately erect, close to Binadhan-11	Selected
	MFOL-866	Spreading	X
	MFOL-1289	Spreading	X
	MFOL-729	Spreading	X
	MFOL-842	Spreading	X
OzT8 + OzT9	MFOL-471	Moderately erect, close to Binadhan-11	Selected
	MFOL-544	Moderately erect, close to Binadhan-11	Selected
	MFOL-579	Moderately erect, close to Binadhan-11	Selected
	MFOL-491	Spreading	X
	MFOL-518	Spreading	X

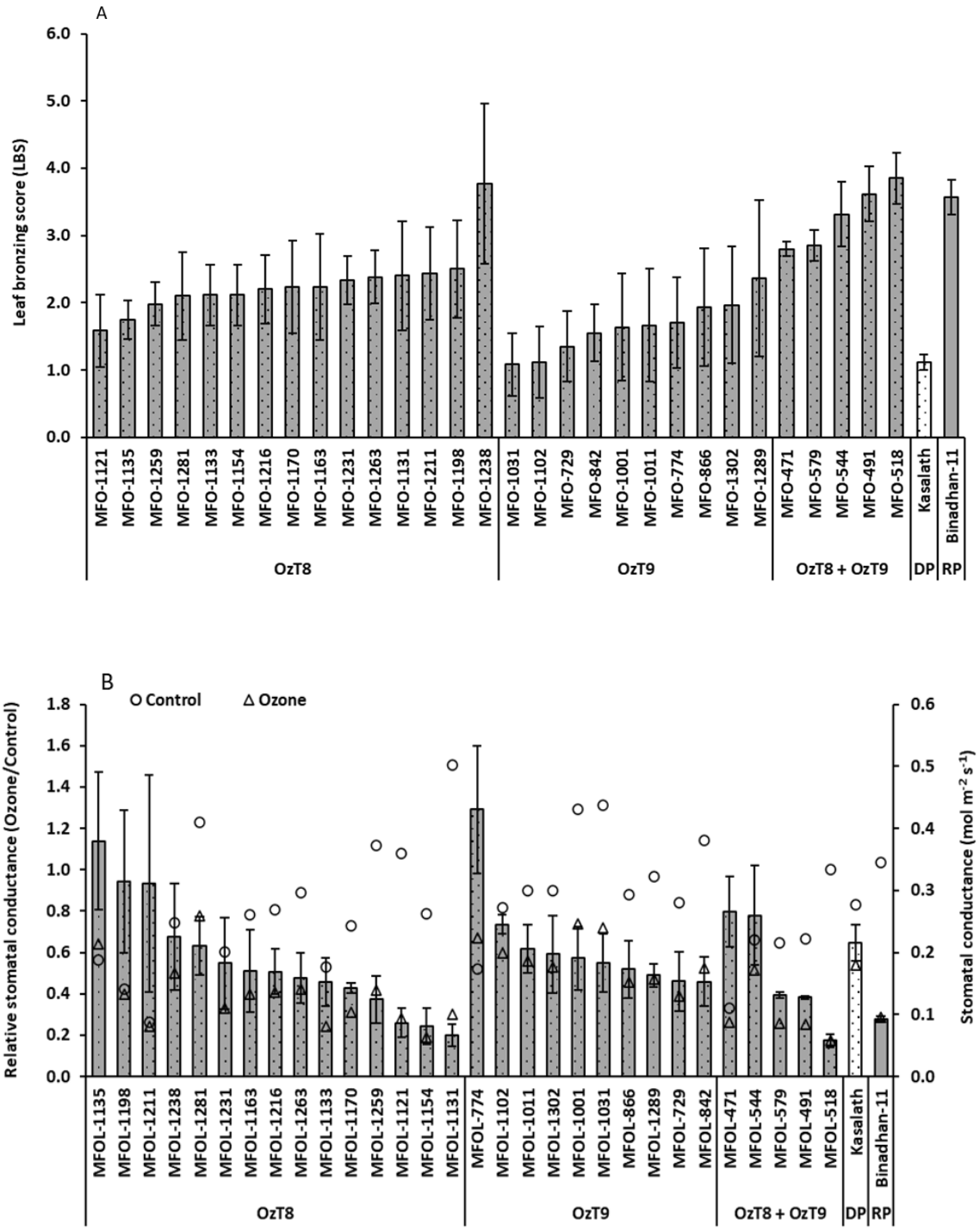

Figure 14 (A) Leaf bronzing scores of breeding lines derived from the cross Binadhan-11 × Kasalath at 38 DAO. Bars represent mean values with standard errors (n = 3). (B) Relative stomatal conductance of the breeding lines (Binadhan-11 × Kasalath). Bars represent mean relative values with standard errors (n = 3). Circular and triangular markers indicate absolute values under control and ozone treatments, respectively. DP refers to the donor parent (Kasalath), and RP refers to the recipient parent (Binadhan-11).

4.3.3 Genotypic variation in leaf bronzing score (LBS)

Breeding lines from BRRI Dhan28 X Kasalath cross

Significant reductions in leaf bronzing score (LBS) were observed in breeding lines carrying the *OzT8* and/or *OzT9* QTLs compared to the recipient parent BRRI dhan28 under ozone stress conditions at both measurement time points (Figure 15A, B). At 80 DAO exposure, breeding lines containing only *OzT9* exhibited the lowest average LBS (2.83), followed by lines carrying *OzT8* (3.31) and those containing both (*OzT8* + *OzT9*) *QTLs* (3.43). Among all genotypes, MFOL-328 (2.67), MFOL-1926 (2.92), and MFOL-1956 (2.92), all of which harbored *OzT9*, exhibited the lowest LBS values. Additionally, MFOL-1491, which contained both QTLs (*OzT8* + *OzT9*), showed a reduced LBS of 2.92(Figure 15A). Similarly, at 109 DAO, breeding lines carrying only *OzT9* again showed the lowest average LBS (3.78), followed by lines with both (*OzT8* + *OzT9*) QTLs (4.08) and those with *OzT8* (4.50). Among individual genotypes, the lowest LBS was recorded for MFOL-1956 (3.33) and MFOL-1491 (3.33), which contained *OzT9* and both QTLs (*OzT8* + *OzT9*), respectively. This was followed by MFOL-328 (3.50), which also carried *OzT9* (Figure 15B).

Breeding lines from Binadhan-11 X Kasalath cross

At 80 DAO, breeding lines containing only *OzT8* exhibited the LBS of 3.2, followed by lines harboring *OzT9* (4.1) and those containing both (*OzT8* + *OzT9*) QTLs (4.3). Among the genotypes, MFOL-1135 (2.6) and MFOL-1281 (2.8), both of which carried *OzT8*, and MFOL-1001 (3.33), also containing *OzT9*, demonstrated the lowest LBS values(Figure 16A). Similarly, at 109 DAO, breeding lines with only *OzT8* again showed the lowest mean LBS (3.9), followed by lines carrying *OzT9* (4.50) and those harboring both (*OzT8* + *OzT9*) QTLs (4.9). At the genotype level, the lowest LBS was observed in MFOL-1135 and MFOL-1281 (3.0), both containing *OzT9*, followed by MFOL-1001 (4.3) and MFOL-471 (4.3), which harbored *OzT9* and both QTLs (*OzT8* + *OzT9*), respectively (Figure 16B).

These results suggested that breeding lines carrying the *OzT8* and/or *OzT9* QTLs exhibit significantly reduced leaf bronzing scores (LBS) under ozone stress compared to the recipient parents. Breeding lines with *OzT9* consistently displayed the lowest LBS at both 80 and 109 DAO in the BRRI Dhan28 × Kasalath cross, while those with *OzT8* performed better in the Binadhan-11 × Kasalath cross. The presence of both QTLs provided moderate LBS reductions,

but individual QTLs, particularly *OzT9* in BRRI Dhan28-derived lines and *OzT8* in Binadhan-11-derived lines, demonstrated superior performance.

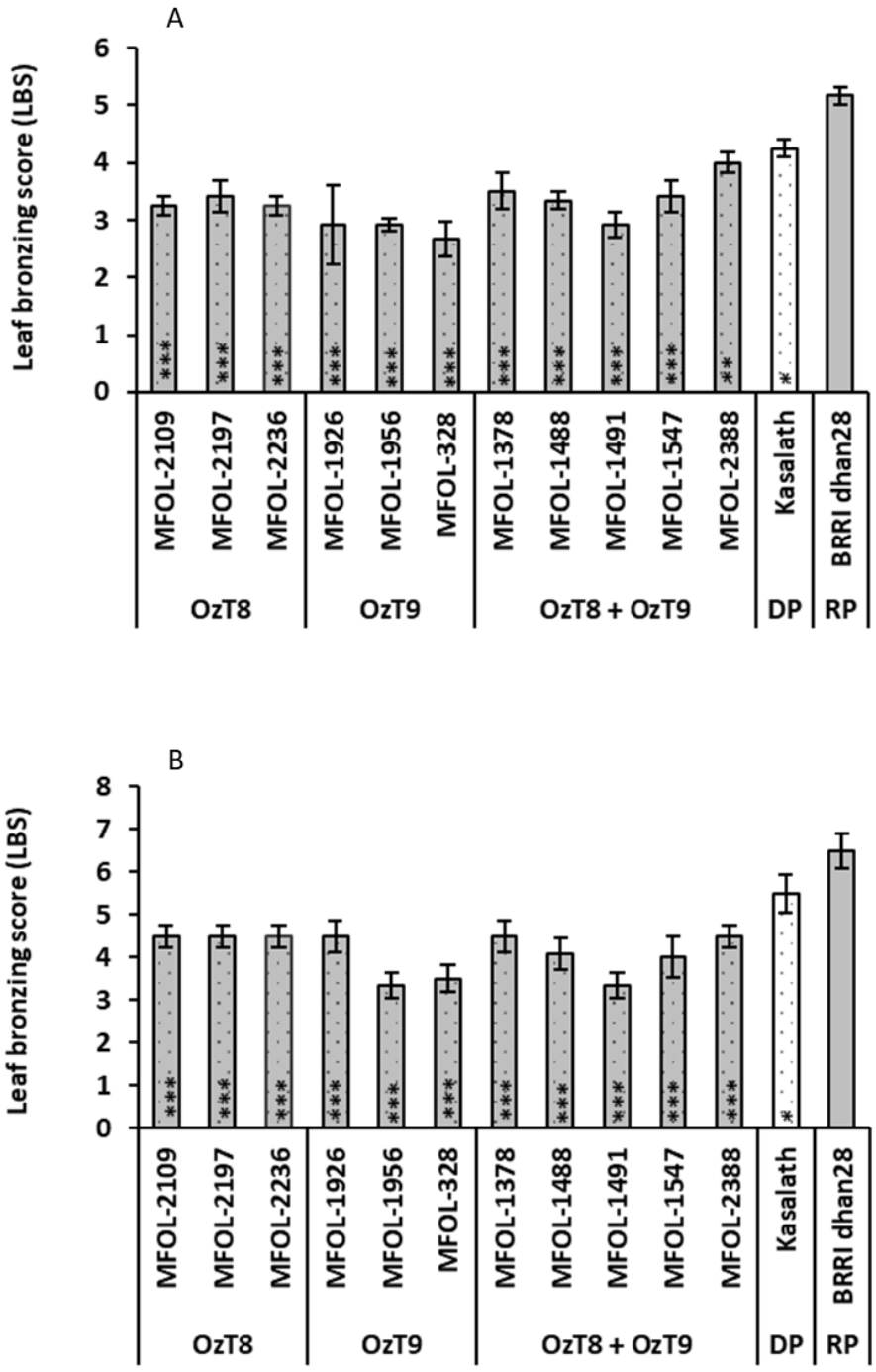

Figure 15 Leaf bronzing scores of selected breeding lines carrying *OzT8* and/or *OzT9* derived from the cross BRRI dhan28 × Kasalath under ozone stress at (A) 80 DAO and (B) 109 DAO. The bar graphs display the mean and standard error of relative values (n = 3). Asterisks within the bars indicate significant differences between the genotypes and the recipient parent (BRRI dhan28), as determined by Dunnett's test (*P < 0.05, **P < 0.01, ***P < 0.001). DP, donor parent, and RP, recipient parent.

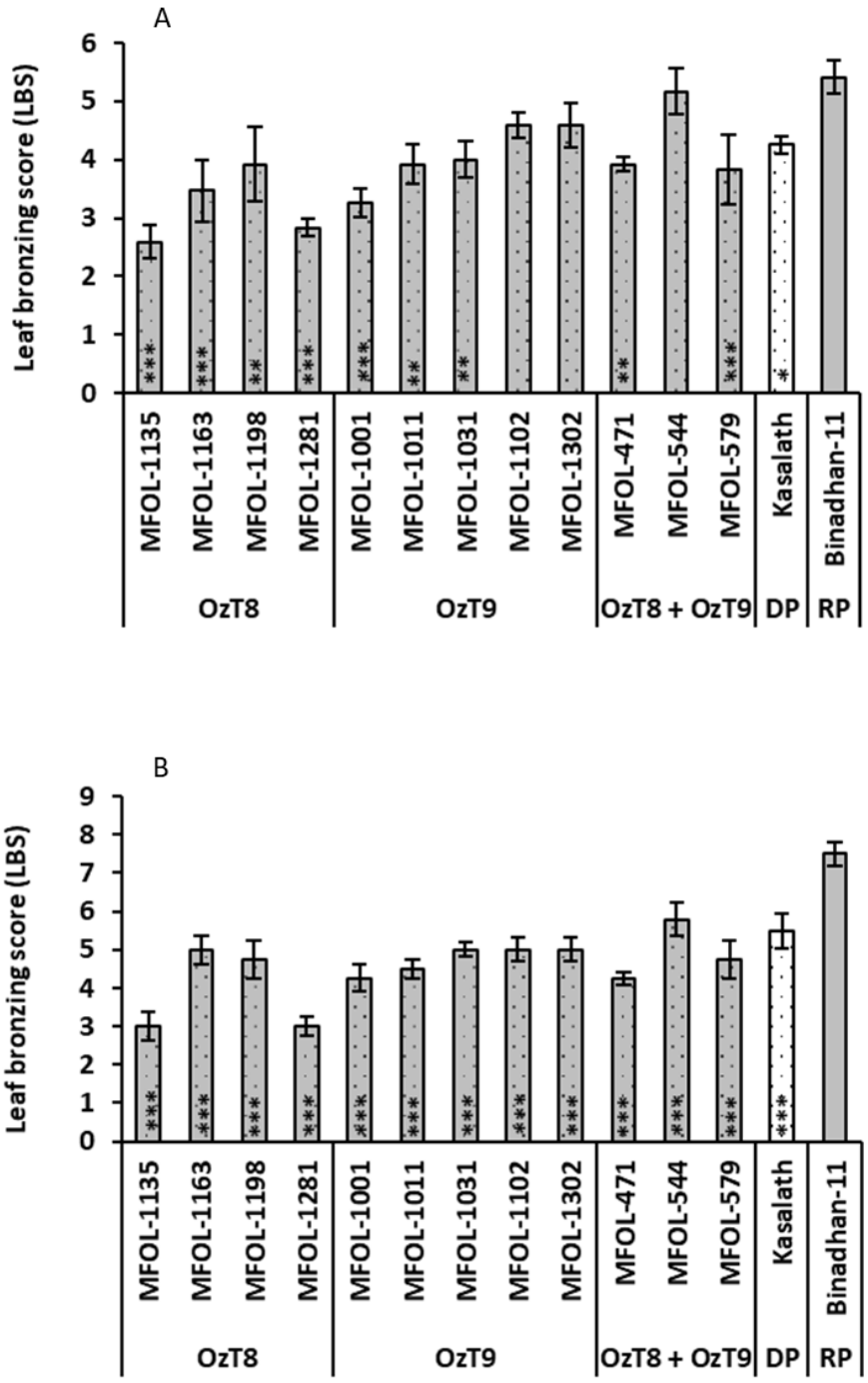

Figure 16 Leaf bronzing scores of selected breeding lines carrying *OzT8* and/or *OzT9* derived from the cross Binadhan-11 × Kasalath under ozone stress at (A) 80 DAO and (B) 109 DAO. The bar graphs display the mean and standard error of relative values (n = 3). Asterisks within the bars indicate significant differences between the genotypes and the recipient parent (Binadhan-11), as determined by Dunnett's test (*P < 0.05, **P < 0.01, ***P < 0.001). DP, donor parent, and RP, recipient parent.

4.3.4 Evaluation of breeding lines in response to plant foliar pigments

Breeding lines from BRRI Dhan28 X Kasalath cross

At 80 DAO, breeding lines carrying both QTLs (*OzT8* + *OzT9*) exhibited the highest average relative NDVI, followed by those containing only *OzT9* or *OzT8*. A similar trend was observed at 109 DAO (Figure 17A, B). Among all genotypes evaluated at 80 DAO, MFOL-2388 demonstrated the highest relative NDVI, followed by MFOL-1926 (*OzT9*), MFOL-1488 (*OzT8* + *OzT9*), and MFOL-1378 (*OzT8* + *OzT9*) (Figure 17A). At 109 DAO, the highest relative NDVI among individual genotypes was recorded for MFOL-328 (*OzT9*), followed by MFOL-1378, MFOL-1488, and MFOL-1491, all of which carried both QTLs (*OzT8* + *OzT9*) (Figure 17B).

At 80 DAO, breeding lines carrying both QTLs (*OzT8* + *OzT9*) exhibited the highest average relative Lic2, followed by lines containing only *OzT8* and *OzT9* (Figure 19A). Similarly, at 109 DAO, breeding lines with both QTLs (*OzT8* + *OzT9*) again demonstrated the highest average relative Lic2, followed by those carrying only *OzT9* or *OzT8* (Figure 19B). Among all genotypes assessed at 80 DAO, MFOL-2197 (*OzT8*) showed the highest relative Lic2, followed by MFOL-1488, MFOL-2388, and MFOL-1378, all of which contained both QTLs (*OzT8* + *OzT9*) (Figure 19A). At 109 DAO, the genotype with the highest relative Lic2 was MFOL-1378 (*OzT8* + *OzT9*), followed by MFOL-2388 (*OzT8* + *OzT9*), MFOL-328 (*OzT9*), and MFOL-1491 (*OzT8* + *OzT9*) (Figure 19B).

Breeding lines carrying both QTLs (*OzT8* + *OzT9*) exhibited the highest average relative NBI, followed by lines containing only *OzT8* and *OzT9* at 80 DAO (Figure 21A). However, at 109 DAO, breeding lines with *OzT9* QTL demonstrated the highest average relative NBI, followed by those carrying both QTLs (*OzT8* + *OzT9*) and QTL *OzT8* (Figure 21B). Among all genotypes assessed at 80 DAO, MFOL-2388 showed the highest relative NBI, followed by MFOL-1547 and MFOL-1488, all containing both QTLs (*OzT8* + *OzT9*) (Figure 21A). At 109 DAO, the genotype with the highest relative NBI was MFOL-1547 (*OzT8* + *OzT9*), followed by MFOL-1926 (*OzT9*) and MFOL-2388 (*OzT8* + *OzT9*) (Figure 21B).

Breeding lines from Binadhan-11 X Kasalath cross

At 80 DAO exposure, breeding lines containing *OzT9* exhibited the highest average relative NDVI values, followed by lines carrying *OzT8* and those containing both QTLs (*OzT8* + *OzT9*) (Figure 18A). However, at 109 DAO, breeding lines containing *OzT8* recorded the highest average relative NDVI values, followed by lines with *OzT9* and those carrying both QTLs (*OzT8*

+ *OzT9*) (Figure 18B). Among all genotypes evaluated at 80 DAO, the highest relative NDVI was observed in MFOL-1031 (*OzT9*), followed by MFOL-1102 (*OzT9*), MFOL-1001 (*OzT9*), MFOL-579 (*OzT8* + *OzT9*), and MFOL-1163 (*OzT8*). Conversely, at 109 DAO, the highest relative NDVI was recorded for MFOL-1135 (*OzT8*), followed by MFOL-1163 (*OzT8*), MFOL-579 (*OzT8* + *OzT9*), and MFOL-1031 (*OzT9*).

Breeding lines carrying the *OzT9* QTL exhibited the highest average relative Lic2 values at 80 DAO exposure, followed by lines containing *OzT8* and those possessing both QTLs (*OzT8* + *OzT9*) (Figure 20A). However, at 109 DAO, lines carrying *OzT8* recorded the highest average relative Lic2 values, followed by those containing *OzT9* and lines harboring both QTLs (*OzT8* + *OzT9*) (Figure 20B). Among the genotypes evaluated at 80 DAO, the highest relative Lic2 value was observed in MFOL-1102 (*OzT9*), followed by MFOL-1135 (*OzT8*) and MFOL-1031 (*OzT9*). In contrast, at 109 DAO, the highest relative Lic2 value was recorded for MFOL-1135 (*OzT8*), followed by MFOL-1163 (*OzT8*) and MFOL-1011 (*OzT9*).

At 80 DAO, breeding lines with only QTL *OzT9* exhibited the highest average relative NBI, followed by those with only QTL *OzT8*, and then lines with both QTLs (*OzT8* + *OzT9*) (Figure 22A). A comparable pattern was observed at 109 DAO (Figure 22B). Among all genotypes assessed at 80 DAO, the line MFOL-1102, carrying QTL *OzT9*, demonstrated the highest relative NBI, followed by MFOL-1135 and MFOL-1281, both of which harbor QTL *OzT8* (Figure 22A). Similarly, at 109 DAO, the highest relative NBI was observed in MFOL-1135 (*OzT8*), followed by MFOL-1302 and MFOL-1031, both of which contained QTL *OzT9* (Figure 22B).

Together, these results suggested that breeding lines from the BRRI Dhan28 × Kasalath cross demonstrated that lines containing both QTLs (*OzT8* + *OzT9*) exhibited the highest average relative NDVI, Lic2, and NBI values at both 80 and 109 DAO, with notable performance by genotypes MFOL-2388, MFOL-1378, and MFOL-1488. For the Binadhan-11 × Kasalath cross, lines carrying *OzT9* QTL outperformed others in average relative NDVI and Lic2 at 80 DAO, while those with *OzT8* QTL showed higher values at 109 DAO. At 80 DAO, the highest relative NBI was recorded in lines carrying only QTL *OzT9*, whereas at 109 DAO, *OzT8* QTL lines demonstrated superior NBI values. Key genotypes like MFOL-1135, MFOL-1031, MFOL-1102, and MFOL-1163 showed superior performance across metrics. Overall, genotypes carrying both QTLs (*OzT8* + *OzT9*) generally performed better in the BRRI Dhan28 cross, while individual QTLs showed dominance in the Binadhan-11 cross depending on the specific trait

and observation period. These results emphasize the impact of particular QTLs on physiological characteristics, varying by genotype and developmental stages.

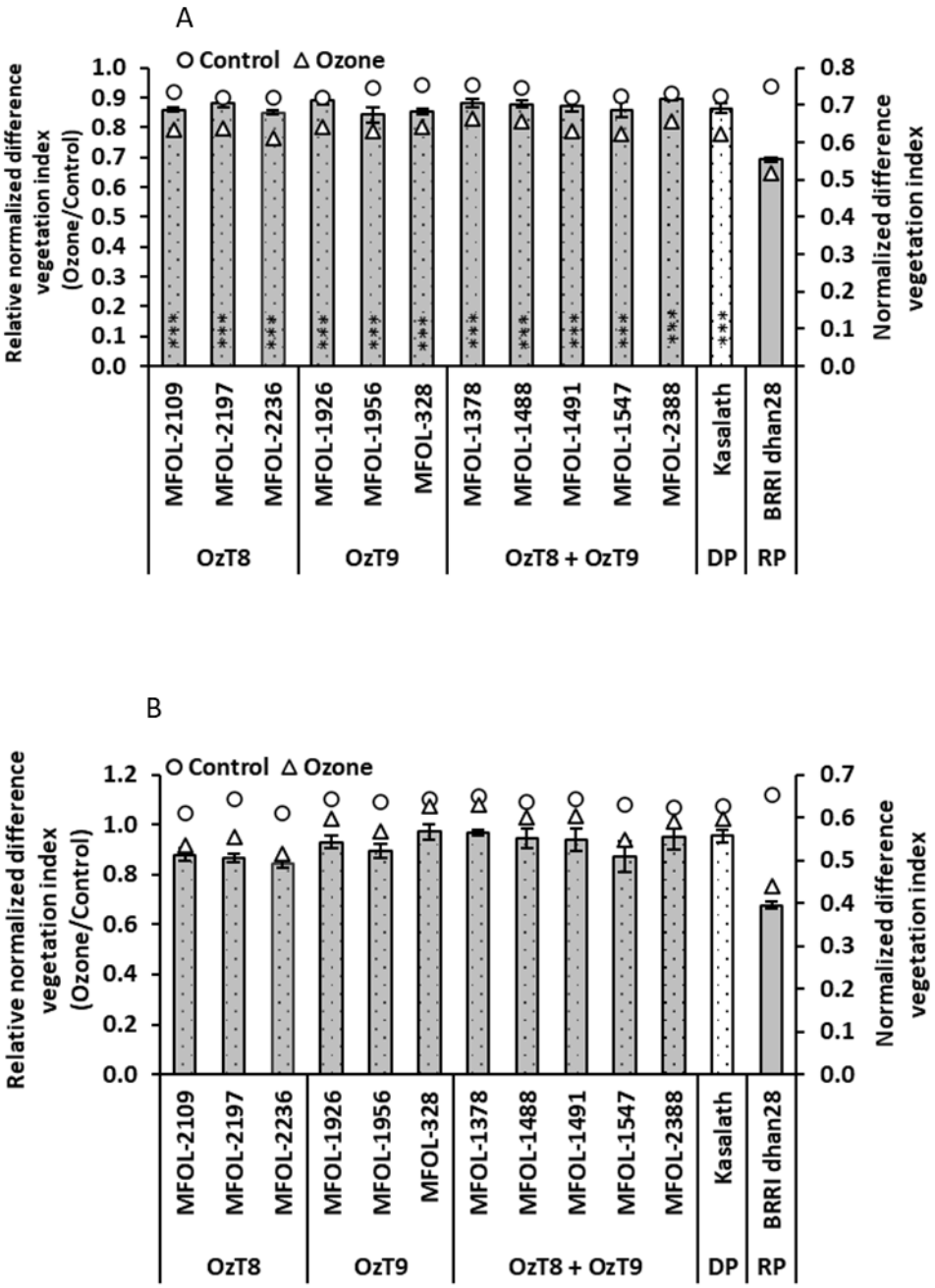

Figure 17 Normalized difference vegetation index of selected breeding lines carrying *OzT8* and/or *OzT9* derived from the cross BRRI dhan28 × Kasalath under ozone stress and control conditions at (A) 80 DAO and (B) 109 DAO. The bar graphs display the mean and standard error of relative values (n = 3), while the circles and triangles represent absolute values for the control and ozone-treated groups, respectively. Asterisks within the bars indicate significant differences between the genotypes and the recipient parent (BRRI dhan28), as determined by Dunnett's test (*P < 0.05, **P < 0.01, ***P < 0.001). DP, donor parent, and RP, recipient parent.

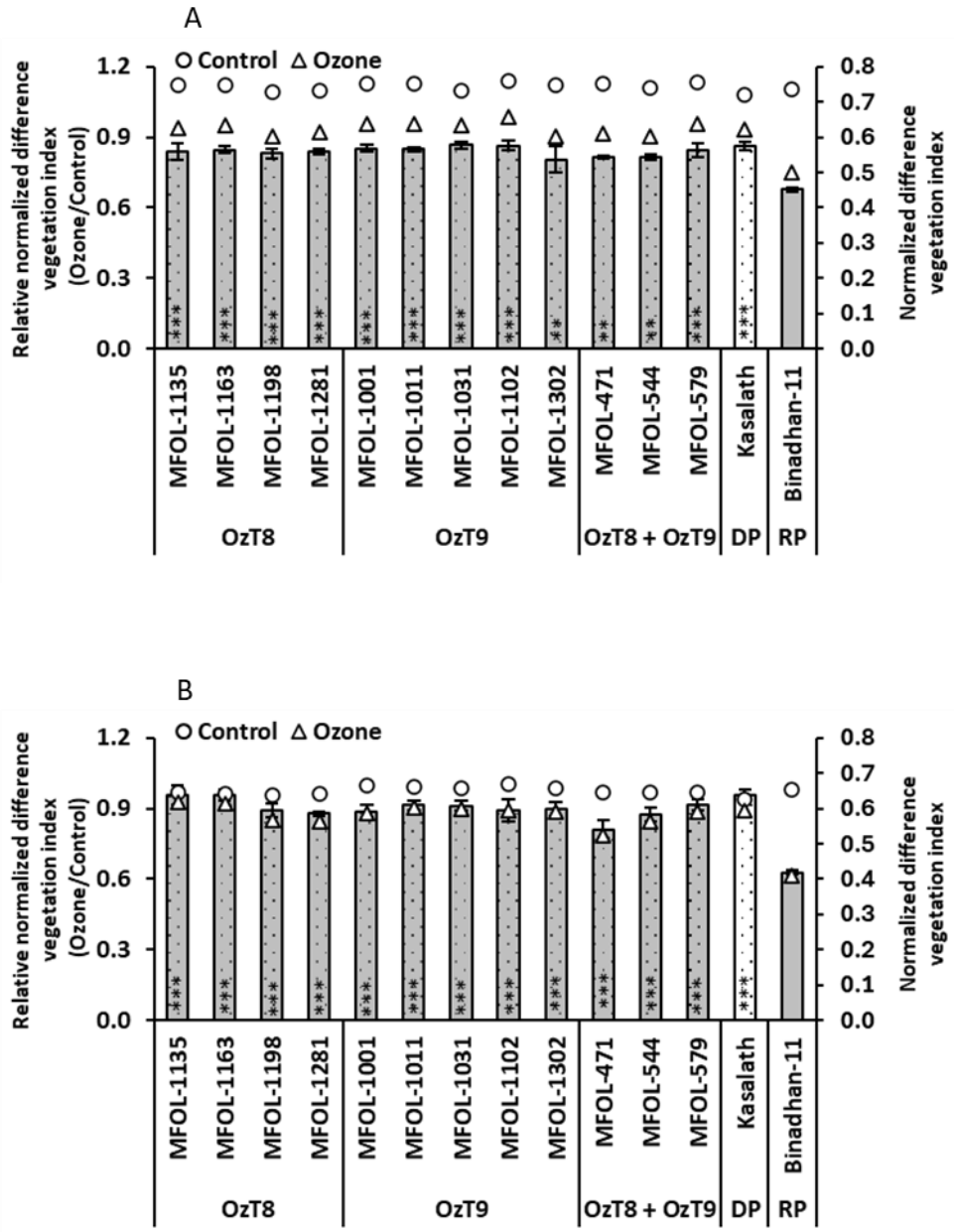

Figure 18 Normalized difference vegetation index of selected breeding lines carrying *OzT8* and/or *OzT9* derived from the cross Binadhan-11 × Kasalath under ozone stress and control conditions at (A) 80 DAO and (B) 109 DAO. The bar graphs display the mean and standard error of relative values (n = 3), while the circles and triangles represent absolute values for the control and ozone-treated groups, respectively. Asterisks within the bars indicate significant differences between the genotypes and the recipient parent (Binadhan-11), as determined by Dunnett's test (*P < 0.05, **P < 0.01, ***P < 0.001). DP, donor parent, and RP, recipient parent.

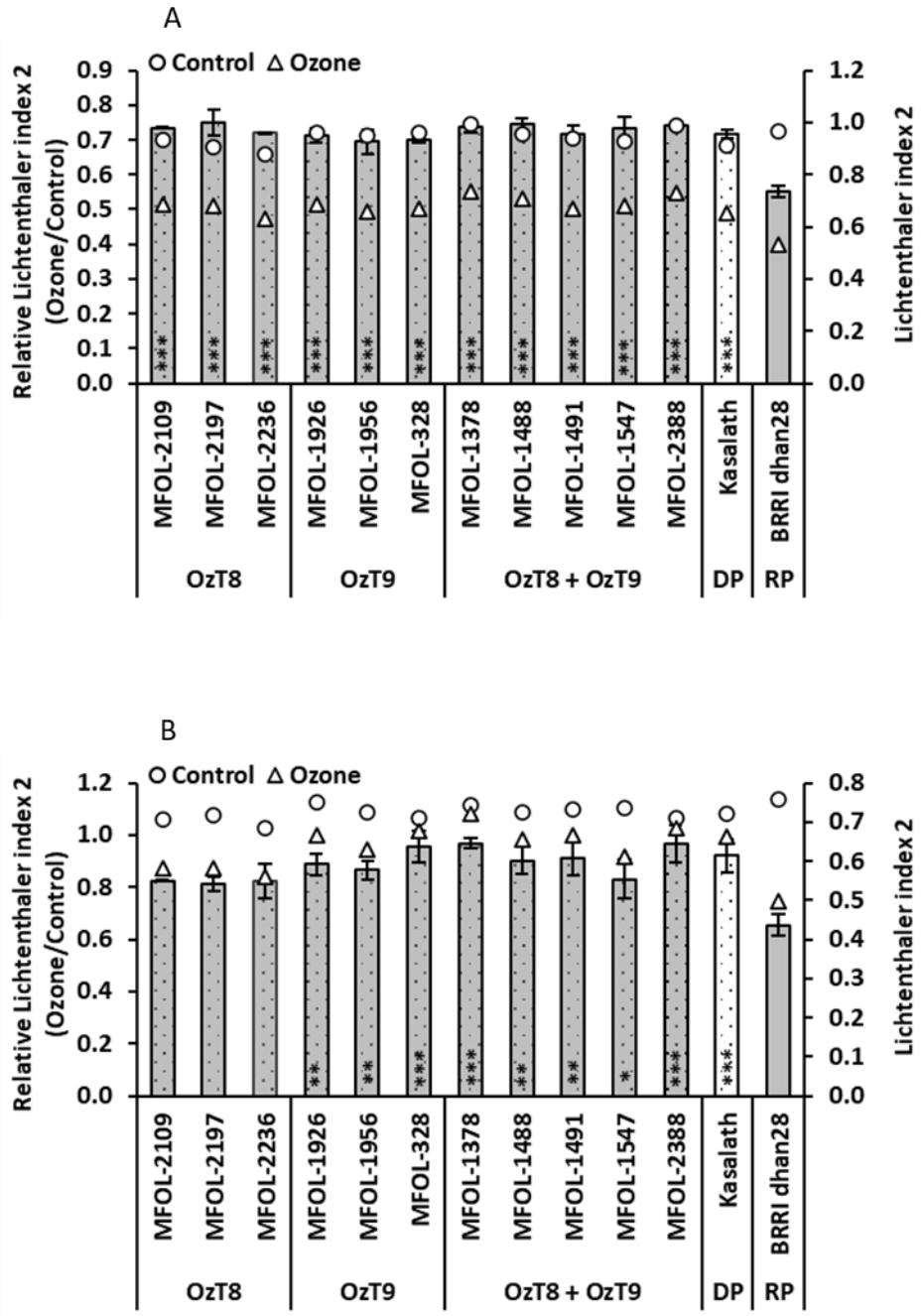

Figure 19 Lichtenthaler index 2 of selected breeding lines carrying *OzT8* and/or *OzT9* derived from the cross BRRI dhan28 × Kasalath under ozone stress and control conditions at (A) 80 DAO and (B) 109 DAO. The bar graphs display the mean and standard error of relative values (n = 3), while the circles and triangles represent absolute values for the control and ozone-treated groups, respectively. Asterisks within the bars indicate significant differences between the genotypes and the recipient parent (BRRI dhan28), as determined by Dunnett's test (*P < 0.05, **P < 0.01, ***P < 0.001). DP, donor parent, and RP, recipient parent.

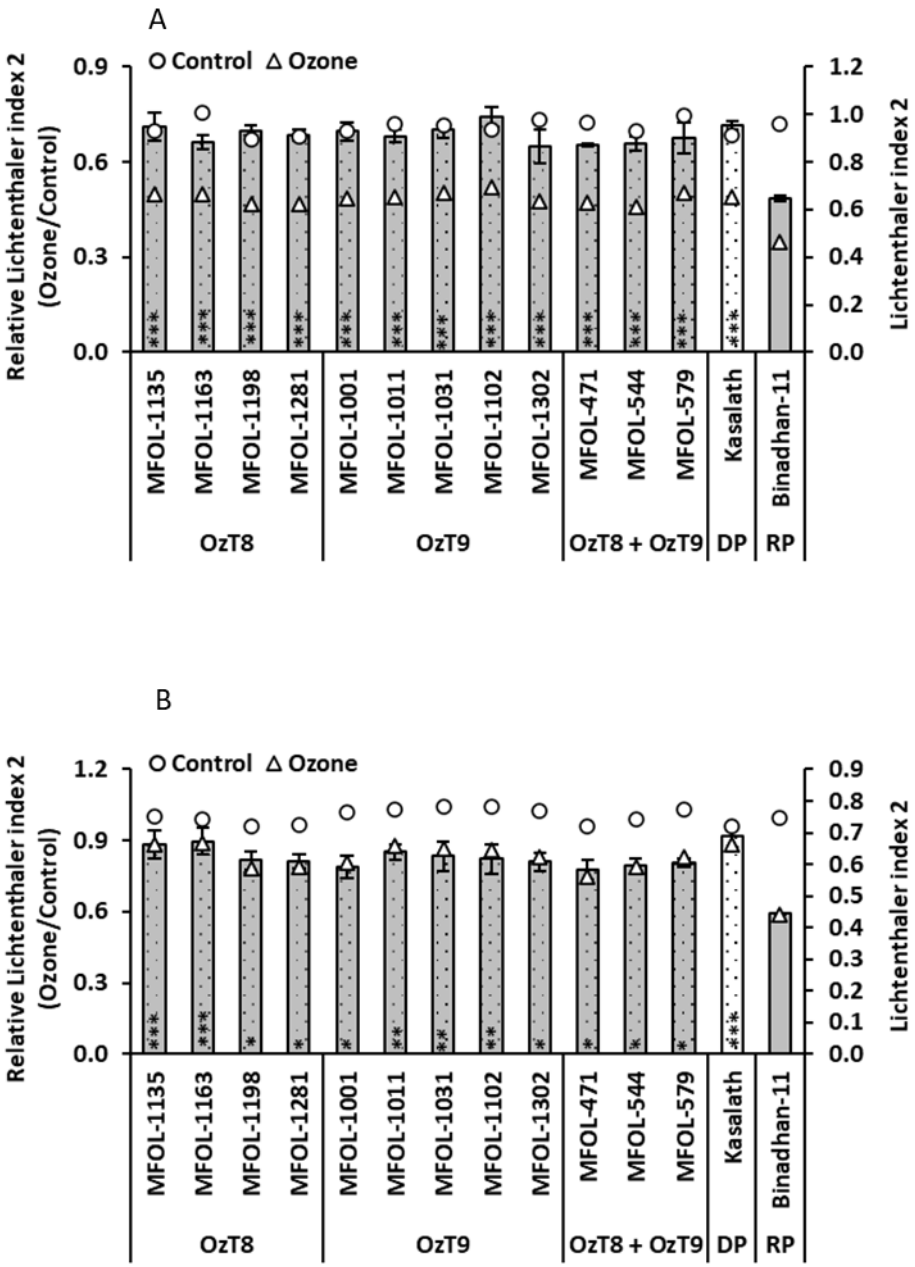

Figure 20 Lichtenthaler index 2 of selected breeding lines carrying *OzT8* and/or *OzT9* derived from the cross Binadhan-11 × Kasalath under ozone stress and control conditions at (A) 80 DAO and (B) 109 DAO. The bar graphs display the mean and standard error of relative values (n = 3), while the circles and triangles represent absolute values for the control and ozone-treated groups, respectively. Asterisks within the bars indicate significant differences between the genotypes and the recipient parent (Binadhan-11), as determined by Dunnett's test (*P < 0.05, **P < 0.01, ***P < 0.001). DP, donor parent, and RP, recipient parent.

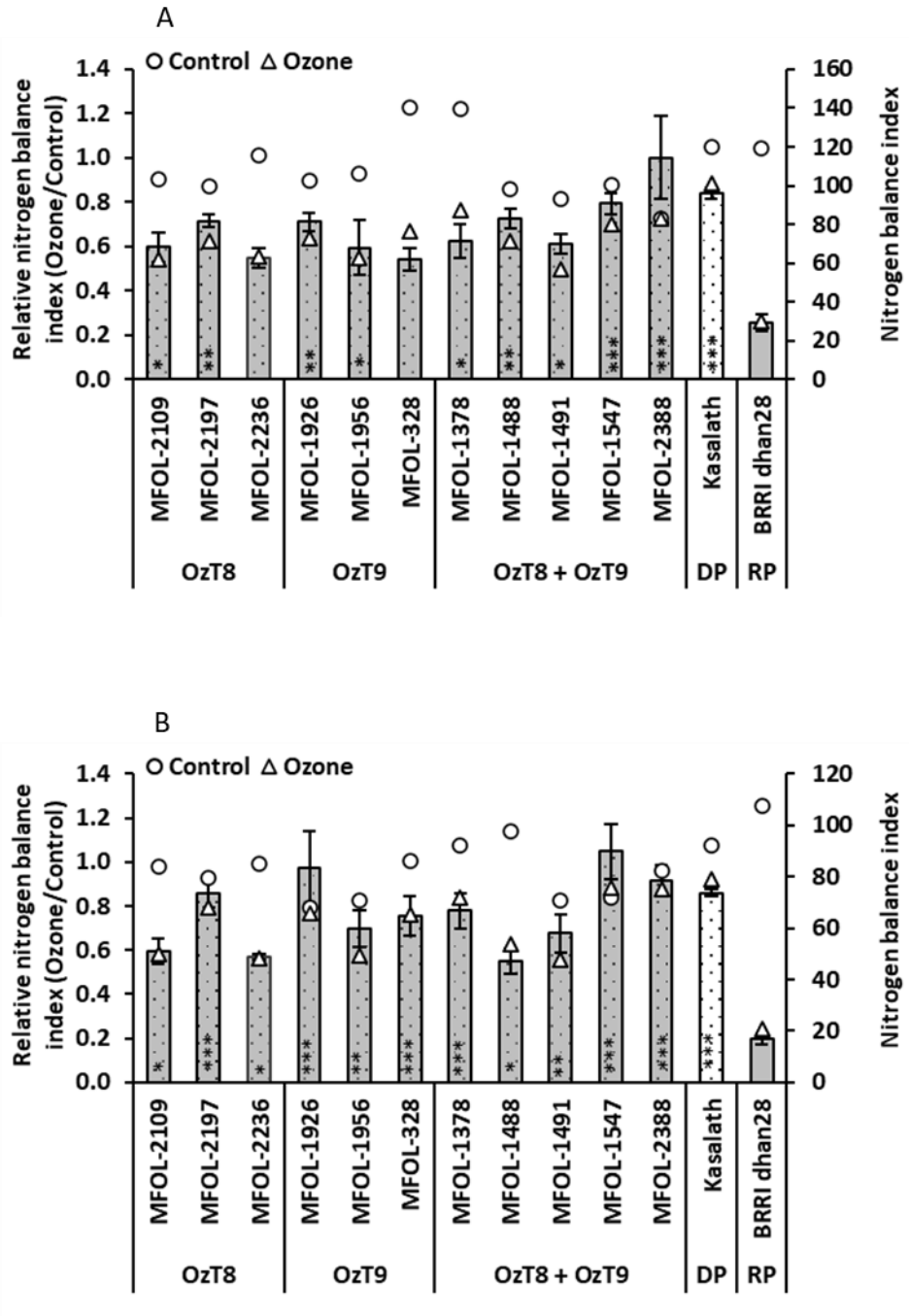

Figure 21 Nitrogen balance index of selected breeding lines carrying *OzT8* and/or *OzT9* derived from the cross BRRI dhan28 × Kasalath under ozone stress and control conditions at (A) 80 DAO and (B) 109 DAO. The bar graphs display the mean and standard error of relative values (n = 3), while the circles and triangles represent absolute values for the control and ozone-treated groups, respectively. Asterisks within the bars indicate significant differences between the genotypes and the recipient parent (BRRI dhan28), as determined by Dunnett's test (*P < 0.05, **P < 0.01, ***P < 0.001). DP, donor parent, and RP, recipient parent.

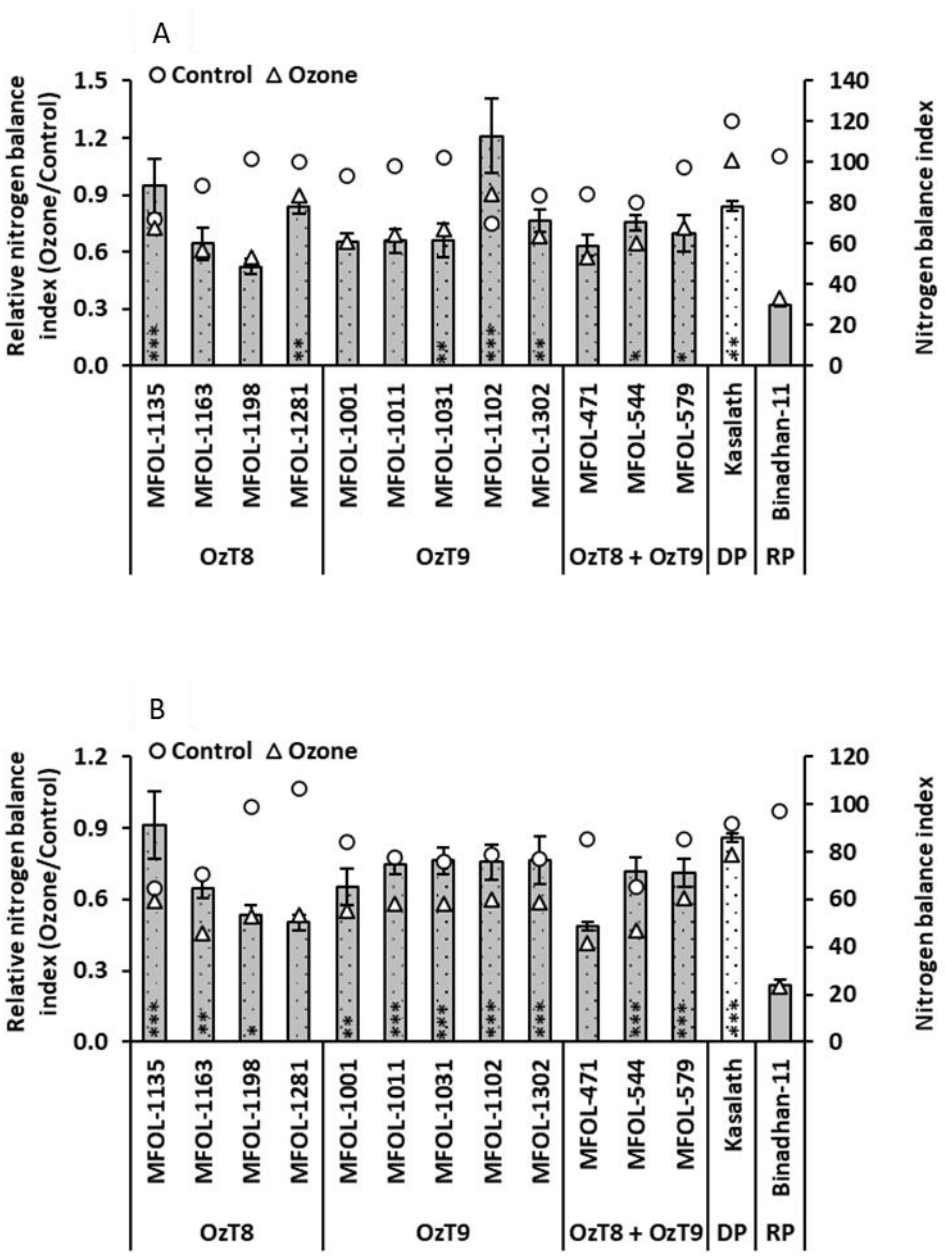

Figure 22 Nitrogen balance index of selected breeding lines carrying *OzT8* and/or *OzT9* derived from the cross Binadhan-11 × Kasalath under ozone stress and control conditions at (A) 80 DAO and (B) 109 DAO. The bar graphs display the mean and standard error of relative values (n = 3), while the circles and triangles represent absolute values for the control and ozone-treated groups, respectively. Asterisks within the bars indicate significant differences between the genotypes and the recipient parent (Binadhan-11), as determined by Dunnett's test (*P < 0.05, **P < 0.01, ***P < 0.001). DP, donor parent, and RP, recipient parent.

4.3.5 Assessment of breeding lines for photosynthetic efficiency

Breeding lines from BRRI Dhan28 X Kasalath cross

The quantum efficiency of photosystem II (PhiPS2) was evaluated in selected breeding lines of BRRI dhan28 at 80 and 109 DAO. At 80 DAO, the breeding lines MFOL-2236 (*OzT8*), MFOL-1926 (*OzT9*), MFOL-328 (*OzT9*), MFOL-1488 (*OzT8* + *OzT9*), and MFOL-2388 (*OzT8* + *OzT9*) exhibited significantly higher PhiPS2 compared to the recurrent parent, BRRI dhan28 (Figure 23A). By 109 DAO, all breeding lines demonstrated significantly improved relative PhiPS2 BRRI dhan28 (Figure 23B). Lines carrying the *OzT9* QTL alone displayed the highest average relative PhiPS2 at 80 DAO, followed by those containing both QTLs (*OzT8* + *OzT9*), and then lines with *OzT8* alone (Figure 23A). At 109 DAO, breeding lines possessing both QTLs (*OzT8* + *OzT9*) showed the highest average relative PhiPS2, with lines carrying *OzT9* alone and *OzT8* alone ranking second and third, respectively (Figure 23B). Among individual genotypes at 80 DAO, MFOL-1488 (*OzT8* + *OzT9*) recorded the highest relative PhiPS2, followed by MFOL-1926 (*OzT9*) and MFOL-2236 (OzT8) (Figure 23A). At 109 DAO, the highest relative PhiPS2 was observed in MFOL-1491 (*OzT8* + *OzT9*), with MFOL-328 (OzT9) and MFOL-1488 (*OzT8* + *OzT9*) ranking second and third, respectively (Figure 23B).

None of the breeding lines exhibited a statistically significant electron transport rate (ETR) compared to the recipient parent, BRRI dhan28, at 80 and 109 DAO (Figure 25A, B). At 80 DAO, lines carrying the *OzT8* QTL alone demonstrated the highest mean relative ETR, followed by those with the *OzT9* QTL and lines harboring both QTLs (*OzT8* + *OzT9*) (Figure 25A). By 109 DAO, the highest mean relative ETR was observed in breeding lines possessing both QTLs (*OzT8* + *OzT9*), with lines carrying *OzT8* and *OzT9* individually ranking second and third, respectively (Figure 25B). Among individual genotypes at 80 DAO, MFOL-2236 (*OzT8*) displayed the highest relative ETR, followed by MFOL-1378 (*OzT8* + *OzT9*) and MFOL-2109 (*OzT8*) (Figure 25A). At 109 DAO, the genotype MFOL-1547 (*OzT8* + *OzT9*) exhibited the highest relative ETR, with MFOL-2236 (*OzT8*) and MFOL-1488 (*OzT8* + *OzT9*) ranked as the second and third highest, respectively (Figure 25B).

Breeding lines from Binadhan-11 X Kasalath cross

At 80 DAO, the genotypes MFOL-1135, MFOL-1163, and MFOL-1281, all of which harbor the *OzT8* QTL, along with MFOL-1031 (*OzT9*), exhibited significantly higher relative PhiPS2 values compared to the recipient parent, Binadhan-11 (Figure 24A). At 109 DAO, the breeding lines

MFOL-1135 (*OzT8*), MFOL-1001, MFOL-1011, and MFOL-1102, all harboring the *OzT9* QTL, demonstrated significantly improved relative PhiPS2 (Figure 24B). At 80 DAO, lines carrying only the *OzT8* QTL showed the highest average relative PhiPS2, followed by those with both QTLs (*OzT8* + *OzT9*), and those with *OzT9* alone (Figure 24A). However, at 109 DAO, lines containing the *OzT9* QTL alone exhibited the highest average relative PhiPS2, while those with *OzT8* alone and those with both QTLs (*OzT8* + *OzT9*) ranked second and third, respectively (Figure 24B). Among individual genotypes at 80 DAO, MFOL-1163 (*OzT8*) recorded the highest relative PhiPS2, followed by MFOL-1031 (*OzT9*), MFOL-1281 (*OzT8*), and MFOL-1135 (*OzT8*) (Figure 24A). At 109 DAO, MFOL-1135 (*OzT8*) achieved the highest relative PhiPS2, followed by MFOL-1011, MFOL-1001, MFOL-1102, and MFOL-1302, all of which carry the *OzT9* QTL (Figure 24B).

None of the breeding lines exhibited a statistically significant electron transport rate (ETR) compared to the recipient parent, Binadhan-11, at 80 and 109 DAO (Figure 26A, B). At 80 DAO, lines carrying the *OzT9* QTL alone demonstrated the highest average relative ETR, followed by lines harboring the *OzT8* QTL and those containing both QTLs (*OzT8* + *OzT9*) (Figure 26A). At 109 DAO, lines carrying the *OzT8* QTL exhibited the highest average relative ETR, with lines carrying the *OzT9* QTL and those possessing both QTLs (*OzT8* + *OzT9*) ranking second and third, respectively (Figure 26B). Among individual genotypes at 80 DAO, MFOL-1135 (*OzT8*) displayed the highest relative ETR, followed by MFOL-1302 (*OzT9*) and MFOL-1031 (*OzT9*) (Figure 26A). At 109 DAO, the highest relative ETR was observed in MFOL-1281 (*OzT8*), with MFOL-1011 (*OzT9*) and MFOL-1135 (*OzT8*) ranking second and third, respectively (Figure 26B).

Together, these results suggested that among the QTLs, *OzT9* alone showed the highest PhiPS2 at 80 DAO, while at 109 DAO, lines with both QTLs (*OzT8* + *OzT9*) exhibited the highest PhiPS2 in the BRRI dhan28 cross. In the Binadhan-11 cross, *OzT8* alone performed best at 80 DAO, but *OzT9* surpassed other QTL combinations by 109 DAO for PhiPS2. The top-performing genotypes for PhiPS2 in the BRRI dhan28 cross were MFOL-1488 (*OzT8* + *OzT9*) and MFOL-1491 (*OzT8* + *OzT9*), while in the Binadhan-11 cross, MFOL-1163 (*OzT8*) and MFOL-1135 (*OzT8*) excelled. Although significant improvements in PhiPS2 were observed, none of the breeding lines showed statistically significant enhancements in ETR compared to their respective recipient parents.

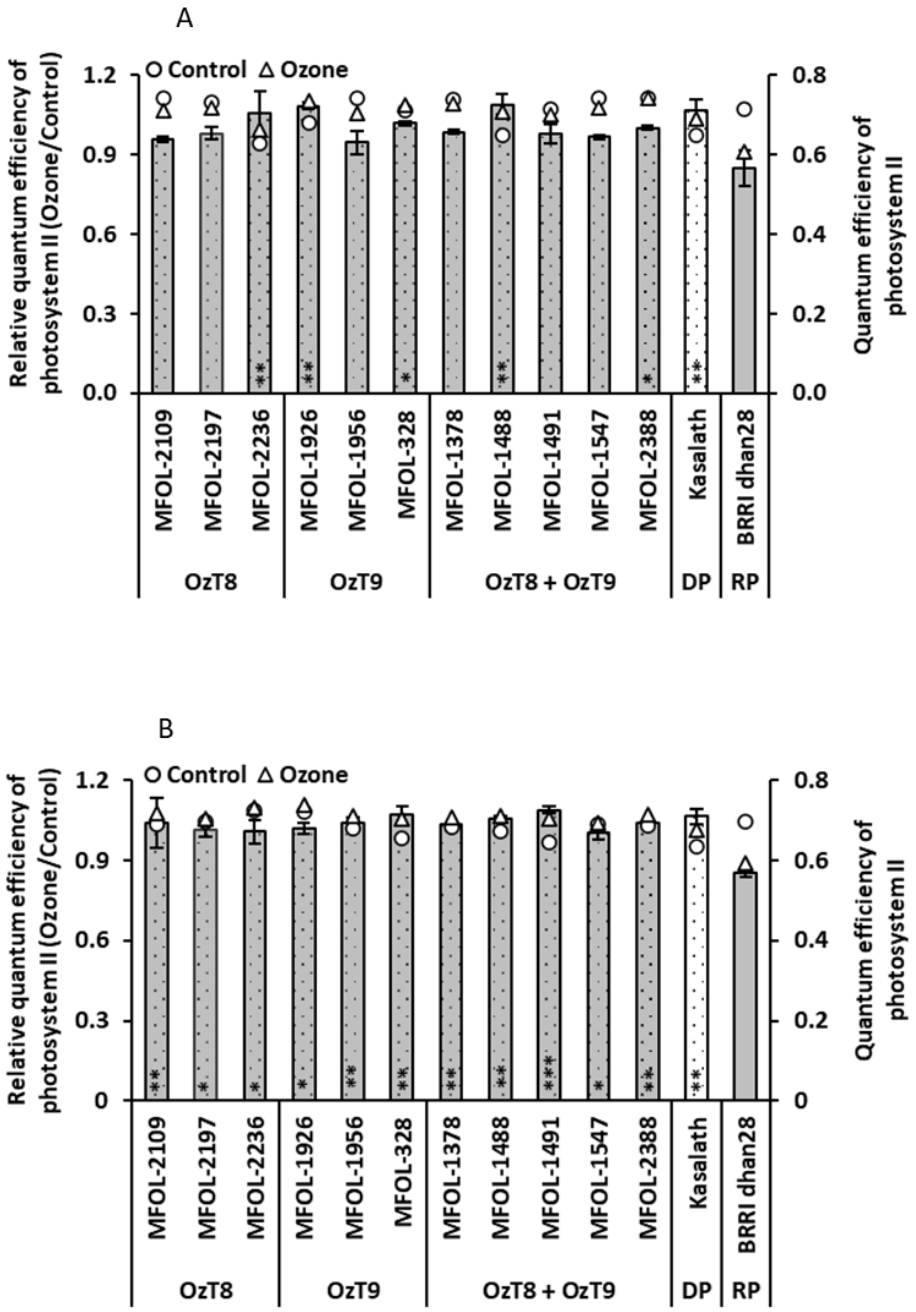

Figure 23 Quantum efficiency of photosystem II (PhiPS2) of selected breeding lines carrying *OzT8* and/or *OzT9* derived from the cross BRRI dhan28 × Kasalath under ozone stress and control conditions at (A) 80 DAO and (B) 109 DAO. The bar graphs display the mean and standard error of relative values (n = 3), while the circles and triangles represent absolute values for the control and ozone-treated groups, respectively. Asterisks within the bars indicate significant differences between the genotypes and the recipient parent (BRRI dhan28), as determined by Dunnett's test (*P < 0.05, **P < 0.01, ***P < 0.001). DP, donor parent, and RP, recipient parent.

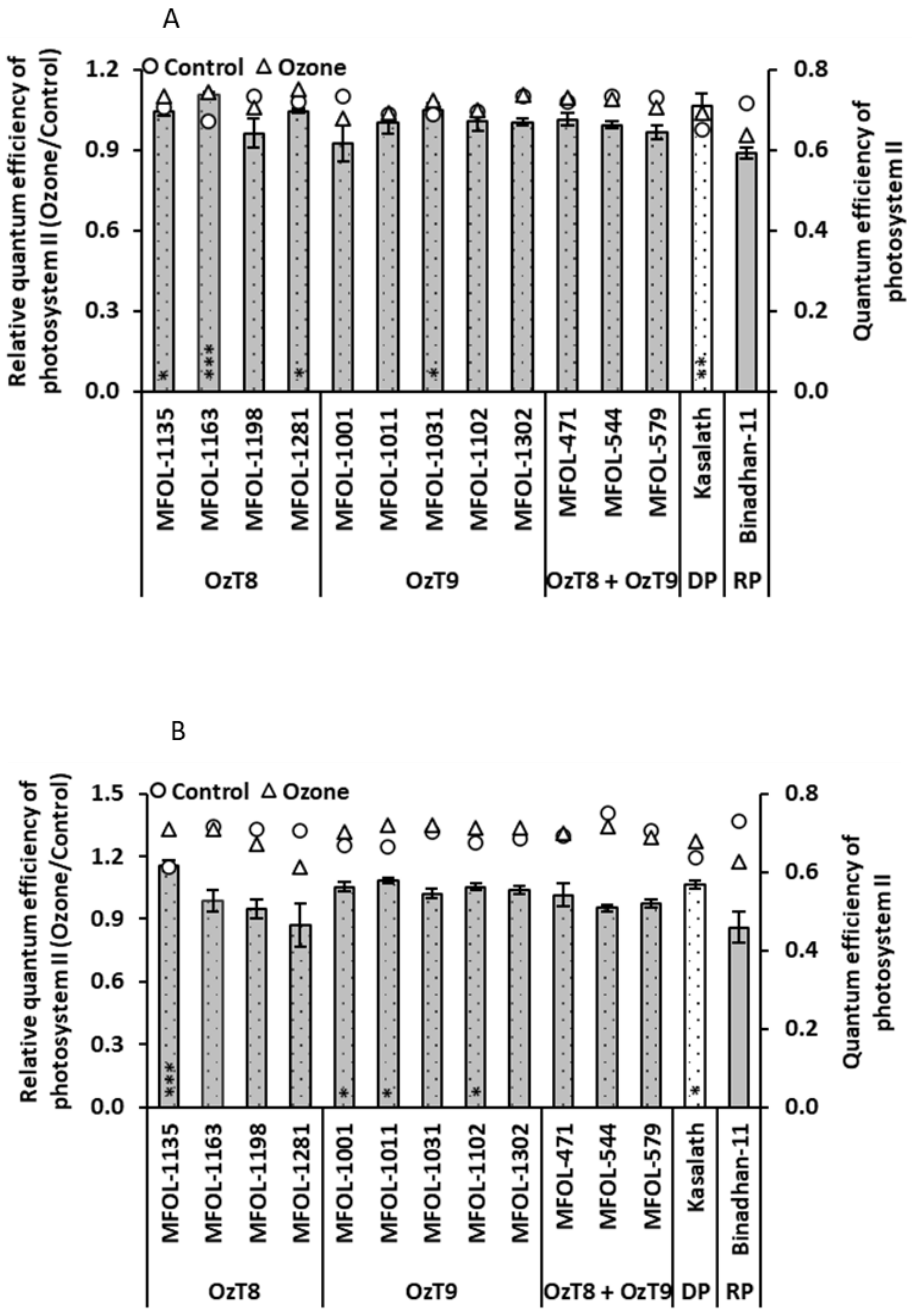

Figure 24 Quantum efficiency of photosystem II (PhiPS2) of selected breeding lines carrying *OzT8* and/or *OzT9* derived from the cross Binadhan-11 × Kasalath under ozone stress and control conditions at (A) 80 DAO and (B) 109 DAO. The bar graphs display the mean and standard error of relative values (n = 3), while the circles and triangles represent absolute values for the control and ozone-treated groups, respectively. Asterisks within the bars indicate significant differences between the genotypes and the recipient parent (Binadhan-11), as determined by Dunnett's test (*P < 0.05, **P < 0.01, ***P < 0.001). DP, donor parent, and RP, recipient parent.

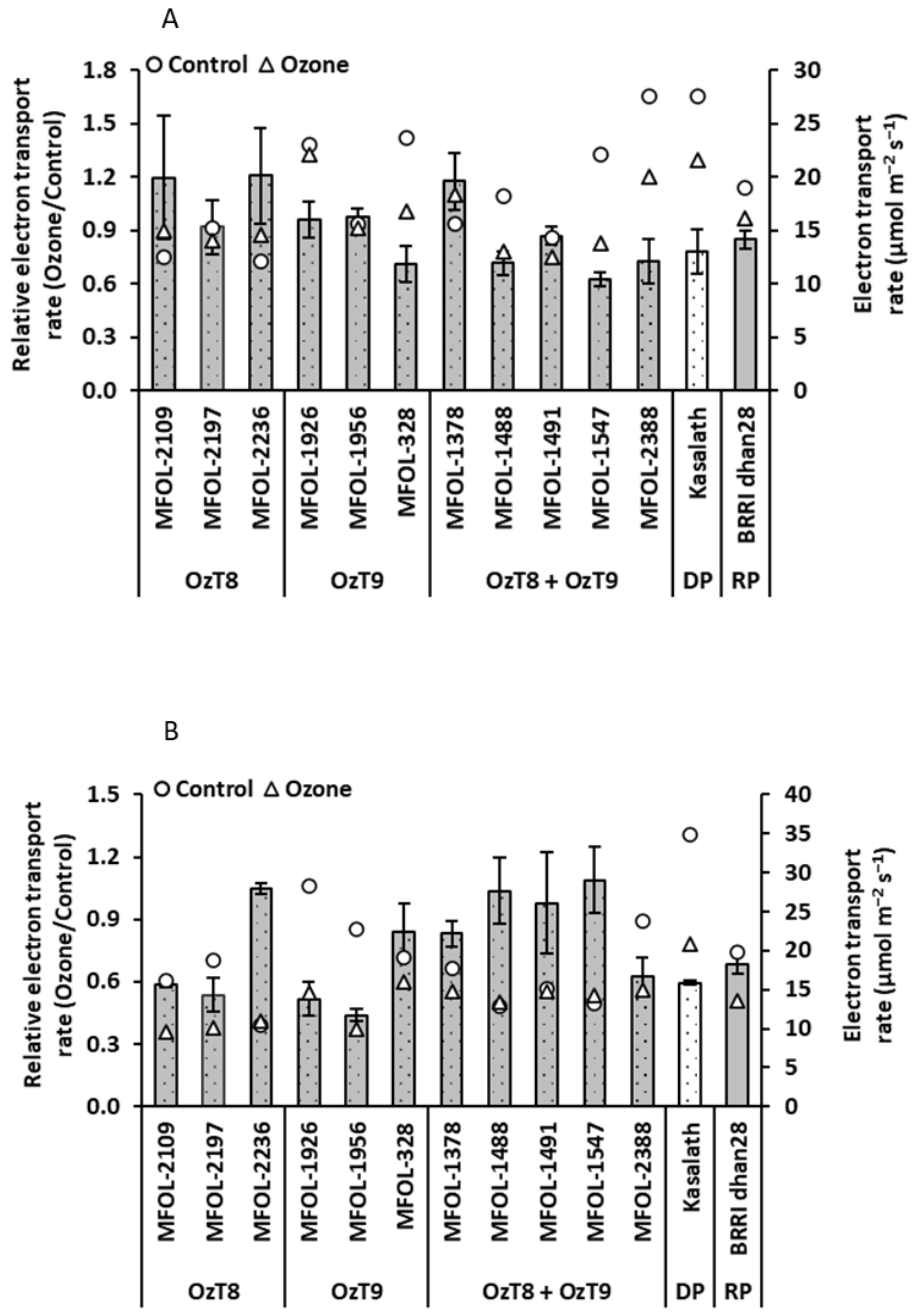

Figure 25 Electron transport rate (ETR) of selected breeding lines carrying *OzT8* and/or *OzT9* derived from the cross BRRI dhan28 × Kasalath under ozone stress and control conditions at (A) 80 DAO and (B) 109 DAO. The bar graphs display the mean and standard error of relative values (n = 3), while the circles and triangles represent absolute values for the control and ozone-treated groups, respectively. There are no significant differences between the genotypes and the recipient parent (BRRI dhan28), as determined by Dunnett's test (*P < 0.05, **P < 0.01, ***P < 0.001). DP, donor parent, and RP, recipient parent.

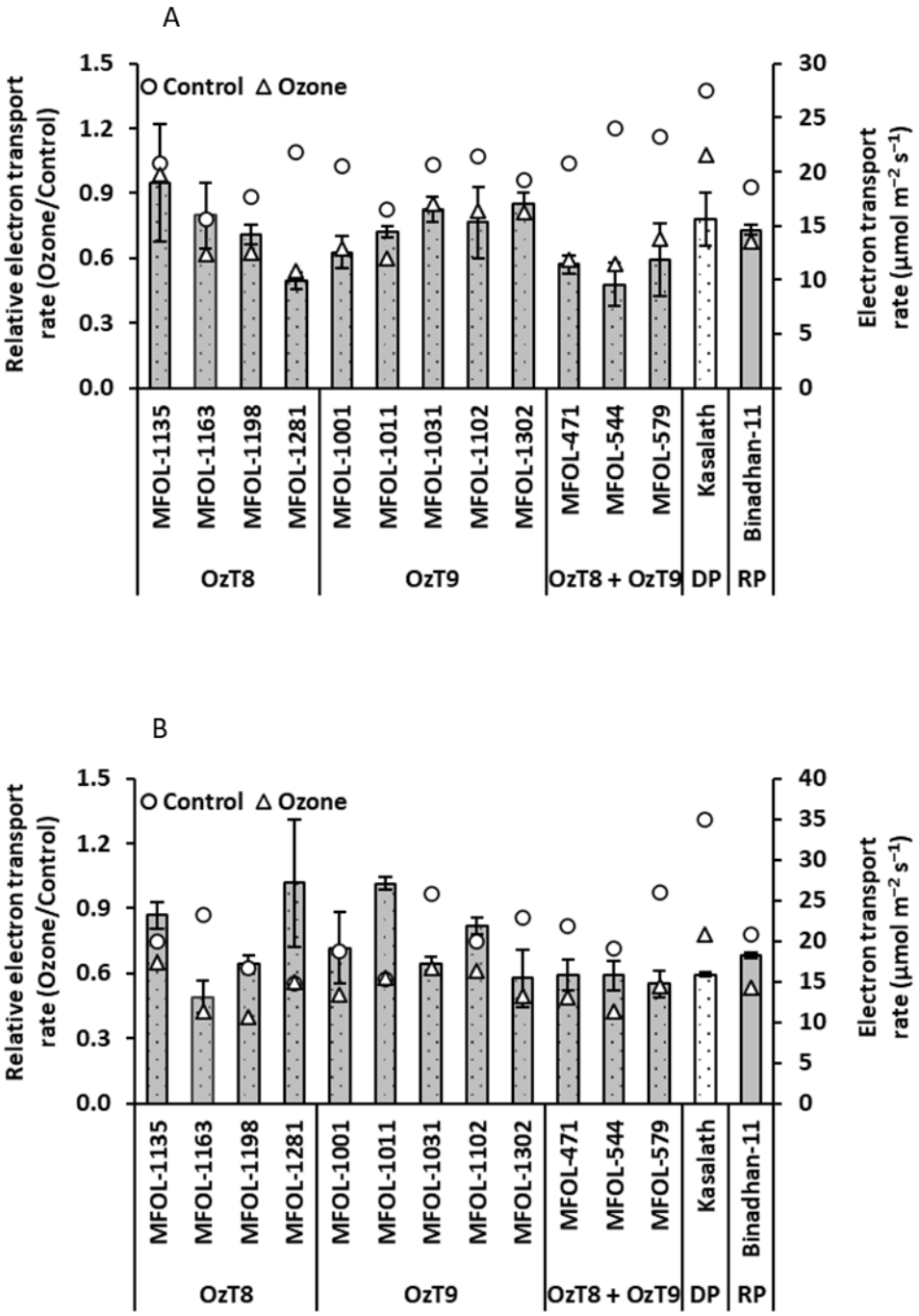

Figure 26 Electron transport rate (ETR) of selected breeding lines carrying *OzT8* and/or *OzT9* derived from the cross Binadhan-11 × Kasalath under ozone stress and control conditions at (A) 80 DAO and (B) 109 DAO. The bar graphs display the mean and standard error of relative values (n = 3), while the circles and triangles represent absolute values for the control and ozone-treated groups, respectively. There are no significant differences between the genotypes and the recipient parent (Binadhan-11), as determined by Dunnett's test (*P < 0.05, **P < 0.01, ***P < 0.001). DP, donor parent, and RP, recipient parent.

4.3.6 Gas exchange dynamics in breeding lines

Breeding lines from BRRI Dhan28 X Kasalath cross

At 80 DAO, the breeding line MFOL-328, carrying the *OzT9* QTL, exhibited significantly higher stomatal conductance (gsw) than its recipient parent, BRRI dhan 28. However, at 109 DAO, none of the breeding lines demonstrated better relative gsw than BRRI dhan 28. Breeding lines carrying both QTLs (*OzT8* + *OzT9*) displayed the highest average relative gsw across 80 and 109 DAO, followed by lines carrying *OzT9* alone and *OzT8* alone, ranking second and third, respectively (Figure 27A, B). Among individual genotypes at 80 DAO, MFOL-328 (*OzT9*) recorded the highest relative gsw, followed by MFOL-2388 (*OzT8* + *OzT9*) and MFOL-1491 (*OzT8* + *OzT9*) (Figure 27A). At 109 DAO, the highest relative gsw was observed in MFOL-1926 (*OzT9*), with MFOL-1378 (*OzT8* + *OzT9*) and MFOL-2388 (*OzT8* + *OzT9*) ranking second and third, respectively (Figure 27B).

Breeding lines from Binadhan-11 X Kasalath cross

At 80 DAO, the breeding line MFOL-1198, which carries the *OzT8* QTL, and MFOL-544, carrying both QTLs (*OzT8* + *OzT9*), exhibited significantly higher stomatal conductance (gsw) compared to the recipient parent, Binadhan-11. However, by 109 DAO, none of the breeding lines demonstrated a superior relative gsw compared to Binadhan-11 (Figure 28A, B). At 80 DAO, breeding lines with the *OzT8* QTL displayed the highest average relative gsw, followed by lines carrying both QTLs (*OzT8* + *OzT9*), and those with *OzT9* alone (Figure 28A). Similarly, at 109 DAO, lines with *OzT8* maintained the highest average relative gsw, followed by lines carrying *OzT9* and those carrying both QTLs (*OzT8* + *OzT9*) (Figure 28B). Among individual genotypes, MFOL-544 (*OzT8* + *OzT9*) exhibited the highest relative gsw at 80 DAO, followed by MFOL-1198 (*OzT8*) and MFOL-1135 (*OzT8*) (Figure 28A). In contrast, at 109 DAO, MFOL-1031 (*OzT9*) showed the highest relative gsw, with MFOL-1163 (*OzT8*) and MFOL-1302 (*OzT9*) ranking second and third, respectively (Figure 28B).

We selected six breeding lines in the BRRI dhan 28 background and six breeding lines in the Binadhan-11 background to measure the CO_2 assimilation rate (µmol m^{-2} s^{-1}), transpiration rate (mol m^{-2} s^{-1}), and intercellular CO_2 concentration (µmol mol^{-1}). Our selection included two lines from each QTL group for the measurement at 116 DAO.

Breeding lines from BRRI Dhan28 X Kasalath cross

At 116 DAO, none of the breeding lines exhibited a significantly higher relative transpiration rate than BRRI dhan28. Among the lines, those carrying the *OzT9* QTL demonstrated the highest average relative transpiration rate, followed by lines with the *OzT8* QTL and those carrying both QTLs (*OzT8* + *OzT9*), which ranked second and third, respectively (Figure 29A). Within the BRRI dhan28 genotypes, MFOL-2236 (*OzT8*) recorded the highest transpiration rate, followed by MFOL-328 (*OzT9*) and MFOL-1956 (*OzT9*) (Figure 29A).

Similarly, none of the breeding lines exhibited a significantly higher relative intercellular CO_2 concentration than BRRI dhan28 at 116 DAO. Breeding lines possessing the *OzT8* QTL demonstrated the highest average relative intercellular CO_2 concentration, followed by those carrying both QTLs and then lines with the *OzT9* QTL, ranking second and third, respectively (Figure 30A). Among the individual genotypes, MFOL-2197 (*OzT8*) exhibited the highest transpiration rate, followed by MFOL-2388 (*OzT8* + *OzT9*) and MFOL-2236 (*OzT8*) (Figure 30A).

Breeding lines derived from BRRI dhan28 exhibited a significantly higher relative net CO_2 assimilation rate than the parental line, BRRI dhan28 (Figure 31A). Those carrying both QTLs (*OzT8* + *OzT9*) demonstrated the highest average relative net CO_2 assimilation rate among the lines evaluated. Lines carrying the *OzT9* QTL ranked second, while those with the *OzT8* QTL ranked third (Figure 31A). Among individual genotypes, MFOL-1547 (*OzT8* + *OzT9*) displayed the highest relative net CO_2 assimilation rate, followed by MFOL-2388 (*OzT8* + *OzT9*) and MFOL-1956 (*OzT9*) (Figure 31A).

Breeding lines from Binadhan-11 X Kasalath cross

None of the breeding lines exhibited a significantly higher relative transpiration rate than Binadhan-11 at 116 DAO. Breeding lines harboring the *OzT8* QTL demonstrated the highest average relative transpiration rate, followed by lines with the *OzT9* QTL and those possessing both QTLs (*OzT8* + *OzT9*), which ranked second and third, respectively (Figure 29B). Among individual genotypes, MFOL-1135 (*OzT8*) recorded the highest transpiration rate, followed by MFOL-544 (*OzT8* + *OzT9*) and MFOL-1102 (*OzT9*) (Figure 29B).

At 116 DAO, none of the breeding lines exhibited a significantly higher relative intercellular CO_2 concentration than Binadhan-11. Among the evaluated lines, those carrying both QTLs (*OzT8* + *OzT9*) exhibited the highest average relative intercellular CO_2 concentration, followed by lines carrying the *OzT8* QTL, and finally, those with the *OzT9* QTL, ranking second and third,

respectively (Figure 30B). Among the individual genotypes, MFOL-471 (*OzT8* + *OzT9*) showed the highest relative intercellular CO_2 concentration, followed by MFOL-1198 (*OzT8*), MFOL-544 (*OzT8* + *OzT9*), and MFOL-1102 (*OzT9*) (Figure 30B).

Breeding lines derived from Binadhan-11 exhibited a significantly higher relative net CO_2 assimilation rate than Binadhan-11(Figure 31B). Among the evaluated lines, those carrying both QTLs (*OzT8* + *OzT9*) demonstrated the highest average relative net CO_2 assimilation rate, followed by lines possessing the *OzT8* QTL and those with the *OzT9* QTL, which ranked second and third, respectively (Figure 31B). Among the individual genotypes, MFOL-544 (*OzT8* + *OzT9*) showed the highest relative net CO_2 assimilation rate, followed by MFOL-471 (*OzT8* + *OzT9*) and MFOL-1102 (*OzT9*) (Figure 31B).

Overall, the findings highlighted that in the BRRI dhan28 × Kasalath cross, the best-performing breeding lines for stomatal conductance (gsw) at 80 DAO were MFOL-328 (*OzT9*), while MFOL-1926 (*OzT9*) exhibited the highest gsw at 109 DAO. Lines carrying both QTLs (*OzT8* + *OzT9*) demonstrated the highest relative net CO_2 assimilation rates at 116 DAO, with MFOL-1547 (*OzT8* + *OzT9*) being the top-performing genotype. In the Binadhan-11 × Kasalath cross, MFOL-1198 (*OzT8*) and MFOL-544 (*OzT8* + *OzT9*) outperformed at 80 DAO for gsw, while MFOL-1031 (*OzT9*) excelled at 109 DAO. At 116 DAO, lines with both QTLs showed superior CO_2 assimilation rates, with MFOL-544 (*OzT8* + *OzT9*) ranking highest. Across both crosses, breeding lines with combined QTLs (*OzT8* + *OzT9*) consistently exhibited superior gas exchange parameters, particularly for net CO_2 assimilation rates.

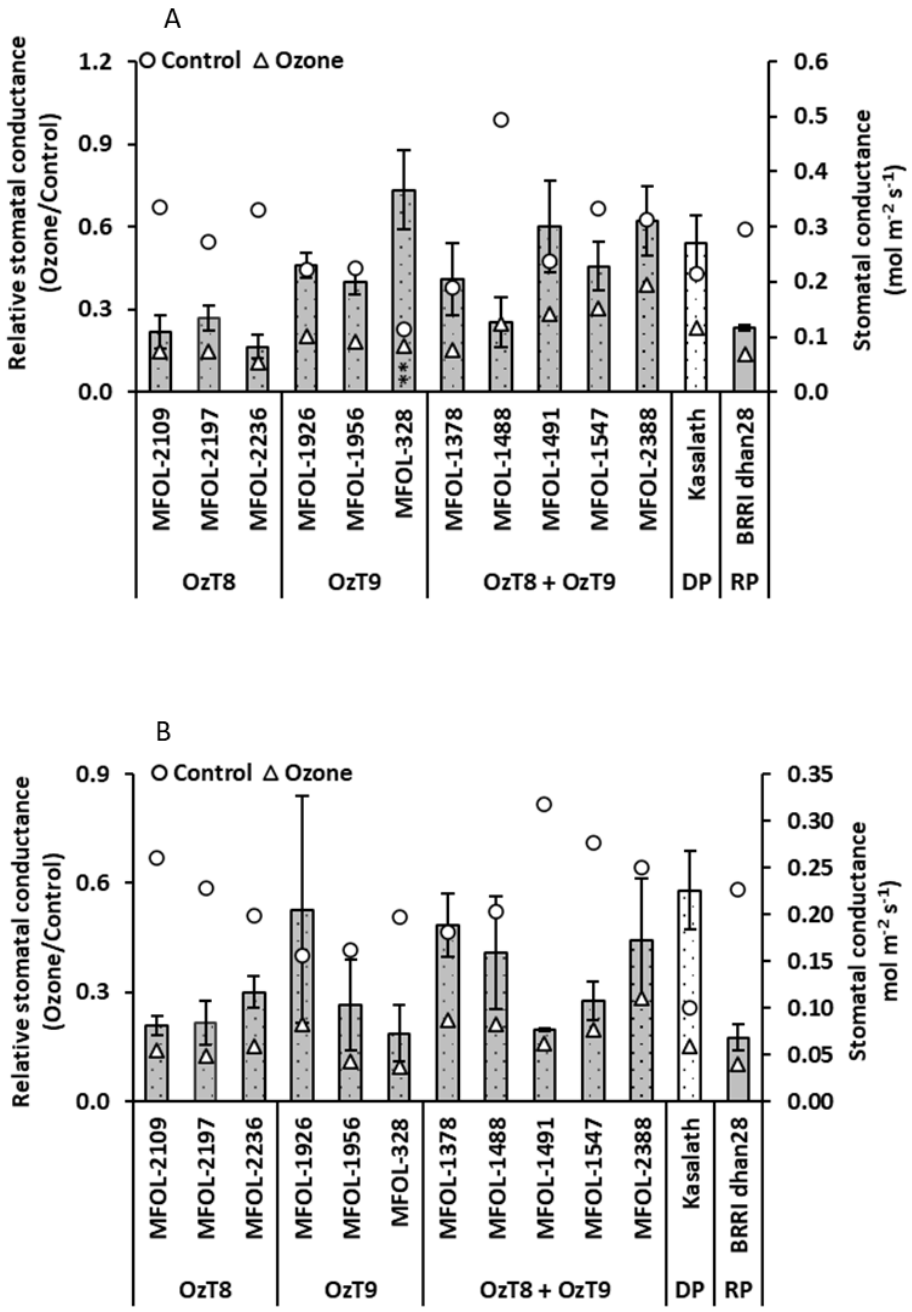

Figure 27 Stomatal conductance(mol m^{-2} s^{-1}) of selected breeding lines carrying *OzT8* and/or *OzT9* derived from the cross BRRI dhan28 × Kasalath under ozone stress and control conditions at (A) 80 DAO and (B) 109 DAO. The bar graphs display the mean and standard error of relative values (n = 3), while the circles and triangles represent absolute values for the control and ozone-treated groups, respectively. Asterisks within the bars indicate significant differences between the genotypes and the recipient parent (BRRI dhan28), as determined by Dunnett's test (*P < 0.05, **P < 0.01, ***P < 0.001). DP, donor parent, and RP, recipient parent.

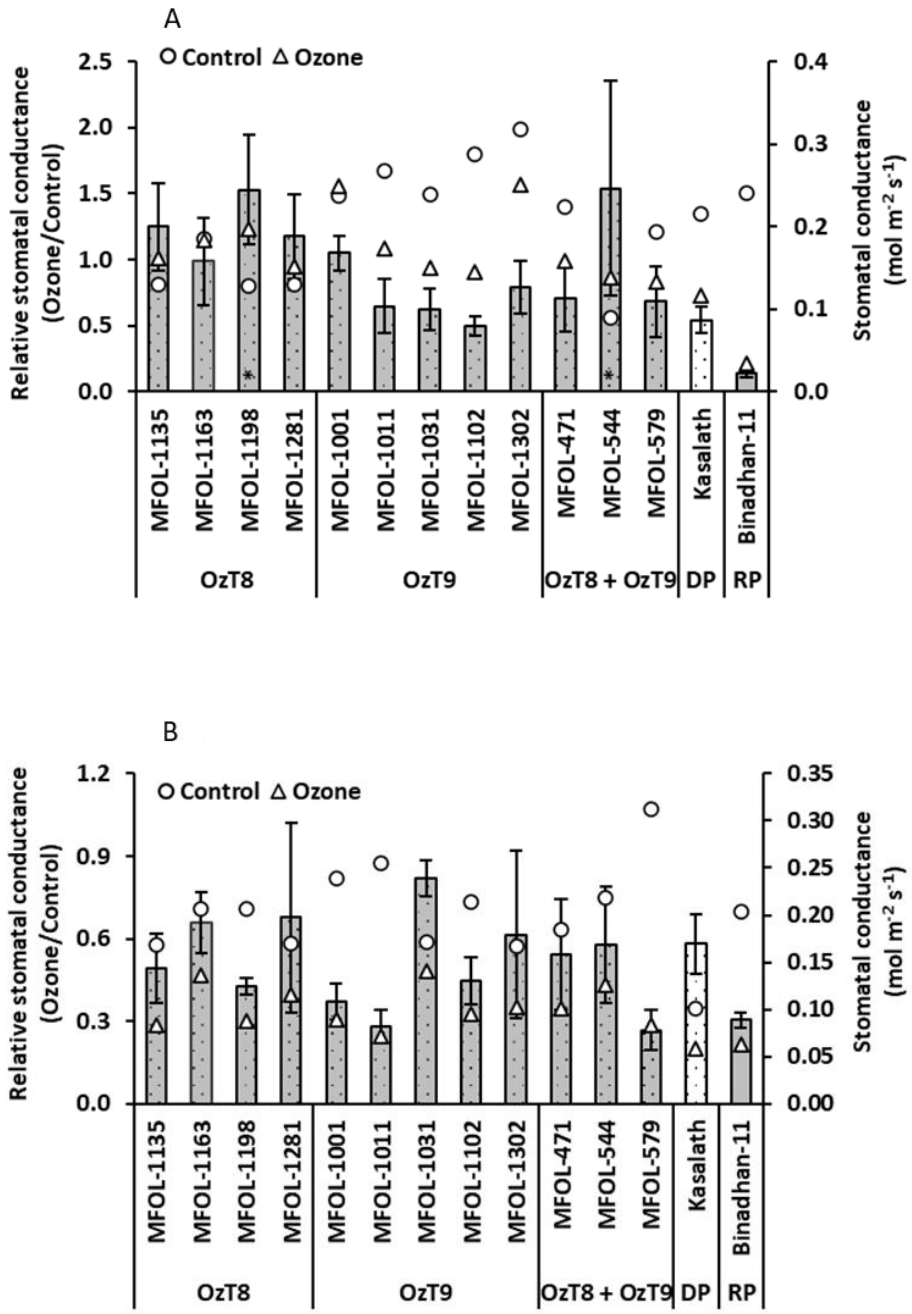

Figure 28 Stomatal conductance(mol m^{-2} s^{-1}) of selected breeding lines carrying *OzT8* and/or *OzT9* derived from the cross Binadhan-11 × Kasalath under ozone stress and control conditions at (A) 80 DAO and (B) 109 DAO. The bar graphs display the mean and standard error of relative values (n = 3), while the circles and triangles represent absolute values for the control and ozone-treated groups, respectively. Asterisks within the bars indicate significant differences between the genotypes and the recipient parent (Binadhan-11), as determined by Dunnett's test (*P < 0.05, **P < 0.01, ***P < 0.001). DP, donor parent, and RP, recipient parent.

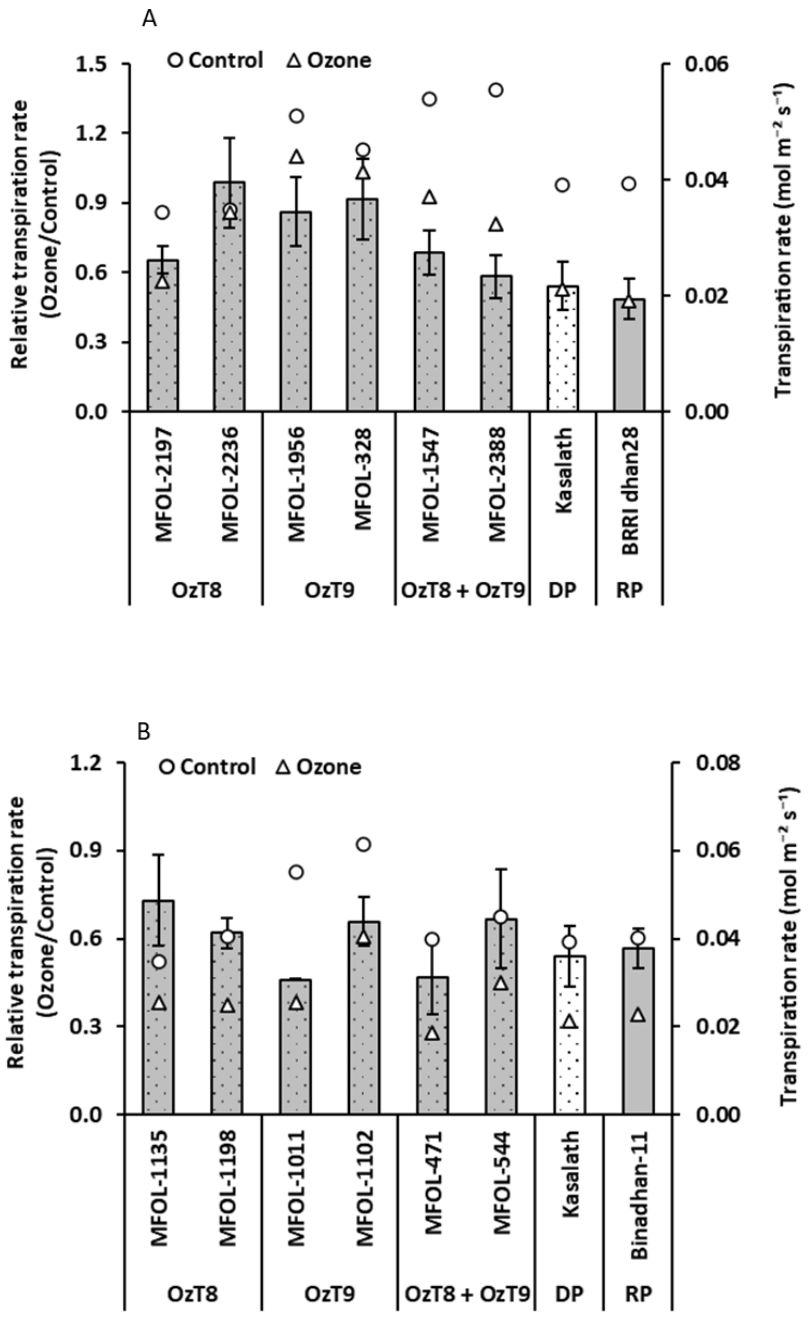

Figure 29 Transpiration rate (mol m^{-2} s^{-1}) of selected breeding lines carrying *OzT8* and/or *OzT9* derived from the cross (A) BRRI dhan28 × Kasalath and (B) Binadhan-11 × Kasalath under ozone stress and control conditions at 116 DAO. The bar graphs display the mean and standard error of relative values (n = 3), while the circles and triangles represent absolute values for the control and ozone-treated groups, respectively. There are no significant differences between the genotypes and the recipient parent (BRRI dhan28 or Binadhan-11), as determined by Dunnett's test (*P < 0.05, **P < 0.01, ***P < 0.001). DP, donor parent, and RP, recipient parent.

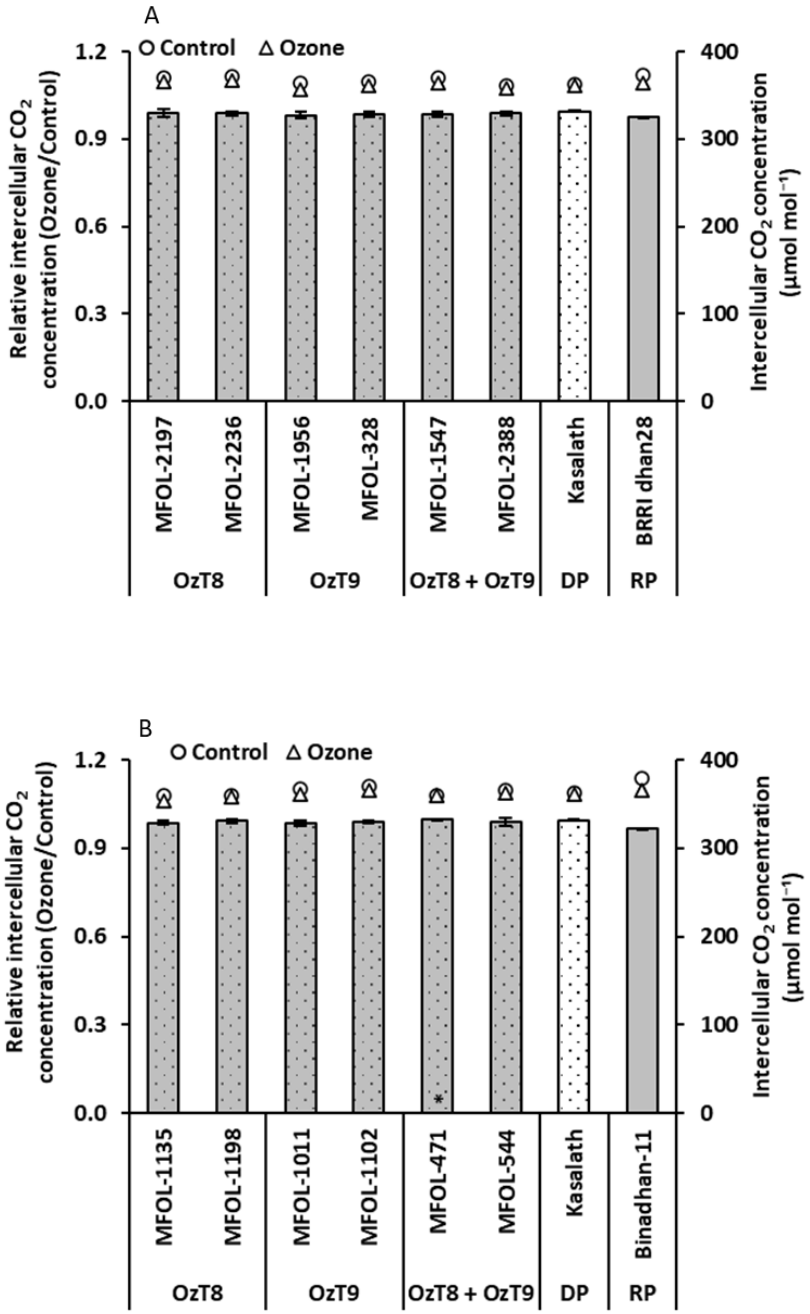

Figure 30 Intercellular CO_2 concentration (µmol mol^{-1}) of selected breeding lines carrying *OzT8* and/or *OzT9* derived from the cross (A) BRRI dhan28 × Kasalath and (B) Binadhan-11 × Kasalath under ozone stress and control conditions at 116 DAO. The bar graphs display the mean and standard error of relative values (n = 3), while the circles and triangles represent absolute values for the control and ozone-treated groups, respectively. There are no significant differences between the genotypes and the recipient parent (BRRI dhan28 or Binadhan-11), as determined by Dunnett's test (*P < 0.05, **P < 0.01, ***P < 0.001). DP, donor parent, and RP, recipient parent.

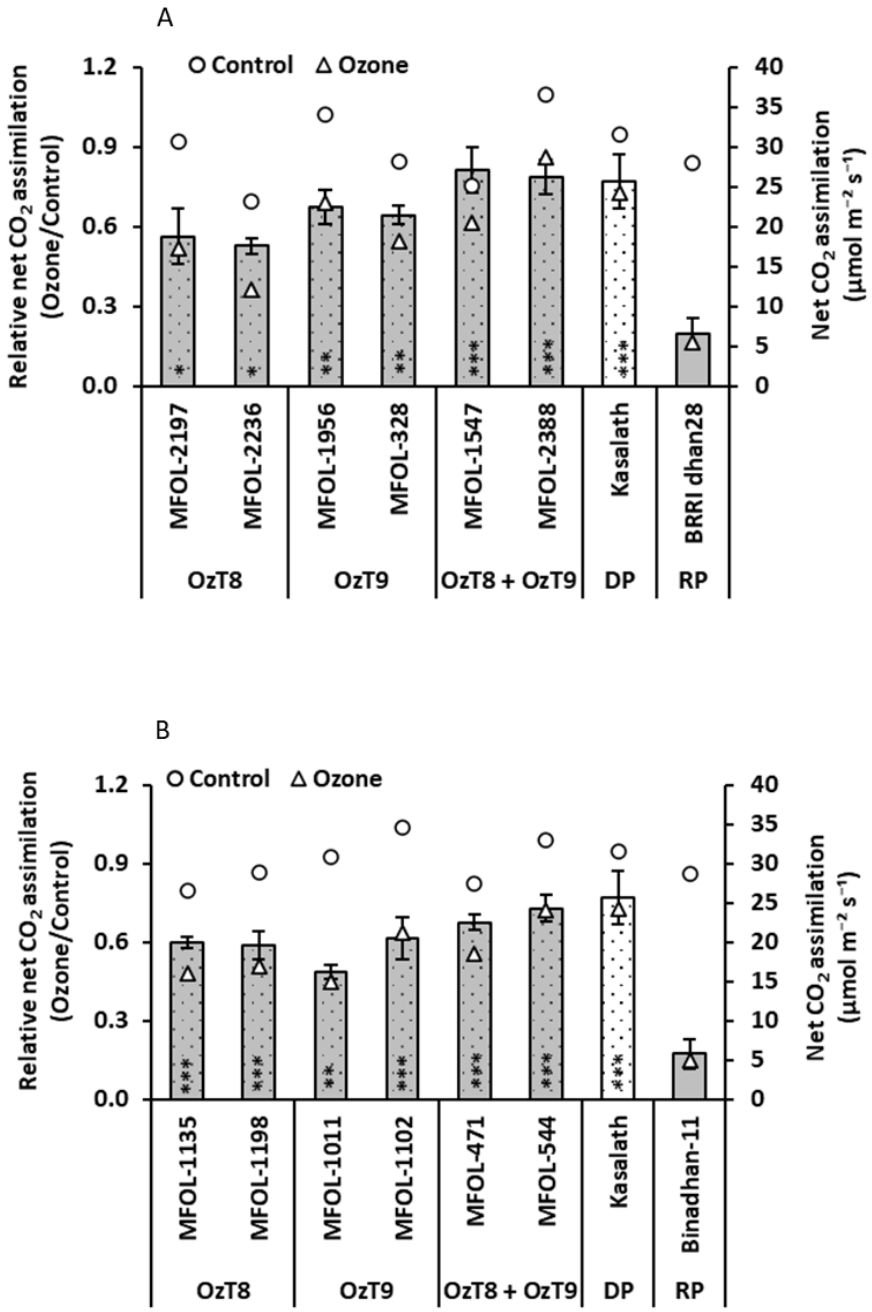

Figure 31 CO_2 assimilation rate (µmol m^{-2} s^{-1}) of selected breeding lines carrying *OzT8* and/or *OzT9* derived from the cross (A) BRRI dhan28 × Kasalath and (B) Binadhan-11 × Kasalath under ozone stress and control conditions at 116 DAO. The bar graphs display the mean and standard error of relative values (n = 3), while the circles and triangles represent absolute values for the control and ozone-treated groups, respectively. Asterisks within the bars indicate significant differences between the genotypes and the recipient parent (BRRI dhan28 or Binadhan-11), as determined by Dunnett's test (*P < 0.05, **P < 0.01, ***P < 0.001). DP, donor parent, and RP, recipient parent.

4.3.7 Assessment of breeding lines based on biochemical traits

Breeding lines from BRRI Dhan28 X Kasalath cross

At 50 DAO, all breeding lines derived from BRRI dhan28 exhibited significantly lower malondialdehyde (MDA) concentration compared to the recipient parent variety, BRRI dhan28. Among these lines, those carrying the *OzT9* QTL showed the lowest mean relative MDA concentration, followed by lines harboring the *OzT8* QTL and those possessing both QTLs (*OzT8* + *OzT9*), which ranked second and third, respectively (Figure 32A). Among the BRRI dhan28-derived genotypes, MFOL-328 (*OzT9*) recorded the lowest relative MDA concentration, followed by MFOL-1956 (*OzT9*), MFOL-1491 *(OzT8* + *OzT9*), and MFOL-1547 (*OzT8* + *OzT9*) (Figure 32A).

Breeding lines from Binadhan-11 X Kasalath cross

At 50 DAO, all breeding lines derived from Binadhan-11 exhibited significantly lower malondialdehyde (MDA) concentrations than the recipient parent line, Binadhan-11. Among these lines, those carrying the *OzT8* QTL displayed the lowest mean relative MDA concentration, followed by lines carrying both QTLs (*OzT8* + *OzT9*) and those carrying only the *OzT9* QTL (Figure 32B). Within the Binadhan-11-derived genotypes, MFOL-1135 (*OzT8*) recorded the lowest relative MDA concentration, followed by MFOL-1198 (*OzT8*), MFOL-1281 (*OzT8*), and MFOL-471 (*OzT8* + *OzT9*) (Figure 32B).

Taken together, the data suggested that among the BRRI dhan28-derived lines, the *OzT9* QTL demonstrated the best performance, with MFOL-328 (*OzT9*) recording the lowest relative MDA concentration, followed by MFOL-1956 (*OzT9*), MFOL-1491 (*OzT8* + *OzT9*), and MFOL-1547 (*OzT8 + OzT9*). For the Binadhan-11-derived lines, the *OzT8* QTL was the best-performing, with MFOL-1135 (*OzT8*) exhibiting the lowest relative MDA concentration, followed by MFOL-1198 (*OzT8*), MFOL-1281 (*OzT8*), and MFOL-471 (*OzT8* + *OzT9*).

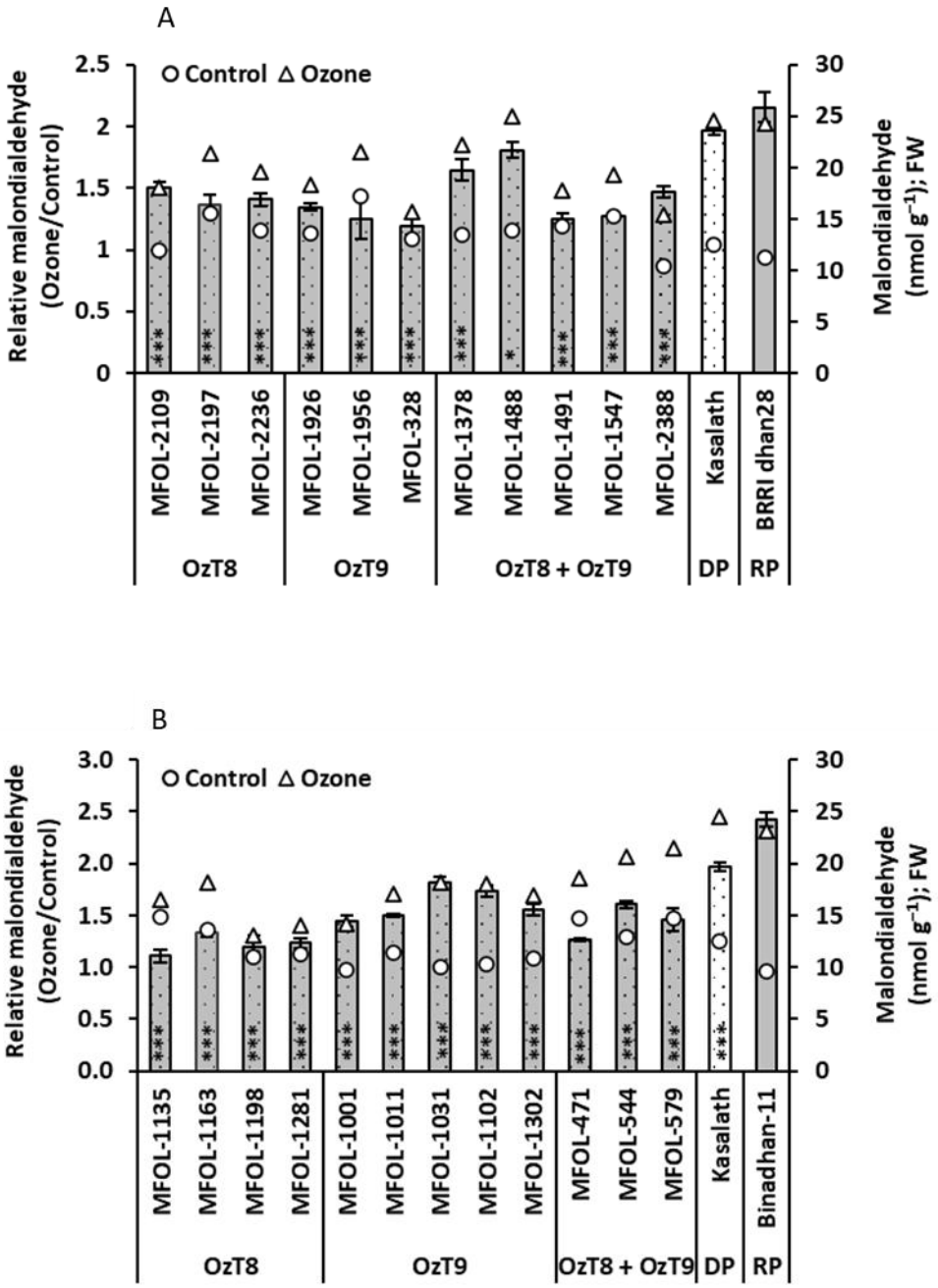

Figure 32 Malondialdehyde (nmol g^{-1}); FW of selected breeding lines carrying *OzT8* and/or *OzT9* derived from the cross (A) BRRI dhan28 × Kasalath and (B) Binadhan-11 × Kasalath under ozone stress and control conditions at 50 DAO. The bar graphs display the mean and standard error of relative values (n = 3), while the circles and triangles represent absolute values for the control and ozone-treated groups, respectively. Asterisks within the bars indicate significant differences between the genotypes and the recipient parent (BRRI dhan28 or Binadhan-11), as determined by Dunnett's test (*P < 0.05, **P < 0.01, ***P < 0.001). DP, donor parent, and RP, recipient parent.

4.3.8 Evaluation of breeding lines in response to yield components

We assessed several yield components associated with straw and grain yields in breeding lines derived from the BRRI dhan28 × Kasalath and Binadhan-11 × Kasalath crosses. Notably, two breeding lines, MFOL-1031 (carrying *OzT9* from Binadhan-11) and MFOL-2109 (carrying *OzT8* from BRRI dhan28), exhibited a very low grain count and were excluded from the yield component analysis.

Under ozone treatment, reductions were observed in all measured traits, including plant height, panicle number, filled grain number, grain yield, and straw biomass, with mean values consistently lower than those recorded under control conditions. However, the statistical significance of these reductions varied (Tables 8, 9). Analysis of variance (ANOVA) revealed that ozone treatment significantly affected plant height in breeding lines from the Binadhan-11 × Kasalath cross (Table 9). In contrast, no significant treatment effects were observed for any traits in breeding lines derived from the BRRI dhan28 × Kasalath cross (Table 8).

Significant genotype effects were detected for all traits in both crosses, but interactions between genotype and ozone treatment were generally non-significant. The sole exception was the panicle number in the BRRI dhan28 × Kasalath cross, where a significant interaction was observed (Table 8).

Breeding lines from BRRI Dhan28 X Kasalath cross

None of the breeding lines derived from BRRI dhan28 demonstrated a significantly higher plant height than the recipient parent variety, BRRI dhan28. Among these lines, those carrying the *OzT8* QTL exhibited the highest mean relative plant height, followed by lines with the *OzT9* QTL and, finally, lines possessing both QTLs (*OzT8* + *OzT9*), which ranked second and third, respectively (Figure 33A). Specifically, within the BRRI dhan28-derived genotypes, MFOL-1956 (*OzT9*) recorded the highest relative plant height, followed by MFOL-2197 (*OzT8*) and MFOL-1378 (*OzT8* + *OzT9*) (Figure 33A).

Breeding lines derived from BRRI dhan28, including MFOL-1378, MFOL-1488, MFOL-1547, MFOL-2388, MFOL-1926, MFOL-1956, and MFOL-328, exhibited significantly higher relative panicle numbers compared to the recipient parent variety, BRRI dhan28. Among these, lines carrying both QTLs (*OzT8* + *OzT9*) demonstrated the highest mean relative panicle number, followed by those with the *OzT9* QTL and then those with the *OzT8* QTL (Figure 34A). Notably, MFOL-1378 (*OzT8* + *OzT9*) recorded the highest relative panicle number, followed by MFOL-

1547 (*OzT8* + *OzT9*), MFOL-1926 (*OzT9*), MFOL-1488 (*OzT8* + *OzT9*), and MFOL-2388 (*OzT8* + *OzT9*) (Figure 34A).

None of the breeding lines derived from BRRI dhan28 showed a significantly higher relative filled grain number compared to the recipient parent, BRRI dhan28. Among these lines, those carrying the *OzT9* QTL exhibited the highest average relative filled grain number, followed by lines harboring both QTLs (*OzT8* + *OzT9*), and then those with the *OzT8* QTL alone (Figure 35A). Among the BRRI dhan28-derived genotypes, MFOL-1926 (*OzT9*) recorded the highest relative filled grain number, followed by MFOL-1488 (*OzT8* + *OzT9*) and MFOL-1378 (*OzT8* + *OzT9*) (Figure 35A).

None of the breeding lines derived from BRRI dhan28 exhibited a significantly higher relative grain yield than the recipient parent variety, BRRI dhan28. However, among these lines, those carrying the *OzT9* QTL demonstrated the highest mean relative grain yield, followed by lines with both the *OzT8* and *OzT9* QTLs, and then those possessing only the *OzT8* QTL (Figure 36A). Within the BRRI dhan28-derived genotypes, MFOL-1926 (*OzT9*) achieved the highest relative grain yield, followed by MFOL-1488 (*OzT8* + *OzT9*) and MFOL-1491 (*OzT8* + *OzT9*) (Figure 36A).

Similarly, no breeding lines derived from BRRI dhan28 exhibited a significantly higher relative straw biomass than the recipient parent variety, BRRI dhan28. However, lines containing both QTLs (*OzT8* + *OzT9*) showed the highest mean relative straw biomass, followed by lines with the *OzT9* QTL alone, and then those with the *OzT8* QTL alone (Figure 37A). Among the genotypes derived from BRRI dhan28, MFOL-1488 recorded the highest relative straw biomass, followed by MFOL-1378 and MFOL-1547, all of which carried both QTLs (*OzT8* + *OzT9*) (Figure 37A).

Breeding lines from Binadhan-11 X Kasalath cross

Similarly, none of the breeding lines derived from Binadhan-11 exhibited significantly higher plant height than the recipient parent, Binadhan-11. As observed with Binadhan-11, lines carrying the *OzT8* QTL showed the highest mean relative plant height, followed by lines with the *OzT9* QTL and those with both QTLs (*OzT8* + *OzT9*), ranking second and third, respectively (Figure 33B). Among the Binadhan-11-derived genotypes, MFOL-1302 (*OzT9*) achieved the highest relative plant height, followed by MFOL-1198 (*OzT8*) and MFOL-1281 (*OzT8*) (Figure 33B).

Most breeding lines derived from Binadhan-11, including MFOL-544, MFOL-471, MFOL-1302, MFOL-1011, MFOL-1198, MFOL-1163, and MFOL-1135, demonstrated significantly higher relative panicle numbers compared to the recipient parent variety. Among these lines, those carrying both QTLs (*OzT8* + *OzT9*) exhibited the highest mean relative panicle number, followed by lines with the *OzT9* QTL alone and those with the *OzT8* QTL (Figure 34B). Notably, MFOL-544 (*OzT8* + *OzT9*) recorded the highest relative panicle number among the Binadhan-11-derived genotypes, followed by MFOL-1135 (*OzT8*), MFOL-1198 (*OzT8*), MFOL-1011 (*OzT9*), and MFOL-1302 (*OzT9*) (Figure 34B).

None of the breeding lines derived from Binadhan-11 exhibited a significantly higher relative filled grain number than the recipient parent, Binadhan-11. However, among these lines, those with the *OzT8* QTL demonstrated the highest mean relative filled grain number, followed by lines with the *OzT9* QTL and those with both QTLs (*OzT8* + *OzT9*) (Figure 35B). Among the Binadhan-11-derived genotypes, MFOL-1163 (*OzT8*) achieved the highest relative filled grain number, followed by MFOL-1102 (*OzT9*) and MFOL-1198 (*OzT8*) (Figure 35B).

None of the breeding lines derived from Binadhan-11 demonstrated a significantly higher relative grain yield than the recipient parent, Binadhan-11. Among these lines, those with the *OzT8* QTL exhibited the highest mean relative grain yield, followed by lines with the *OzT9* QTL and those with both QTLs (*OzT8* + *OzT9*) (Figure 36B). Among the Binadhan-11-derived genotypes, MFOL-1163 (*OzT8*) achieved the highest relative grain yield, followed by MFOL-1102 (*OzT9*), MFOL-1198 (*OzT8*), and MFOL-471 (*OzT8* + *OzT9*) (Figure 36B).

Similarly, no breeding lines derived from Binadhan-11 showed a significantly higher relative straw biomass than the recipient parent, Binadhan-11. Among these lines, those carrying the *OzT8* QTL exhibited the highest mean relative straw biomass, followed by lines with the *OzT9* QTL and those containing both QTLs (*OzT8* + *OzT9*) (Figure 37B). Among the Binadhan-11-derived genotypes, MFOL-1198 (*OzT8*) demonstrated the highest relative straw biomass, followed by MFOL-1135 (*OzT8*) and MFOL-1102 (*OzT9*) (Figure 37B).

Taken together, the results indicate that the breeding lines from the BRRI Dhan28 × Kasalath cross showed *OzT9* as the best-performing QTL, with MFOL-1926 excelling in filled grain number and grain yield, while MFOL-1488 (*OzT8* + *OzT9*) exhibited superior straw biomass and was among the top for grain yield. Lines carrying both QTLs (*OzT8* + *OzT9*), such as MFOL-1378, performed best in panicle number and straw biomass. Breeding lines from the

Binadhan-11 × Kasalath cross highlighted *OzT8* as the best-performing QTL, with MFOL-1163 excelling in grain yield and filled grain number, while MFOL-1198 showed the highest straw biomass. In both crosses, QTL combinations like *OzT8* + *OzT9* enhanced panicle numbers and straw biomass (for BRRI Dhan28 × Kasalath cross) but did not significantly outperform recipient parents in overall grain yield or filled grain numbers.

Table 8 Descriptive statistics and analysis of variance (ANOVA) of agronomic traits of breeding lines originating from BRRI dhan28 X Kasalath under ozone stress and control conditions.

Traits	Date	LS means (treatment)				ANOVA					
		Control		Ozone		Ozone-Treatment		Genotype		Interaction	
		Mean	SD	Mean	SD	Pr(>F)	F values	Pr(>F)	F values	Pr(>F)	F values
Plant height (cm)	Harvest	105.24	13.64	93.47	14.03	0.0817	60.07	**<0.0001**	68.52	0.3827	1.08
Panicle number	Harvest	4.11	0.93	3.65	0.97	0.1521	16.86	**<0.0001**	12.68	**0.0169**	2.23
Filled grain number	Harvest	216.40	113.92	179.51	118.94	0.2457	6.06	**<0.0001**	9.74	0.4728	0.98
Grain yield (g)	Harvest	3.45	1.81	2.83	1.88	0.2301	6.99	**<0.0001**	8.75	0.4033	1.06
Straw biomass (g)	Harvest	13.45	3.78	11.48	3.84	0.1274	24.30	**<0.0001**	20.34	0.3505	1.12

Note: Mean values of all genotypes are shown. LS, least square means; SD, standard deviation.

Table 9 Descriptive statistics and analysis of variance (ANOVA) of agronomic traits of breeding lines originating from Binadhan-11 X Kasalath under ozone stress and control conditions.

Traits	Date	LS means (treatment)				ANOVA					
		Control		Ozone		Ozone-Treatment		Genotype		Interaction	
		Mean	SD	Mean	SD	Pr(>F)	F values	Pr(>F)	F values	Pr(>F)	F values
Plant height (cm)	Harvest	105.96	11.48	92.51	11.94	**0.0429**	219.66	**<0.0001**	42.72	0.2678	1.23
Panicle number	Harvest	4.19	0.87	3.58	0.76	0.2026	9.22	**<0.0001**	4.61	0.1237	1.52
Filled grain number	Harvest	234.99	91.83	193.88	122.4	0.2264	7.25	**<0.0001**	4.89	0.6468	0.80
Grain yield (g)	Harvest	4.86	1.80	4.02	2.48	0.2349	6.69	**0.0013**	2.93	0.5998	0.85
Straw biomass (g)	Harvest	14.31	3.99	12.65	4.80	0.2008	9.39	**<0.0001**	9.92	0.7906	0.66

Note: Mean values of all genotypes are shown. LS, least square means; SD, standard deviation.

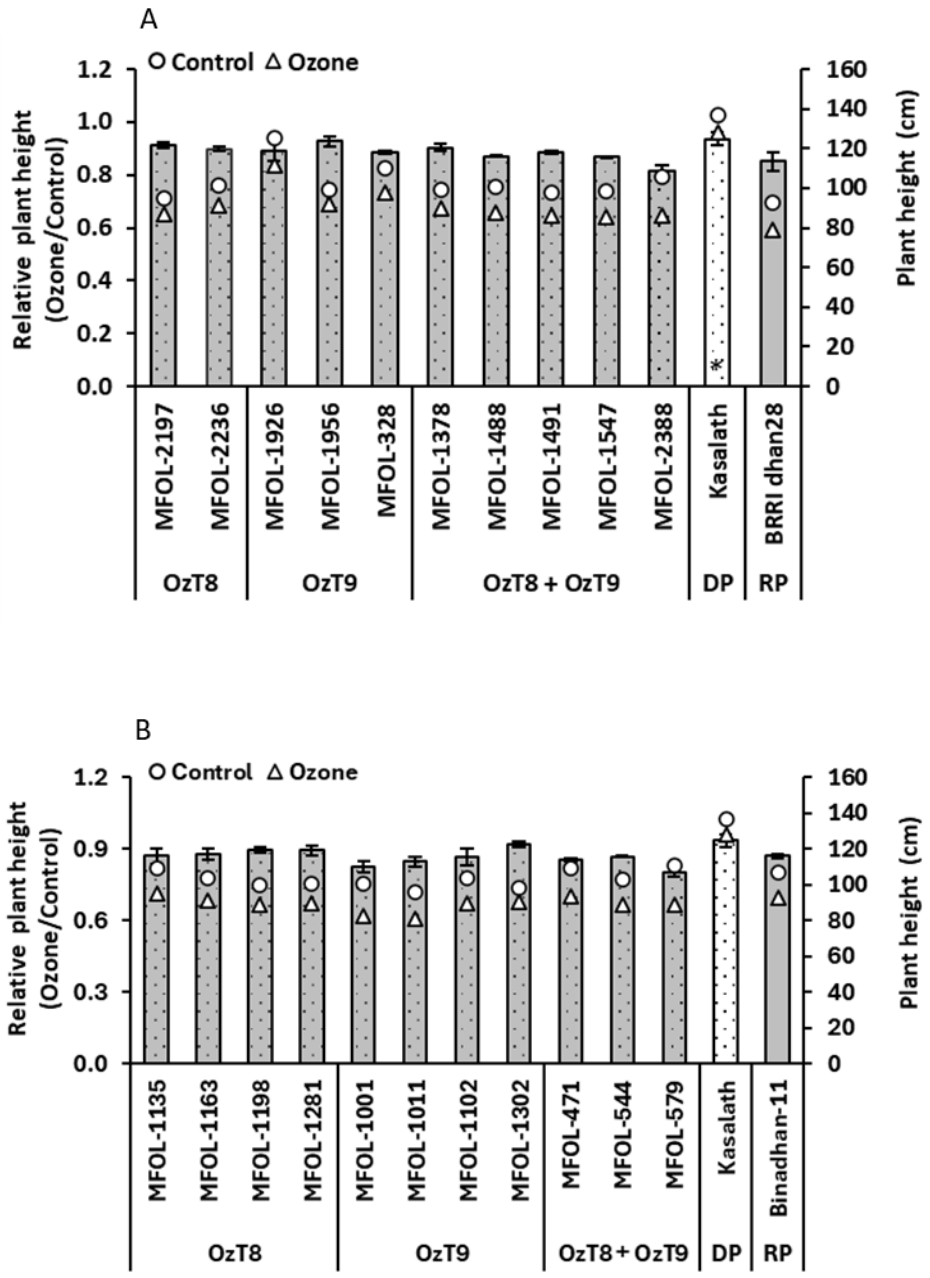

Figure 33 Plant height (cm) of selected breeding lines carrying *OzT8* and/or *OzT9* derived from the cross (A) BRRI dhan28 × Kasalath and (B) Binadhan-11 × Kasalath under ozone stress and control conditions. The bar graphs display the mean and standard error of relative values (n = 3), while the circles and triangles represent absolute values for the control and ozone-treated groups, respectively. Asterisks within the bars indicate significant differences between the genotypes and the recipient parent (BRRI dhan28 or Binadhan-11), as determined by Dunnett's test (*P < 0.05, **P < 0.01, ***P < 0.001). DP, donor parent, and RP, recipient parent.

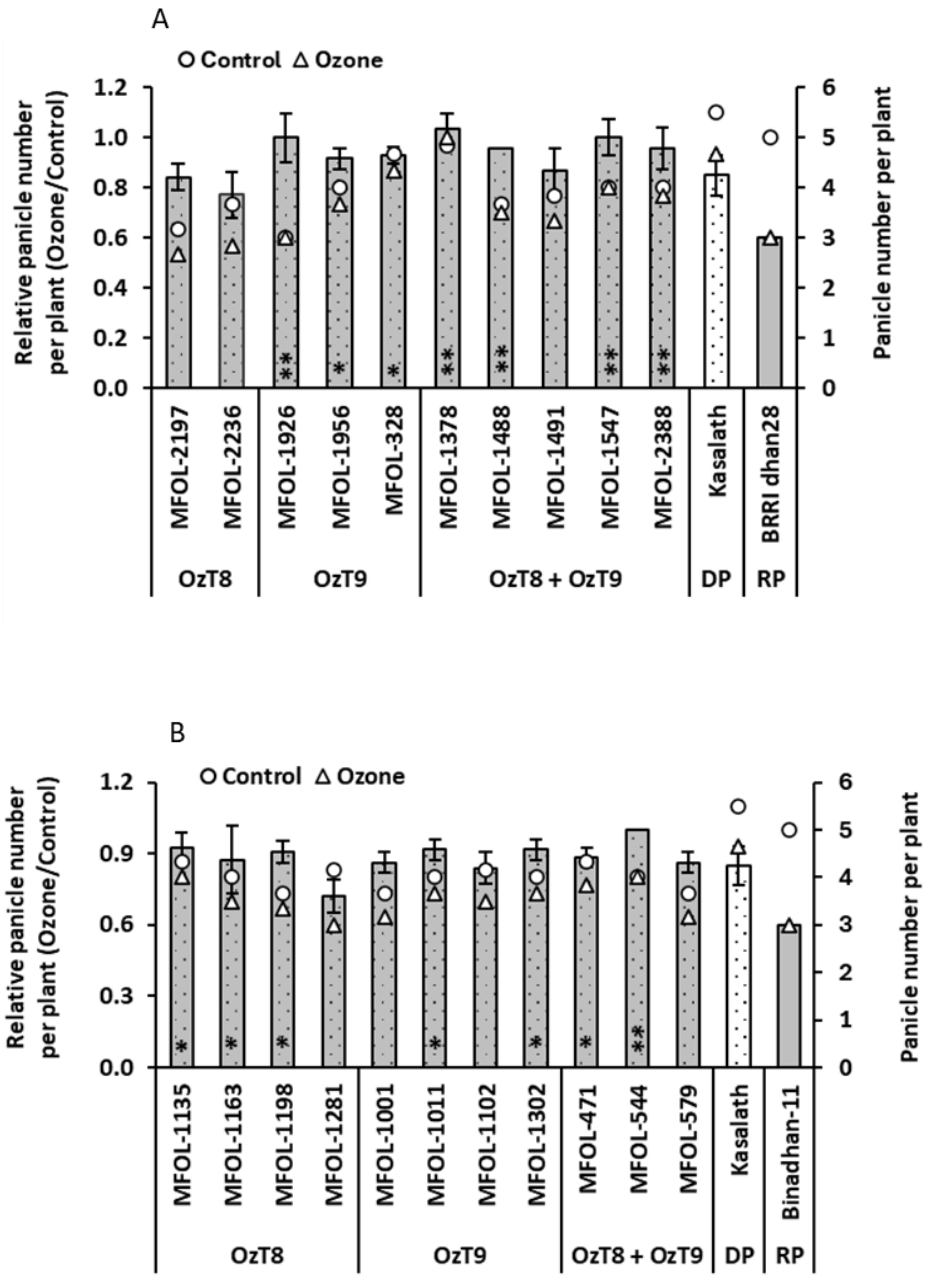

Figure 34 Panicle number of selected breeding lines carrying *OzT8* and/or *OzT9* derived from the cross (A) BRRI dhan28 × Kasalath and (B) Binadhan-11 × Kasalath under ozone stress and control conditions. The bar graphs display the mean and standard error of relative values (n = 3), while the circles and triangles represent absolute values for the control and ozone-treated groups, respectively. Asterisks within the bars indicate significant differences between the genotypes and the recipient parent (BRRI dhan28 or Binadhan-11), as determined by Dunnett's test (*P < 0.05, **P < 0.01, ***P < 0.001). DP, donor parent, and RP, recipient parent.

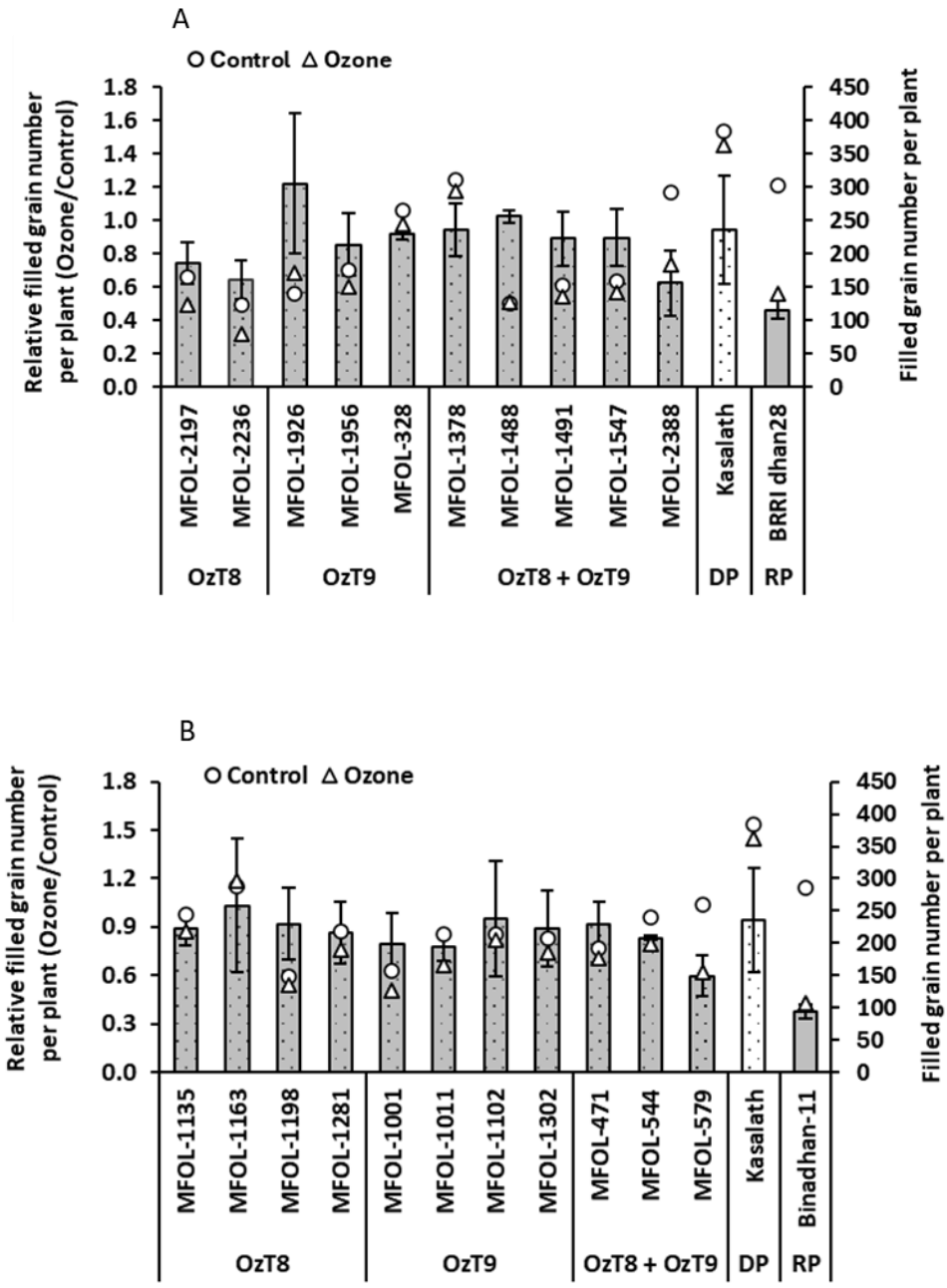

Figure 35 Filled grain number of selected breeding lines carrying *OzT8* and/or *OzT9* derived from the cross (A) BRRI dhan28 × Kasalath and (B) Binadhan-11 × Kasalath under ozone stress and control conditions. The bar graphs display the mean and standard error of relative values (n = 3), while the circles and triangles represent absolute values for the control and ozone-treated groups, respectively. Asterisks within the bars indicate significant differences between the genotypes and the recipient parent (BRRI dhan28 or Binadhan-11), as determined by Dunnett's test (*P < 0.05, **P < 0.01, ***P < 0.001). DP, donor parent, and RP, recipient parent.

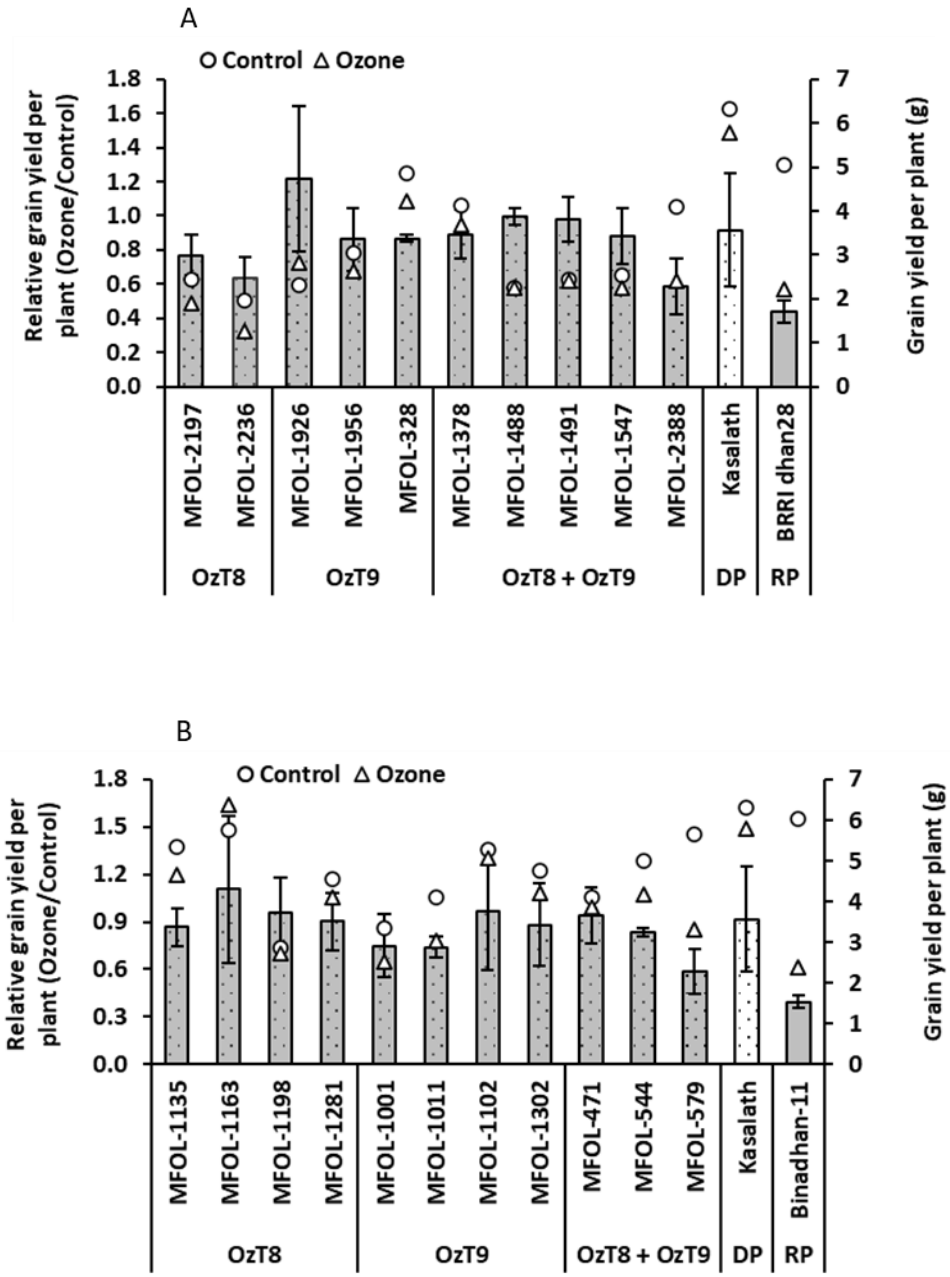

Figure 36 Grain yield (g) of selected breeding lines carrying *OzT8* and/or *OzT9* derived from the cross (A) BRRI dhan28 × Kasalath and (B) Binadhan-11 × Kasalath under ozone stress and control conditions. The bar graphs display the mean and standard error of relative values (n = 3), while the circles and triangles represent absolute values for the control and ozone-treated groups, respectively. Asterisks within the bars indicate significant differences between the genotypes and the recipient parent (BRRI dhan28 or Binadhan-11), as determined by Dunnett's test (*P < 0.05, **P < 0.01, ***P < 0.001). DP, donor parent, and RP, recipient parent.

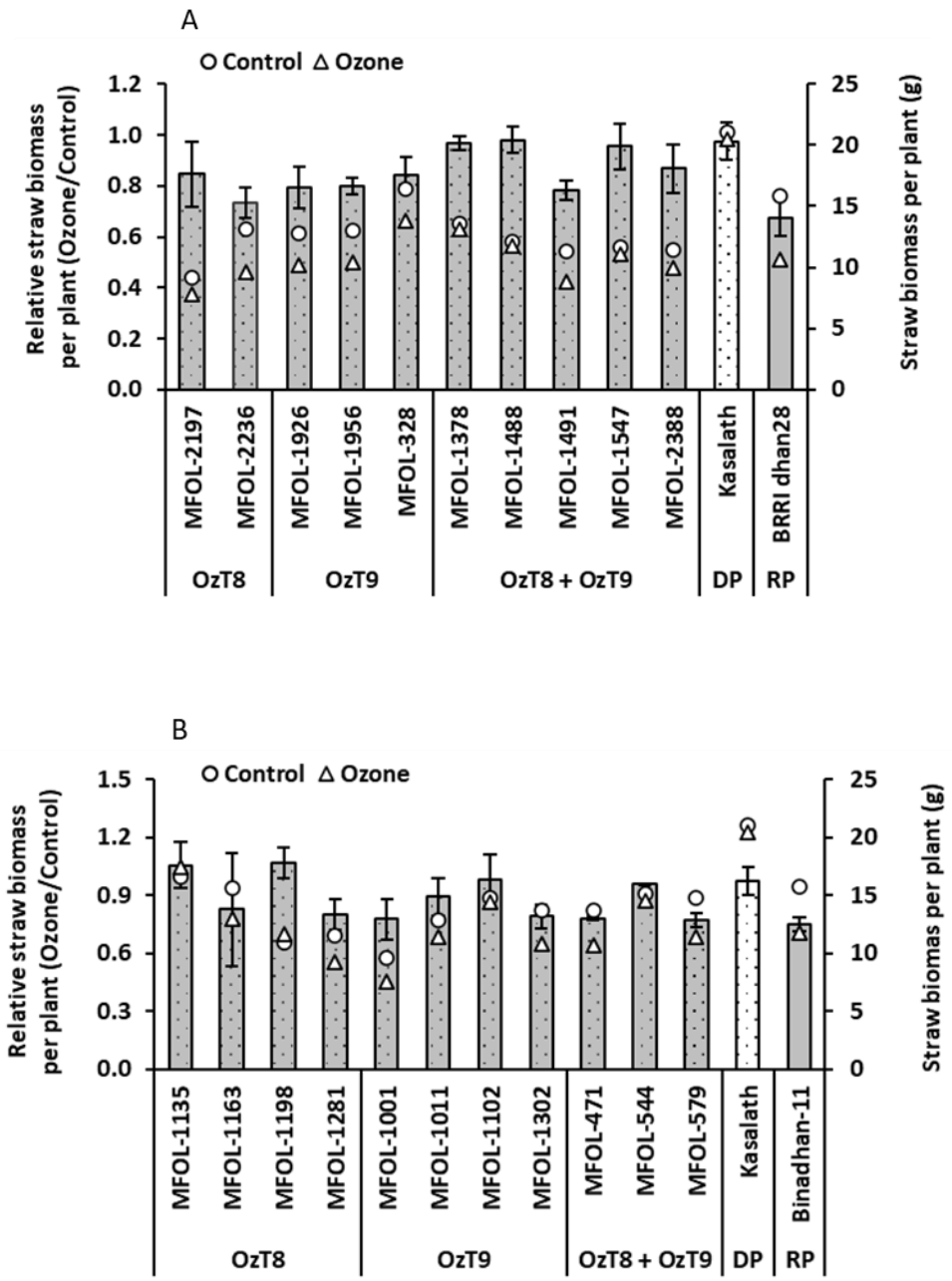

Figure 37 Straw biomass (g) of selected breeding lines carrying *OzT8* and/or *OzT9* derived from the cross (A) BRRI dhan28 × Kasalath and (B) Binadhan-11 × Kasalath under ozone stress and control conditions. The bar graphs display the mean and standard error of relative values (n = 3), while the circles and triangles represent absolute values for the control and ozone-treated groups, respectively. Asterisks within the bars indicate significant differences between the genotypes and the recipient parent (BRRI dhan28 or Binadhan-11), as determined by Dunnett's test (*P < 0.05, **P < 0.01, ***P < 0.001). DP, donor parent, and RP, recipient parent.

4.3.9 Line selection for further comprehensive experiment

Additionally, we excluded certain experimental lines from the planned comprehensive (Experiment 3 + 4) study. The evaluation focused on the final grain yield per plant and key plant morphological characteristics.

Breeding lines from BRRI Dhan28 X Kasalath cross

We selected the following breeding lines from the BRRI dhan28 background: MFOL-2197 and MFOL-2236, which harbor *OzT8*; MFOL-1956 and MFOL-328, which harbor *OzT9*; and MFOL-1378, MFOL-1488, MFOL-1491, and MFOL-1547, which harbor both QTLs (*OzT8* + *OzT9*). We discarded MFOL-1926 (*OzT9*), which excelled in many evaluated traits, due to its severe grain-shattering characteristics, which made it unsuitable for agronomic use. Similarly, we excluded MFOL-2388 (*OzT8 + OzT9*) despite its exceptional performance across several traits because it showed significant yield loss under ozone stress.

Breeding lines from Binadhan-11 X Kasalath cross

We selected the following breeding lines from the Binadhan-11 background: MFOL-1135 and MFOL-1198, harboring *OzT8*; MFOL-1011, MFOL-1102, and MFOL-1302, harboring *OzT9*; and MFOL-471 and MFOL-544, harboring both QTLs (*OzT8* + *OzT9*). However, we excluded MFOL-1163 (*OzT8*) and MFOL-1281 (*OzT8*) despite their superior performance across several traits because they were lodged at harvest, which made them unsuitable for agronomic use. We also excluded MFOL-1001 (*OzT9*) due to severe yield loss under ozone stress and poor performance across most measured traits. Similarly, we discarded MFOL-579 (*OzT8 + OzT9*) because it exhibited severe yield loss under ozone stress.

4.4 Experiment 3 + 4: Comprehensive evaluation of ozone-tolerant rice (*Oryza sativa* L.) breeding lines through physiological and agronomic trait analysis

In this section, we first discuss the results of the third experiment, which we conducted in a climate-controlled greenhouse at the University of Giessen's research station between April and October 2023 to identify the most suitable ozone-tolerant rice varieties for deployment in ozone-affected regions such as Bangladesh. Subsequently, we present the results of a preliminary field trial (fourth experiment) that we conducted in Bangladesh from December 2023 to June 2024.

Experiment 3

4.4.1 Effects of ozone stress on physiological and agronomic traits

We evaluated 19 breeding lines for their morphological, physiological, and yield-related traits under ozone stress conditions. Among these, we derived 10 lines from the cross between BRRI dhan28 and Kasalath and nine from the cross between Binadhan-11 and Kasalath. Based on previous experimental results, we selected eight lines from the BRRI dhan28 × Kasalath cross and included two new breeding lines. Similarly, from the Binadhan-11 × Kasalath cross, we selected seven lines from prior experiments and added two new breeding lines.

Breeding lines from BRRI Dhan28 X Kasalath cross

The Leaf Bronzing Score (LBS), which indicates visible damage, showed a marked increase under ozone stress at later stages, particularly at 33, 60, and 75 DAO (Table 10). This suggests progressive damage to leaf tissues with prolonged exposure to ozone, with significant genotype and genotype × treatment interaction effects, indicating genetic variability in the response (Table 10).

The Normalized difference vegetation index (NDVI), an indicator of canopy health, remained relatively stable under ozone stress at early stages (16 DAO) but showed significant declines at later stages, particularly at 75 DAO (Table 10). These reductions indicate a delayed impact of ozone stress on the canopy's health. Significant genotype and interaction effects at all measured stages further emphasize variability among lines. Similarly, the chlorophyll-to-carotenoid ratio (Lic2), exhibited significant reductions compared to control conditions at later stages, particularly at 75 DAO (Table 10). Ozone stress also reduced the Nitrogen balance index (NBI) at later stages, particularly at 75 DAO, which may indicate nitrogen metabolism

or allocation disruptions. We observed significant genotype and genotype × treatment interaction effects concerning NBI, while the treatment effect was statistically insignificant (Table 10).

Table 10 Descriptive statistics and analysis of variance (ANOVA) for physiological traits of breeding lines derived from the cross between BRRI dhan28 and Kasalath under ozone stress and control conditions.

Traits	Date	LS means (treatment)				ANOVA					
		Control		Ozone		Ozone-Treatment		Genotype		Interaction	
		Mean	SD	Mean	SD	Pr(>F)	F values	Pr(>F)	F values	Pr(>F)	F values
LBS	16 DAO	0.00	0.00	0.11	0.43	0.892	0.029	0.694	0.746	0.694	0.746
	33 DAO	0.00	0.00	2.06	1.24	0.340	7.397	**<0.000**	19.587	**<0.000**	19.587
	60 DAO	0.00	0.00	2.79	1.32	0.269	16.402	**<0.000**	14.740	**<0.000**	14.740
	75 DAO	0.00	0.00	3.27	1.26	0.232	27.059	**<0.000**	23.654	**<0.000**	23.654
NDVI	16 DAO	0.65	0.05	0.65	0.04	0.860	0.045	**<0.000**	13.299	**0.003**	2.682
	33 DAO	0.65	0.03	0.63	0.03	0.326	3.892	**0.000**	7.200	**0.011**	2.261
	60 DAO	0.64	0.06	0.60	0.06	0.487	0.837	**0.000**	6.915	**0.000**	3.371
	75 DAO	0.60	0.07	0.51	0.09	**0.03**	16.468	**0.002**	2.793	**0.000**	5.326
Lic2	16 DAO	0.81	0.08	0.84	0.08	**0.000**	20.335	**0.000**	5.262	0.406	1.046
	33 DAO	0.85	0.06	0.80	0.07	0.119	3.308	**0.000**	4.756	0.392	1.061
	60 DAO	0.79	0.09	0.71	0.08	0.118	16.328	**0.000**	5.660	**0.006**	2.443
	75 DAO	0.72	0.14	0.60	0.09	**0.003**	22.327	0.118	1.532	0.898	0.508
NBI	16 DAO	30.66	11.35	30.29	9.24	0.775	0.141	**0.000**	7.333	**0.015**	2.178
	33 DAO	32.16	7.01	31.85	8.03	0.953	0.023	**0.000**	8.332	**0.000**	3.231
	60 DAO	28.22	8.94	22.47	7.07	0.316	5.369	**0.015**	2.176	**0.003**	2.640
	75 DAO	19.77	6.43	14.08	5.91	0.214	8.321	**0.000**	5.775	**0.018**	2.126
gsw (mol m^{-2} s^{-1})	16 DAO	0.49	0.21	0.19	0.15	**0.001**	215.702	**0.001**	3.017	**0.004**	2.539
	33 DAO	0.43	0.18	0.12	0.12	0.109	88.054	**0.000**	7.582	**0.000**	3.783
	60 DAO	0.39	0.18	0.15	0.13	**0.000**	177.775	0.056	1.778	**0.015**	2.185
	75 DAO	0.23	0.17	0.11	0.08	0.104	13.978	**0.019**	2.101	0.138	1.475

PhiPS2	16 DAO	0.71	0.05	0.71	0.04	0.886	0.032	**0.021**	2.087	0.011	2.280
	33 DAO	0.62	0.11	0.55	0.14	0.186	4.593	**0.008**	2.349	0.044	1.860
	60 DAO	0.59	0.13	0.53	0.14	0.376	3.318	**0.001**	3.048	0.077	1.676
	75 DAO	0.48	0.12	0.48	0.11	0.938	0.007	**0.031**	1.962	0.721	0.718
ETR (µmol m^{-2} s^{-1})	16 DAO	76.32	33.08	51.28	21.88	0.709	1.563	**0.009**	2.344	0.664	0.776
	33 DAO	78.52	31.77	62.15	39.41	0.680	0.433	**0.000**	4.908	0.060	1.757
	60 DAO	58.39	22.33	49.95	22.25	0.699	0.369	**0.000**	3.745	0.013	2.233
	75 DAO	48.43	17.85	38.39	10.18	0.452	2.731	**0.000**	4.78	0.533	0.907
A (µmol m^{-2} s^{-1})	65 DAO	55.21	9.19	44.48	8.97	0.234	28.872	**0.000**	4.659	**0.014**	2.247
E (mol m^{-2} s^{-1})	65 DAO	0.04	0.01	0.03	0.01	0.151	2.087	**0.000**	4.848	0.062	1.775
Ci (µmol mol^{-1})	65 DAO	365.33	26.25	359.62	20.00	0.666	0.697	0.640	0.799	0.998	0.180

Note: Mean values of all genotypes are shown. LS, least square means; DAO, days after ozone; SD, standard deviation; LBS, leaf bronzing score; NDVI, normalized difference vegetation index; Lic2, Lichtenthaler index 2; NBI, nitrogen balance index; gsw, stomatal conductance(mol m^{-2} s^{-1}); PhiPS2, quantum efficiency of photosystem II; ETR, electron transport rate (µmol m^{-2} s^{-1}); A, CO_2 assimilation rate (µmol m^{-2} s^{-1}); E, transpiration rate (mol m^{-2} s^{-1}); Ci, intercellular CO_2 concentration (µmol mol^{-1}).

Stomatal conductance (gsw) was particularly sensitive to ozone stress, showing substantial reductions across all stages, with pronounced treatment effects at 16 and 60 DAO (Table 10). This suggests that stomatal closure under ozone stress limits gas exchange, a key physiological response. Significant genotypic effects (at 16, 30, and 75 DAO) and genotype × treatment interactions (at 16, 30, and 60 DAO) highlight the variation among genotypes in their ability to regulate stomata under ozone stress (Table 10). The Quantum Efficiency of Photosystem II (PhiPS2) and Electron Transport Rate (ETR), key indicators of photosynthetic efficiency, also demonstrated reductions under ozone stress. Although the decline in PhiPS2 was moderate, ETR showed consistent declines under stress at all stages. These changes indicate the detrimental impact of ozone on photosynthetic efficiency and energy transfer processes. Significant genotype effects for these traits suggest the potential for selecting genotypes with superior photosynthetic efficiency under stress conditions (Table 10). Furthermore, the CO_2 assimilation rate (A) was decreased under ozone stress, as observed at 65 DAO, highlighting compromised photosynthetic capacity. Other physiological traits such as transpiration rate (E) and intercellular CO_2 concentration (Ci) showed minor variations, with limited statistical significance in their responses to ozone stress (Table 10).

Further, we assessed the agronomic performance of the breeding lines under both control and ozone stress conditions. Ozone stress reduced the mean number of days to flowering compared to the control, although this reduction was not statistically significant (Table 11). Similarly, ozone stress decreased the days to maturity, but the treatment effect remained nonsignificant. In contrast, genotypes exhibited highly significant effects, and genotype × treatment interactions were significant for both traits, highlighting the differential responses of the genotypes to ozone stress (Table 11). Under ozone stress, plant height was slightly reduced compared to control conditions. However, the treatment effect was non-significant, whereas genotype was a significant factor (Table 11).

For the tiller number, we observed an increase in ozone stress compared to the control, but neither treatment nor genotype-treatment interaction significantly influenced this trait. However, genotype effects were significant. In contrast, panicle number showed minimal differences between treatments, with no significant treatment effects, though genotype significantly impacted this trait (Table 11). The number of filled grains per panicle decreased under ozone stress compared to control conditions. Despite this decline, the treatment effect

was not statistically significant, but genotype played a significant role. However, the number of unfilled grains increased under ozone stress compared to control, with significant genotype contributions and interaction between genotype and treatment. Additionally, unfilled grain weight exhibited a significant increase under stress, with treatment, genotype, and interaction effects being significant (Table 11). Thousand-grain weight, a critical yield determinant, was marginally reduced under stress compared to control conditions. While the treatment effect was not significant, genotype and interaction significantly influenced this trait (Table 11).

In terms of grain yield, a reduction from control to ozone stress was observed, although the treatment effect was not statistically significant. Genotype was a major determinant, highlighting genetic differences in yield potential under ozone stress. A similar trend was seen for straw biomass, which decreased under ozone stress compared to control, with genotype having a significant effect but treatment remaining non-significant (Table 11). Interestingly, the harvest index, an indicator of resource allocation between grain and biomass, increased under ozone stress compared to control. While treatment effects were not significant, genotype and genotype-treatment interaction had significant influences, indicating genetic variability in the ability to maintain a higher harvest index under ozone stress conditions (Table 11).

Table 11 Descriptive statistics and analysis of variance (ANOVA) of agronomic traits of breeding lines originating from BRRI dhan28 X Kasalath under ozone stress and control conditions.

Traits	LS means (treatment)				ANOVA					
	Control		Ozone		Ozone-Treatment		Genotype		Interaction	
	Mean	SD	Mean	SD	Pr(>F)	F values	Pr(>F)	F values	Pr(>F)	F values
Days to flowering	96.02	5.91	91.88	5.77	0.1993	16.61	**<0.0000**	147.22	**0.0000**	5.19
Days to maturity	131.18	5.65	125.16	5.36	0.0931	46.79	**<0.0000**	175.44	**<0.0000**	10.65
Plant height (cm)	132.11	15.70	127.10	15.88	0.8023	3.36	**<0.0000**	133.09	0.9885	0.28
Tiller number	10.21	2.61	11.13	2.38	0.4248	2.06	**0.0000**	4.11	0.7564	0.68
Panicle number	9.94	2.62	9.76	2.26	0.8111	0.12	**0.0000**	4.48	0.3593	1.10
Filled grain number	1333.51	306.78	1208.93	314.14	0.4106	3.93	**0.0000**	8.00	0.112	1.55
Unfilled grain number	137.48	123.40	201.27	181.40	0.2811	14.21	**<0.0000**	52.25	**0.0000**	6.21
Unfilled grain weight (g)	0.41	0.33	0.64	0.50	**0.0001**	58.08	**<0.0000**	34.87	**0.0000**	4.93
Thousand-grain weight (g)	18.52	1.88	18.15	1.92	0.4902	5.18	**<0.0000**	175.64	**0.0000**	6.13
Grain yield (g)	24.42	5.31	21.70	5.35	0.3364	8.20	**0.0000**	7.43	0.0644	1.73
Straw biomass (g)	26.69	7.70	22.68	6.89	0.4757	5.85	**<0.0000**	23.79	0.9367	0.44
Harvest index	48.19	4.89	49.14	4.24	0.6784	0.36	**<0.0000**	14.86	**0.0023**	2.70

Note: Mean values of all genotypes are shown. LS, least square means; SD, standard deviation.

Breeding lines from Binadhan-11 X Kasalath cross

Leaf bronzing score (LBS) increased significantly under ozone stress, with noticeable effects starting at 33 DAO and peaking at 75 DAO. ANOVA revealed highly significant effects for genotype and genotype-treatment interactions, suggesting substantial variation among genotypes in response to ozone (Table 12). The normalized difference vegetation index (NDVI), although stable initially (16 DAO), declined under ozone stress at later stages (75 DAO), with consistent significance for genotype effects. Similarly, the Lichtenthaler index 2 (Lic2) demonstrated a marked reduction under ozone stress, especially at 60 and 75 DAO, with highly significant genotype and genotype-treatment interactions at these time points (Table 12). The nitrogen balance index (NBI) exhibited a complex response to ozone stress, with notable reductions becoming more evident only at 60 DAO. Our analysis revealed highly significant effects of genotype and their interactions on NBI (Table 12).

The stomatal conductance (gsw) decreased sharply under ozone stress across all time points, notably at 16 and 33 DAO, with highly significant genotype and interaction effects. For quantum efficiency of photosystem II (PhiPS2), minor reductions were observed under ozone stress, with significant genotype and treatment interaction at 33 DAO. The electron transport rate (ETR) followed a similar trend, declining markedly under stress, particularly at 16 and 75 DAO, with significant genotype effects at all time points and genotype-treatment interactions at several stages (Table 12).

Furthermore, ozone stress also negatively affected photosynthesis parameters, including CO_2 assimilation rate (A) and transpiration rate (E), while intercellular CO_2 concentration (Ci) showed minimal variation between treatments. Statistical analysis consistently highlighted the significant effects of genotype on these traits, and we did not observe genotype-treatment interactions for intercellular CO_2 concentration (Ci) (Table 12).

Across the measured agronomic traits, we observed a less dramatic effect of ozone stress compared to the control condition. For instance, days to flowering and maturity decreased slightly under ozone stress compared to control conditions, although these differences were not statistically significant (Table 13). Similarly, plant height and grain yield reductions were observed, but treatment effects alone were not significant for these traits. Notable variability was evident in grain yield components, with filled grain number decreasing significantly under ozone stress, as indicated by significant genotype × treatment interactions (Table 13).

Table 12 Descriptive statistics and analysis of variance (ANOVA) for physiological traits of breeding lines derived from the cross between Binadhan-11 and Kasalath under ozone stress and control conditions.

Traits	Date	LS means (treatment)				ANOVA					
		Control		Ozone		Ozone-Treatment		Genotype		Interaction	
		Mean	SD	Mean	SD	Pr(>F)	F values	Pr(>F)	F values	Pr(>F)	F values
LBS	16 DAO	0.00	0.00	0.56	0.99	0.200	11.762	**0.000**	8.154	**0.000**	8.154
	33 DAO	0.00	0.00	2.00	1.21	0.275	15.314	**<0.000**	14.819	**<0.000**	14.819
	60 DAO	0.00	0.00	2.38	1.20	0.249	21.495	**<0.000**	15.569	**<0.000**	15.569
	75 DAO	0.00	0.00	3.03	1.34	0.213	36.478	**<0.000**	17.03	**<0.000**	17.03
NDVI	16 DAO	0.66	0.05	0.66	0.04	0.888	0.030	**<0.000**	12.551	0.065	1.770
	33 DAO	0.66	0.03	0.65	0.03	0.309	4.000	**<0.000**	14.806	**0.011**	2.348
	60 DAO	0.66	0.05	0.65	0.05	0.851	0.052	**<0.000**	46.448	**<0.000**	17.413
	75 DAO	0.67	0.07	0.63	0.07	0.114	10.296	**<0.000**	23.865	**0.000**	5.485
Lic2	16 DAO	0.83	0.08	0.87	0.29	0.599	0.595	0.318	1.159	0.304	1.179
	33 DAO	0.87	0.05	0.82	0.08	0.151	2.700	**0.000**	10.379	0.508	0.928
	60 DAO	0.82	0.07	0.79	0.08	**0.000**	25.232	**<0.000**	25.980	**0.000**	10.265
	75 DAO	0.84	0.10	0.78	0.10	0.104	3.652	**<0.000**	24.442	**0.009**	2.390
NBI	16 DAO	32.56	9.08	33.58	9.35	0.945	0.008	**0.000**	8.680	**0.050**	1.861
	33 DAO	40.20	10.70	39.18	9.53	0.789	0.291	**0.001**	3.199	**0.001**	3.221
	60 DAO	37.74	9.34	29.74	7.38	0.959	0.013	**0.000**	5.496	0.716	0.709
	75 DAO	32.51	9.06	33.05	12.49	0.890	0.073	**<0.000**	23.491	**0.000**	8.366
gsw (mol m^{-2} s^{-1})	16 DAO	0.42	0.22	0.17	0.10	**0.002**	111.713	**0.000**	6.541	**0.000**	5.331
	33 DAO	0.28	0.16	0.12	0.11	**0.000**	48.707	**<0.000**	21.739	**0.020**	2.152
	60 DAO	0.35	0.16	0.16	0.12	0.070	15.977	**0.019**	2.169	**0.000**	4.753
	75 DAO	0.21	0.16	0.11	0.08	**0.000**	65.042	**0.004**	2.604	**0.023**	2.112

PhiPS2	16 DAO	0.72	0.04	0.72	0.03	0.644	0.350	0.142	1.489	0.250	1.264
	33 DAO	0.64	0.09	0.59	0.13	0.110	3.999	0.027	2.063	**0.008**	2.446
	60 DAO	0.60	0.11	0.59	0.11	**0.003**	8.768	0.420	1.028	0.080	1.696
	75 DAO	0.53	0.12	0.53	0.12	0.932	0.009	0.271	1.229	0.669	0.757
ETR (µmol m^{-2} s^{-1})	16 DAO	69.16	33.24	48.33	21.36	0.465	1.281	**0.001**	3.065	0.344	1.123
	33 DAO	75.10	36.01	67.64	41.21	0.870	0.055	**0.000**	6.127	**0.007**	2.474
	60 DAO	62.18	25.75	56.49	22.89	0.817	0.127	**0.007**	2.480	**0.035**	1.983
	75 DAO	52.02	19.50	41.12	11.06	0.422	4.339	**0.002**	2.855	**0.037**	1.952
A (µmol m^{-2} s^{-1})	65 DAO	46.63	9.17	44.34	13.22	0.687	0.404	**0.000**	8.502	**0.000**	3.816
E (mol m^{-2} s^{-1})	65 DAO	0.03	0.01	0.02	0.01	0.148	2.750	**0.000**	6.059	**0.025**	2.123
Ci (µmol mol^{-1})	65 DAO	354.30	29.91	344.58	17.94	0.458	2.501	**0.001**	3.124	0.839	0.565

Note: Mean values of all genotypes are shown. LS, least square means; DAO, days after ozone; SD, standard deviation; LBS, leaf bronzing score; NDVI, normalized difference vegetation index; Lic2, Lichtenthaler index 2; NBI, nitrogen balance index; gsw, stomatal conductance(mol m^{-2} s^{-1}); PhiPS2, quantum efficiency of photosystem II; ETR, electron transport rate (µmol m^{-2} s^{-1}); A, CO_2 assimilation rate (µmol m^{-2} s^{-1}); E, transpiration rate (mol m^{-2} s^{-1}); Ci, intercellular CO_2 concentration (µmol mol^{-1}).

Genotypic effects were highly significant for all the measured traits, underscoring substantial variability among the breeding lines. Genotype × treatment interactions were significant for key traits such as days to maturity, grain yield, and harvest index, suggesting differential responses of genotypes to ozone stress. Traits such as tiller number, panicle number, unfilled grain weight, and harvest index remained relatively stable, with no significant treatment effects observed (Table 13).

Overall, the results from both crosses demonstrate that ozone stress adversely affects key physiological traits, particularly those related to photosynthesis and stomatal regulation. The significant genotype × treatment interactions observed for several traits, including LBS, NDVI, NBI, and gsw, underscore the genetic variability in response to ozone stress. Similarly, the results underscore the differential sensitivity of agronomic traits to ozone stress. While treatment alone often had limited significance, the pronounced effects of genotype and genotype-treatment interactions suggest that genotypes play a critical role in determining performance under stress conditions.

Table 13 Descriptive statistics and analysis of variance (ANOVA) of agronomic traits of breeding lines originating from Binadhan-11 X Kasalath under ozone stress and control conditions.

Traits	LS means (treatment)				ANOVA					
	Control		Ozone		Ozone-Treatment		Genotype		Interaction	
	Mean	SD	Mean	SD	Pr(>F)	F values	Pr(>F)	F values	Pr(>F)	F values
Days to flowering	124.66	13.24	120.15	13.37	0.1560	103.35	**<0.0000**	135.00	0.0598	1.80
Days to maturity	158.05	13.09	152.14	13.17	0.1221	234.59	**<0.0000**	474.12	**0.0003**	3.39
Plant height (cm)	114.22	21.01	112.00	20.28	0.3865	2.93	**<0.0000**	331.07	0.539	0.89
Tiller number	9.80	2.82	9.72	2.89	0.9637	0.00	**<0.0000**	7.15	0.1113	1.58
Panicle number	9.66	2.81	9.30	2.67	0.7776	0.35	**<0.0000**	5.52	0.1317	1.52
Filled grain number	877.39	331.07	821.83	359.74	0.7367	1.02	**<0.0000**	63.90	**0.0315**	2.01
Unfilled grain number	51.40	45.46	52.61	50.42	0.8654	0.05	**<0.0000**	9.94	0.6472	0.78
Unfilled grain weight (g)	0.20	0.19	0.19	0.20	0.5535	0.46	**0.0000**	6.69	0.6291	0.80
Thousand-grain weight (g)	22.38	2.48	21.74	2.24	0.5896	4.09	**0.0000**	85.50	0.81	0.60
Grain yield (g)	19.24	6.18	17.42	6.76	0.6837	2.28	**<0.0000**	37.67	**0.0107**	2.35
Straw biomass (g)	36.30	9.62	32.71	8.95	0.6961	2.43	**<0.0000**	9.35	0.3618	1.10
Harvest index	34.57	6.90	34.31	7.30	0.8773	0.07	**<0.0000**	57.31	**0.0273**	2.06

Note: Mean values of all genotypes are shown. LS, least square means; SD, standard deviation.

4.4.2 Associations among the measured traits

We analyzed the interrelationships between traits by conducting a correlation analysis and principal component analysis (PCA). This approach allowed us to examine the relationships among morphological, physiological, and yield-related traits, focusing specifically on grain yield and straw biomass. For this analysis, we used relative values calculated as the ratio of the trait value under the stress treatment to its value under the control. Additionally, data collected at various growth stages were averaged to compute relative values that reflect the overall responses of different genotypes throughout the growth period.

Breeding lines from BRRI Dhan28 X Kasalath cross

The stress response indicator, leaf bronzing score (LBS), showed a negative correlation with all non-destructive indices (NDVI, Lic2, and NBI), photosynthetic traits (gsw, PhiPS2, ETR, and A), and yield-related trait (panicle number) (Figure 38). This relationship highlights that visible stress symptoms are closely associated with physiological inefficiencies and reductions in yield. Furthermore, non-destructive indices like the normalized difference vegetation index (NDVI) and nitrogen balance index (NBI) were positively correlated with both yield and photosynthetic parameters, showcasing their potential as reliable indicators of plant health under stress. Among the Photosynthetic parameters, stomatal conductance (gsw), quantum efficiency of photosystem II (PhiPS2) and electron transport rate (ETR) were positively correlated with grain yield (GY), underscoring the critical role of photosynthetic efficiency in determining yield outcomes. Grain yield (GY) showed a significant positive correlation with panicle number (PN) and filled grain number (FGN), demonstrating their direct contributions to productivity. Harvest index (HI) was positively associated with GY but negatively correlated with straw biomass (SB), suggesting efficient biomass partitioning to grains is vital for higher yields (Figure 38).

The Principal Component Analysis (PCA) biplot illustrates that the first principal component (Dim1) explains 44.5% of the total variance, while the second principal component (Dim2) accounts for 17.3% of the total variance. These two dimensions (Dim1 and Dim2) explain a combined 61.8% of the total variance (Figure 39).

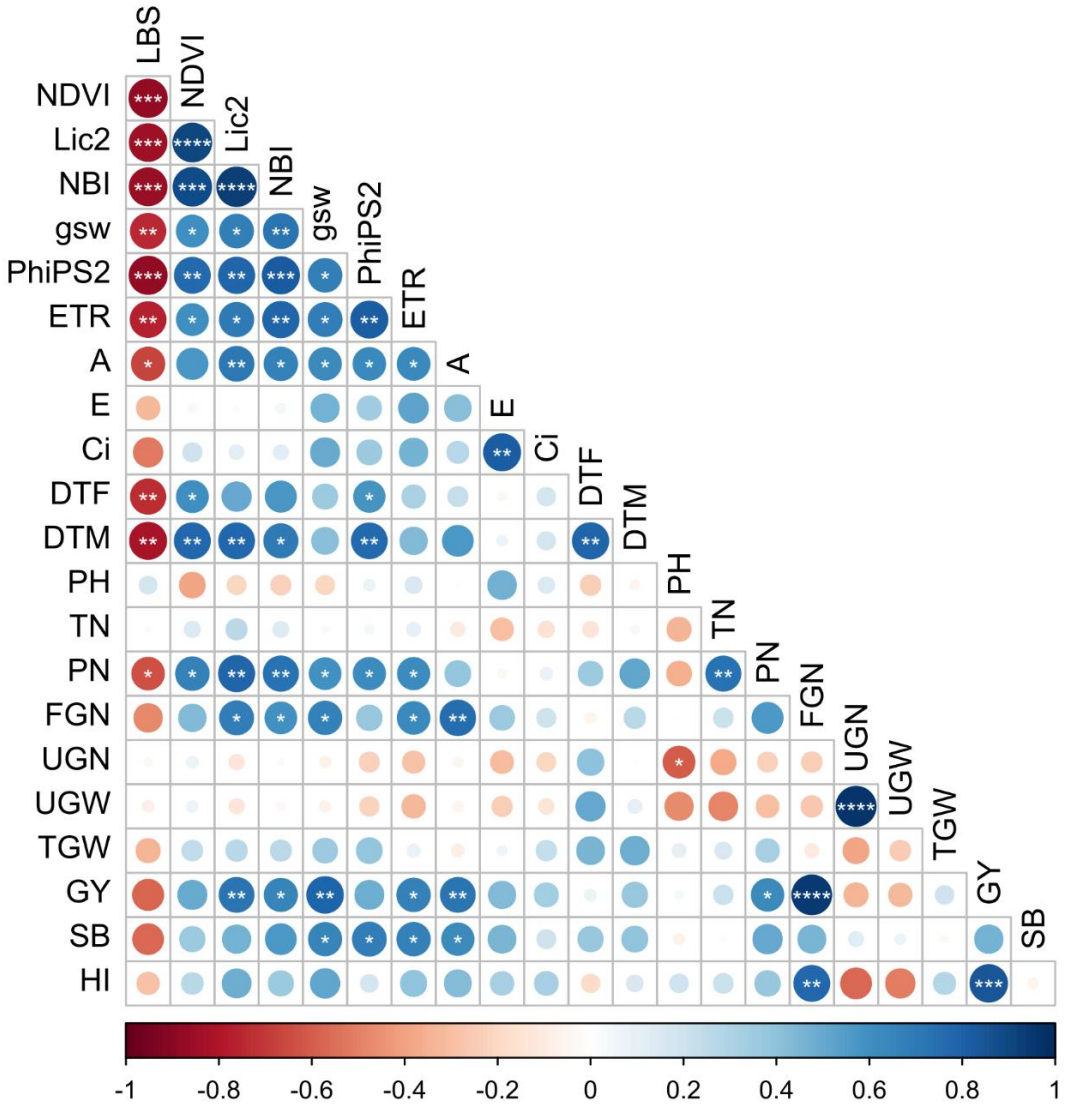

Figure 38 Pearson correlation matrix for morphological, physiological, and yield-related traits of rice breeding lines carrying *OzT8* and/or *OzT9* derived from the cross BRRI dhan28 × Kasalath under ozone stress and control conditions. Asterisk indicates statistically significant correlation at *p < 0.05; ** p < 0.01; p < 0.001; ***; p < 0.0001****. LBS, leaf bronzing score; NDVI, normalized difference vegetation index; Lic2, Lichtenthaler index 2; NBI, nitrogen balance index; gsw, stomatal conductance; PhiPS2, quantum efficiency of photosystem II; ETR, electron transport rate; A, CO_2 assimilation rate; E, transpiration rate ; Ci, intercellular CO_2 concentration; DTF, days to flowering; DTM, days to maturity; PH, plant height; TN, tiller number; PN, panicle number; FGN, filled grain number; UFGN, unfilled grain number; UGW, unfilled grain weight; TGW, thousand-grain weight; GY, grain yield; SB, straw biomass; HI, harvest index. Relative values (ratio of value for plants grown under stress conditions relative to the control condition) were used except for LBS (n = 12).

Variables such as days to flowering (DTF), days to maturity (DTM), normalized difference vegetation index (NDVI), nitrogen balance index (NBI), Lichtenthaler index 2 (Lic2), quantum efficiency of photosystem II (PhiPS2), panicle number (PN), and straw biomass (SB) form a tightly linked cluster, indicating that these traits are strongly related and contributing to Dim1. Another grouping involves the photosynthetic and transpiration-related traits, including CO_2 assimilation rate (A), stomatal conductance (gsw), electron transport rate (ETR), transpiration rate (E), filled grain number (FGN), grain yield (GY) and harvest index (HI) are closely associated, highlighting their interdependence and also aligned along Dim1 (Figure 39).

In contrast, leaf bronzing score (LBS) showed a negative correlation with all non-destructive indices (NDVI, Lic2, and NBI), photosynthetic traits (gsw, PhiPS2, ETR, and A), and yield-related traits (panicle number, straw biomass), as evidenced by the vectors pointing in opposite directions, suggesting that increased leaf bronzing under ozone stress is associated with a decline in crop physiological activity and yield performance (Figure 39).

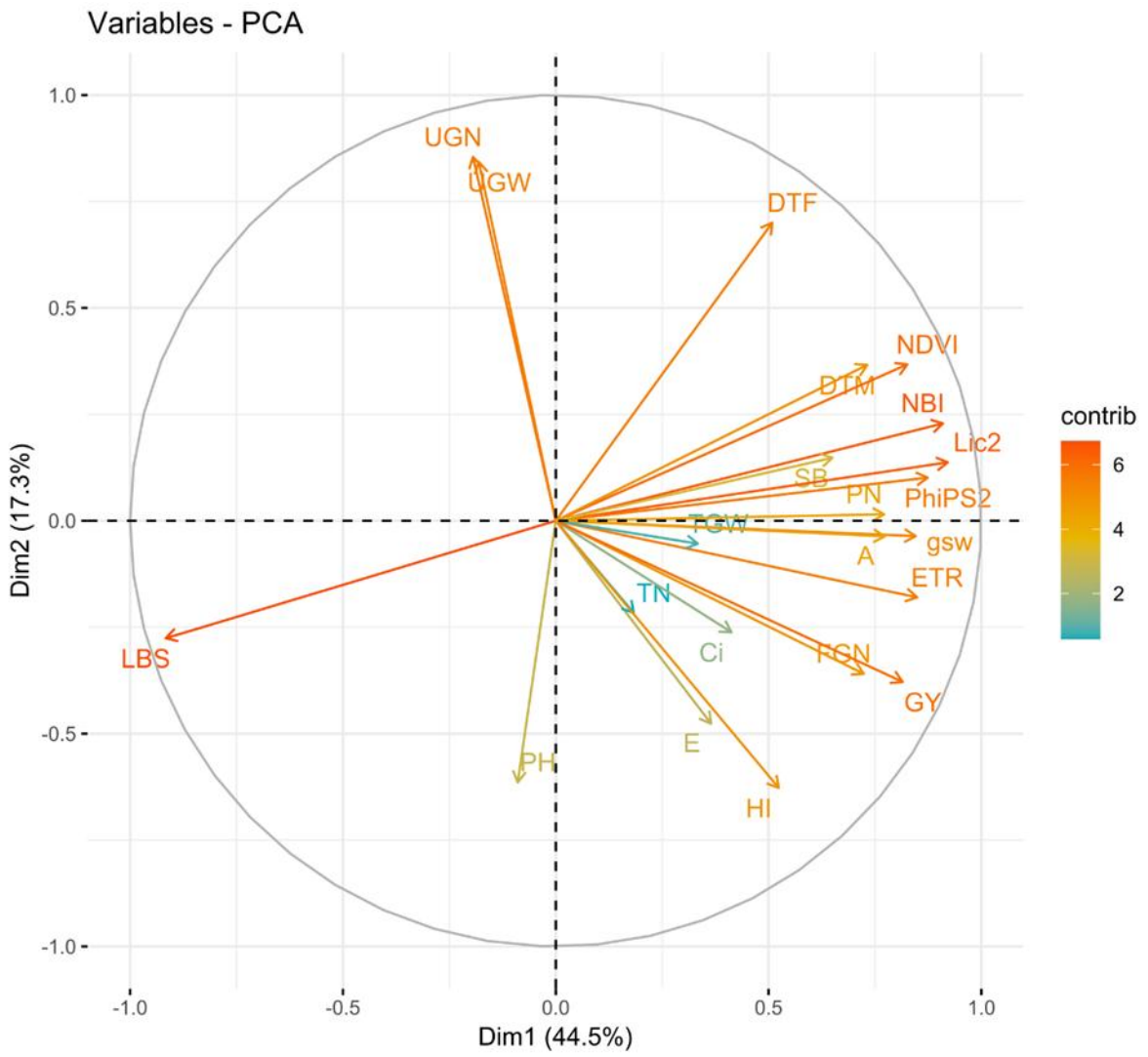

Figure 39 Principal component analysis (PCA) biplot showing the distributions of the measured traits of rice breeding lines carrying *OzT8* and/or *OzT9* derived from the cross BRRI dhan28 × Kasalath under ozone stress and control conditions. LBS, leaf bronzing score; NDVI, normalized difference vegetation index; Lic2, Lichtenthaler index 2; NBI, nitrogen balance index; gsw, stomatal conductance; PhiPS2, quantum efficiency of photosystem II; ETR, electron transport rate; A, CO_2 assimilation rate; E, transpiration rate; Ci, intercellular CO_2 concentration; DTF, days to flowering; DTM, days to maturity; PH, plant height; TN, tiller number; PN, panicle number; FGN, filled grain number; UFGN, unfilled grain number; UGW, unfilled grain weight; TGW, thousand-grain weight; GY, grain yield; SB, straw biomass; HI, harvest index. Relative values (ratio of value for plants grown under stress conditions relative to the control condition) were used except for LBS (n = 12).

Breeding lines from Binadhan-11 X Kasalath cross

LBS exhibited a significant negative correlation with NBI and photosynthetic traits (PhiPS2, ETR, and A), indicating the adverse effects of ozone stress on overall plant performance (Figure 40). In contrast, NDVI and NBI showed a positive correlation with photosynthetic parameters such as PhiPS2, ETR, and A. Notably, among the non-destructive indices, only NBI displayed a significant positive correlation with grain yield (GY) and straw biomass (SB). Among the photosynthetic parameters, stomatal conductance (gsw), quantum efficiency of photosystem II (PhiPS2), and electron transport rate (ETR) were positively correlated with both GY and SB. Additionally, GY and SB were significantly and positively correlated with tiller number (TN), panicle number (PN), and filled grain number (FGN), emphasizing their mutual interdependence and collective role in enhancing productivity (Figure 40).

The Principal Component Analysis (PCA) biplot revealed that the first principal component (Dim1) accounts for 53.1% of the total variance, while the second principal component (Dim2) explains 15% of the total variance. Together, Dim1 and Dim2 capture 68.1% of the total variance (Figure 41). Key variables such as grain yield (GY), straw biomass (SB), harvest index (HI), panicle number (PN), tiller number (TN), filled grain number (FGN), electron transport rate (ETR), and stomatal conductance (gsw) formed a closely linked cluster. Another distinct cluster comprised variables related to phenology and photosynthesis, including days to flowering (DTF), days to maturity (DTM), normalized difference vegetation index (NDVI), nitrogen balance index (NBI), Lichtenthaler index 2 (Lic2), quantum efficiency of photosystem II (PhiPS2), and CO_2 assimilation rate (A). In contrast, LBS, a marker for ozone-induced stress, exhibited a negative association with grain yield and other growth-related parameters (Figure 41).

Based on the Pearson correlation matrix and Principal Component Analysis (PCA) of both crosses, we selected traits for further analysis. Our selection focused on traits significantly correlated with grain yield and/or straw biomass in the crosses BRRI dhan28 and/or Binadhan-11. Additionally, we considered the relatedness of traits as revealed by PCA.

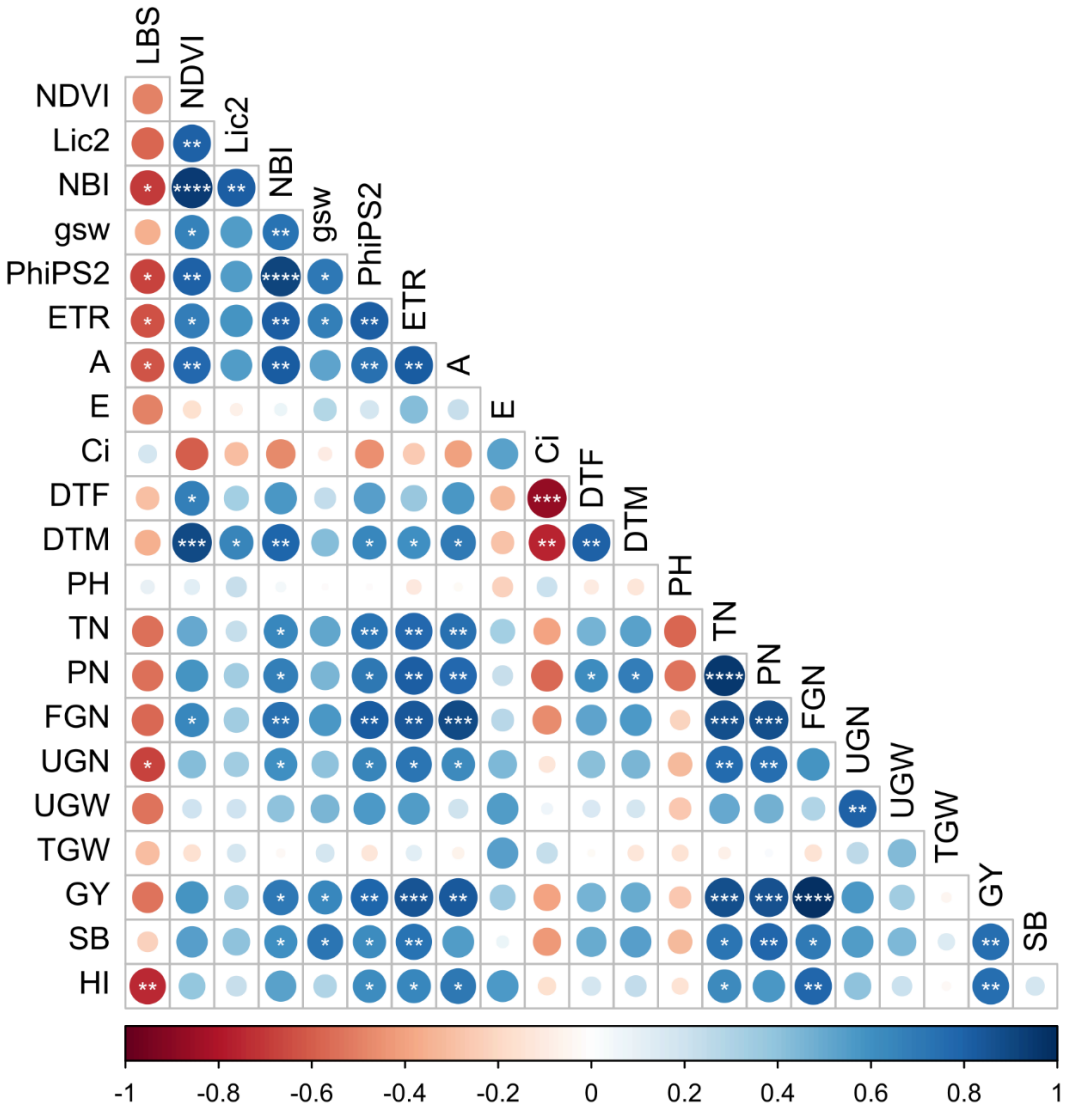

Figure 40 Pearson correlation matrix for morphological, physiological, and yield-related traits of rice breeding lines carrying *OzT8* and/or *OzT9* derived from the cross Binadhan-11 × Kasalath under ozone stress and control conditions. Asterisk indicates statistically significant correlation at *p < 0.05; ** p < 0.01; p < 0.001; ***; p < 0.0001****. LBS, leaf bronzing score; NDVI, normalized difference vegetation index; Lic2, Lichtenthaler index 2; NBI, nitrogen balance index; gsw, stomatal conductance; PhiPS2, quantum efficiency of photosystem II; ETR, electron transport rate; A, CO_2 assimilation rate; E, transpiration rate; Ci, intercellular CO_2 concentration; DTF, days to flowering; DTM, days to maturity; PH, plant height; TN, tiller number; PN, panicle number; FGN, filled grain number; UFGN, unfilled grain number; UGW, unfilled grain weight; TGW, thousand-grain weight; GY, grain yield; SB, straw biomass; HI, harvest index. Relative values (ratio of value for plants grown under stress conditions relative to the control condition) were used except for LBS (n = 11).

From these analyses, we identified the following traits for further investigation: Lichtenthaler index 2 (Lic2), nitrogen balance index (NBI), stomatal conductance (gsw), quantum efficiency of photosystem II (PhiPS2), electron transport rate (ETR), CO_2 assimilation rate (A), tiller number (TN), panicle number (PN), filled grain number (FGN), grain yield (GY), straw biomass (SB), and harvest index (HI).

Moreover, we included leaf bronzing score (LBS) and NDVI due to their strong association with grain yield (GY) and/or straw biomass (SB) as indicated by PCA. We averaged the data collected at different growth stages to evaluate the performance of the breeding lines.

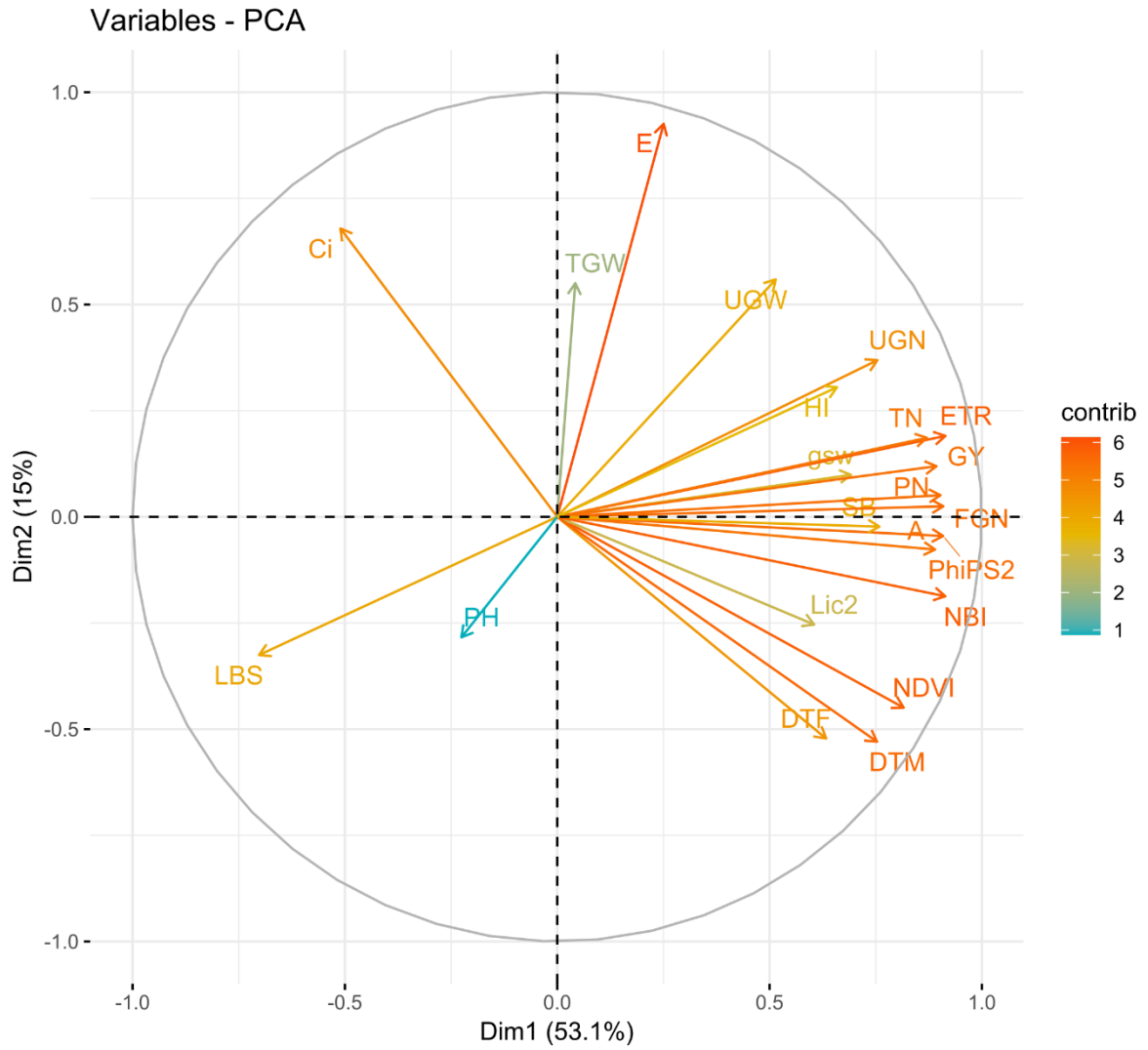

Figure 41 Principal component analysis (PCA) biplot showing the distributions of the measured traits of rice breeding lines carrying *OzT8* and/or *OzT9* derived from the cross Binadhan-11 × Kasalath under ozone stress and control conditions. LBS, leaf bronzing score; NDVI, normalized difference vegetation index; Lic2, Lichtenthaler index 2; NBI, nitrogen balance index; gsw, stomatal conductance; PhiPS2, quantum efficiency of photosystem II; ETR, electron transport rate; A, CO_2 assimilation rate; E, transpiration rate; Ci, intercellular CO_2 concentration; DTF, days to flowering; DTM, days to maturity; PH, plant height; TN, tiller number; PN, panicle number; FGN, filled grain number; UFGN, unfilled grain number; UGW, unfilled grain weight; TGW, thousand-grain weight; GY, grain yield; SB, straw biomass; HI, harvest index. Relative values (ratio of value for plants grown under stress conditions relative to the control condition) were used except for LBS (n = 11).

4.4.3 Assessment of leaf bronzing score and foliar pigments in breeding lines

Breeding lines from BRRI Dhan28 X Kasalath cross

Under ozone stress, we observed a significant reduction in the leaf bronzing score (LBS) among breeding lines carrying the *OzT8* and/or *OzT9* QTLs compared to the recipient parent, BRRI dhan28. Among the genotypes evaluated, lines carrying only *OzT9* exhibited the lowest average LBS (1.77), followed by lines possessing both QTLs (*OzT8* + *OzT9*) (1.81), and those carrying only *OzT8* (2.32). At the individual genotype level, the lowest LBS was recorded for MFOL-1956 (1.64), which carried *OzT9*. This was followed by MFOL-1378 (1.66) and MFOL-1547 (1.77), both of which harbored the combined QTLs (*OzT8* + *OzT9*) (Figure 42A).

Breeding lines possessing both QTLs (*OzT8* + *OzT9*) exhibited the highest mean relative normalized difference vegetation index (NDVI), surpassing those that carried either *OzT9* or *OzT8* individually. Among all genotypes assessed, MFOL-1378 recorded the highest relative NDVI, followed by MFOL-1488 and MFOL-1547. Notably, all three genotypes contained both QTLs (*OzT8* + *OzT9*) (Figure 43A).

Breeding lines possessing both QTLs (*OzT8* + *OzT9*) demonstrated the highest mean relative Lic2 values, surpassing those observed in lines carrying either *OzT9* or *OzT8* individually (Figure 44A). Among the evaluated genotypes, MFOL-1547 (*OzT8* + *OzT9*) exhibited the highest relative Lic2 value, followed by MFOL-328 (*OzT9*) and MFOL-1491 (*OzT8* + *OzT9*) (Figure 44A).

Breeding lines possessing both QTLs (*OzT8* + *OzT9*) demonstrated the highest average relative NBI, with lines carrying only *OzT8* or *OzT9* exhibiting comparatively lower values. Among the genotypes analyzed, MFOL-1491 (*OzT8* + *OzT9*), recorded the highest relative NBI, followed by MFOL-1547 (*OzT8* + *OzT9*) and MFOL-2197 (*OzT8*) (Figure 45A).

Breeding lines from Binadhan-11 X Kasalath cross

Breeding lines carrying only *OzT9* exhibited the lowest average leaf blast severity (LBS) score (1.85), followed by lines with *OzT8* (1.91) and those carrying both QTLs (*OzT8* + *OzT9*) (2.02). These values were significantly lower compared to the recipient parent, Binadhan-11. Among the individual genotypes evaluated, the lowest LBS was observed in MFOL-50 (1.36), which carried both QTLs (*OzT8* + *OzT9*). This was followed by MFOL-1102 (1.61), harboring *OzT9*, and MFOL-60 (1.64), which also carried both QTLs (*OzT8* + *OzT9*) (Figure 42B).

Breeding lines possessing both QTLs (*OzT8* + *OzT9*) exhibited the highest average relative NDVI values, followed by lines containing the *OzT9* and *OzT8* QTLs individually. Among the genotypes evaluated, MFOL-471 (*OzT8* + *OzT9*) displayed the highest relative NDVI, followed by MFOL-1102 (*OzT9*) and MFOL-544 (*OzT8* + *OzT9*) (Figure 43B).

Breeding lines possessing both QTLs (*OzT8* + *OzT9*) demonstrated the highest average relative Lic2 values, as compared to lines carrying either *OzT9* or *OzT8* individually. Among the evaluated genotypes, MFOL-50 (*OzT8* + *OzT9*), exhibited the highest relative Lic2 value, followed by MFOL-1302 (*OzT9*) and MFOL-544 (*OzT8* + *OzT9*) (Figure 44B).

Breeding lines that carried both QTLs (*OzT8* + *OzT9*) demonstrated the highest mean relative NBI values, surpassing those of lines containing either *OzT9* or *OzT8* individually. Among the genotypes analyzed, MFOL-50 (*OzT8* + *OzT9*) exhibited the highest relative NBI, followed by MFOL-471 (*OzT8* + *OzT9*) and MFOL-1102 (*OzT9*) (Figure 45B).

Overall, these results suggested that, for leaf bronzing score (LBS), lines with *OzT9* alone performed best, exhibiting the lowest scores, while those with both *OzT8* and *OzT9* followed closely. Among the genotypes derived from the BRRI dhan28 × Kasalath cross, MFOL-1956 (*OzT9*) recorded the lowest LBS (1.64), while MFOL-1378 (*OzT8* + *OzT9*) achieved the highest NDVI, MFOL-1547 (*OzT8* + *OzT9*) exhibited the highest relative Lic2, and MFOL-1491 (*OzT8* + *OzT9*) recorded the highest NBI. Similarly, in the Binadhan-11 × Kasalath cross, MFOL-50 (*OzT8* + *OzT9*) showed the lowest LBS (1.36), the highest relative Lic2, and the highest NBI, with MFOL-471 (*OzT8* + *OzT9*) leading in NDVI. These findings highlight the superiority of the combined *OzT8* and *OzT9* QTLs for overall performance, with specific genotypes such as MFOL-50, MFOL-1547, and MFOL-1491 standing out as top performers for multiple traits under ozone stress.

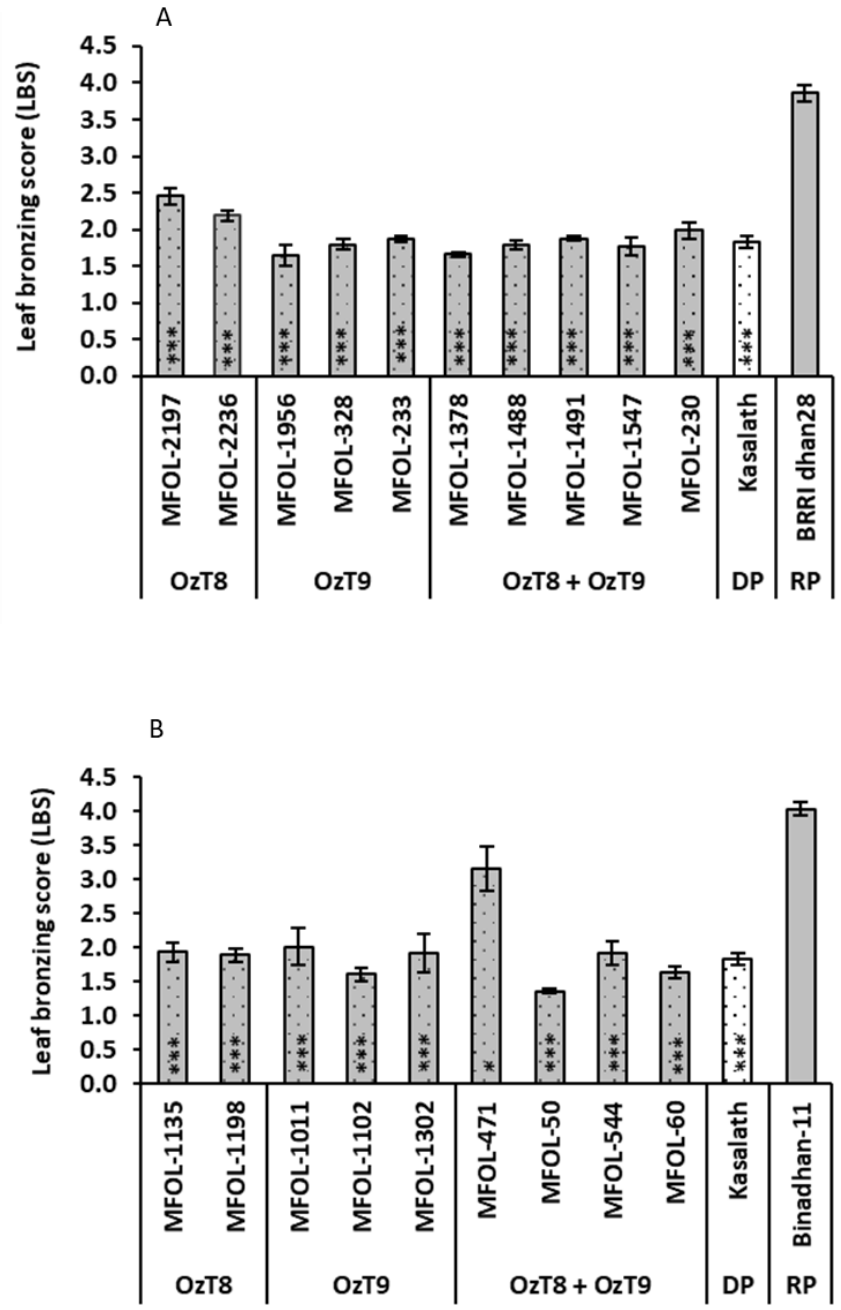

Figure 42 Leaf bronzing scores of selected breeding lines carrying *OzT8* and/or *OzT9* derived from the cross (A) BRRI dhan28 × Kasalath and (B) Binadhan-11 × Kasalath under ozone stress. The bar graphs display the mean and standard error of relative values (n = 4). Asterisks within the bars indicate significant differences between the genotypes and the recipient parent (BRRI dhan28 or Binadhan-11), as determined by Dunnett's test (*P < 0.05, **P < 0.01, ***P < 0.001). DP, donor parent, and RP, recipient parent.

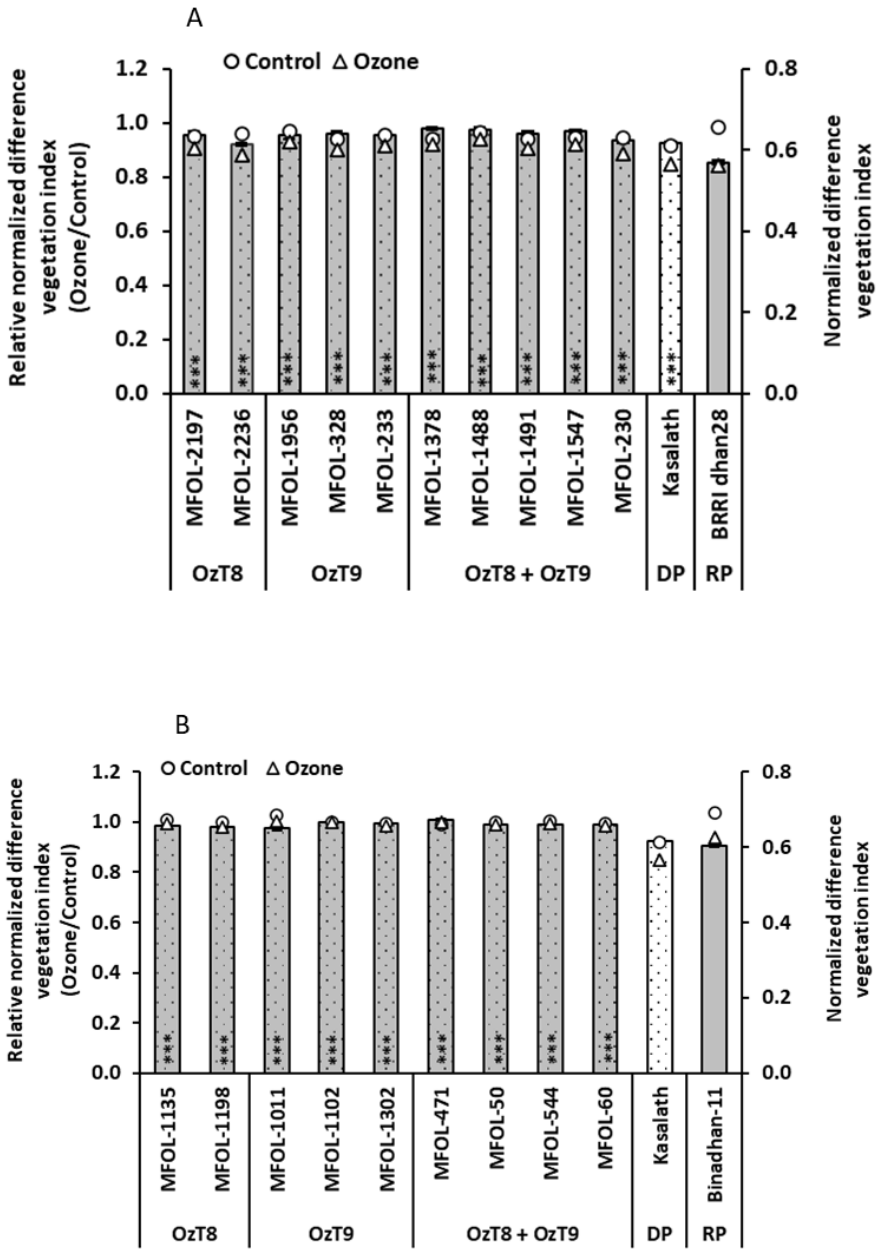

Figure 43 Normalized difference vegetation index of selected breeding lines carrying *OzT8* and/or *OzT9* derived from the cross (A) BRRI dhan28 × Kasalath and (B) Binadhan-11 × Kasalath under ozone stress and control conditions. The bar graphs display the mean and standard error of relative values (n = 4), while the circles and triangles represent absolute values for the control and ozone-treated groups, respectively. Asterisks within the bars indicate significant differences between the genotypes and the recipient parent (BRRI dhan28 or Binadhan-11), as determined by Dunnett's test (*P < 0.05, **P < 0.01, ***P < 0.001). DP, donor parent, and RP, recipient parent.

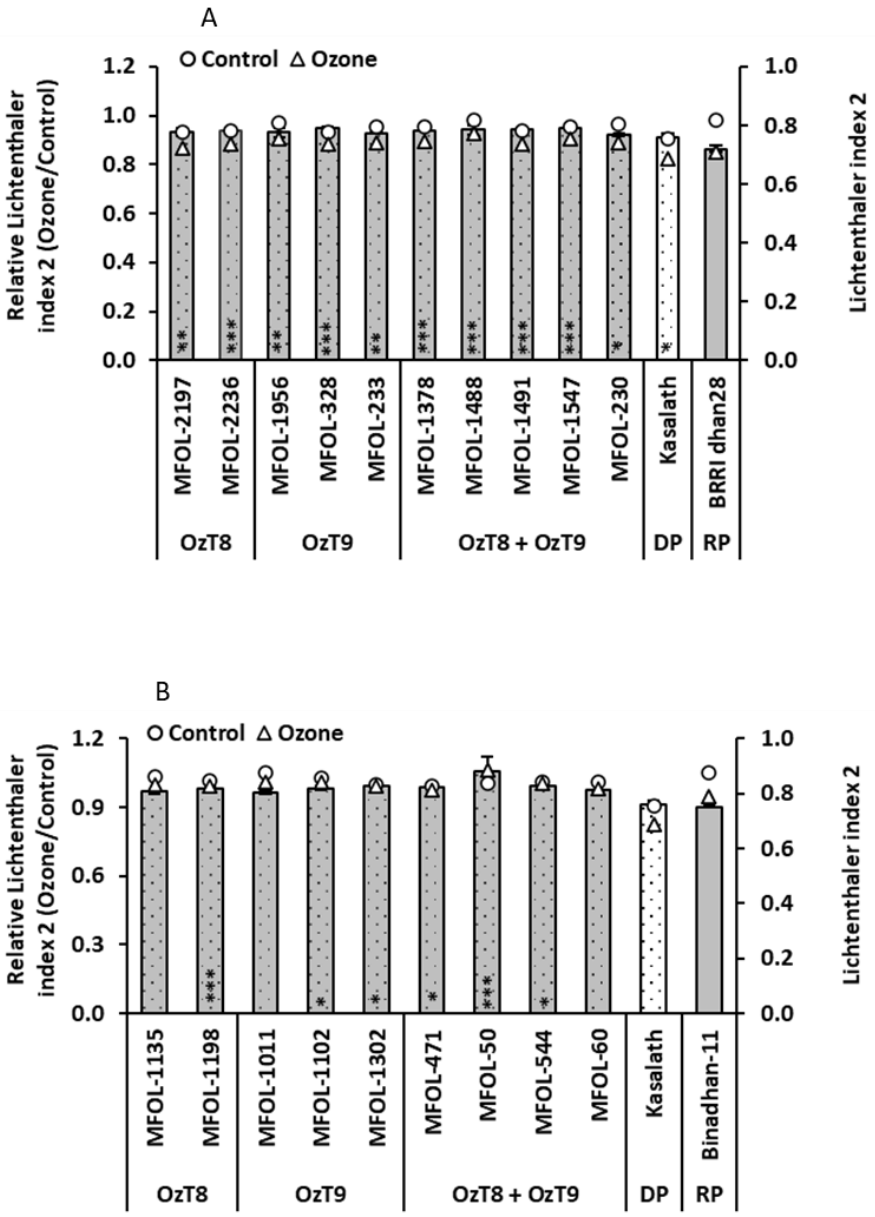

Figure 44 Lichtenthaler index 2 of selected breeding lines carrying *OzT8* and/or *OzT9* derived from the cross (A) BRRI dhan28 × Kasalath and (B) Binadhan-11 × Kasalath under ozone stress and control conditions. The bar graphs display the mean and standard error of relative values (n = 4), while the circles and triangles represent absolute values for the control and ozone-treated groups, respectively. Asterisks within the bars indicate significant differences between the genotypes and the recipient parent (BRRI dhan28 or Binadhan-11), as determined by Dunnett's test (*P < 0.05, **P < 0.01, ***P < 0.001). DP, donor parent, and RP, recipient parent.

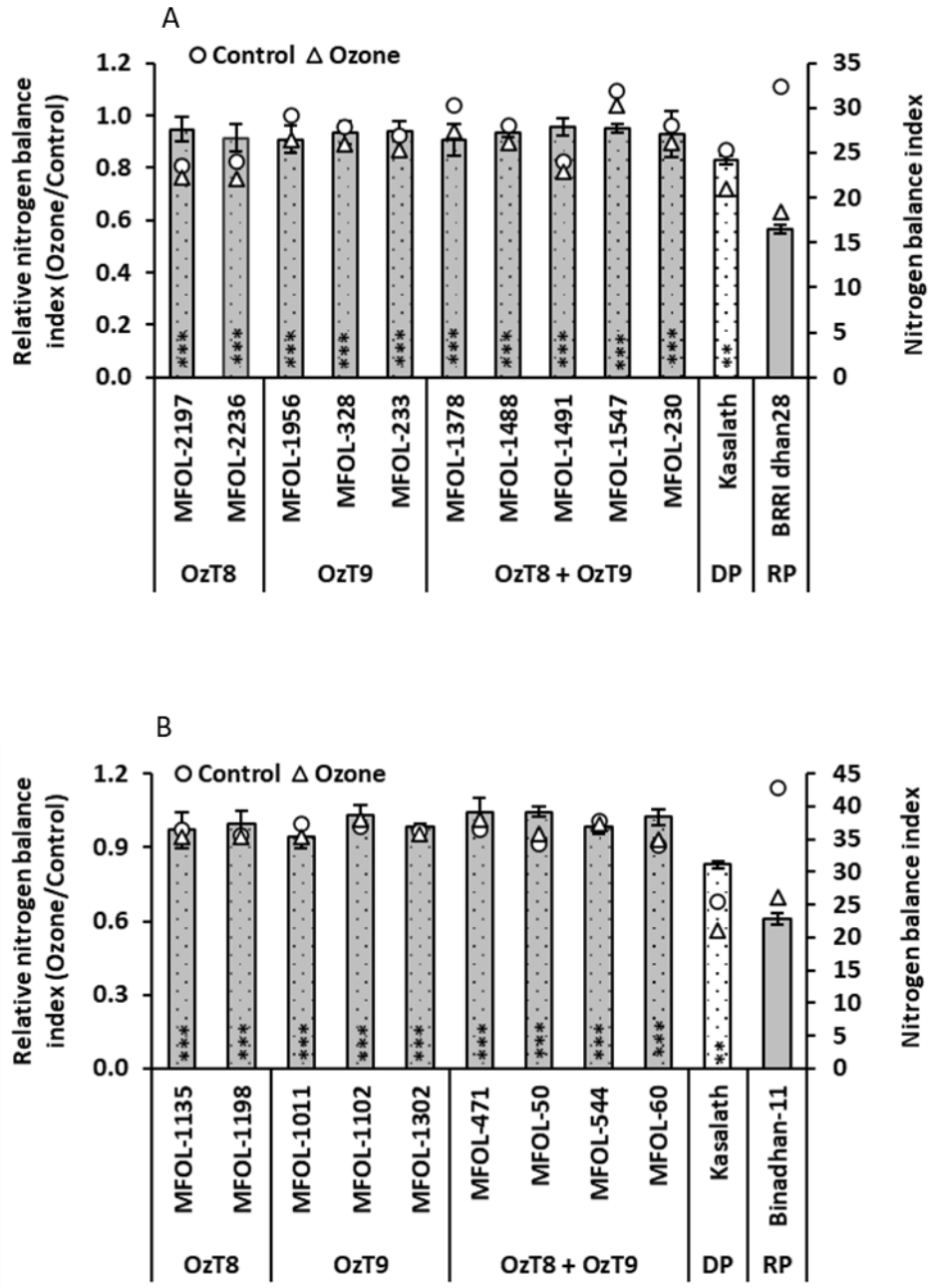

Figure 45 Nitrogen balance index of selected breeding lines carrying *OzT8* and/or *OzT9* derived from the cross (A) BRRI dhan28 × Kasalath and (B) Binadhan-11 × Kasalath under ozone stress and control conditions. The bar graphs display the mean and standard error of relative values (n = 4), while the circles and triangles represent absolute values for the control and ozone-treated groups, respectively. Asterisks within the bars indicate significant differences between the genotypes and the recipient parent (BRRI dhan28 or Binadhan-11), as determined by Dunnett's test (*P < 0.05, **P < 0.01, ***P < 0.001). DP, donor parent, and RP, recipient parent.

4.4.4 Photosynthetic efficiency and gas exchange dynamics in breeding lines

Breeding lines from BRRI Dhan28 X Kasalath cross

Breeding lines carrying *OzT8* exhibited the highest average relative gsw, followed by lines carrying *OzT9* and those possessing both QTLs (*OzT8* + *OzT9*). Among the individual genotypes, MFOL-328 (*OzT9*) demonstrated the highest relative gsw, followed by MFOL-233 (*OzT9*) and MFOL-2197 (*OzT8*) (Figure 46A).

Lines carrying both QTLs (*OzT8* + *OzT9*) exhibited the highest average relative PhiPS2 values, followed by lines containing only the *OzT8* QTL, and then those with only the *OzT9* QTL. Among individual genotypes, MFOL-1378 demonstrated the highest relative PhiPS2, followed by MFOL-230 and MFOL-1547. Notably, all three genotypes possessed both QTLs (*OzT8* + *OzT9*) (Figure 47A).

Lines carrying the *OzT8* QTL exhibited the highest mean relative ETR, followed by lines containing both QTLs (*OzT8* + *OzT9*), and then lines with the *OzT9* QTL alone. Among the individual genotypes, MFOL-1547 (*OzT8* + *OzT9*) recorded the highest relative ETR, with MFOL-2236 (*OzT8*) and MFOL-230 (*OzT8* + *OzT9*) ranking second and third, respectively (Figure 48A).

Breeding lines possessing both QTLs (*OzT8* + *OzT9*) exhibited the highest average relative net CO_2 assimilation rate. Lines carrying only the *OzT8* QTL ranked second, while those with the *OzT9* QTL ranked third. At the genotype level, MFOL-1491 (*OzT8* + *OzT9*) achieved the highest relative net CO_2 assimilation rate, followed by MFOL-2236 (*OzT9*) and MFOL-1488 (*OzT8* + *OzT9*) (Figure 49A).

Breeding lines from Binadhan-11 X Kasalath cross

Breeding lines containing both QTLs (*OzT8* + *OzT9*) exhibited the highest average relative stomatal conductance (gsw), outperforming lines carrying either *OzT9* or *OzT8* individually. Among the specific genotypes evaluated, MFOL-471 (*OzT8* + *OzT9*) recorded the highest relative gsw, followed by MFOL-50 (*OzT8* + *OzT9*) and MFOL-1102 (*OzT9*) (Figure 46B).

Lines containing only the *OzT9* QTL exhibited the highest average relative PhiPS2, followed by lines carrying both QTLs (*OzT8* + *OzT9*), and lastly, those with only the *OzT8* QTL. Among the individual genotypes, MFOL-1102 (*OzT9*) recorded the highest relative PhiPS2, with MFOL-471 (*OzT8* + *OzT9*) and MFOL-60 (*OzT8* + *OzT9*) ranking second and third, respectively (Figure 47B).

Lines carrying the *OzT8* QTL exhibited the highest mean relative electron transport rate (ETR), followed by lines containing both QTLs (*OzT8* + *OzT9*), and then lines with the *OzT9* QTL alone. Among the individual genotypes evaluated, MFOL-1198 (*OzT8*) showed the highest relative ETR, followed by MFOL-471 (*OzT8* + *OzT9*) and MFOL-1302 (*OzT9*) (Figure 48B).

Breeding lines derived from Binadhan-11 exhibited a significantly higher relative net CO_2 assimilation rate than the original Binadhan-11 variety. Those carrying the *OzT8* QTL displayed the highest average relative net CO_2 assimilation rate among the evaluated lines. Lines with both QTLs (*OzT8* + *OzT9*) ranked second, while those carrying the *OzT9* QTL ranked third. At the genotype level, MFOL-1135 (*OzT8*) recorded the highest relative net CO_2 assimilation rate, followed by MFOL-1198 (*OzT8*) and MFOL-1302 (*OzT9*) (Figure 49B).

Together, these results suggested that Breeding lines from the BRRI dhan28 × Kasalath cross with both QTLs (*OzT8* + *OzT9*) showed superior performance in relative PhiPS2 and net CO_2 assimilation rate, with individual genotypes MFOL-1378 and MFOL-1491 excelling in these traits. Lines carrying *OzT8* alone demonstrated the highest relative ETR and second-best net CO_2 assimilation rate, with MFOL-328 (*OzT9*) exhibiting the highest relative stomatal conductance (gsw) and with MFOL-1547 (*OzT8* + *OzT9*) achieving the highest relative electron transport rates (ETR). In the Binadhan-11 × Kasalath cross, lines carrying *OzT8* + *OzT9* had the highest relative stomatal conductance, with MFOL-471 (*OzT8* + *OzT9*) ranking highest among genotypes. Lines carrying only *OzT9* exhibited the highest PhiPS2, with MFOL-1102 (*OzT9*) being the top-performing genotype. *OzT8* lines showed the best ETR, led by MFOL-1198 (*OzT8*), while the highest net CO_2 assimilation rate was observed in MFOL-1135 (*OzT8*). Overall, *OzT8* significantly enhanced photosynthetic efficiency across traits, with combined QTL effects providing synergistic advantages in many cases.

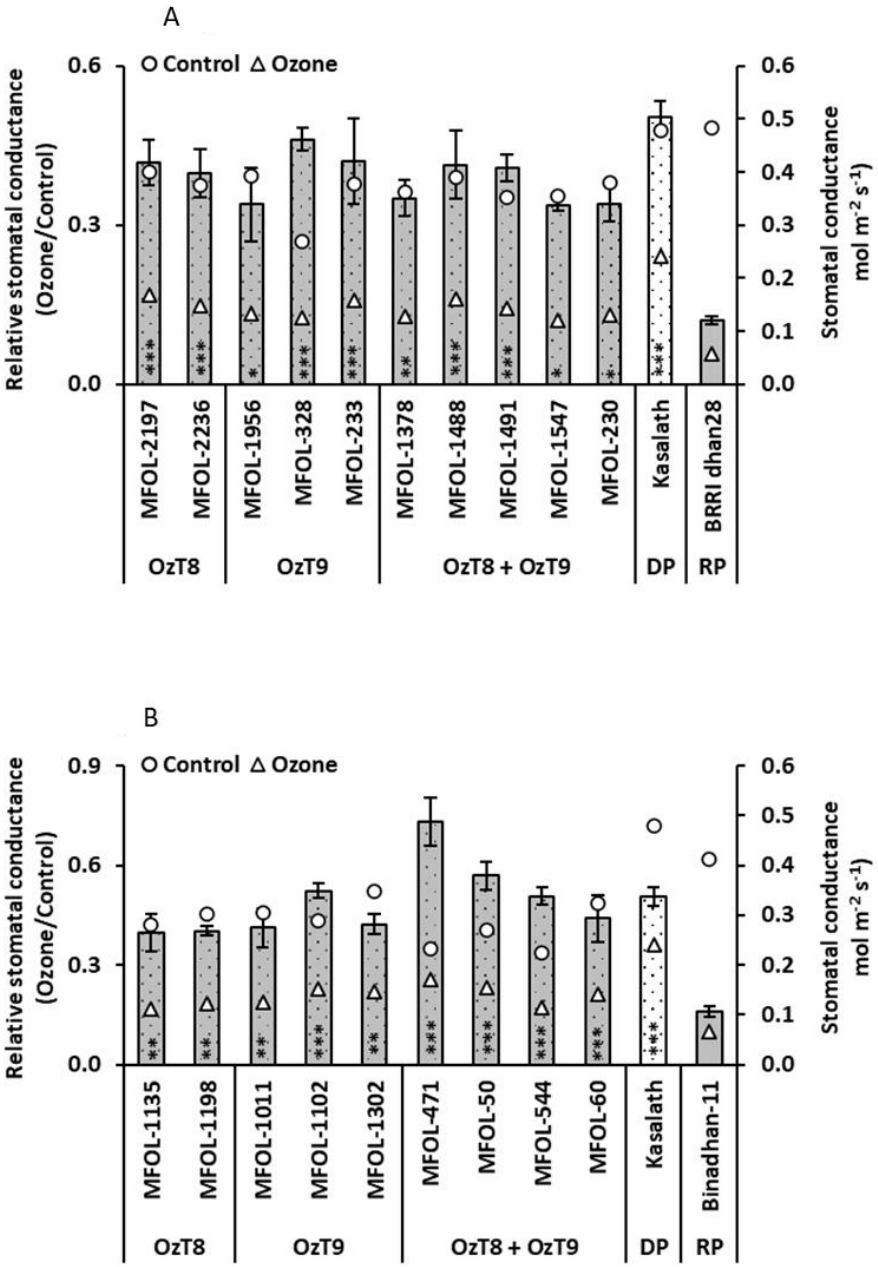

Figure 46 Stomatal conductance(mol m^{-2} s^{-1}) of selected breeding lines carrying *OzT8* and/or *OzT9* derived from the cross (A) BRRI dhan28 × Kasalath and (B) Binadhan-11 × Kasalath under ozone stress and control conditions. The bar graphs display the mean and standard error of relative values (n = 4), while the circles and triangles represent absolute values for the control and ozone-treated groups, respectively. Asterisks within the bars indicate significant differences between the genotypes and the recipient parent (BRRI dhan28 or Binadhan-11), as determined by Dunnett's test (*P < 0.05, **P < 0.01, ***P < 0.001). DP, donor parent, and RP, recipient parent.

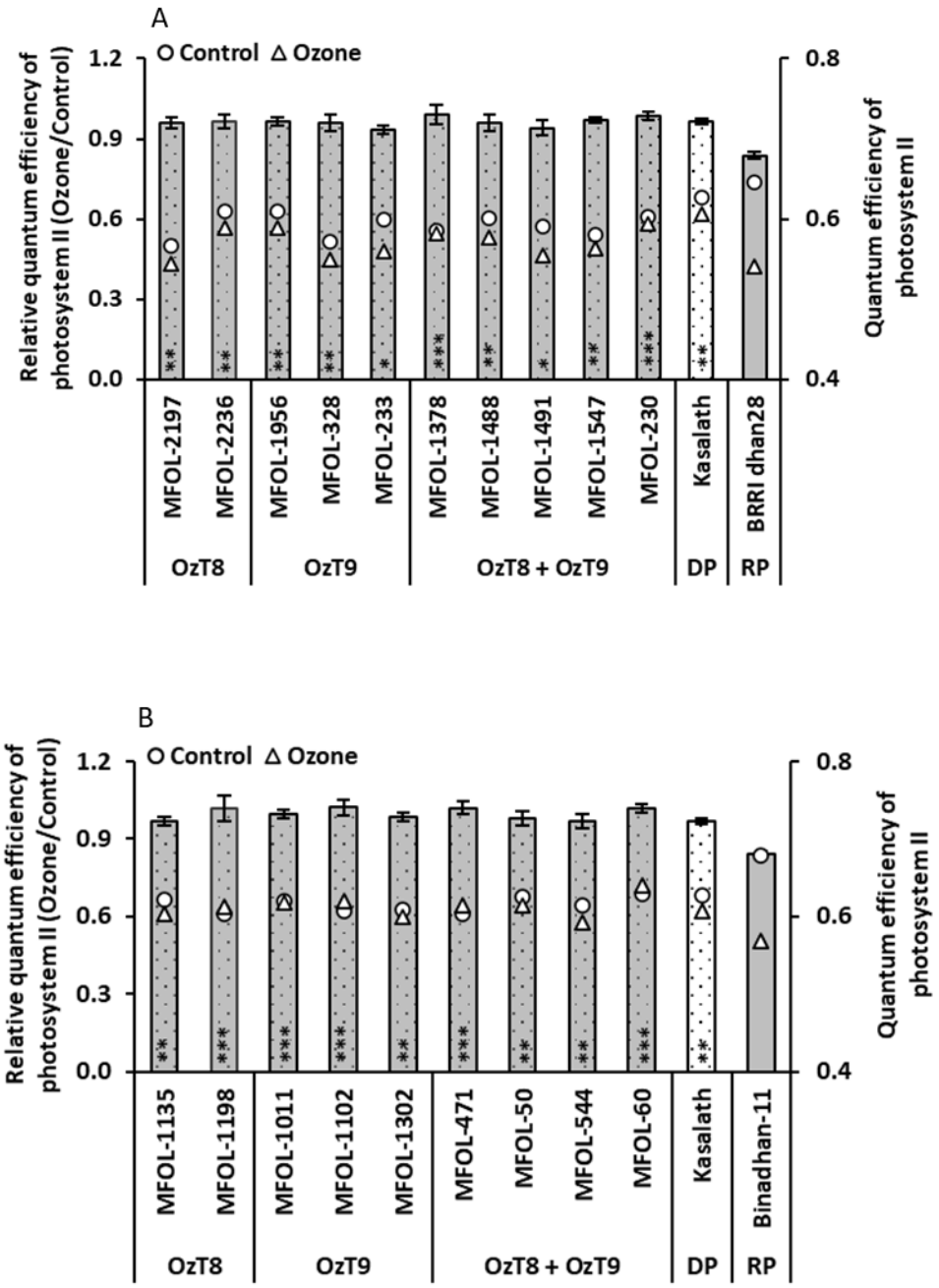

Figure 47 Quantum efficiency of photosystem II (PhiPS2) of selected breeding lines carrying *OzT8* and/or *OzT9* derived from the cross (A) BRRI dhan28 × Kasalath and (B) Binadhan-11 × Kasalath under ozone stress and control conditions. The bar graphs display the mean and standard error of relative values (n = 4), while the circles and triangles represent absolute values for the control and ozone-treated groups, respectively. Asterisks within the bars indicate significant differences between the genotypes and the recipient parent (BRRI dhan28 or Binadhan-11), as determined by Dunnett's test (*P < 0.05, **P < 0.01, ***P < 0.001). DP, donor parent, and RP, recipient parent.

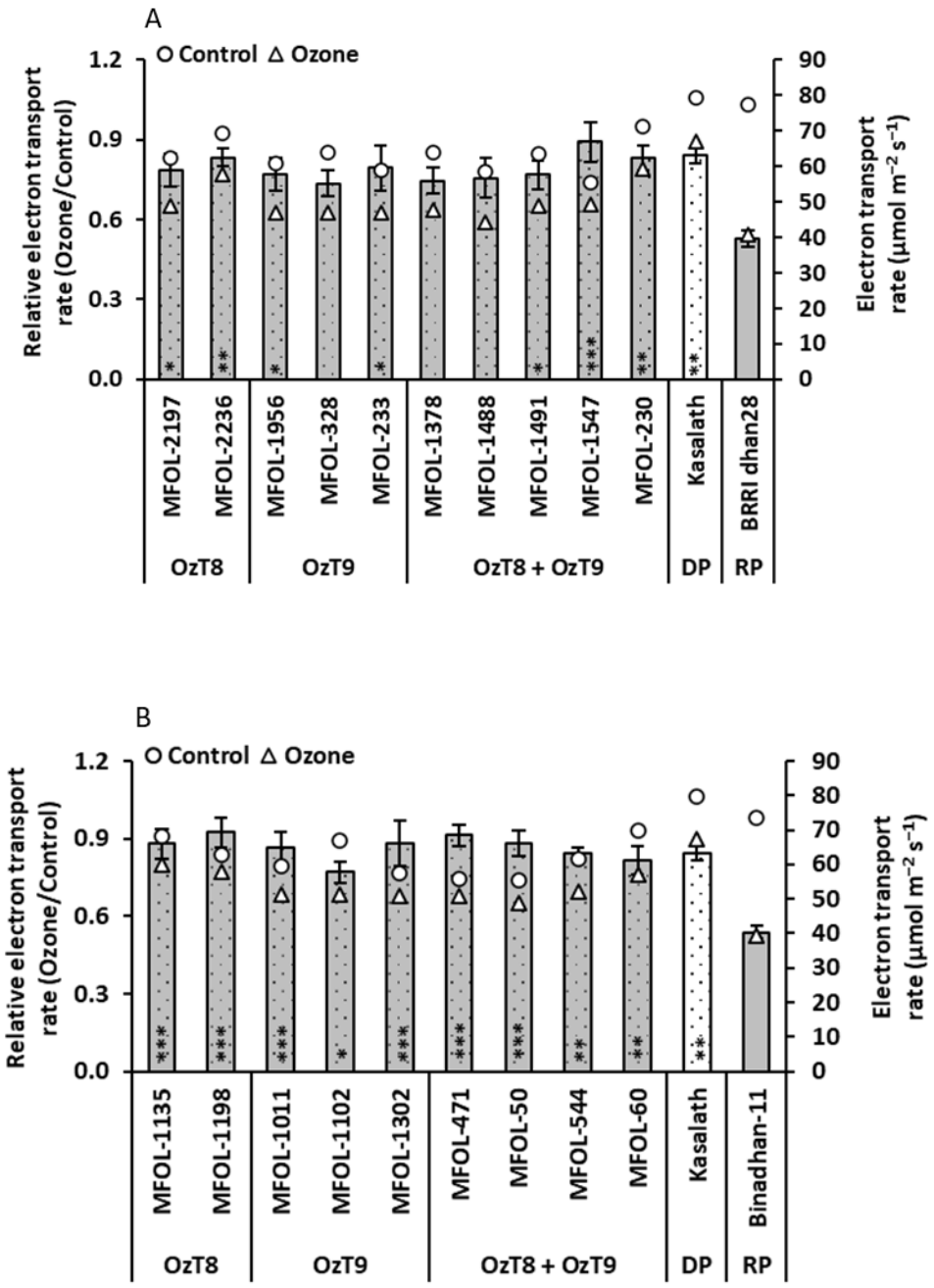

Figure 48 Electron transport rate (ETR) of selected breeding lines carrying *OzT8* and/or *OzT9* derived from the cross (A) BRRI dhan28 × Kasalath and (B) Binadhan-11 × Kasalath under ozone stress and control conditions. The bar graphs display the mean and standard error of relative values (n = 4), while the circles and triangles represent absolute values for the control and ozone-treated groups, respectively. Asterisks within the bars indicate significant differences between the genotypes and the recipient parent (BRRI dhan28 or Binadhan-11), as determined by Dunnett's test (*P < 0.05, **P < 0.01, ***P < 0.001). DP, donor parent, and RP, recipient parent.

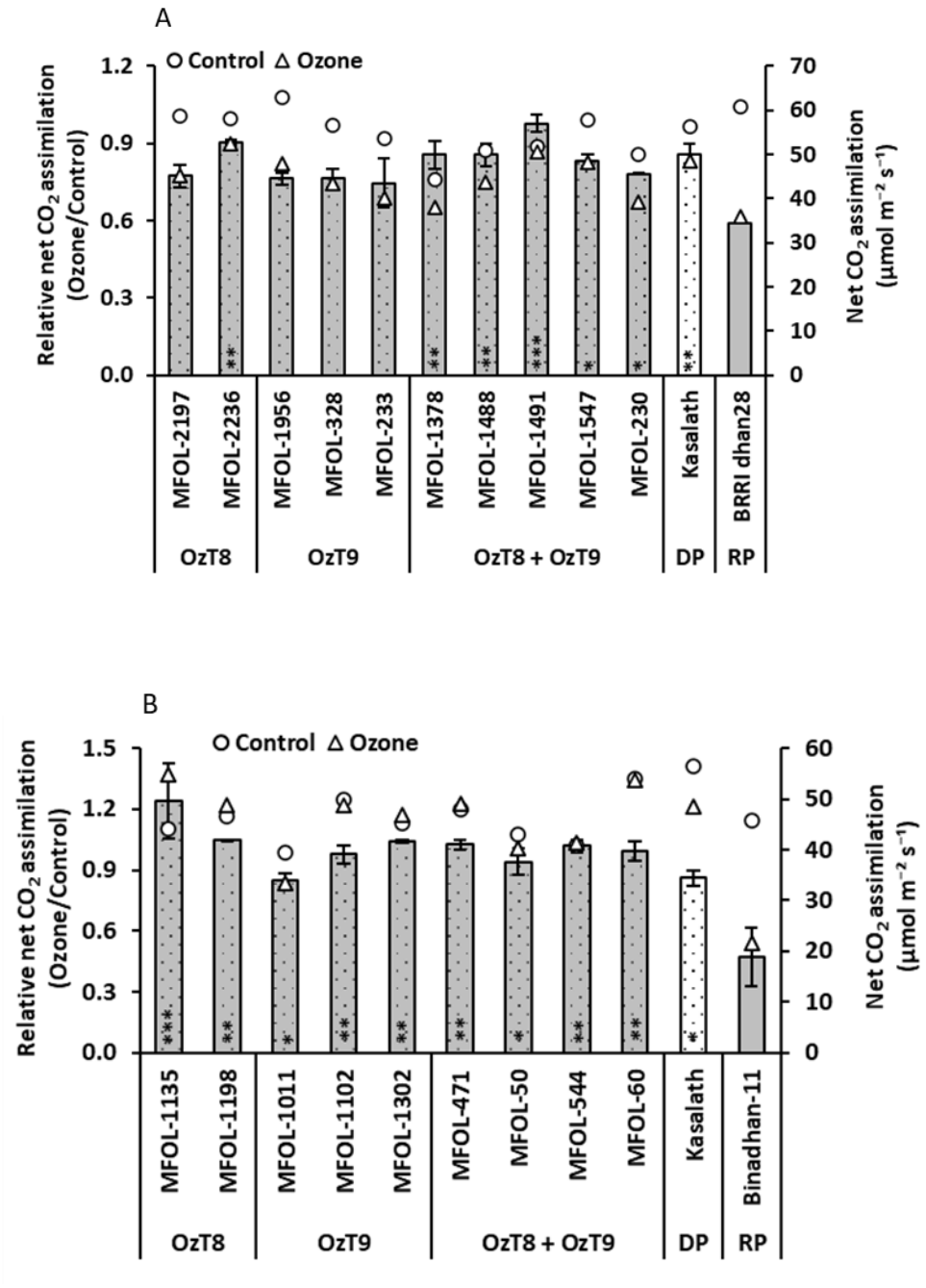

Figure 49 CO_2 assimilation rate (µmol m^{-2} s^{-1}) of selected breeding lines carrying *OzT8* and/or *OzT9* derived from the cross (A) BRRI dhan28 × Kasalath and (B) Binadhan-11 × Kasalath under ozone stress and control conditions at 65 DAO. The bar graphs display the mean and standard error of relative values (n = 4), while the circles and triangles represent absolute values for the control and ozone-treated groups, respectively. Asterisks within the bars indicate significant differences between the genotypes and the recipient parent (BRRI dhan28 or Binadhan-11), as determined by Dunnett's test (*P < 0.05, **P < 0.01, ***P < 0.001). DP, donor parent, and RP, recipient parent.

4.4.5 Evaluating yield-related traits in breeding lines

Breeding lines from BRRI Dhan28 X Kasalath cross

None of the breeding lines derived from BRRI dhan28 exhibited significantly higher relative tiller numbers than the recipient parent, BRRI dhan28. Among the lines evaluated, those carrying the *OzT8* QTL exhibited the highest mean relative tiller numbers, followed by lines with the *OzT9* QTL and those harboring both QTLs (*OzT8* + *OzT9*). Notably, the line MFOL-328 (*OzT9*) demonstrated the highest relative tiller number, followed by MFOL-1547 (*OzT8* + *OzT9*) and MFOL-1378 (*OzT8* + *OzT9*) (Figure 50A).

Breeding lines derived from BRRI dhan28, including MFOL-2197, MFOL-2236, MFOL-328, MFOL-233, MFOL-1378, MFOL-1491, and MFOL-1547, exhibited significantly higher relative panicle numbers compared to the recipient parent variety, BRRI dhan28. Among these lines, those carrying the *OzT9* QTL showed the highest mean relative panicle numbers, followed by lines carrying the *OzT8* QTL and those with both QTLs (*OzT8* + *OzT9*). At the individual genotype level, MFOL-328 (*OzT9*) demonstrated the highest relative panicle number, followed by MFOL-233 (*OzT9*) and MFOL-1547 (*OzT8* + *OzT9*), as shown in Figure 51A.

The breeding lines MFOL-2197, MFOL-2236, MFOL-328, MFOL-1488, MFOL-1491, and MFOL-1547 demonstrated a significantly higher relative number of filled grains compared to the recipient parent, BRRI dhan28. Lines carrying both QTLs (*OzT8* + *OzT9*) exhibited the highest average relative filled grain number, followed by those carrying only the *OzT8* QTL, and then by lines with the *OzT9* QTL. Among the BRRI dhan28-derived genotypes, MFOL-2236 (*OzT8*) showed the highest relative filled grain number, followed by MFOL-1491 and MFOL-1547, both of which carried the combined QTLs (*OzT8* + *OzT9*) (Figure 52A).

Breeding lines MFOL-2197, MFOL-2236, MFOL-328, MFOL-1488, MFOL-1491, and MFOL-1547 demonstrated significantly higher relative grain yields compared to the recipient parent variety, BRRI dhan28. Notably, among these lines, those carrying the *OzT8* QTL exhibited the highest mean relative grain yield, followed by lines carrying the *OzT9* QTL and those with both QTLs (*OzT8* + *OzT9*). Specifically, the genotype MFOL-2236 (*OzT8*) recorded the highest relative grain yield, followed by MFOL-1491 (*OzT8* + *OzT9*) and MFOL-328 (*OzT9*) (Figure 53A).

Among the breeding lines evaluated, only MFOL-2236 and MFOL-1378 demonstrated significantly higher relative straw biomass than the recipient parent variety, BRRI dhan28. Lines carrying the *OzT8* QTL exhibited the highest mean relative straw biomass, followed by those possessing both QTLs (*OzT8* + *OzT9*) and lines with the *OzT9* QTL alone. Notably, MFOL-2236 (*OzT8*) recorded the highest relative straw biomass among all genotypes, followed by MFOL-1378 (*OzT8* + *OzT9*) and MFOL-233 (*OzT8* + *OzT9*) (Figure 54A).

We evaluated the harvest index (HI), a critical parameter for plant breeders, which measures the ratio of economic yield (e.g., grain) to total above-ground biomass. The breeding lines MFOL-328, MFOL-1488, MFOL-1491, and MFOL-1547 achieved significantly higher relative HI compared to the recipient parent, BRRI dhan28. Lines carrying the *OzT8* QTL recorded the highest average relative HI, followed by those carrying the *OzT9* QTL and those carrying both QTLs (*OzT8* + *OzT9*). Among the genotypes, MFOL-328 (*OzT9*) achieved the highest relative HI, while MFOL-1547 and MFOL-1491, both carrying the combined QTLs (*OzT8* + *OzT9*), ranked second and third, respectively (Figure 55A).

Breeding lines from Binadhan-11 X Kasalath cross

All breeding lines derived from Binadhan-11, except for MFOL-1302, exhibited significantly higher relative tiller numbers than the recipient parent, Binadhan-11. Among the evaluated lines, those possessing the *OzT8* QTL exhibited the highest mean relative tiller numbers, followed by lines carrying both QTLs (*OzT8* + *OzT9*), and lines harboring the *OzT9* QTL alone. At the individual genotype level, MFOL-1135 (*OzT8*) demonstrated the highest relative tiller number, followed by MFOL-1011 (*OzT9*) and MFOL-60 (*OzT8* + *OzT9*) (Figure 50B).

Similarly, all breeding lines derived from Binadhan-11 exhibited significantly higher relative panicle numbers than the recipient parent variety. Among these, lines carrying the *OzT8* QTL demonstrated the highest mean relative panicle numbers, followed by lines carrying both QTLs (*OzT8* + *OzT9*) and those carrying the *OzT9* QTL alone. Notably, the genotype MFOL-1135 (*OzT8*) achieved the highest relative panicle number among the Binadhan-11-derived lines, followed by MFOL-1011 (*OzT9*) and MFOL-1198 (*OzT8*), as illustrated in Figure 51B.

All breeding lines, except MFOL-544, showed significantly higher relative filled grain numbers compared to the recipient parent, Binadhan-11. Among these lines, those carrying the *OzT8* QTL exhibited the highest mean relative filled grain number, followed by lines with the *OzT9* QTL and those carrying both QTLs (*OzT8* + *OzT9*). Specifically, the genotype MFOL-1135 (*OzT8*) recorded the highest relative filled grain number, followed by MFOL-471 (*OzT8* + *OzT9*) and MFOL-1198 (*OzT8*) (Figure 52B).

Similarly, all breeding lines, except for MFOL-544, exhibited significantly higher relative grain yield than the recipient parent, Binadhan-11. Among these lines, those carrying the *OzT8* QTL demonstrated the highest mean relative grain yield, followed by lines with the *OzT9* QTL and those possessing both QTLs (*OzT8* + *OzT9*). Within the Binadhan-11-derived genotypes, MFOL-1135 (*OzT8*) recorded the highest relative grain yield, followed by MFOL-471 (*OzT8* + *OzT9*) and MFOL-1198 (*OzT8*), as illustrated in Figure 53B.

Among the breeding lines evaluated, MFOL-1135, MFOL-1011, and MFOL-471 exhibited significantly higher relative straw biomass compared to the recipient parent, Binadhan-11. Lines carrying the *OzT8* QTL displayed the highest mean relative straw biomass, followed by lines carrying both QTLs (*OzT8* + *OzT9*) and those with the *OzT9* QTL alone. Among the individual genotypes, MFOL-471 (*OzT8* + *OzT9*) recorded the highest relative straw biomass, followed by MFOL-1102 (*OzT9*) and MFOL-1135 (*OzT8*), as shown in Figure 54B.

The breeding lines MFOL-1135, MFOL-1198, MFOL-1011, MFOL-1102, MFOL-1302, and MFOL-60 exhibited a significantly higher relative harvest index compared to the recipient parent, Binadhan-11. Among these lines, those carrying the *OzT9* QTL displayed the highest average relative harvest index, followed by lines carrying the *OzT8* QTL and those possessing both QTLs (*OzT8* + *OzT9*). Notably, the genotype MFOL-1302 (*OzT9*) achieved the highest relative harvest index, with MFOL-1135 (*OzT8*) and MFOL-60 (*OzT8* + *OzT9*) ranking second and third, respectively (Figure 55B).

The results together demonstrated that in the BRRI Dhan28 × Kasalath cross, lines carrying the *OzT8* QTL exhibited the highest relative values for grain yield, straw biomass, and harvest index, with MFOL-2236 (*OzT8*) being the top-performing line for grain yield and straw

biomass, while MFOL-328 (*OzT9*) led in harvest index. Similarly, in the Binadhan-11 × Kasalath cross, lines with the *OzT8* QTL consistently outperformed others in relative tiller and panicle numbers, with MFOL-1135 (*OzT8*) achieving the highest grain yield, straw biomass, and filled grain number. Across both crosses, the combination of *OzT8* and *OzT9* QTLs further enhanced multiple traits, though individual QTL contributions varied by trait and genotype. Overall, MFOL-2236 and MFOL-1135 emerged as the best-performing lines in their respective crosses.

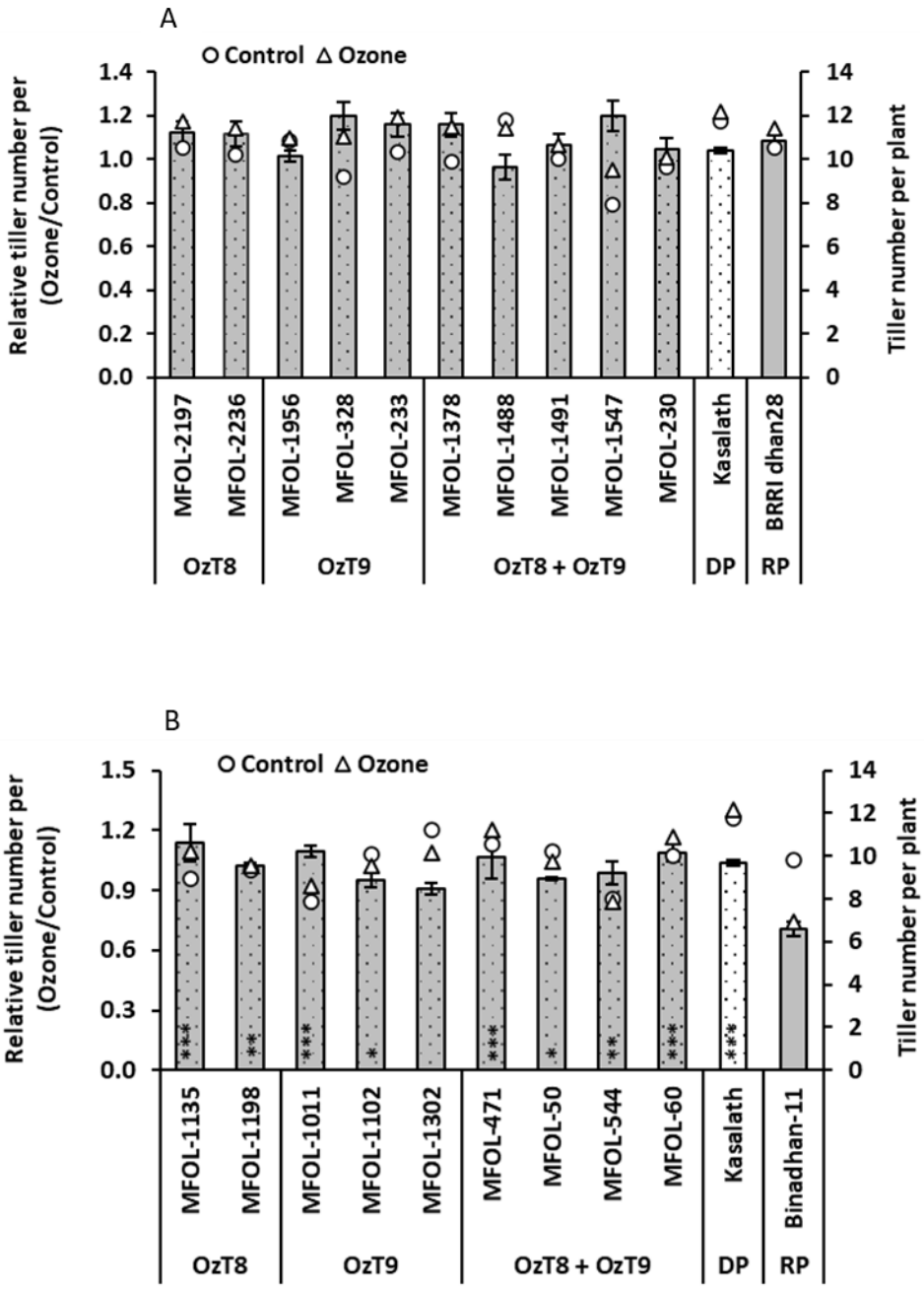

Figure 50 Tiller number of selected breeding lines carrying *OzT8* and/or *OzT9* derived from the cross (A) BRRI dhan28 × Kasalath and (B) Binadhan-11 × Kasalath under ozone stress and control conditions. The bar graphs display the mean and standard error of relative values (n = 4), while the circles and triangles represent absolute values for the control and ozone-treated groups, respectively. Asterisks within the bars indicate significant differences between the genotypes and the recipient parent (BRRI dhan28 or Binadhan-11), as determined by Dunnett's test (*P < 0.05, **P < 0.01, ***P < 0.001). DP, donor parent, and RP, recipient parent.

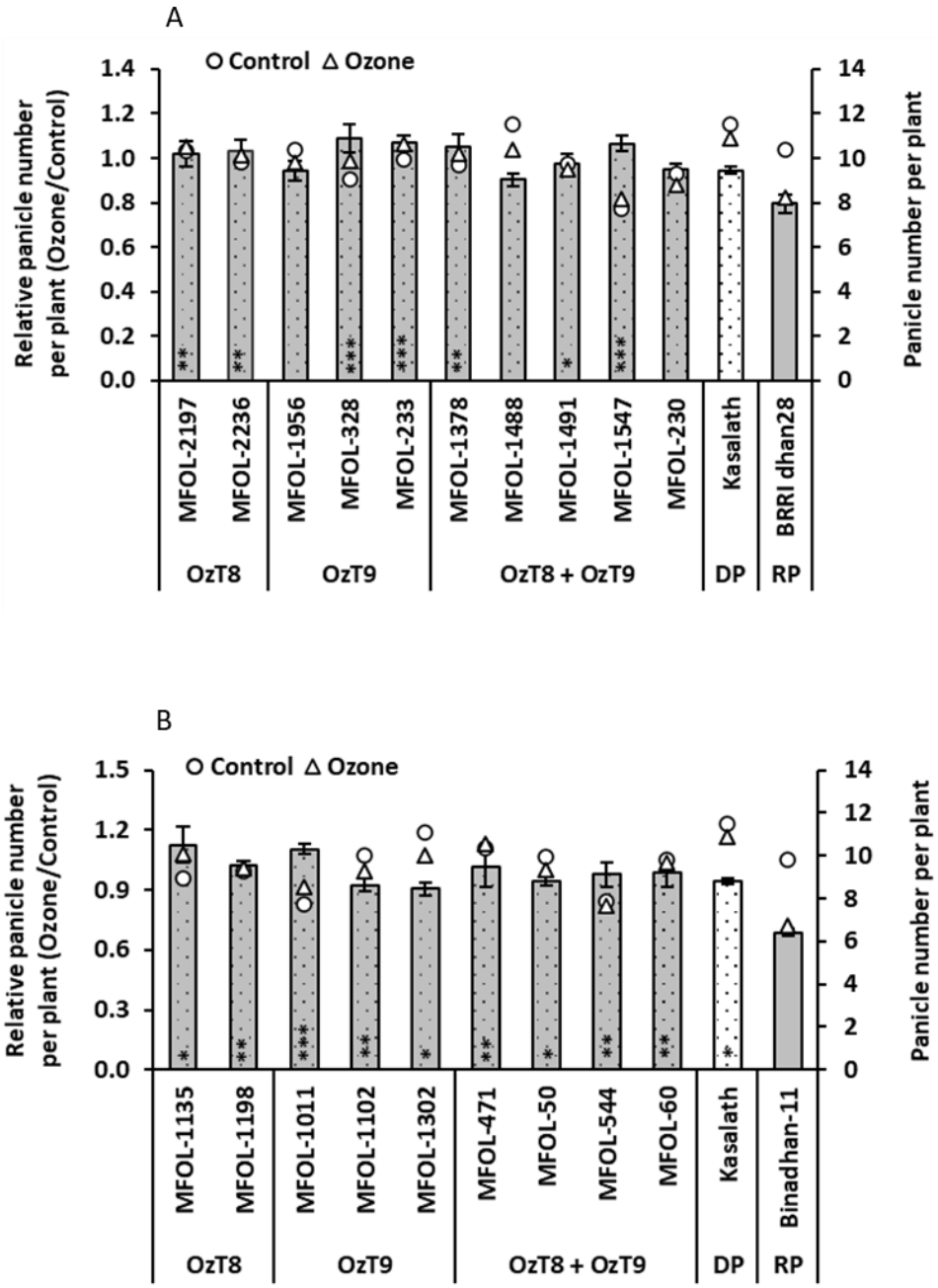

Figure 51 Panicle number of selected breeding lines carrying *OzT8* and/or *OzT9* derived from the cross (A) BRRI dhan28 × Kasalath and (B) Binadhan-11 × Kasalath under ozone stress and control conditions. The bar graphs display the mean and standard error of relative values (n = 4), while the circles and triangles represent absolute values for the control and ozone-treated groups, respectively. Asterisks within the bars indicate significant differences between the genotypes and the recipient parent (BRRI dhan28 or Binadhan-11), as determined by Dunnett's test (*P < 0.05, **P < 0.01, ***P < 0.001). DP, donor parent, and RP, recipient parent.

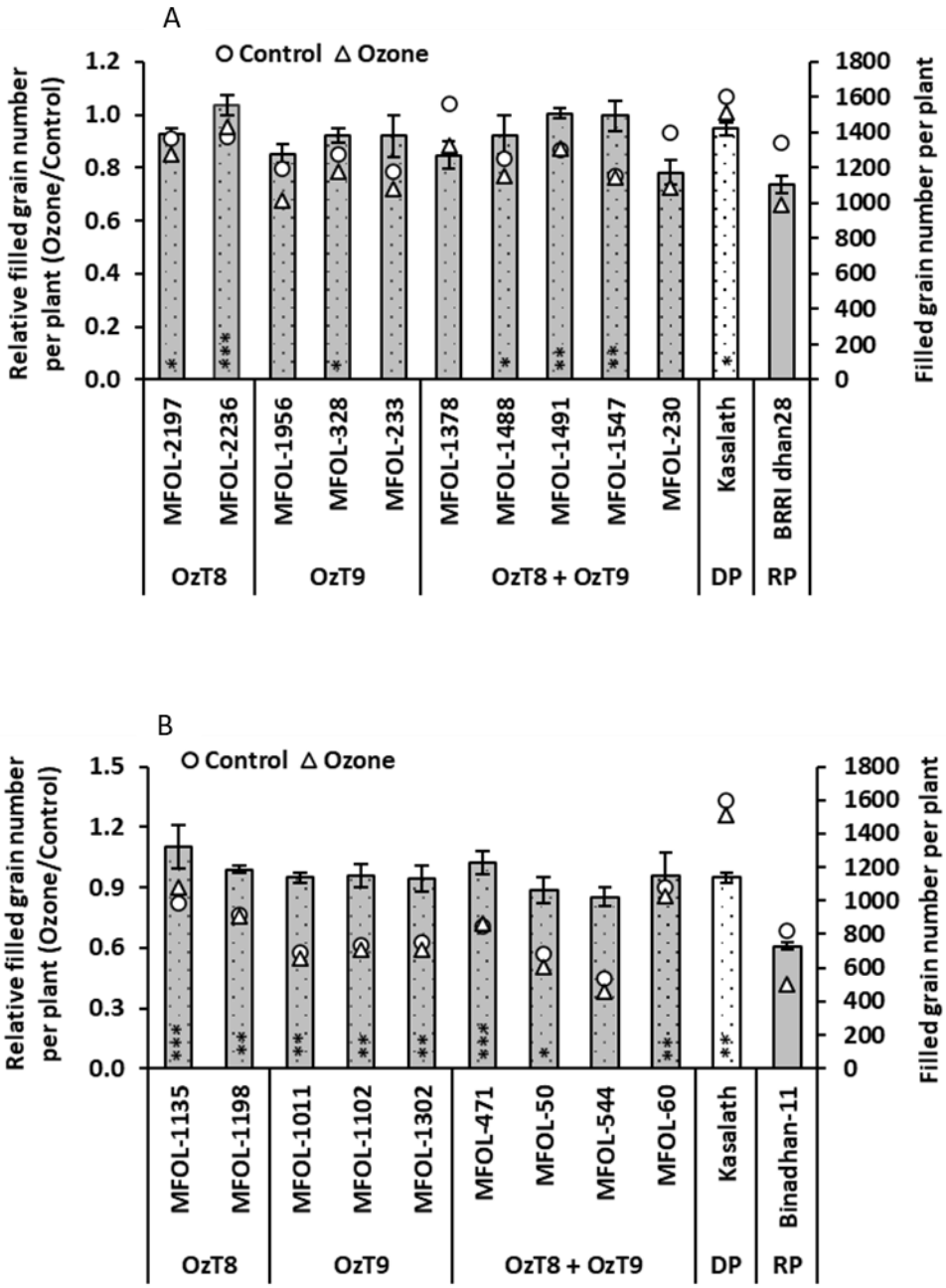

Figure 52 Filled grain number of selected breeding lines carrying *OzT8* and/or *OzT9* derived from the cross (A) BRRI dhan28 × Kasalath and (B) Binadhan-11 × Kasalath under ozone stress and control conditions. The bar graphs display the mean and standard error of relative values (n = 4), while the circles and triangles represent absolute values for the control and ozone-treated groups, respectively. Asterisks within the bars indicate significant differences between the genotypes and the recipient parent (BRRI dhan28 or Binadhan-11), as determined by Dunnett's test (*P < 0.05, **P < 0.01, ***P < 0.001). DP, donor parent, and RP, recipient parent.

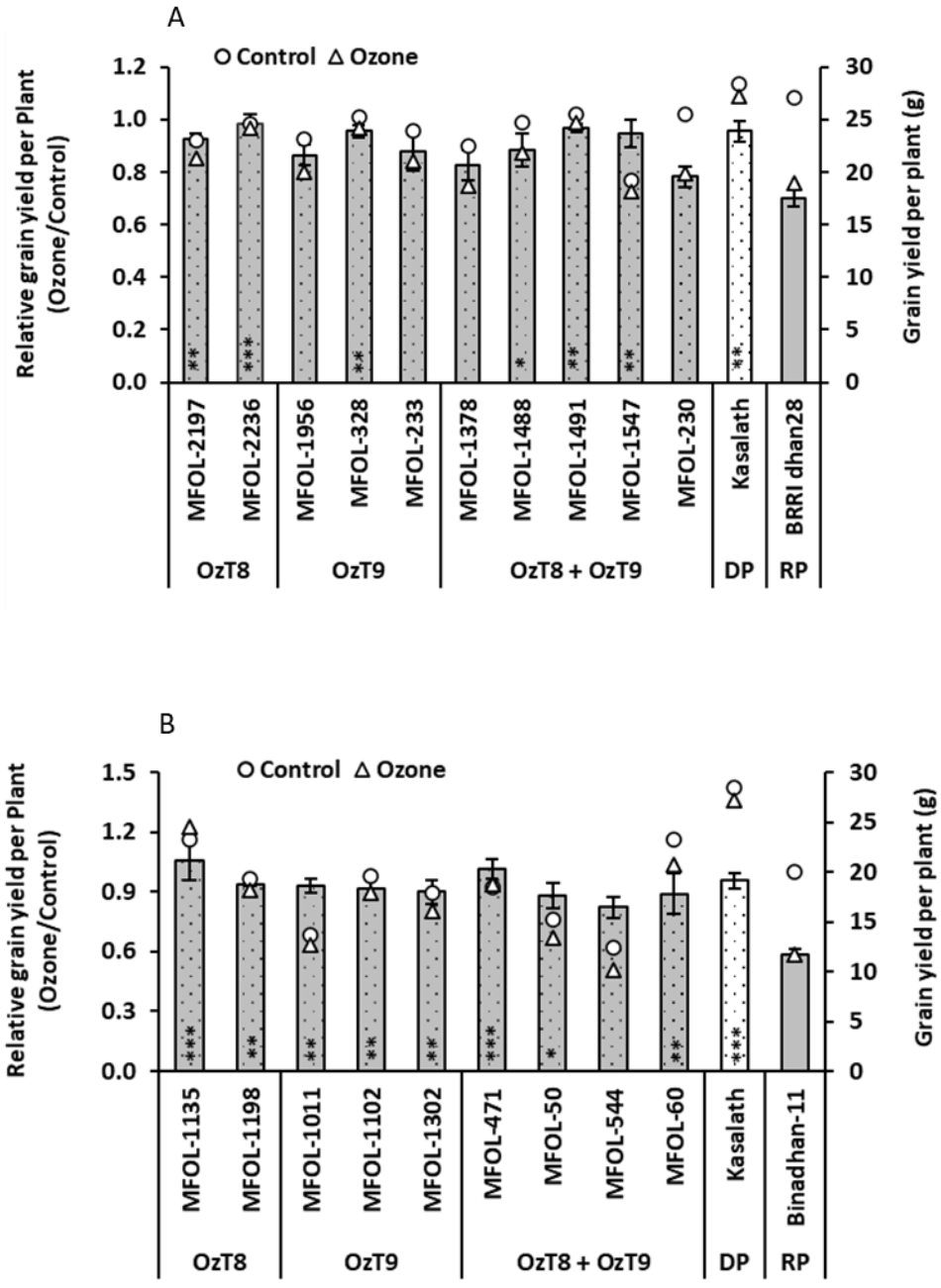

Figure 53 Grain yield (g) of selected breeding lines carrying *OzT8* and/or *OzT9* derived from the cross (A) BRRI dhan28 × Kasalath and (B) Binadhan-11 × Kasalath under ozone stress and control conditions. The bar graphs display the mean and standard error of relative values (n = 4), while the circles and triangles represent absolute values for the control and ozone-treated groups, respectively. Asterisks within the bars indicate significant differences between the genotypes and the recipient parent (BRRI dhan28 or Binadhan-11), as determined by Dunnett's test (*P < 0.05, **P < 0.01, ***P < 0.001). DP, donor parent, and RP, recipient parent.

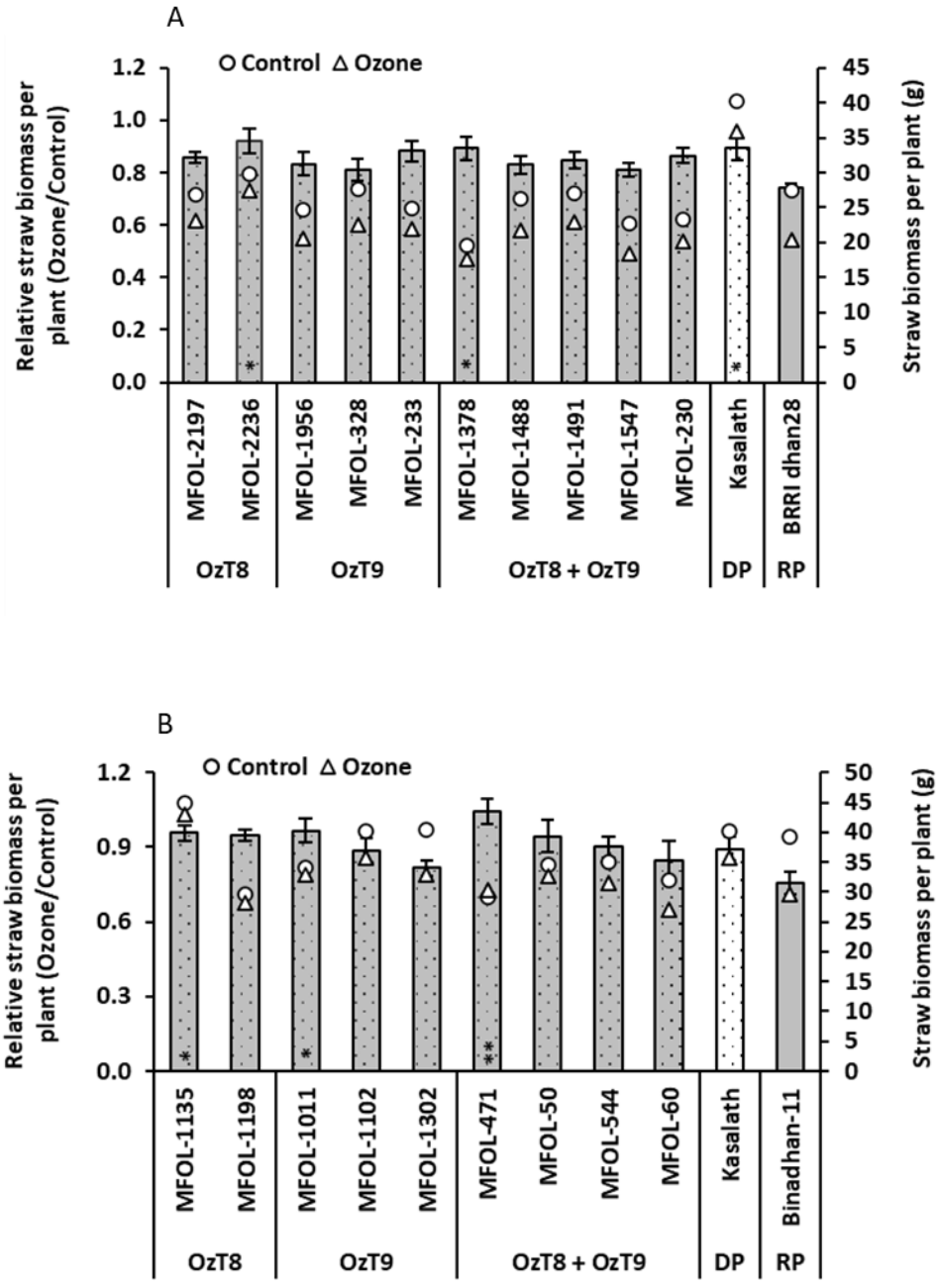

Figure 54 Straw biomass (g) of selected breeding lines carrying *OzT8* and/or *OzT9* derived from the cross (A) BRRI dhan28 × Kasalath and (B) Binadhan-11 × Kasalath under ozone stress and control conditions. The bar graphs display the mean and standard error of relative values (n = 4), while the circles and triangles represent absolute values for the control and ozone-treated groups, respectively. Asterisks within the bars indicate significant differences between the genotypes and the recipient parent (BRRI dhan28 or Binadhan-11), as determined by Dunnett's test (*P < 0.05, **P < 0.01, ***P < 0.001). DP, donor parent, and RP, recipient parent.

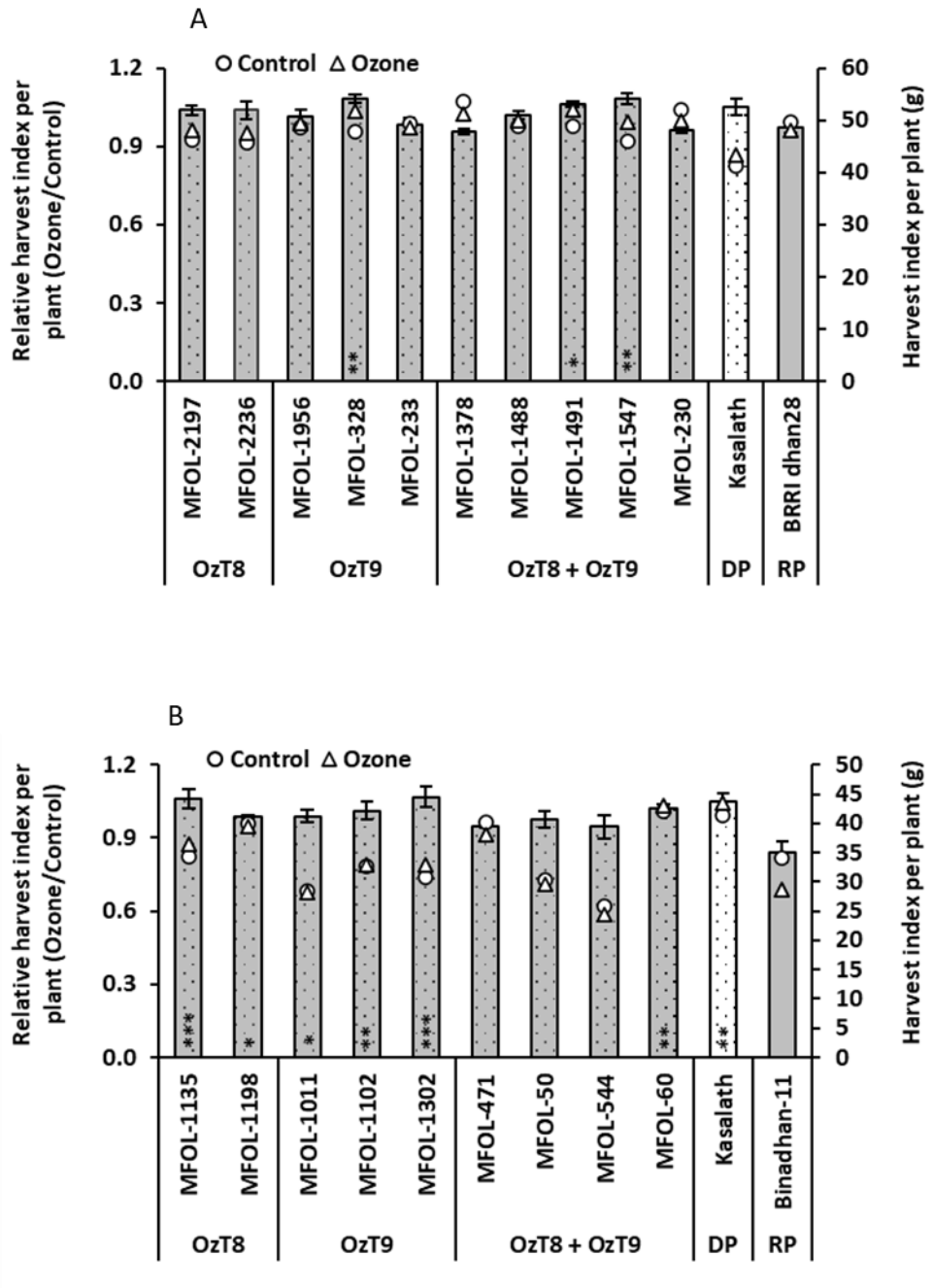

Figure 55 Harvest index of selected breeding lines carrying *OzT8* and/or *OzT9* derived from the cross (A) BRRI dhan28 × Kasalath and (B) Binadhan-11 × Kasalath under ozone stress and control conditions. The bar graphs display the mean and standard error of relative values (n = 4), while the circles and triangles represent absolute values for the control and ozone-treated groups, respectively. Asterisks within the bars indicate significant differences between the genotypes and the recipient parent (BRRI dhan28 or Binadhan-11), as determined by Dunnett's test (*P < 0.05, **P < 0.01, ***P < 0.001). DP, donor parent, and RP, recipient parent.

4.4.6 Line selection for evaluation under ambient ozone conditions

Further, we selected breeding lines for a field experiment in Bangladesh based on their grain yield per plant. The experiment was conducted under ambient ozone conditions to assess the performance and adaptability of the selected lines in real-world environmental scenarios.

Breeding lines from BRRI Dhan28 X Kasalath cross

We selected the breeding lines MFOL-2236, MFOL-1956, MFOL-328, MFOL-1491, and MFOL-1547 from the BRRI dhan28 background. MFOL-2236 carries *OzT8*, MFOL-1956 and MFOL-328 carry *OzT9*, while MFOL-1491 and MFOL-1547 harbor both *OzT8* and *OzT9*. We prioritized MFOL-2236 over MFOL-2197 due to its superior physiological traits and yield performance. We excluded MFOL-233 because it exhibited a higher LBS than the other lines carrying *OzT9*. Similarly, we eliminated MFOL-230, MFOL-1378, and MFOL-1488 due to their higher yield losses.

Breeding lines from Binadhan-11 X Kasalath cross

We selected the following breeding lines from the Binadhan-11 background for further evaluation: MFOL-1135, carrying *OzT8*; MFOL-1102 and MFOL-1302, carrying *OzT9*; and MFOL-471 and MFOL-60, carrying both *OzT8* and *OzT9*. We prioritized MFOL-1135 over MFOL-1198 due to its superior yield performance. We excluded MFOL-1011 because it exhibited a higher LBS than the other lines carrying *OzT9*. Similarly, we excluded MFOL-544 and MFOL-50 because of their higher yield losses.

Experiment 4

4.4.7 Yield performance of breeding lines under ambient ozone conditions

We evaluated the breeding lines and their parents under ambient ozone conditions in Bangladesh. However, before conducting a multilocation trial, we focused on assessing the yield performance of the breeding lines, including grain yield, straw biomass, and harvest index.

Breeding lines from BRRI Dhan28 X Kasalath cross

Breeding lines MFOL-1956, MFOL-328, MFOL-1491, and MFOL-1547, showed significantly higher relative grain yields than the recipient parent variety, BRRI dhan28. Among these lines, those containing both QTLs (*OzT8* + *OzT9*) had the highest mean relative grain yield, followed by lines with the *OzT9* QTL and then those with the *OzT8* QTL. Specifically, the genotype MFOL-1491 (*OzT8* + *OzT9*) recorded the highest relative grain yield, followed by MFOL-1547 (*OzT8* + *OzT9*) and MFOL-1956 (*OzT9*) (Figure 56A).

All breeding lines also produced significantly higher relative straw biomass than the recipient parent variety, BRRI dhan28. Lines with the *OzT9* QTL had the highest mean relative straw biomass, followed by those containing both QTLs (*OzT8* + *OzT9*) and then those with the *OzT8* QTL. Notably, MFOL-1956 (*OzT9*) recorded the highest relative straw biomass among all genotypes, followed by MFOL-1491 (*OzT8* + *OzT9*) and MFOL-2236 (*OzT8*) (Figure 57A).

None of the breeding lines achieved a significantly higher relative harvest index (HI) than BRRI dhan28. However, lines containing both QTLs (*OzT8* + *OzT9*) exhibited the highest mean relative HI, followed by those with the *OzT9* QTL and then the *OzT8* QTL. Among the genotypes, MFOL-1547 (*OzT8* + *OzT9*) achieved the highest relative HI, with MFOL-1491 (*OzT8* + *OzT9*) and MFOL-1956 (*OzT9*) ranking second and third, respectively (Figure 58A).

Breeding lines from Binadhan-11 X Kasalath cross

The breeding lines MFOL-1302, MFOL-471, and MFOL-60 showed significantly higher relative grain yield compared to the recipient parent, Binadhan-11. Among these lines, genotypes carrying both QTLs (*OzT8* + *OzT9*) exhibited the highest mean relative grain yield, followed by those with the *OzT9* QTL, and then those with the *OzT8* QTL. Within the Binadhan-11-derived

genotypes, MFOL-60 (*OzT8* + *OzT9*) had the highest relative grain yield, followed by MFOL-1302 (*OzT9*) and MFOL-471 (*OzT8* + *OzT9*), as shown in Figure 56B.

None of the breeding lines produced significantly higher relative straw biomass than the recipient parent, Binadhan-11. However, among the lines, those carrying both QTLs (*OzT8* + *OzT9*) demonstrated the highest mean relative straw biomass, followed by those with the *OzT8* QTL and then those with the *OzT9* QTL. Specifically, MFOL-60 (*OzT8* + *OzT9*) recorded the highest relative straw biomass, followed by MFOL-1302 (*OzT9*) and MFOL-471 (*OzT8* + *OzT9*) (Figure 57B).

The breeding lines MFOL-1102, MFOL-1302, and MFOL-60 displayed significantly higher relative harvest index compared to the recipient parent, Binadhan-11. Genotypes containing both QTLs (*OzT8* + *OzT9*) had the highest mean relative harvest index, followed by lines with the *OzT9* QTL and then those with the *OzT8* QTL. Among the individual genotypes, MFOL-60 (*OzT8* + *OzT9*) achieved the highest relative harvest index, with MFOL-1102 (*OzT8*) and MFOL-1302 (*OzT8*) ranking second and third, respectively (Figure 58B).

Overall, the findings highlighted that lines containing both QTLs (*OzT8* + *OzT9*) consistently demonstrated superior performance, followed by lines with the *OzT9* QTL and those with the *OzT8* QTL. Among BRRI dhan28-derived lines, MFOL-1491 (*OzT8* + *OzT9*) showed the highest grain yield, while MFOL-1956 (*OzT9*) excelled in straw biomass, and MFOL-1547 (*OzT8* + *OzT9*) achieved the highest HI. Similarly, within Binadhan-11-derived lines, MFOL-60 (*OzT8* + *OzT9*) led in all three performance metrics, including grain yield, straw biomass, and HI. This categorization highlights the strong influence of QTLs, particularly the combination of *OzT8* and *OzT9*, in enhancing yield-related traits.

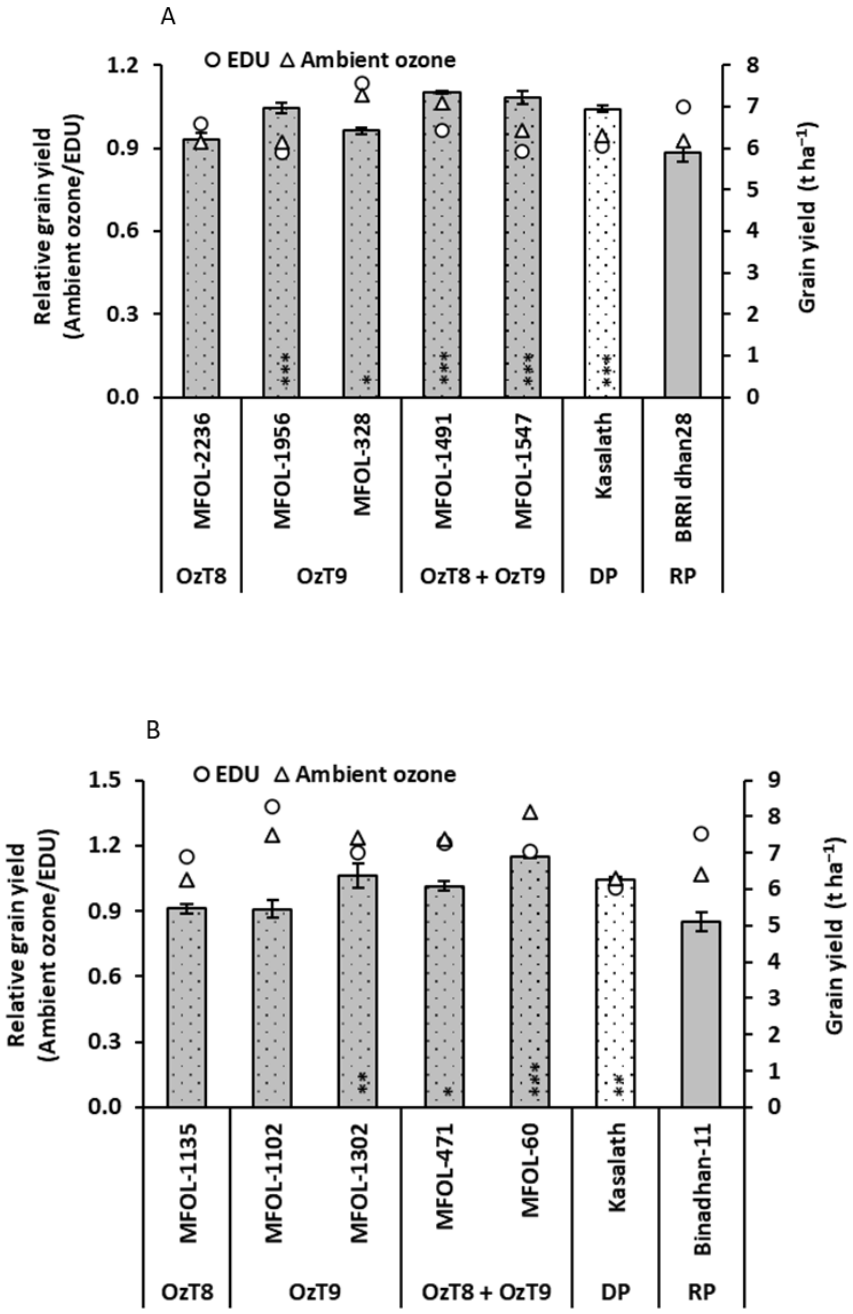

Figure 56 Grain yield (t ha^{-1}) of selected breeding lines carrying *OzT8* and/or *OzT9* derived from the cross (A) BRRI dhan28 × Kasalath and (B) Binadhan-11 × Kasalath under ambient ozone and with the application of antiozonant, ethylenediurea (EDU). The bar graphs display the mean and standard error of relative values (n = 3), while the circles and triangles represent absolute values for the ethylenediurea (EDU) and ambient ozone-treated groups, respectively. Asterisks within the bars indicate significant differences between the genotypes and the recipient parent (BRRI dhan28 or Binadhan-11), as determined by Dunnett's test (*P < 0.05, **P < 0.01, ***P < 0.001). DP, donor parent, and RP, recipient parent.

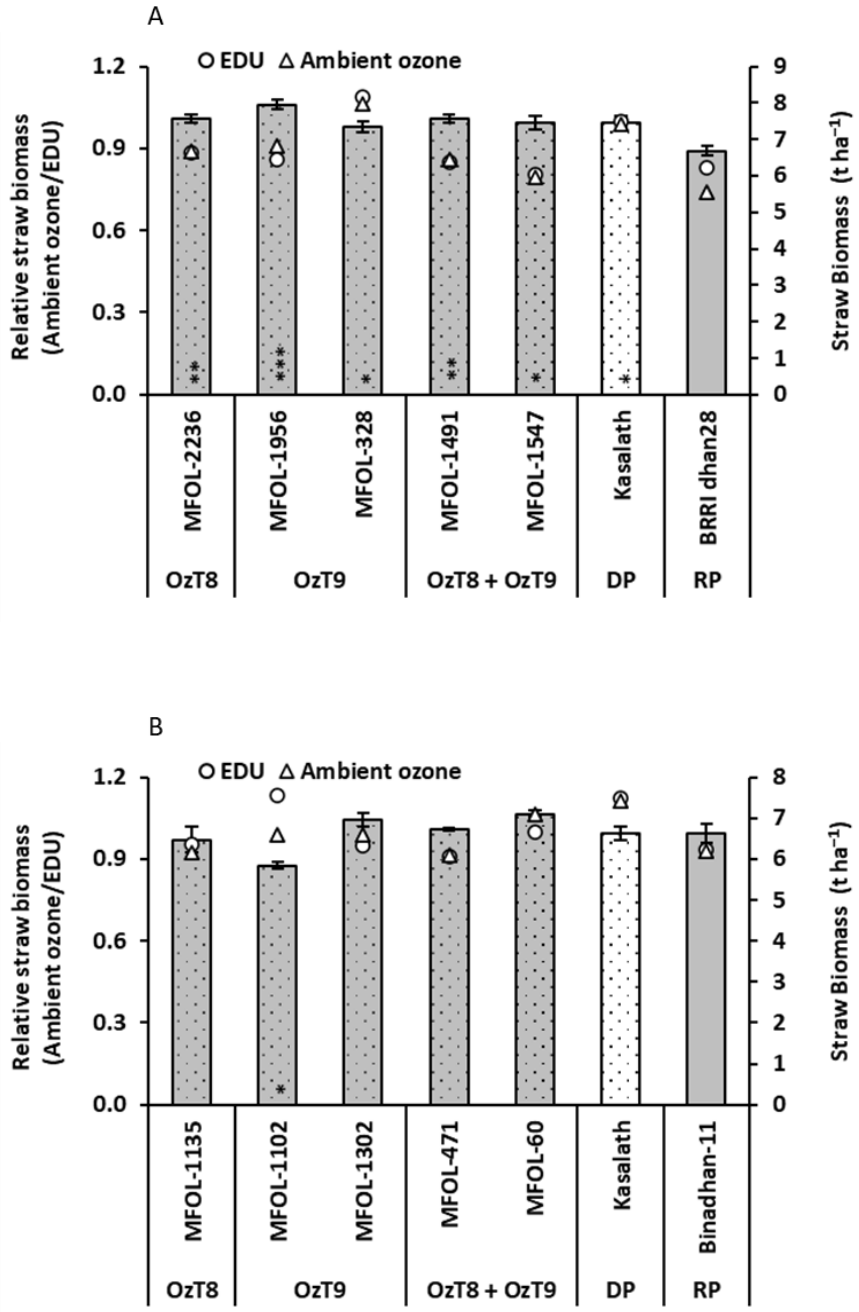

Figure 57 Straw biomass (t ha^{-1}) of selected breeding lines carrying *OzT8* and/or *OzT9* derived from the cross (A) BRRI dhan28 × Kasalath and (B) Binadhan-11 × Kasalath under ambient ozone and with the application of antiozonant, ethylenediurea (EDU). The bar graphs display the mean and standard error of relative values (n = 3), while the circles and triangles represent absolute values for the ethylenediurea (EDU) and ambient ozone-treated groups, respectively. Asterisks within the bars indicate significant differences between the genotypes and the recipient parent (BRRI dhan28 or Binadhan-11), as determined by Dunnett's test (*P < 0.05, **P < 0.01, ***P < 0.001). DP, donor parent, and RP, recipient parent.

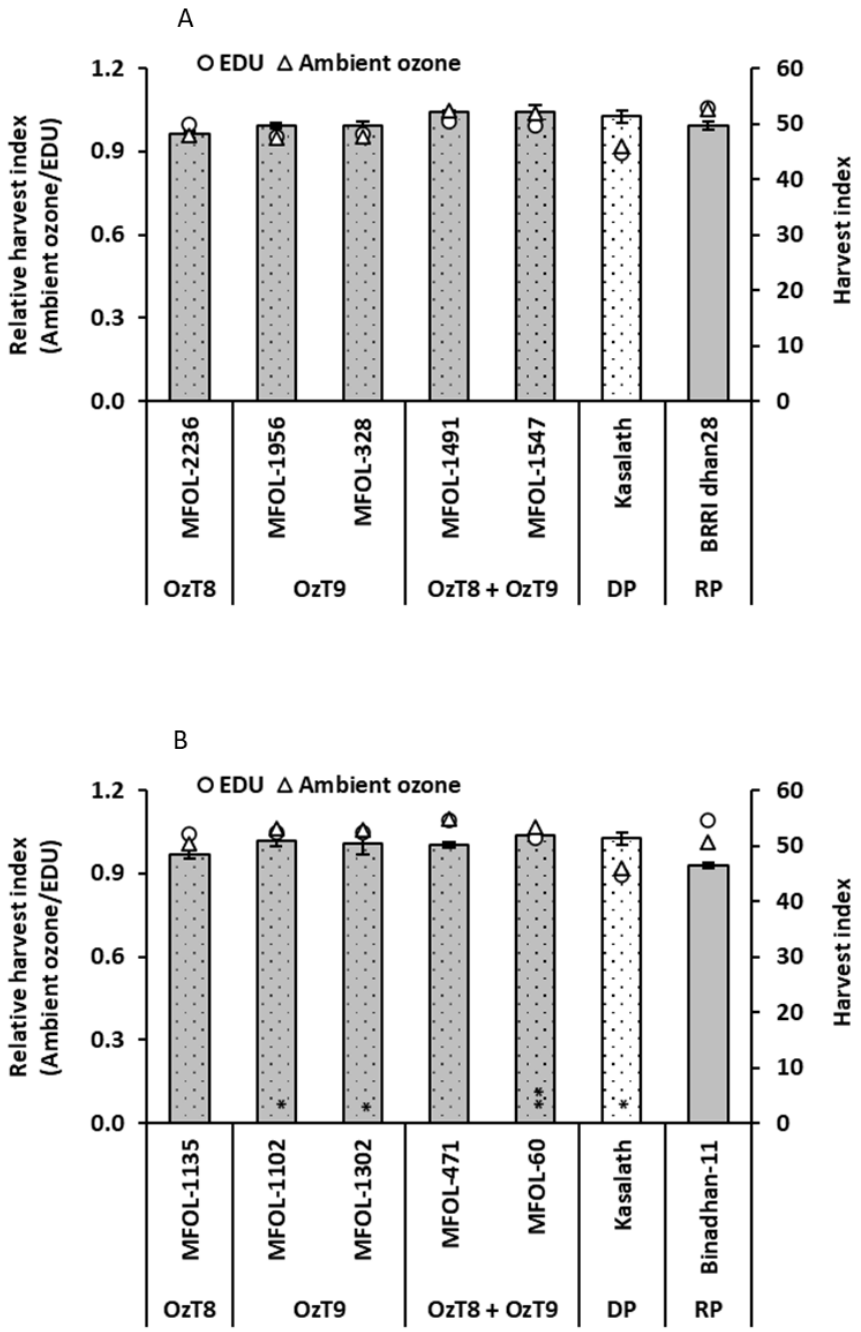

Figure 58 Harvest index of selected breeding lines carrying *OzT8* and/or *OzT9* derived from the cross (A) BRRI dhan28 × Kasalath and (B) Binadhan-11 × Kasalath under ambient ozone and with the application of antiozonant, ethylenediurea (EDU). The bar graphs display the mean and standard error of relative values (n = 3), while the circles and triangles represent absolute values for the ethylenediurea (EDU) and ambient ozone-treated groups, respectively. Asterisks within the bars indicate significant differences between the genotypes and the recipient parent (BRRI dhan28 or Binadhan-11), as determined by Dunnett's test (*P < 0.05, **P < 0.01, ***P < 0.001). DP, donor parent, and RP, recipient parent.

5 Discussion

5.1 Interactions between ozone and blast stress

The first objective of the initial study was to investigate the interactions between ozone exposure and blast stress in rice plants. Notably, many of the traits measured in this study demonstrated significant interactions between ozone and blast treatment (Tables 2 and 3). In order to quantify stress symptoms, we employed visual scoring scales. LBS as a measure for visible ozone damage (Ueda et al., 2015a, 2015b; Ashrafuzzaman et al., 2017; Begum et al., 2020) and BSS as a measure for blast severity (Challagulla et al., 2015; Hensawang et al., 2017; Devi et al., 2020) have repeatedly been used in previous studies and are thus well established. In this experiment, under combined ozone and blast treatment, ozone exposure reduced blast severity (Table 2, Supplementary Table 4). Symptoms of oxidative stress triggered by ozone appeared as chlorosis and brown spots on the leaves, while diamond-shaped light tan lesions with necrotic borders (Supplementary Figure 1) characterized blast symptoms. The differential appearance of LBS and BSS helped us to distinguish between ozone and blast injury in combined ozone and blast treatment. A previous report showed that rice blast fungus infection potential was inhibited by 200 ppb of acute ozone exposure for 3 days (Hur et al., 2002). However, in that experiment, they grew the blast conidia under ozone exposure and then inoculated plants which had not been exposed to ozone. Thus, they did not investigate plant reactions to single or combined stresses. When used at appropriate concentrations, ozone could trigger defense against pathogens (Pazarlar et al., 2017), as ozone generates ROS, which forms part of the primary defense mechanism in plants against pathogens (Torres et al., 2006; Huang et al., 2019). Our data suggested that long-term chronic ozone fumigation at 100 ppb did not favor the environment for blast conidia growth and infection. As a hemibiotrophic (Park et al., 2009; Fernandez & Orth, 2018) fungal pathogen, *M*. *oryzae* requires living cells at the initial period (biotrophy). Thus, their feeding may be inhibited by ozone-induced leaf senescence and cell death (Violini, 1995). Inside the plant, ozone-induced ROS may accelerate defense-like responses, including cell wall strengthening (e.g., through lignification) and induction of pathogen-associated defense genes (Sandermann et al., 1998; Fiscus et al., 2005). Some other biotrophic fungal pathogens also showed decreased disease severity under ozone fumigation, e.g., powdery mildew in barley (Mikkelsen et al., 2015), in wheat (Pazarlar et al., 2017), and cucumber (Khan & Khan, 1999).

However, young wheat plants showed a severe powdery mildew (biotrophic) attack when exposed to 80 to 160 ppb of ozone, while at a concentration of 240 ppb, powdery mildew attack was significantly reduced. In that study, very high ozone concentration enhanced the premature senescence of the wheat leaf, which inhibited the powdery mildew growth (Tiedemann, 1992).

We employed a set of vegetation indices to estimate ozone and blast effects on foliar pigments at individual plant levels through non-destructive measurements (Sims & Gamon, 2002; Meroni et al., 2009; López López et al., 2016). For different host-pathogen interactions, reductions in pigment concentrations are the most notable adverse effects resulting from pathogen infection (Lichtenthaler & Miehé, 1997; Baker, 2008). Apart from the commonly used NDVI, ozone responsive vegetation index Lic2 (Begum et al., 2020) was significantly positively correlated with grain yield in the blast and ozone and blast treatment. In many stressful situations, chlorophyll degrades faster than carotenoids (Peñuelas et al., 1995; Liu et al., 2011), as reflected in Lic2. However, in the combined stress, the additional blast infection did not escalate the damaging effect.

One possible explanation for the mitigating effect of ozone on blast infection could be phytoalexin-type cellular compounds (Skärby & Pell, 1979). The chemical substance phytoalexin inhibits the fungus development and is formed or activated only when the host plants contact the parasite (Harborne, 1993). However, ozone resembles fungal elicitors, and phytoalexins were induced by ozone in soybean (Keen & Taylor, 1975), pine needles (Sandermann, 1996), and in grapevine (Schubert et al., 1997). Rice infected with *M. oryzae* showed resistant disease reactions probably through activation of ROS and phytoalexin production (Yang et al., 2017). In addition, ozone activates salicylic acid-dependent signaling pathways previously shown to be associated with the activation of pathogen defense reactions (Sharma et al., 1996; Rao & Davis, 1999). In tobacco, the ozone-induced salicylic acid signaling pathway increased tolerance towards the tobacco mosaic virus (Yalpani et al., 1994).

Regarding the grain yield, a significant decline was seen in ozone and ozone and blast compared to blast or control. However, the most blast susceptible CO39 and Koshihikari contributed to a likewise significant yield loss in the blast treatment compared to control. In

our study, season-long high ozone (103 ppb) treatment caused a 37% yield loss in rice (Table 3). For comparison, Ashrafuzzaman et al. (2017) reported grain yield losses in rice exceeding 26% after season-long ozone fumigation with an average ozone concentration of 77 ppb. Yield loss for the blast was around 17%, but in the combined ozone and blast, these yield losses from individual stresses did not simply sum up, but were only slightly and nonsignificantly higher than in the ozone alone treatment. In a previous study, the fungal disease powdery mildew combined with 100 ppb ozone did also not exacerbate yield loss in cucumber (Khan & Khan, 1999). However, the reported yield loss due to blast is higher than for ozone (Mills et al., 2018b; Sakulkoo et al., 2018), which is the opposite of our results. We exposed the plants to ozone for an entire season with a relatively high average concentration of 103 ppb ozone. Furthermore, only two out of nine genotypes were ozone tolerant in our experiment. Also, the genotypes used in this study showed no significant yield loss due to blast except for susceptible CO39 and Koshihikari. These factors may have resulted in higher yield losses due to ozone than due to blast.

These data address the first question of the first study, showing that ozone exposure does not increase plant sensitivity to blast. Instead, it reduces the formation of visible blast symptoms. Additionally, blast inoculation does not heighten ozone sensitivity. However, in-depth physiological or genetic causes need to be explored in further studies.

5.2 Contrasting genotypic response to blast disease and ozone

The second objective of the initial study was to explore whether ozone and blast tolerance are positively or negatively correlated in different rice genotypes. Judged by visual injury, some of the genotypes showed both ozone and blast susceptibility (CO39, Koshihikari, Nipponbare). The ozone-tolerant Kasalath showed 1% BSS (Supplementary table 4), which is considered a resistant reaction to blast inoculation (Hensawang et al., 2017; Xiao et al., 2017), whereas the ozone tolerant L81 (derived from Kasalath as one of its parents) showed blast susceptibility (Supplementary Table 4). It is possible that blast sensitivity in L81 was inherited from its second parent Nipponbare (Y. Wang et al., 2014b), which showed a similar level of blast sensitivity. In contrast, Kasalath showed a broad spectrum of resistance reactions against standard differential blast isolates from the Philippines and Japan in a previous study (Ebitani et al., 2011). Kasalath is also considered a donor for blast resistance QTL (Hayasaka

et al., 1995; Takehisa et al., 2009). On the other hand, ozone susceptible Binadhan-11, Kitaake, IR64, and BRRI dhan28 showed blast resistance. Similar to visual injury, differential ozone or blast tolerance or susceptibility were also represented by vegetation indices and other physiological traits such as stomatal conductance and lipid peroxidation. Yield and yield components did not demonstrate any additive or interactive effect regarding blast or ozone tolerance (Table 3, Figure 9). In addition, LBS and BSS were not significantly correlated in combined stress (Figure 10C).

Ozone can induce plant-signaling cascades similar to a pathogen response, ultimately leading to PCD (Sandermann et al., 1998; Kangasjärvi et al., 2005). Moreover, PCD is an essential pathway of pathogen response in plant leaves (Huysmans et al., 2017), which is involved in the formation of ozone stress symptoms (Ueda et al., 2015a, 2015b). Therefore, balancing the interplay of redox homeostasis and PCD pathways is essential for simultaneous ozone and pathogen tolerant breeding (Mills et al., 2018b). In our study Kasalath, the donor for both ozone and blast tolerant QTL did not show any apparent conflict between the ozone and blast tolerance in combined ozone and blast stress. This genotype was resistant to both blast and ozone. In a recent study targeting ozone tolerance and fungal resistance breeding, Mashaheet et al. (2020) tested eight key rust-susceptible wheat genotypes for ozone tolerance and found differential responses. For example, bread wheat genotypes Thatcher and LMPG 6 showed severe sensitivity to ozone, whereas Chinese Spring showed tolerance for ozone-induced visible symptoms and biomass production. Taken together, our data suggest that despite the partly overlapping physiological responses to ozone and blast disease and the interactive effects of these stresses on rice plants (Tables 2 and 3), tolerance or resistance to these stress factors are genetically independent traits. Thus, we can assume that breeding for tolerance against one trait would not necessarily compromise the other trait.

5.3 Breeding efficiency and genotypic advancements

Our initial study gave us sufficient confidence to develop and evaluate ozone-tolerant rice (*Oryza sativa* L.). We achieved this by introgressing the ozone tolerance quantitative trait loci (QTLs), *OzT8* and *OzT9*, into two ozone-sensitive Bangladeshi rice varieties, BRRI dhan28 and Binadhan-11. The marker-assisted backcrossing approach successfully introgressed *OzT8* and *OzT9* into BRRI dhan28 and Binadhan-11, as evidenced by genotypic data confirming the

presence of the target QTLs in advanced breeding generations (Figure 11, 12; Supplementary Table 3). The use of genotyping-by-sequencing (GBS) and KASP markers allowed for the precise selection of individuals carrying the desired alleles, ensuring the efficient transfer of tolerance traits while recovering the genetic background of the recipient parents (Poland et al., 2012; He et al., 2014; Ertiro et al., 2015; Rasheed et al., 2016; Sandhu et al., 2022).

KASP markers have emerged as powerful tools in rice breeding programs for the introgression of QTLs, particularly in developing stress-tolerant varieties. Their efficiency and precision in identifying QTLs associated with abiotic stresses—drought, salinity, and submergence—have made them increasingly popular among rice breeders. KASP markers offer a cost-effective and flexible approach, facilitating the rapid selection of desirable traits and enabling the integration of multiple QTLs into elite cultivars. This technology significantly enhances the resilience of rice varieties against environmental stresses (Steele et al., 2018; Muthu et al., 2020). In rice, these markers have been utilized in conjunction with genotyping-by-sequencing to identify salt-tolerant introgression lines derived from crosses between salt-tolerant and salt-sensitive varieties (Bundó et al., 2022). A study on Korean japonica rice varieties demonstrated the utility of KASP markers in mapping QTLs for bakanae disease resistance, with the successful development and application of 771 markers (Cheon et al., 2019). Additionally, KASP markers have been employed in association mapping studies to identify novel QTLs for nitrogen use efficiency (NUE). For instance, researchers developed KASP SNP markers at a newly identified NUE-related locus (*RM5748*) to investigate putative NUE-related genes and validate their effects (Liu et al., 2016). Furthermore, the pyramiding of multiple QTLs, such as those for drought tolerance (*qDTY1*.1) and salinity tolerance (*Saltol*), has proven effective in improving both yield and survival under abiotic stress conditions (Dhawan et al., 2021). Beyond rice, KASP markers have also been widely applied in other cereal crops, including wheat (Grewal et al., 2019; Ur Rehman et al., 2021; Jiang et al., 2023), barley (Hill et al., 2019), and maize (Awata et al., 2020; Jagtap et al., 2020; Chen et al., 2021), highlighting their broad applicability in plant breeding.

We adapted the methodology proposed by Hospital & Charcosset (1997) and employed 41 KASP markers for background genotyping, achieving a marker density of one per 10.49 Mb, based on the estimated rice genome size of 430 Mb. While no definitive guidelines exist for the minimum number of markers required for background selection in rice, previous studies suggest that a range from 48 (Siwach et al., 2004; Tang et al., 2022) to 386 (Iftekharuddaula

et al., 2011; Kim et al., 2021) well-distributed markers can be effective for various breeding applications. In our breeding lines derived from BRRI dhan28 and Binadhan-11 backgrounds, we observed a progressive increase in homozygosity for target alleles alongside a substantial recovery of the recipient parent genome (together average >87.93%). These findings demonstrate the efficacy of marker-assisted selection (MAS) in generating lines that are genetically and phenotypically similar to the recipient parents (Figures 11, 12; Supplementary Table 3). Prior research has indicated that low-density marker sets can be effective in breeding populations with strong linkage disequilibrium (LD), yielding prediction accuracies comparable to those of high-density arrays (Werner et al., 2018; Larkin et al., 2019).

5.4 Ozone concentration in greenhouse experiment resembles high-risk field conditions

Two controlled greenhouse experiments were conducted to simulate high-risk ozone exposure scenarios similar to those in field environments, particularly in ozone-affected regions such as Bangladesh. The average ozone concentration across both experiments was 99.1 ppb during the 7-hour treatment period (9:00 AM–4:00 PM). Individually, the ozone concentration in the first experiment, which focused on evaluating breeding lines (Experiment 2), was 91 ppb; in the second experiment (Experiment 3), it was 107 ppb. These concentrations align with those observed in several rice-growing Asian countries, including China, India, and Bangladesh, where ambient ozone levels frequently exceed the critical threshold for crop damage due to increasing emissions of ozone precursor pollutants (Ainsworth, 2017; Brauer et al., 2016). China, the largest emitter of nitrogen oxides (NOx) in Asia, experiences rising surface ozone levels, particularly during the rice-growing season when daily average ozone concentrations exceed 50 ppb in some regions (Tang et al., 2013; Feng et al., 2015). Recent studies highlight a consistent upward trend in ozone pollution across various parts of the country. For example, Wang et al. (2020) reported that during 2013–2017, the fourth-highest daily maximum 8-hour average (MDA8) ozone concentrations were approximately 86.0 ± 14.7 ppb — significantly surpassing the levels observed in Europe and the USA. This trend has persisted, with Tian (2023) documenting a marked increase in ozone levels in densely populated provinces such as Henan and Hubei in Central China. Similarly, India has reported 8-hour daily average concentrations surpassing 100 ppb, particularly in urban areas such as Pune (Roy et al., 2009). Moreover, the increasing trend of ozone pollution

is linked to rapid urbanization and industrialization in India, which has led to a rise in emissions of ozone precursors (Gao et al., 2020; Shandilya, 2024).

In Bangladesh, the estimated daily maximum ozone concentration reached 72 ppb in 2013 (Brauer et al., 2016). A review by Frei (2015) confirmed that rice-growing seasons across the Indian subcontinent face a high risk of ozone-induced yield losses. Given the increasing trends in ground-level ozone across these regions (Brauer et al., 2016), the concentrations used in our controlled experiments will likely become even more representative of future ambient conditions. As ozone levels continue to rise, they are expected to routinely exceed the established damage threshold for rice (40 ppb), posing a significant challenge to food security in rice-producing nations.

Furthermore, the lack of a comprehensive nationwide air quality monitoring system beyond Dhaka's metropolitan area limits the direct measurement of ozone levels in Bangladesh, (Rahman et al., 2019). Consequently, estimates of air pollution in Bangladesh largely rely on satellite-based data sources, such as the Sentinel-5 mission of Copernicus ESA (Islam et al., 2021) and the NASA Aura Ozone Monitoring Instrument (OMI) (Ziemke et al., 2006). Recent field experiments have provided the first direct evidence of ground-level ozone concentrations in Bangladesh. Observations during the dry season revealed average daytime ozone levels ranging from 59.4 ppb to 84.2 ppb, with peak concentrations reaching 190 ppb (Frei et al., 2024). Additionally, in our own field experiment (Experiment 4), the recorded average ozone concentration was 88 ppb, closely aligning with the greenhouse conditions used in our study. This suggests that the ozone concentrations employed for testing our breeding lines accurately simulated field conditions, and in some cases, the selected lines demonstrated tolerance to even slightly higher ozone exposure than those observed in the field. Our findings demonstrate differential responses among breeding lines and their sensitive recipient parents under ozone stress. Key physiological markers, including Leaf Bronzing Score (LBS) (Figures 15, 16, 42), chlorophyll degradation (NDVI) (Figures 17, 18, 43), stomatal conductance (gsw) (Figures 27, 28, 46), and oxidative stress indicators such as Malondialdehyde (MDA) (Figure 32), provide strong validation for the employed ozone concentrations. Moreover, variations in grain yield (Figures 36, 53) and photosynthetic efficiency (Figures 31, 49) further confirm that ozone-induced stress responses observed in the greenhouse accurately mimic real-world conditions. This highlights the effectiveness of

greenhouse-based screening for identifying and selecting ozone-tolerant rice lines before their deployment in field environments.

5.5 Physiological and biochemical responses of breeding lines exhibiting tolerance to ozone stress

The findings from both greenhouse experiments revealed significant variations in the physiological and biochemical responses of the breeding lines under ozone stress. Several breeding lines exhibited superior performance compared to their recipient parents, BRRI dhan28 and Binadhan-11. Ozone stress induced an increase in the leaf bronzing score (LBS), a well-established visible marker of oxidative damage in rice plants (Frei et al., 2008; Sawada & Kohno, 2009; Ueda et al., 2015b; Alam et al., 2022). The breeding lines derived from BRRI dhan28 × Kasalath and Binadhan-11 × Kasalath displayed distinct genotypic variations in response to ozone exposure. While control plants showed no visible symptoms, ozone-treated plants exhibited a progressive increase in LBS over time, with significant differences observed at 80 and 109 days after ozone exposure (DAO) in Experiment 2 (Tables 4, 5). However, in Experiment 3, although LBS gradually increased over time, the differences were not statistically significant (Tables 10, 12). Previous studies have suggested that the severity of LBS is influenced by both the duration and concentration of ozone exposure (Sarkar & Agrawal, 2010; Arshad, 2021; Jo et al., 2024). Notably, breeding lines carrying *OzT8* and/or *OzT9* exhibited a significant reduction in LBS, particularly at later stages of ozone exposure, indicating a potential role of these loci in conferring tolerance to ozone stress (Figures 15, 16, 42). *OsORAP1* has been proposed as a candidate gene underlying the ozone tolerance QTL *OzT9*, which is associated with foliar symptom formation under ozone stress. Therefore, breeding lines with tolerant *OsORAP1* introgression could contribute to the reduction of ozone-induced symptoms (Ueda et al., 2015b; Ashrafuzzaman et al., 2020). In our experiments, lines carrying *OzT9* demonstrated reduced leaf injury in both Experiments 2 and 3 within BRRI dhan28-derived lines (Figures 15, 42A, Supplementary Figure 2). In contrast, *OzT8* was more effective in reducing leaf injury in Binadhan-11-derived lines in Experiment 2 (Figure 16). However, in Experiment 3, lines carrying *OzT9* exhibited reduced leaf injury (Figure 42B, Supplementary Figure 2). Overall, breeding lines carrying the *OzT9 QTL* consistently exhibited the lowest LBS, whereas lines harboring *OzT8* alone showed moderate

reductions. Lines containing both QTLs (*OzT8* + *OzT9*) displayed an intermediate response. These findings suggest that the presence of these QTLs helps mitigate visible oxidative damage, likely through enhanced antioxidative mechanisms or reduced ozone uptake (Ueda et al., 2015b; Frei, 2015; Tsukahara et al., 2015; Ashrafuzzaman et al., 2017; Begum et al., 2020).

Since LBS assessment involves a degree of subjective judgment, we further evaluated oxidative stress by measuring malondialdehyde (MDA) concentration as a biochemical marker (Brosset et al., 2020) in Experiment 2. Breeding lines carrying the *OzT8* and/or *OzT9* QTLs exhibited lower MDA levels compared to their recurrent parents (Figure 32), indicating enhanced antioxidative defense mechanisms and improved stress tolerance. Similar to the LBS results, BRRI dhan28-derived lines carrying *OzT9* effectively reduced MDA levels. In contrast, in Experiment 2, Binadhan-11-derived lines carrying *OzT8* showed a more pronounced reduction in MDA levels (Figure 32). This observation aligns with previous studies, which have reported that ozone-tolerant genotypes often accumulate lower MDA levels due to their superior protection against oxidative stress (Ashrafuzzaman et al., 2020; Alam et al., 2022).

To evaluate the impact of ozone stress on foliar pigments at the individual plant level (Pettorelli et al., 2005; Ashrafuzzaman et al., 2017), we measured vegetation indices, including the normalized difference vegetation index (NDVI) and Lichtenthaler index 2 (Lic2), using non-destructive methods (Sims & Gamon, 2002; Meroni et al., 2009; López López et al., 2016). A significant reduction in NDVI and Lic2 values across multiple measurement days (Tables 4, 5, 10, and 12) indicated a decline in chlorophyll content under ozone stress, highlighting the sensitivity of these indices as key indicators of plant pigment composition. The observed decline in NDVI suggests that ozone-induced oxidative stress accelerates chlorophyll degradation (Ribas, 2005; Gielen et al., 2007; Ashrafuzzaman et al., 2017; Y. Feng et al., 2022), thereby impairing photosynthetic efficiency (Shah et al., 2017). Although the effect of ozone treatment was not consistently significant, even at later stages in Experiment 3, genotypic differences were evident (Tables 10, 12). Breeding lines carrying both QTLs (*OzT8* + *OzT9*) exhibited higher NDVI values (Figure 43, Supplementary Figure 3), suggesting enhanced chlorophyll retention in both BRRI dhan and Binadhan-11-derived breeding lines. Among the single QTLs, lines carrying *OzT9* alone displayed the highest NDVI values, indicating that this QTL is crucial in protecting photosynthetic pigments under ozone stress

(Supplementary Figure 3). The ability of plants to maintain chlorophyll content under ozone stress has also been reported in other studies, such as in wheat (Begum et al., 2020; Y. Feng et al., 2022) and rice (Ashrafuzzaman et al., 2017; Alam et al., 2022). Similarly, the ozone-responsive vegetation index Lic2, which reflects the balance between chlorophyll and carotenoids, exhibited significant reductions under ozone exposure (Tables 4, 5, 10, and 12), particularly at later stages in both Experiments 2 and 3. Under ozone stress, chlorophyll degradation is typically accelerated, whereas carotenoid synthesis may increase as an antioxidant defense mechanism, or their degradation may occur at a slower rate. These shifts in the chlorophyll-to-carotenoid ratio support the use of indices such as Lic2 as reliable physiological indicators of ozone stress, measurable non-invasively and at high throughput via spectral reflectance (Begum et al., 2020; Frei et al., 2024). Notably, in Experiment 3, lines containing both QTLs (*OzT8* + *OzT9*) exhibited the highest relative Lic2 values (Figure 44; Supplementary Figure 4), suggesting a potential synergistic role in chlorophyll stability and oxidative stress protection. The preservation of NDVI and Lic2 values in QTL-carrying lines indicates that these genotypes (Figure 43, 44) may possess an enhanced ability to regulate pigment degradation, possibly through increased antioxidant enzyme activity (Alam et al., 2021) or reduced ozone-induced reactive oxygen species (ROS) accumulation (Ashrafuzzaman et al., 2020), as also observed in Experiment 2 (Figure 32).

Another critical physiological parameter affected by ozone stress is the nitrogen balance index (NBI), which indicates plant nitrogen status and protein synthesis (Li et al., 2015; Padilla et al., 2016). In our study, ozone exposure generally reduced NBI values across all breeding lines, particularly at 80 and 109 DAO in Experiment 2 (Tables 4 and 5), suggesting a disruption in nitrogen metabolism. However, in Experiment 3, no substantial decline in NBI values was observed (Tables 10, 12). Ozone stress is known to impair nitrogen assimilation by inhibiting nitrate reductase activity (Y. Z. Huang et al., 2012), thereby reducing nitrogen availability for essential physiological processes such as chlorophyll synthesis and protein formation (Akhtar et al., 2024; Feng et al., 2024). Notably, breeding lines carrying both QTLs (*OzT8* + *OzT9*) exhibited significantly higher NBI values than those carrying either *OzT8* or *OzT9* alone (Figure 45; Supplementary Figure 5). This suggests that combining these QTLs may play a role in maintaining nitrogen homeostasis under ozone stress. The ability of these lines to sustain higher NBI values despite ozone exposure indicates an enhanced capacity for nitrogen uptake,

assimilation, or remobilization, thereby supporting growth and metabolic functions under stress conditions.

5.6 Improved gas exchange and photosynthetic efficiency in breeding lines

Stomatal conductance (gsw), a key determinant of gas exchange, was significantly reduced under ozone stress in both experiments (Tables 4, 5, 10, and 12). Stomatal regulation is crucial in the plant's response to ozone stress, limiting ozone uptake into the leaves (Vahisalu et al., 2010; Moldau et al., 2011; Chen et al., 2011). However, ozone exposure can also cause stomatal sluggishness, impairing the plant's ability to dynamically adjust to fluctuating ozone concentrations (Paoletti & Grulke, 2010; Sun et al., 2012). This presents a challenge for plants, as they must balance stomatal conductance to sustain photosynthesis while mitigating ozone-induced damage (Hoshika et al., 2018; Nowroz et al., 2024). Despite this challenge, tolerant plants exhibit a more stable stomatal conductance, as observed in this study and supported by previous research (Alam et al., 2022; Frei et al., 2024). In our third experiment, we observed an average reduction of 87.94% in stomatal conductance in BRRI dhan28, whereas the breeding lines showed an average reduction of 61.32% (Figure 46A). Similarly, Binadhan-11 exhibited an 84.02% reduction, while the breeding lines showed a 51.92% reduction (Figure 46B). In contrast, the ozone-tolerant donor plant Kasalath exhibited a lower reduction of 49.56% (Figure 46). However, the performance of different QTL combinations in both genetic backgrounds was inconclusive in our study (Supplementary Figure 6). Although all QTL combinations resulted in improved stomatal conductance compared to the sensitive recipient lines, the specific effects varied (Figures 27, 28, 46).

Photosynthetic efficiency parameters, such as the quantum efficiency of photosystem II (PhiPS2) and the electron transport rate (ETR), showed no significant reduction under ozone stress (Tables 4, 5, 10, and 12), indicating that the breeding lines maintained their photosynthetic capacity despite the oxidative stress (Figures 23, 24, 25, 26, 47, 48). It is well-established that various environmental stressors, including ozone, can impair PSII functionality (Sperdouli et al., 2021; Orts et al., 2024) and significantly reduce ETR (Ohashi et al., 2006; Xu et al., 2007; Kerner et al., 2011; Nowroz et al., 2024). Although all QTL combinations resulted in improved PhiPS2 and ETR compared to the sensitive recipient lines, a consistent pattern across experiments and recipient parents was not observed (Figures 23, 24, 25, 26, 47, 48; Supplementary Figure 7,8).

Further, ozone stress significantly affects plant photosynthesis, reducing carbon assimilation and overall plant productivity (Mäenpää et al., 2011; Fares et al., 2013; Choquette et al., 2019). However, in both of our experiments (2,3), we did not observe a significant reduction in the net CO_2 assimilation rate (A), an integrated measure of photosynthetic capacity (Tcherkez & Limami, 2019), as shown in Tables 4, 5, 10, and 12. Despite this, significant genotypic differences were evident. Specifically, a drastic reduction in net CO_2 assimilation rate (A) was observed only in the sensitive recipient parents (Figures 31, 49). The ability of tolerant plants to maintain net CO_2 assimilation under ozone stress has also been reported in previous studies (Nouchi et al., 1995; Degl'Innocenti et al., 2002; Du et al., 2018).

Furthermore, we measured additional photosynthesis-related traits, including transpiration rate (E) and intercellular CO_2 concentration (Ci). However, our analysis did not reveal any significant correlation between these traits and yield (Figures 38, 39, 40, and 41).

5.7 Breeding line exhibits yield stability under ozone stress conditions

While evaluating breeding lines' physiological, biochemical, and photosynthetic responses, we observed tolerance behavior under ozone stress, which was further reflected in yield-related traits (Table 8, 9, 11, 13). Despite the adverse effects of ozone, the breeding lines harboring *OzT8* and/or *OzT9* demonstrated superior agronomic performance compared to their recipient parents under stress conditions (Figures 34, 35, 36, 37, 50, 51, 52, 53, 54, 55). Key traits such as reduced leaf bronzing score (LBS), sustained vegetation indices, lower malondialdehyde (MDA) levels, and improved gas exchange and photosynthesis were associated with enhanced yield components, including higher grain yield and straw biomass (Q. Wang et al., 2014; Phothi et al., 2016; Periyasamy et al., 2020).

In our second experiment, BRRI dhan28 exhibited an average yield loss of 55.81% under ozone stress. In contrast, the breeding lines derived from BRRI dhan28 showed a yield loss ranging from no loss to a maximum of 41.22% (Figure 36A). Similarly, Binadhan-11 showed a 60.45% yield loss due to ozone, while its derived breeding lines exhibited yield losses ranging from none to a maximum of 41.59% (Figure 36B). The average yield loss in BRRI dhan28 in the third experiment was 29.81%. However, the breeding lines derived from BRRI dhan28 showed significantly reduced yield losses, ranging from a minimum of 1.66% to a maximum of 21.79% under ozone stress (Figure 53A). Similarly, Binadhan-11 experienced a yield loss of 41.34%, whereas its breeding lines displayed no yield loss to a maximum of 17.83% (Figure 53B). In

our field study (Experiment 4), BRRI dhan28 exhibited an average yield loss of 11.87% under ozone stress. In contrast, the breeding lines derived from BRRI dhan28 showed a yield loss ranging from no loss to a maximum of 6.72% (Figure 56A). Similarly, Binadhan-11 had a yield loss of 15.01%, while its breeding lines experienced losses ranging from none to a maximum of 9.16% (Figure 56B). The yield loss observed in BRRI dhan28 and Binadhan-11 aligns with findings from previous ozone fumigation studies (Ashrafuzzaman et al., 2017; Alam et al., 2022; Frei et al., 2024). The introgression of the QTLs *OzT8* and/or *OzT9* conferred ozone stress tolerance to the breeding lines, enabling them to maintain a comparable stable yield across varying ozone concentrations. In our experiments, the donor Kasalath exhibited a relatively lower yield reduction, with an 8.28% reduction in the second experiment and 4.36% in the third, while no yield loss was observed in the field experiment (Figures 36, 53, 56). These findings are consistent with its previously reported ozone tolerance in several ozone fumigation studies (Frei et al., 2008; Alam et al., 2022; Frei et al., 2024). The number of filled grains was the primary yield component responsible for the smaller yield reductions observed in the breeding lines compared to the more significant reductions in recipient parents under greenhouse conditions (Figures 38, 40). Since this trait is determined relatively early in the plant growth cycle during the panicle initiation stage (Fageria, 2007; Xu et al., 2020), these findings further confirm the tolerance of the breeding lines throughout the growth cycle.

Another important trait of interest is the reduction of straw biomass under ozone stress, with *OzT8* being primarily identified as a key factor influencing biomass under these conditions (Chen et al., 2011). Results from our third experiment showed a similar trend in both genetic backgrounds, confirming a lower reduction in biomass for breeding lines harboring the QTL *OzT8* (Figure 54; Supplementary Figure 9). However, this trend was not observed in the field experiment, where *OzT8* exhibited an intermediate response alone (Figure 57; Supplementary Figure 10).

The harvest index (HI) is critical for crop improvement for cereal breeders, particularly for enhancing yield efficiency. HI is a key indicator of how effectively a plant converts biomass into economically valuable grain (Sinclair, 1998; Asefa, 2019). In our greenhouse experiments, we observed diverse responses; however, in the field experiment, plants carrying both QTLs (*OzT8* + *OzT9*) consistently exhibited a higher harvest index (Figure 58; Supplementary Figure 11, 12). Breeders prioritize HI because it reflects the physiological capacity of different genotypes and offers valuable insights into their genetic potential for yield improvement

(Bhatt, 1976; Sinclair, 2019). These findings underscore the importance of incorporating both QTLs (*OzT8* + *OzT9*) to develop ozone-tolerant rice varieties.

5.8 Pyramiding of *OzT8* and *OzT9* QTLs enhances ozone stress tolerance in breeding lines

One of our primary objectives was to compare the performance of two ozone-tolerance QTLs, *OzT8* and *OzT9*. Our findings suggest that *OzT8* and *OzT9*, either independently or in combination with other QTLs, influence multiple physiological and biochemical parameters that contribute to ozone stress mitigation, although with varying degrees of effectiveness depending on the genetic background of the recipient lines. To evaluate the distinct performance of these QTLs, we analyzed net CO_2 assimilation rates (A) from the third experiment as an indicator of physiological performance (Fares et al., 2013; Reguera et al., 2013; Liu et al., 2020) and grain yield data from both the third experiment and a field trial, as grain yield is the primary target in stress-tolerant rice breeding (Sakamoto & Matsuoka, 2008; Pang et al., 2017; Du et al., 2020), to assess their impact under ozone stress.

In the BRRI dhan28 genetic background, breeding lines carrying both QTLs (*OzT8* + *OzT9*) exhibited significantly higher net CO_2 assimilation rates compared to lines carrying *OzT9* alone. However, no significant difference was observed between lines with *OzT8* alone and those with *OzT8* + *OzT9*, suggesting that *OzT8* plays a more dominant role in enhancing photosynthesis under ozone stress (Supplementary Figure 13A). A similar trend was observed in the Binadhan-11 background: lines with *OzT8* had significantly higher net CO_2 assimilation rates than those with *OzT9* alone, while the difference between *OzT8* and both QTls (*OzT8* + *OzT9*) remained statistically non-significant (Supplementary Figure 13B). *OzT8* is primarily associated with maintaining high photosynthetic rates despite ozone-induced stomatal closure (Chen et al., 2011), a characteristic also evident in our experiments.

Grain yield data from both genetic backgrounds revealed no statistically significant differences among the QTL combinations, although lines with *OzT8* showed comparatively lower yield reduction under ozone stress (Supplementary Figure 14). In the field experiment, breeding lines carrying both QTLs (*OzT8* + *OzT9*) exhibited significantly higher grain yields compared to lines with either QTL alone (Supplementary Figure 15). This result supports the conclusion that the combined effect of *OzT8* and *OzT9* enhances rice yield under ozone stress (Y. Wang et al., 2014b; Jing et al., 2016; Alam et al., 2022). Although the relationship between physiological traits and yield in our study was not entirely straightforward, the improved

physiological performance of breeding lines carrying both QTLs likely contributed to their superior grain yield under ozone stress. Our findings also highlight the importance of pyramiding multiple tolerance loci to enhance resilience against complex stressors like ozone (Ravelombola et al., 2021; Guo et al., 2024).

5.9 *OsORAP1* Plays a Key Role in Reducing LBS

We performed multiple crosses and genotyped the resulting progenies to identify breeding lines with recombination in both QTLs. However, we did not obtain suitable lines with recombination in the *OzT8* QTL (Supplementary Table 3). In contrast, several breeding lines showed recombination for the *OzT9* QTL, which is associated with foliar symptom formation under ozone stress (Ueda et al., 2015b). Additionally, we identified breeding lines lacking the previously proposed introgression of *OzT9* but carrying the tolerant *OsORAP1* introgression (Supplementary Table 3, 5).

We evaluated the symptom formation score in all recombinant lines and found no statistically significant differences between the lines, irrespective of genetic background (Supplementary Figure 16). This suggests that the tolerant *OsORAP1* introgression is more critical in reducing symptom formation than *OzT9*. For instance, breeding line MFOL-1102, which lacks the *OzT9* introgression but carries the tolerant *OsORAP1* introgression, exhibited the lowest leaf bronzing score (LBS) in the Binadhan-11 background (Supplementary Figure 16B). Similarly, breeding line MFOL-1547 showed a lower LBS in the BRRI dhan28 background (Supplementary Figure 16A). These results strongly support the role of *OsORAP1* as a candidate gene for mitigating leaf bronzing, in agreement with previous studies (Ueda et al., 2015a, 2015b; Ashrafuzzaman et al., 2020; Frei et al., 2024).

Although reduced leaf bronzing may not directly enhance yield, it could improve rice straw quality for ruminant herbivores (Y. Wang et al., 2014b). Additionally, while *OzT9* introgression did not significantly affect symptom formation, it remains relevant for breeding ozone-tolerant rice, as this QTL has been associated with key agronomic traits such as reduced spikelet sterility (Y. Wang et al., 2014b), decreased chalkiness (Jing et al., 2016), and improved rice straw quality (Frei et al., 2011), particularly when combined with another ozone tolerance QTL, *OzT8*. Additionally, genes within the *OzT9* interval are likely to interact with *OsORAP1* (Ueda et al., 2015a, 2015b), suggesting a complex genetic interplay underlying ozone

tolerance. The recombinant lines developed in this study thus serve as valuable genetic resources for the fine-mapping of *OzT9* in future research.

6 Conclusion

This study investigated the interactions between ozone exposure and blast disease in rice, focusing on the contrasting responses of different genotypes and the potential for breeding ozone-tolerant varieties through marker-assisted selection. The data suggest that chronic ozone exposure slightly mitigated blast severity, but no significant reciprocal effect was observed. Additionally, the combined stress treatment did not result in an additive increase in stress intensity. No consistent synergy or trade-off was found regarding genotype tolerance to individual or combined stresses, indicating that tolerance to one stress does not necessarily compromise tolerance to the other.

Marker-assisted backcrossing successfully introgressed the quantitative trait loci (QTLs) *OzT8* and *OzT9* into BRRI dhan28 and Binadhan-11. Kompetitive Allele-Specific PCR (KASP) markers enabled precise selection and efficient recovery of the recipient genome, achieving over 87.93% genome recovery. This confirmed the utility of KASP markers for developing stress-resilient rice varieties. Greenhouse experiments accurately simulated high-risk ozone exposure scenarios, closely reflecting real-world field conditions in Bangladesh and other Asian countries. Physiological markers such as the leaf bronzing score (LBS), chlorophyll degradation, oxidative stress indicators, and gas exchange traits validated the robustness of these conditions. Breeding lines carrying *OzT8* and *OzT9* showed significant reductions in LBS and malondialdehyde (MDA) levels, indicating enhanced antioxidative defense mechanisms. Retained chlorophyll content, improved vegetation indices (NDVI and Lic2), and enhanced gas exchange (gsw, PhiPS2, ETR, A) further demonstrated greater photosynthetic capacity under ozone stress. The synergistic effects of *OzT8* and *OzT9* helped mitigate visible oxidative damage and maintain nitrogen balance.

Despite ozone's adverse effects, breeding lines consistently displayed superior yield stability compared to their sensitive recipient parents. In field experiments, some breeding lines showed minimal or no yield loss, confirming their resilience and adaptability to real-world environments. However, since the field experiment was conducted at a single location, multi-location trials are necessary for further validation.

The evaluation of recombinant lines revealed that the *OsORAP1* introgression is more critical in reducing leaf bronzing symptoms than *OzT9* alone, suggesting *OsORAP1* as a key genetic resource for breeding ozone-tolerant rice. Therefore, the developed breeding lines

incorporating *OzT8*, *OzT9,* and *OsORAP1* offer a strong foundation for future breeding programs targeting combined ozone tolerance in rice.

References

Agathokleous, E. (2017). Perspectives for elucidating the ethylenediurea (EDU) mode of action for protection against O_3 phytotoxicity. *Ecotoxicology and Environmental Safety*, 142, 530–537. https://doi.org/10.1016/j.ecoenv.2017.04.057

Agathokleous, E., Belz, R. G., Calatayud, V., De Marco, A., Hoshika, Y., Kitao, M., Saitanis, C. J., Sicard, P., Paoletti, E., & Calabrese, E. J. (2019a). Predicting the effect of ozone on vegetation via linear non-threshold (LNT), threshold and hormetic dose-response models. *Science of the Total Environment*, 649, 61–74. https://doi.org/10.1016/j.scitotenv.2018.08.264

Agathokleous, E., Araminiene, V., Belz, R. G., Calatayud, V., De Marco, A., Domingos, M., Feng, Z., Hoshika, Y., Kitao, M., Koike, T., Paoletti, E., Saitanis, C. J., Sicard, P., & Calabrese, E. J. (2019b). A quantitative assessment of hormetic responses of plants to ozone. *Environmental Research*, 176, 108527. https://doi.org/10.1016/j.envres.2019.108527

Agathokleous, E., Frei, M., Knopf, O. M., Muller, O., Xu, Y., Nguyen, T. H., Gaiser, T., Liu, X., Liu, B., Saitanis, C. J., Shang, B., Alam, M. S., Feng, Y., Ewert, F., & Feng, Z. (2023). Adapting crop production to climate change and air pollution at different scales. *Nature Food, 4*(10), 854–865. https://doi.org/10.1038/s43016-023-00858-y

Agathokleous, E., Kitao, M., & Kinose, Y. (2018). A review study on ozone phytotoxicity metrics for setting critical levels in Asia. *Asian Journal of Atmospheric Environment*, 12, 1–16. https://doi.org/10.5572/ajae.2018.12.1.001

Agathokleous, E., Saitanis, C. J., & Koike, T. (2015). Tropospheric O_3, the nightmare of wild plants: A review study. *Journal of Agricultural Meteorology, 71*(2), 142–152. https://doi.org/10.2480/agrmet.D-14-00008

Ainsworth, E. A. (2008). Rice production in a changing climate: A meta-analysis of responses to elevated carbon dioxide and elevated ozone concentration. *Global Change Biology, 14*(7), 1642–1650. https://doi.org/10.1111/j.1365-2486.2008.01594.x

Ainsworth, E. A. (2017). Understanding and improving global crop response to ozone pollution. *The Plant Journal, 90*(5), 886–897. https://doi.org/10.1111/tpj.13298

Ainsworth, E. A., Yendrek, C. R., Sitch, S., Collins, W. J., & Emberson, L. D. (2012). The effects of tropospheric ozone on net primary productivity and implications for climate

change. *Annual Review of Plant Biology*, 63, 637–661. https://doi.org/10.1146/annurev-arplant-042110-103829

Akhtar, K., Ain, N. U., Prasad, P. V. V., Naz, M., Aslam, M. M., Djalovic, I., Riaz, M., Ahmad, S., Varshney, R. K., He, B., & Wen, R. (2024). Physiological, molecular, and environmental insights into plant nitrogen uptake, and metabolism under abiotic stresses. *The Plant Genome, 17*(2), e20461. https://doi.org/10.1002/tpg2.20461

Akhtar, N., Yamaguchi, M., Inada, H., Hoshino, D., Kondo, T., Fukami, M., Funada, R., & Izuta, T. (2010). Effects of ozone on growth, yield and leaf gas exchange rates of four Bangladeshi cultivars of rice (Oryza sativa L.). *Environmental Pollution*, 158(9), 2970–2976. https://doi.org/10.1016/j.envpol.2010.05.026

Akimoto, H. (2003). Global air quality and pollution. *Science*, 302(5651), 1716–1719. https://doi.org/10.1126/science.1092666

Alam, M. S., Abdel-Latef, A. A. H., & Ashrafuzzaman, M. (2021). Ozone and enzymatic and non-enzymatic antioxidant enzymes in plants. In A. A. H. Abdel Latef (Ed.), *Organic solutes, oxidative stress, and antioxidant enzymes under abiotic stressors* (1st ed., pp. 365–386). CRC Press. https://doi.org/10.1201/9781003022879-17

Alam, M. S., Maina, A. W., Feng, Y., Wu, L.-B., & Frei, M. (2022). Interactive effects of tropospheric ozone and blast disease (*Magnaporthe oryzae*) on different rice genotypes. *Environmental Science and Pollution Research*, 29, 48893–48907. https://doi.org/10.1007/s11356-022-19282-z

Ali, S., Gautam, R. K., Mahajan, R., Krishnamurthy, S. L., Sharma, S. K., Singh, R. K., & Ismail, A. M. (2013). Stress indices and selectable traits in *SALTOL* QTL introgressed rice genotypes for reproductive stage tolerance to sodicity and salinity stresses. *Field Crops Research, 154*, 65–73. https://doi.org/10.1016/j.fcr.2013.06.011

Alpuerto, V. L. E., Norton, G. W., Alwang, J., & Ismail, A. M. (2009). Economic impact analysis of marker-assisted breeding for tolerance to salinity and phosphorous deficiency in rice. *Review of Agricultural Economics*, 31(4), 779–792.

Amann, M., & Lutz, M. (2000). The revision of the air quality legislation in the European Union related to ground-level ozone. *Journal of Hazardous Materials, 78*(1–3), 41–62. https://doi.org/10.1016/S0304-3894(00)00216-8

Apel, K., & Hirt, H. (2004). Reactive oxygen species: Metabolism, oxidative stress, and signal transduction. *Annual Review of Plant Biology*, 55, 373–399. https://doi.org/10.1146/annurev.arplant.55.031903.141701

Arshad, A. (2021). A growth and biochemistry of ten high yielding genotypes of Pakistani rice (*Oryza sativa* L.) at maturity under elevated tropospheric ozone. *Heliyon*, 7(10), e08198. https://doi.org/10.1016/j.heliyon.2021.e08198

Asefa, G. (2019). The role of harvest index in improving crop productivity: A review. *Journal of Natural Sciences Research*, 9(6), 24–28. https://doi.org/10.7176/jnsr/9-6-04

Ashmore, M. R. (2005). Assessing the future global impacts of ozone on vegetation. *Plant, Cell & Environment*, 28(8), 949–964. https://doi.org/10.1111/j.1365-3040.2005.01341.x

Ashrafuzzaman, M., Haque, Z., Ali, B., Mathew, B., Yu, P., Hochholdinger, F., de Abreu Neto, J. B., McGillen, M. R., Ensikat, H.-J., Manning, W. J., & Frei, M. (2018). Ethylenediurea (EDU) mitigates the negative effects of ozone in rice: Insights into its mode of action. *Plant, Cell & Environment*, 41(12), 2882–2898. https://doi.org/10.1111/pce.13423

Ashrafuzzaman, M., Henry, R., & Frei, M. (2021). Molecular breeding for improving ozone tolerance in rice: recent progress and future perspectives. In M. A. Hossain, L. Hassan, K. M. Iftekharuddaula, A. Kumar, & R. Henry (Eds.), *Molecular breeding for rice abiotic stress tolerance and nutritional quality* (pp. 180–200). John Wiley & Sons. https://doi.org/10.1002/9781119633174.ch9

Ashrafuzzaman, M., Lubna, F. A., Holtkamp, F., Manning, W. J., Kraska, T., & Frei, M. (2017). Diagnosing ozone stress and differential tolerance in rice (*Oryza sativa* L.) with ethylenediurea (EDU). *Environmental Pollution, 230*, 339–350. https://doi.org/10.1016/j.envpol.2017.06.055

Ashrafuzzaman, M., Ueda, Y., & Frei, M. (2020). Natural sequence variation at the *OsORAP1* locus is a marker for ozone tolerance in Asian rice. *Environmental and Experimental Botany, 178*, 104153. https://doi.org/10.1016/j.envexpbot.2020.104153

Avnery, S., Mauzerall, D. L., Liu, J., & Horowitz, L. W. (2011). Global crop yield reductions due to surface ozone exposure: 2. Year 2030 potential crop production losses and economic damage under two scenarios of O_3 pollution. *Atmospheric Environment*, 45(13), 2297–2309. https://doi.org/10.1016/j.atmosenv.2011.01.002

Awata, L. A. O., Beyene, Y., Gowda, M., Suresh, L. M., Jumbo, M. B., Tongoona, P., Danquah, E., Ifie, B. E., Marchelo-Dragga, P. W., Olsen, M., Ogugo, V., Mugo, S., & Prasanna, B. M. (2020). Genetic analysis of QTL for resistance to maize lethal necrosis in multiple mapping populations. *Genes, 11*(1), 32. https://doi.org/10.3390/genes11010032

Baier, M., Kandlbinder, A., Golldack, D., & Dietz, K. J. (2005). Oxidative stress and ozone: Perception, signalling and response. *Plant, Cell & Environment*, 28(8), 1012–1020. https://doi.org/10.1111/j.1365-3040.2005.01326.x

Baker, N. R. (2008). Chlorophyll fluorescence: A probe of photosynthesis in vivo. *Annual Review of Plant Biology, 59*(1), 89–113. https://doi.org/10.1146/annurev.arplant.59.032607.092759

Begum, H., Alam, M. S., Feng, Y., Koua, P., Ashrafuzzaman, M., Shrestha, A., Kamruzzaman, M., Dadshani, S., Ballvora, A., Naz, A. A., & Frei, M. (2020). Genetic dissection of bread wheat diversity and identification of adaptive loci in response to elevated tropospheric ozone. *Plant, Cell & Environment*, 43(11), 2650–2665. https://doi.org/10.1111/pce.13864

Bhatt, G. M. (1976). Variation of harvest index in several wheat crosses. *Euphytica*, 25(1), 41–50. https://doi.org/10.1007/BF00041527

Biswas, D. K., Xu, H., Li, Y. G., Liu, M. Z., Chen, Y. H., Sun, J. Z., & Jiang, G. M. (2008). Assessing the genetic relatedness of higher ozone sensitivity of modern wheat to its wild and cultivated progenitors/relatives. *Journal of Experimental Botany, 59*(4), 951–963. https://doi.org/10.1093/jxb/ern022

Boddy, L. (2016). Pathogens of autotrophs. In S. C. Watkinson, N. Money, & L. Boddy (Eds.), *The Fungi* (pp. 245–292). Academic Press. https://doi.org/10.1016/B978-0-12-382034-1.00008-6

Brauer, M., Freedman, G., Frostad, J., van Donkelaar, A., Martin, R. V., Dentener, F., van Dingenen, R., Estep, K., Amini, H., Apte, J. S., Balakrishnan, K., Barregard, L., Broday, D., Feigin, V., Ghosh, S., Hopke, P. K., Knibbs, L. D., Kokubo, Y., Liu, Y., Ma, S., Morawska, L., Texcalac-Sangrador, J. L., Shaddick, G., Anderson, H. R., Vos, T., Forouzanfar, M. H., Burnett, R. T., & Cohen, A. (2016). Ambient air pollution exposure estimation for the global burden of disease 2013. *Environmental Science & Technology*, 50(1), 79–88. https://doi.org/10.1021/acs.est.5b03709

Brosset, A., Saunier, A., Kivimäenpää, M., & Blande, J. D. (2020). Does ozone exposure affect herbivore-induced plant volatile emissions differently in wild and cultivated plants? *Environmental Science and Pollution Research*, 27, 30448–30459. https://doi.org/10.1007/s11356-020-09320-z

Bundó, M., Martín-Cardoso, H., Pesenti, M., Gómez-Ariza, J., Castillo, L., Frouin, J., Serrat, X., Nogués, S., Courtois, B., Grenier, C., Sacchi, G. A., & San Segundo, B. (2022). Integrative approach for precise genotyping and transcriptomics of salt tolerant introgression rice lines. *Frontiers in Plant Science*, 12, 797141. https://doi.org/10.3389/fpls.2021.797141

Burkey, K. O., & Carter, T. E. (2009). Foliar resistance to ozone injury in the genetic base of U.S. and Canadian soybean and prediction of resistance in descendent cultivars using coefficient of parentage. *Field Crops Research, 111*(2), 207–217. https://doi.org/10.1016/j.fcr.2008.12.005

Burton, A. L., Burkey, K. O., Carter, T. E., Jr., Orf, J., & Cregan, P. B. (2016). Phenotypic variation and identification of quantitative trait loci for ozone tolerance in a Fiskeby III × Mandarin (Ottawa) soybean population. *Theoretical and Applied Genetics, 129*, 1113–1125. https://doi.org/10.1007/s00122-016-2687-1

Calatayud, A., & Barreno, E. (2001). Chlorophyll a fluorescence, antioxidant enzymes and lipid peroxidation in tomato in response to ozone and benomyl. *Environmental Pollution*, 115(2), 283–289. https://doi.org/10.1016/S0269-7491(01)00101-4

Carnahan, J. E., Jenner, E. L., & Wat, E. K. W. (1978). Prevention of ozone injury to plants by a new protectant chemical. *Phytopathology, 68*(8), 1225–1229. https://doi.org/10.1094/Phyto-68-1225

Chakraborty, M., Mahmud, N. U., Muzahid, A. N. M., Rabby, S. M. F., & Islam, T. (2020). Oligomycins inhibit *Magnaporthe oryzae Triticum* and suppress wheat blast disease. *PLOS ONE, 15*(8), e0233665. https://doi.org/10.1371/journal.pone.0233665

Challagulla, V., Bhattarai, S., & Midmore, D. J. (2015). In-vitro vs in-vivo inoculation: Screening for resistance of Australian rice genotypes against blast fungus. *Rice Science, 22*(3), 132–137. https://doi.org/10.1016/j.rsci.2015.05.017

Chang, K.-L., Petropavlovskikh, I., Cooper, O. R., Schultz, M. G., & Wang, T. (2017). Regional trend analysis of surface ozone observations from monitoring networks in eastern

North America, Europe and East Asia. *Elementa: Science of the Anthropocene*, 5, 50. https://doi.org/10.1525/elementa.243

Chaudhary, I. J., & Rathore, D. (2020). Relative effectiveness of ethylenediurea, phenyl urea, ascorbic acid and urea in preventing groundnut (*Arachis hypogaea* L) crop from ground level ozone. *Environmental Technology & Innovation*, 19, 100963. https://doi.org/10.1016/j.eti.2020.100963

Chen, C. P., Frei, M., & Wissuwa, M. (2011). The *OzT8* locus in rice protects leaf carbon assimilation rate and photosynthetic capacity under ozone stress. *Plant, Cell & Environment*, 34(7), 1141–1149. https://doi.org/10.1111/j.1365-3040.2011.02312.x

Chen, X., Jia, Y., & Wu, B. M. (2019). Evaluation of rice responses to the blast fungus *Magnaporthe oryzae* at different growth stages. *Plant Disease,* 103(1), 132–136. https://doi.org/10.1094/PDIS-12-17-1873-RE

Chen, X., Wang, Z., Shangguan, Y., Yu, J., Hu, B., Shen, Q., Xue, J., Zhang, X., & Shi, Z. (2023). Estimating monthly surface ozone using multi-source satellite products in China based on Deep Forest model. Atmospheric Environment, 307, 119819. https://doi.org/10.1016/j.atmosenv.2023.119819

Chen, Z., Tang, D., Ni, J., Li, P., Wang, L., Zhou, J., Li, C., Lan, H., Li, L., & Liu, J. (2021). Development of genic KASP SNP markers from RNA-Seq data for map-based cloning and marker-assisted selection in maize. *BMC Plant Biology*, 21, Article 157. https://doi.org/10.1186/s12870-021-02932-8

Chengqi, Z., Yuxuan, Y., Tian, Q., Yafan, H., Jifeng, Y., & Zhicheng, S. (2023). Drought-tolerant rice at molecular breeding eras: an emerging reality. *Rice Science, 31*(4). https://doi.org/10.1016/j.rsci.2023.11.005

Cheon, K.-S., Jeong, Y.-M., Lee, Y.-Y., Oh, J., Kang, D.-Y., Oh, H., Kim, S. L., Kim, N., Lee, E., Baek, J., Kim, K.-H., Won, Y. J., Cho, Y.-I., Han, J.-H., & Ji, H. (2019). Kompetitive allele-specific PCR marker development and quantitative trait locus mapping for bakanae disease resistance in Korean *japonica* rice varieties. *Plant Breeding and Biotechnology*, 7(3), 208–219. https://doi.org/10.9787/PBB.2019.7.3.208

Cho, K., Tiwari, S., Agrawal, S. B., Torres, N. L., Agrawal, M., Sarkar, A., Shibato, J., Agrawal, G. K., Kubo, A., & Rakwal, R. (2011). Tropospheric ozone and plants: Absorption, responses, and consequences. In D. M. Whitacre (Ed.), *Reviews of Environmental*

Contamination and Toxicology (Vol. 212, pp. 61–111). Springer. https://doi.org/10.1007/978-1-4419-8453-1_3

Chojak-Koźniewska, J., Kuźniak, E., & Zimny, J. (2018). The effects of combined abiotic and pathogen stress in plants: Insights from salinity and *Pseudomonas syringae* pv. *lachrymans* interaction in cucumber. *Frontiers in Plant Science*, 9, 1691. https://doi.org/10.3389/fpls.2018.01691

Choquette, N. E., Ogut, F., Wertin, T. M., Montes, C. M., Sorgini, C. A., Morse, A. M., Brown, P. J., Leakey, A. D. B., McIntyre, L. M., & Ainsworth, E. A. (2019). Uncovering hidden genetic variation in photosynthesis of field-grown maize under ozone pollution. *Global Change Biology, 25*(12), 4327–4338. https://doi.org/10.1111/gcb.14794

Cohen, S. P., & Leach, J. E. (2019). Abiotic and biotic stresses induce a core transcriptome response in rice. *Scientific Reports, 9*, 6273. https://doi.org/10.1038/s41598-019-42731-8

Collard, B. C. Y., & Mackill, D. J. (2008). Marker-assisted selection: An approach for precision plant breeding in the twenty-first century. *Philosophical Transactions of the Royal Society B: Biological Sciences, 363*(1491), 557–572. https://doi.org/10.1098/rstb.2007.2170

Conklin, P. L., & Barth, C. (2004). Ascorbic acid, a familiar small molecule intertwined in the response of plants to ozone, pathogens, and the onset of senescence. *Plant, Cell & Environment*, 27(8), 959–970. https://doi.org/10.1111/j.1365-3040.2004.01203.x

Conklin, P. L., Pallanca, J. E., Last, R. L., & Smirnoff, N. (1997). L-ascorbic acid metabolism in the ascorbate-deficient Arabidopsis mutant vtc1. *Plant Physiology*, 115(3), 1277–1285. https://doi.org/10.1104/pp.115.3.1277

Conklin, P. L., Saracco, S. A., Norris, S. R., & Last, R. L. (2000). Identification of ascorbic acid-deficient Arabidopsis thaliana mutants. *Genetics, 154*(2), 847–856. https://doi.org/10.1093/genetics/154.2.847

Conklin, P. L., Williams, E. H., & Last, R. L. (1996). Environmental stress sensitivity of an ascorbic acid-deficient Arabidopsis mutant. *Proceedings of the National Academy of Sciences of the United States of America*, 93(18), 9970–9974. https://doi.org/10.1073/pnas.93.18.9970

Cooper, O. R., Parrish, D. D., Stohl, A., Trainer, M., Nédélec, P., Thouret, V., Cammas, J. P., Oltmans, S. J., Johnson, B. J., Tarasick, D., Leblanc, T., McDermid, I. S., Jaffe, D., Gao,

R., Stith, J., Ryerson, T., Aikin, K., Campos, T., Weinheimer, A., & Avery, M. A. (2010). Increasing springtime ozone mixing ratios in the free troposphere over western North America. *Nature*, 463, 344–348. https://doi.org/10.1038/nature08708

Dachler, M. (2023). *Welternährung: Status quo und Ausblick zur globalen Ernährungslage*. Springer. https://doi.org/10.1007/978-3-662-66904-4

Das, S., Pal, D., & Sarkar, A. (2021). Particulate matter pollution and global agricultural productivity. In V. Kumar Singh, R. Singh, & E. Lichtfouse (Eds.), *Sustainable Agriculture Reviews 50* (Vol. 50, pp. 79–107). Springer International Publishing. https://doi.org/10.1007/978-3-030-63249-6_4

David, L. M., Ravishankara, A. R., Brewer, J. F., Sauvage, B., Thouret, V., Venkataramani, S., & Sinha, V. (2019). Tropospheric ozone over the Indian subcontinent from 2000 to 2015: Data set and simulation using GEOS-Chem chemical transport model. *Atmospheric Environment*, 219, 117039. https://doi.org/10.1016/j.atmosenv.2019.117039

Debaje, S. B. (2014). Estimated crop yield losses due to surface ozone exposure and economic damage in India. *Environmental Science and Pollution Research, 21*(12), 7329–7338. https://doi.org/10.1007/s11356-014-2657-6

Degl'Innocenti, E., Guidi, L., Nali, C., & Soldatini, G. F. (2002). Characterisation of the photosynthetic response of tobacco leaves to ozone: CO_2 assimilation and chlorophyll fluorescence. *Journal of Plant Physiology, 159*(8), 845–853. https://doi.org/10.1078/0176-1617-00519

Deng, S., Gu, Z., Yang, N., Li, L., Yue, X., Que, Y., Sun, G., Wang, Z., & Wang, J. (2016). Identification and characterization of the peroxin 1 gene *MoPEX1* required for infection-related morphogenesis and pathogenicity in *Magnaporthe oryzae*. *Scientific Reports*, 6, 36292. https://doi.org/10.1038/srep36292

Devi, S. J. S. R., Singh, K., Umakanth, B., Vishalakshi, B., Sudhakara Rao, K. V., Suneel, B., Sharma, S. K., Kadambari, G. K. M., Prasad, M. S., Senguttvel, P., Syamaladevi, D. P., & Madhav, M. S. (2020). Identification and characterization of a large effect QTL from *Oryza glumaepatula* revealed *Pi68*(t) as putative candidate gene for rice blast resistance. *Rice*, 13, 17. https://doi.org/10.1186/s12284-020-00378-4

Dewan, S., Bamola, S., & Lakhani, A. (2024). Addressing ozone pollution to promote United Nations sustainable development goal 2: Ensuring global food security. *Chemosphere, 347*, 140693. https://doi.org/10.1016/j.chemosphere.2023.140693

Dhawan, G., Kumar, A., Dwivedi, P., Gopala Krishnan, S., Pal, M., Vinod, K. K., Nagarajan, M., Bhowmick, P. K., Bollinedi, H., Ellur, R. K., Ravikiran, K. T., Kumar, P., & Singh, A. K. (2021). Introgression of *qDTY1*.1 governing reproductive stage drought tolerance into an elite Basmati rice variety "Pusa Basmati 1" through marker assisted backcross breeding. *Agronomy, 11*(2), 202. https://doi.org/10.3390/agronomy11020202

Dipta, B., Sood, S., Mangal, V., Bhardwaj, V., Thakur, A. K., Kumar, V., & Singh, B. (2024). KASP: A high-throughput genotyping system and its applications in major crop plants for biotic and abiotic stress tolerance. *Molecular Biology Reports*, 51, 508. https://doi.org/10.1007/s11033-024-09455-z

Dong, D., & Wang, J. (2023). Air pollution as a substantial threat to the improvement of agricultural total factor productivity: Global evidence. *Environment International*, 173, 107842. https://doi.org/10.1016/j.envint.2023.107842

Du, B., Kreuzwieser, J., Winkler, J. B., Ghirardo, A., Schnitzler, J.-P., Ache, P., Alfarraj, S., Hedrich, R., White, P., & Rennenberg, H. (2018). Physiological responses of date palm (Phoenix dactylifera) seedlings to acute ozone exposure at high temperature. *Environmental Pollution, 242*, 905–913. https://doi.org/10.1016/j.envpol.2018.07.059

Du, C., Pei, J., & Feng, Z. (2024). Unraveling the complex interactions between ozone pollution and agricultural productivity in China's main winter wheat region using an interpretable machine learning framework. *Science of The Total Environment*, 954, 176293. https://doi.org/10.1016/j.scitotenv.2024.176293

Du, Y., Xi, Y., Cui, T., Anten, N. P. R., Weiner, J., Li, X., Turner, N. A., Zhao, Y., & Li, F. (2020). Yield components, reproductive allometry and the tradeoff between grain yield and yield stability in dryland spring wheat. *Field Crops Research, 257*, 107930. https://doi.org/10.1016/j.fcr.2020.107930

Ebitani, T., Hayashi, N., Omoteno, M., Ozaki, H., Yano, M., Morikawa, M., & Fukuta, Y. (2011). Characterization of *Pi13*, a blast resistance gene that maps to chromosome 6 in *indica* rice (*Oryza sativa* L. variety, Kasalath). *Breeding Science, 61*(3), 251–259. https://doi.org/10.1270/jsbbs.61.251

Emberson, L. D., Pleijel, H., Ainsworth, E., Van den Berg, M., Ren, W., Osborne, S., Mills, G., Pandey, D., Dentener, F., Buker, P., Ewert, F., Koeble, R., & Van Dingenen, R. (2018). Ozone effects on crops and consideration in crop models. *European Journal of Agronomy, 100*, 19–34. https://doi.org/10.1016/j.eja.2018.06.002

Ernst, D., Schraudner, M., Langebartels, C., & Sandermann, H., Jr. (1992). Ozone-induced changes of mRNA levels of β-1,3-glucanase, chitinase and 'pathogenesis-related' protein 1b in tobacco plants. *Plant Molecular Biology, 20*(4), 673–682. https://doi.org/10.1007/BF00046452

Ertiro, B. T., Ogugo, V., Worku, M., Das, B., Olsen, M., Labuschagne, M., & Semagn, K. (2015). Comparison of Kompetitive Allele Specific PCR (KASP) and genotyping by sequencing (GBS) for quality control analysis in maize. *BMC Genomics, 16*, 908. https://doi.org/10.1186/s12864-015-2180-2

Fageria, N. K. (2007). Yield physiology of rice. *Journal of Plant Nutrition*, 30(6), 843–879. https://doi.org/10.1080/15226510701374831

Fann, N., Baker, K. R., Chan, E. A. W., Eyth, A., Macpherson, A., Miller, E., & Snyder, J. (2018). Assessing human health $PM_{2.5}$ and ozone impacts from U.S. oil and natural gas sector emissions in 2025. *Environmental Science & Technology*, 52(15), 8095–8103. https://doi.org/10.1021/acs.est.8b02050

Fares, S., Vargas, R., Detto, M., Goldstein, A. H., Karlik, J., Paoletti, E., & Vitale, M. (2013). Tropospheric ozone reduces carbon assimilation in trees: Estimates from analysis of continuous flux measurements. *Global Change Biology, 19*(8), 2427–2443. https://doi.org/10.1111/gcb.12222

Feng, Y., Alam, M. S., Yan, F., & Frei, M. (2024). Alteration of carbon and nitrogen allocation in winter wheat under elevated ozone. *Plant Science*, 338, 111924. https://doi.org/10.1016/j.plantsci.2023.111924

Feng, Y., Nguyen, T. H., Alam, M. S., Emberson, L., Gaiser, T., Ewert, F., & Frei, M. (2022). Identifying and modelling key physiological traits that confer tolerance or sensitivity to ozone in winter wheat. *Environmental Pollution, 304*, 119251. https://doi.org/10.1016/j.envpol.2022.119251

Feng, Z., & Kobayashi, K. (2009). Assessing the impacts of current and future concentrations of surface ozone on crop yield with meta-analysis. *Atmospheric Environment, 43*(8), 1510–1519. https://doi.org/10.1016/j.atmosenv.2008.11.033

Feng, Z., Agathokleous, E., Yue, X., Oksanen, E., Paoletti, E., Sase, H., Gandin, A., Koike, T., Calatayud, V., Yuan, X., Liu, X., De Marco, A., Jolivet, Y., Kontunen-Soppela, S., Hoshika, Y., Saji, H., Li, P., Li, Z., Watanabe, M., & Kobayashi, K. (2021). Emerging challenges of ozone impacts on Asian plants: Actions are needed to protect ecosystem health. *Ecosystem Health and Sustainability, 7*(1), Article 1911602. https://doi.org/10.1080/20964129.2021.1911602

Feng, Z., Hu, E., Wang, X., Jiang, L., & Liu, X. (2015). Ground-level O_3 pollution and its impacts on food crops in China: A review. *Environmental Pollution*, 199, 42–48. https://doi.org/10.1016/j.envpol.2015.01.016

Feng, Z., Kobayashi, K., & Ainsworth, E. A. (2008). Impact of elevated ozone concentration on growth, physiology, and yield of wheat (*Triticum aestivum* L.): A meta-analysis. *Global Change Biology, 14*(11), 2696–2708. https://doi.org/10.1111/j.1365-2486.2008.01673.x

Feng, Z., Pang, J., Nouchi, I., Kobayashi, K., Yamakawa, T., & Zhu, J. (2010a). Apoplastic ascorbate contributes to the differential ozone sensitivity in two varieties of winter wheat under fully open-air field conditions. *Environmental Pollution*, 158(12), 3539–3545. https://doi.org/10.1016/j.envpol.2010.08.019

Feng, Z., Wang, S., Szantoi, Z., Chen, S., & Wang, X. (2010b). Protection of plants from ambient ozone by applications of ethylenediurea (EDU): A meta-analytic review. *Environmental Pollution*, 158(10), 3236–3242. https://doi.org/10.1016/j.envpol.2010.07.009

Feng, Z., Xu, Y., Kobayashi, K., Dai, L., Zhang, T., Agathokleous, E., Calatayud, V., Paoletti, E., Mukherjee, A., Agrawal, M., Park, R. J., Oak, Y. J., & Yue, X. (2022). Ozone pollution threatens the production of major staple crops in East Asia. *Nature Food, 3*(1), 47–56. https://doi.org/10.1038/s43016-021-00422-6

Fernandez, J., & Orth, K. (2018). Rise of a cereal killer: The biology of *Magnaporthe oryzae* biotrophic growth. *Trends in Microbiology, 26*(7), 582–597. https://doi.org/10.1016/j.tim.2017.12.007

Fiscus, E. L., Booker, F. L., & Burkey, K. O. (2005). Crop responses to ozone: Uptake, modes of action, carbon assimilation and partitioning. *Plant, Cell & Environment*, 28(8), 997–1011. https://doi.org/10.1111/j.1365-3040.2005.01349.x

Fowler, D., Amann, M., Anderson, R., Ashmore, M., Cox, P., Depledge, M., Derwent, D., Grennfelt, P., Hewitt, N., Hov, O., Jenkin, M., Kelly, F., Liss, P. S., Pilling, M., Pyle, J., Slingo, J., & Stevenson, D. (2008). *Ground-level ozone in the 21st century: Future trends, impacts and policy implications* (Policy Document 15/08). The Royal Society.

Frei, M. (2015). Breeding of ozone resistant rice: Relevance, approaches and challenges. *Environmental Pollution, 197*, 144–155. https://doi.org/10.1016/j.envpol.2014.12.011

Frei, M., Ashrafuzzaman, M., Piepho, H.-P., Herzog, E., Begum, S. N., & Islam, M. M. (2024). Evidence for tropospheric ozone effects on rice production in Bangladesh. *Science of the Total Environment, 909*, 168560. https://doi.org/10.1016/j.scitotenv.2023.168560

Frei, M., Kohno, Y., Tietze, S., Jekle, M., Hussein, M. A., Becker, T., & Becker, K. (2012). The response of rice grain quality to ozone exposure during growth depends on ozone level and genotype. *Environmental Pollution*, 163, 199–206. https://doi.org/10.1016/j.envpol.2011.12.039

Frei, M., Kohno, Y., Wissuwa, M., Makkar, H. P. S., & Becker, K. (2011). Negative effects of tropospheric ozone on the feed value of rice straw are mitigated by an ozone tolerance QTL. *Global Change Biology, 17*(7), 2319–2329. https://doi.org/10.1111/j.1365-2486.2010.02379.x

Frei, M., Tanaka, J. P., & Wissuwa, M. (2008). Genotypic variation in tolerance to elevated ozone in rice: Dissection of distinct genetic factors linked to tolerance mechanisms. *Journal of Experimental Botany, 59*(13), 3741–3752. https://doi.org/10.1093/jxb/ern222

Frei, M., Tanaka, J. P., Chen, C. P., & Wissuwa, M. (2010). Mechanisms of ozone tolerance in rice: Characterization of two QTLs affecting leaf bronzing by gene expression profiling and biochemical analyses. *Journal of Experimental Botany, 61*(5), 1405–1417. https://doi.org/10.1093/jxb/erq007

Gaihre, Y. K., Singh, U., Islam, S. M. M., Huda, A., Islam, M. R., Satter, M. A., Sanabria, J., Islam, M. R., & Shah, A. L. (2015). Impacts of urea deep placement on nitrous oxide and nitric oxide emissions from rice fields in Bangladesh. *Geoderma, 259-260*, 370–379. https://doi.org/10.1016/j.geoderma.2015.06.001

Gamon, J. A., Peñuelas, J., & Field, C. B. (1992). A narrow-waveband spectral index that tracks diurnal changes in photosynthetic efficiency. *Remote Sensing of Environment, 41*(1), 35–44. https://doi.org/10.1016/0034-4257(92)90059-S

Gao, M., Gao, J., Zhu, B., Kumar, R., Lu, X., Song, S., Zhang, Y., Jia, B., Wang, P., Beig, G., Hu, J., Ying, Q., Zhang, H., Sherman, P., & McElroy, M. B. (2020). Ozone pollution over China and India: Seasonality and sources. *Atmospheric Chemistry and Physics*, 20(7), 4399–4414. https://doi.org/10.5194/acp-20-4399-2020

Gaudel, A., Cooper, O. R., Ancellet, G., Barret, B., Boynard, A., Burrows, J. P., Clerbaux, C., Coheur, P.-F., Cuesta, J., Cuevas, E., Doniki, S., Dufour, G., Ebojie, F., Foret, G., Garcia, O., Granados-Muñoz, M. J., Hannigan, J. W., Hase, F., Hassler, B., Huang, G., Hurtmans, D., Jaffe, D., Jones, N., Kalabokas, P., Kerridge, B., Kulawik, S., Latter, B., Leblanc, T., Le Flochmoën, E., Lin, W., Liu, J., Liu, X., Mahieu, E., McClure-Begley, A., Neu, J. L., Osman, M., Palm, M., Petetin, H., Petropavlovskikh, I., Querel, R., Rahpoe, N., Rozanov, A., Schultz, M. G., Schwab, J., Siddans, R., Smale, D., Steinbacher, M., Tanimoto, H., Tarasick, D. W., Thouret, V., Thompson, A. M., Trickl, T., Weatherhead, E., Wespes, C., Worden, H. M., Vigouroux, C., Xu, X., Zeng, G., & Ziemke, J. (2018). Tropospheric Ozone Assessment Report: Present-day distribution and trends of tropospheric ozone relevant to climate and global atmospheric chemistry model evaluation. *Elementa: Science of the Anthropocene*, 6(1), 39. https://doi.org/10.1525/elementa.291

Geetha, S., Vasuki, A., Selvam, P. J., Saraswathi, R., Krishnamurthy, S. L., Palanichamy, Manikandan, Dhasarathan, M., Thamodharan, G., & Baskar, M. (2017). Development of sodicity tolerant rice varieties through marker assisted backcross breeding. *Electronic Journal of Plant Breeding*, 8(4), 1013–1021. https://doi.org/10.5958/0975-928X.2017.00151.X

Gielen, B., Löw, M., Deckmyn, G., Metzger, U., Franck, F., Heerdt, C., Matyssek, R., Valcke, R., & Ceulemans, R. (2007). Chronic ozone exposure affects leaf senescence of adult beech trees: a chlorophyll fluorescence approach. *Journal of Experimental Botany, 58*(4), 785–795. https://doi.org/10.1093/jxb/erl222

Gitelson, A. A., Merzlyak, M. N., & Chivkunova, O. B. (2001). Optical properties and nondestructive estimation of anthocyanin content in plant leaves. *Photochemistry*

and Photobiology, 74(1), 38–45. https://doi.org/10.1562/0031-8655(2001)0740038OPANEO2.0.CO2

Grewal, S., Hubbart-Edwards, S., Yang, C., Devi, U., Baker, L., Heath, J., Ashling, S., Scholefield, D., Howells, C., Yarde, J., Isaac, P., King, I. P., & King, J. (2020). Rapid identification of homozygosity and site of wild relative introgressions in wheat through chromosome-specific KASP genotyping assays. *Plant Biotechnology Journal, 18*(3), 743–755. https://doi.org/10.1111/pbi.13241

Guo, C., Wang, X., Wang, Q., Zhao, Z., Xie, B., Xu, L., & Zhang, R. (2024). Plant defense mechanisms against ozone stress: Insights from secondary metabolism. *Environmental and Experimental Botany*, 217, 105553. https://doi.org/10.1016/j.envexpbot.2023.105553

Gupta, S. K., Sharma, M., Majumder, B., Maurya, V. K., Lohani, M., Deeba, F., & Pandey, V. (2018). Impact of ethylenediurea (EDU) on growth, yield and proteome of two winter wheat varieties under high ambient ozone phytotoxicity. *Chemosphere, 196*, 161–173. https://doi.org/10.1016/j.chemosphere.2017.12.150

Höller, S., Meyer, A., & Frei, M. (2014). Zinc deficiency differentially affects redox homeostasis of rice genotypes contrasting in ascorbate level. *Journal of Plant Physiology, 171*(18), 1748–1756. https://doi.org/10.1016/j.jplph.2014.08.012

Hansen, E. M. Ø., Hauggaard-Nielsen, H., Launay, M., Rose, P., & Mikkelsen, T. (2019). The impact of ozone exposure, temperature and CO_2 on the growth and yield of three spring wheat varieties. *Environmental and Experimental Botany, 168*, 103868. https://doi.org/10.1016/j.envexpbot.2019.103868

Harborne, J. B. (1993). Higher plant–lower plant interactions: Phytoalexins and phytotoxins. In *Introduction to ecological biochemistry* (4th ed., pp. 264–297). Academic Press. https://doi.org/10.1016/B978-0-08-091858-7.50014-0

Hasan, N., Choudhary, S., Naaz, N., Sharma, N., & Laskar, R. A. (2021). Recent advancements in molecular marker-assisted selection and applications in plant breeding programmes. *Journal of Genetic Engineering and Biotechnology, 19*(1), Article 128. https://doi.org/10.1186/s43141-021-00231-1

Heath, M. C. (2000). Hypersensitive response-related death. *Plant Molecular Biology, 44*, 321–334. https://doi.org/10.1023/A:1026592509060

Hill, C. B., Wong, D., Tibbits, J., Forrest, K., Hayden, M., Zhang, X.-Q., Westcott, S., Angessa, T. T., & Li, C. (2019). Targeted enrichment by solution-based hybrid capture to identify genetic sequence variants in barley. *Scientific Data, 6*, 12. https://doi.org/10.1038/s41597-019-0011-z

Hodges, D. M., DeLong, J. M., Forney, C. F., & Prange, R. K. (1999). Improving the thiobarbituric acid-reactive-substances assay for estimating lipid peroxidation in plant tissues containing anthocyanin and other interfering compounds. *Planta, 207*, 604–611. https://doi.org/10.1007/s004250050524

Hoshika, Y., Watanabe, M., Carrari, E., Paoletti, E., & Koike, T. (2018). Ozone-induced stomatal sluggishness changes stomatal parameters of Jarvis-type model in white birch and deciduous oak. *Plant Biology*, 20(1), 20–28. https://doi.org/10.1111/plb.12632

Hospital, F. (2009). Challenges for effective marker-assisted selection in plants. *Genetica, 136*(2), 303–310. https://doi.org/10.1007/s10709-008-9307-1

Hossen, M. S., Mano, M., Miyata, A., Baten, M. A., & Hiyama, T. (2012). Surface energy partitioning and evapotranspiration over a double-cropping paddy field in Bangladesh. *Hydrological Processes*, 26(9), 1311–1320. https://doi.org/10.1002/hyp.8232

Huang, H., Ullah, F., Zhou, D.-X., Yi, M., & Zhao, Y. (2019). Mechanisms of ROS regulation of plant development and stress responses. *Frontiers in Plant Science, 10*, 800. https://doi.org/10.3389/fpls.2019.00800

Huang, X., Kurata, N., Wei, X., Wang, Z.-X., Wang, A., Zhao, Q., Zhao, Y., Liu, K., Lu, H., Li, W., Guo, Y., Lu, Y., Zhou, C., Fan, D., Weng, Q., Zhu, C., Huang, T., Zhang, L., Wang, Y., Feng, L., Furuumi, H., Kubo, T., Miyabayashi, T., Yuan, X., Xu, Q., Dong, G., Zhan, Q., Li, C., Fujiyama, A., Toyoda, A., Lu, T., Feng, Q., Qian, Q., Li, J., & Han, B. (2012). A map of rice genome variation reveals the origin of cultivated rice. *Nature*, 490, 497–501. https://doi.org/10.1038/nature1153

Hur, J. S., Kim, J. A., & Koh Y. J. (2002). Inhibitory effects of atmospheric ozone on *Magnaporthe grisea* conidia. *The Plant Pathology Journal, 18*(1), 43-49. https://doi.org/10.5423/PPJ.2002.18.1.043

Huyen, L. T. N., Cuc, L. M., Ismail, A. M., & Ham, L. H. (2012). Introgression the salinity tolerance QTLs *Saltol* into AS996, the elite rice variety of Vietnam. *American Journal of Plant Sciences, 3*(7), 981–987. https://doi.org/10.4236/ajps.2012.37116

Huysmans, M., Lema Asqui, S., Coll, N. S., & Nowack, M. K. (2017). Dying two deaths—programmed cell death regulation in development and disease. *Current Opinion in Plant Biology*, 35, 37–44. https://doi.org/10.1016/j.pbi.2016.11.005

Haagen-Smit, A. J. (1952). Chemistry and physiology of Los Angeles smog. *Industrial & Engineering Chemistry, 44*(6), 1342–1346. https://doi.org/10.1021/ie50510a045

Haagen-Smit, A. J., & Fox, M. M. (1954). Photochemical ozone formation with hydrocarbons and automobile exhaust. *Air Repair*, 4(3), 105–136. https://doi.org/10.1080/00966665.1954.10467649

Hayasaka, H., Takamatsu, M., Kuboki, Y., Yano, M., Matsunaga, K., & Sasaki, T. (1995). Mapping genes conferring rice blast resistance in rice variety Kasalath using RFLP markers. II. Linkage analysis of the resistance gene on chromosome 6. *Breeding Science, 45*(Suppl. 2), 168.

He, J., Zhao, X., Laroche, A., Lu, Z.-X., Liu, H., & Li, Z. (2014). Genotyping-by-sequencing (GBS), an ultimate marker-assisted selection (MAS) tool to accelerate plant breeding. *Frontiers in Plant Science, 5*, 484. https://doi.org/10.3389/fpls.2014.00484

Hensawang, S., Wangwongchai, A., Humphries, U., & Bunsri, T. (2017). *Simulation of severity of rice blast disease in Prachin Buri using plant disease epidemiological model: Simulation of rice blast disease*. In *The 22nd Annual Meeting in Mathematics (AMM 2017)*. Department of Mathematics, Faculty of Science, Chiang Mai University, Chiang Mai, Thailand.

Hospital, F., & Charcosset, A. (1997). Marker-assisted introgression of quantitative trait loci. *Genetics, 147*(3), 1469–1485. https://doi.org/10.1093/genetics/147.3.1469

Huang, Y. Z., Sui, L. H., Wang, W., Geng, C. M., & Yin, B. H. (2012). Visible injury and nitrogen metabolism of rice leaves under ozone stress, and effect on sugar and protein contents in grain. *Atmospheric Environment, 60*, 433–440. https://doi.org/10.1016/j.atmosenv.2012.09.002

Islam, M. S., Tusher, T. R., Roy, S., & Rahman, M. (2021). Impacts of nationwide lockdown due to COVID-19 outbreak on air quality in Bangladesh: A spatiotemporal analysis.

Air Quality, Atmosphere & Health, 14, 351–363. https://doi.org/10.1007/s11869-020-00940-5

Iftekharuddaula, K. M., Newaz, M. A., Salam, M. A., Ahmed, H. U., Mahbub, M. A. A., Septiningsih, E. M., Collard, B. C. Y., Sanchez, D. L., Pamplona, A. M., & Mackill, D. J. (2011). Rapid and high-precision marker assisted backcrossing to introgress the *SUB1* QTL into BR11, the rainfed lowland rice mega variety of Bangladesh. *Euphytica, 178*, 83–97. https://doi.org/10.1007/s10681-010-0272-2

Intergovernmental Panel on Climate Change. (2014). *Climate change 2014: Mitigation of climate change. Contribution of Working Group III to the Fifth Assessment Report of the Intergovernmental Panel on Climate Change* (O. Edenhofer, R. Pichs-Madruga, Y. Sokona, E. Farahani, S. Kadner, K. Seyboth, A. Adler, I. Baum, S. Brunner, P. Eickemeier, B. Kriemann, J. Savolainen, S. Schlömer, C. von Stechow, T. Zwickel, & J.C. Minx, Eds.). Cambridge University Press. https://www.ipcc.ch/site/assets/uploads/2018/02/ipcc_wg3_ar5_full.pdf

Jain, S. L., Arya, B. C., Kumar, A., Ghude, S. D., & Kulkarni, P. S. (2005). Observational study of surface ozone at New Delhi, India. *International Journal of Remote Sensing, 26*(16), 3515–3524. https://doi.org/10.1080/01431160500076616

Jiang, P., Fan, X., Zhang, G., Wu, L., He, Y., Li, C., & Zhang, X. (2023). Cost-effective duplex Kompetitive Allele Specific PCR markers for homologous genes facilitating wheat breeding. *BMC Plant Biology, 23*(1), Article 119. https://doi.org/10.1186/s12870-023-04116-y

Jing, L., Dombinov, V., Shen, S., Wu, Y., Yang, L., Wang, Y., & Frei, M. (2016). Physiological and genotype-specific factors associated with grain quality changes in rice exposed to high ozone. *Environmental Pollution*, 210, 397–408. https://doi.org/10.1016/j.envpol.2016.01.023

Jo, S.-H., Kim, J.-H., Moon, J.-H., Yang, S.-Y., Baek, J.-K., Song, Y.-S., Shon, J.-Y., Chung, N.-J., & Lee, H.-S. (2024). Effects of mineral fertilization (NPK) on combined high temperature and ozone damage in rice. *BMC Plant Biology, 24*(1), 974. https://doi.org/10.1186/s12870-024-05695-0

Jagtap, A. B., Vikal, Y., & Johal, G. S. (2020). Genome-wide development and validation of cost-effective KASP marker assays for genetic dissection of heat stress tolerance in

maize. *International Journal of Molecular Sciences, 21*(19), 7386. https://doi.org/10.3390/ijms21197386

Kihoro, J., Bosco, N. J., Murage, H., Ateka, E., & Makihara, D. (2013). Investigating the impact of rice blast disease on the livelihood of the local farmers in greater Mwea region of Kenya. *SpringerPlus, 2*, 308. https://doi.org/10.1186/2193-1801-2-308

Kangasjärvi, J., Jaspers, P., & Kollist, H. (2005). Signalling and cell death in ozone-exposed plants. *Plant, Cell & Environment*, 28(8), 1021–1036. https://doi.org/10.1111/j.1365-3040.2005.01325.x

Keen, N. T., & Taylor, O. C. (1975). Ozone injury in soybeans: Isoflavonoid accumulation is related to necrosis. *Plant Physiology*, 55(4), 731–733. https://doi.org/10.1104/pp.55.4.731

Kennedy, G., & Burlingame, B. (2003). Analysis of food composition data on rice from a plant genetic resources perspective. *Food Chemistry, 80*(4), 589–596. https://doi.org/10.1016/S0308-8146(02)00507-1

Kerner, R., Winkler, J. B., Dupuy, J.-W., Jürgensen, M., Lindermayr, C., Ernst, D., & Müller-Starck, G. (2011). Changes in the proteome of juvenile European beech following three years exposure to free-air elevated ozone. *iForest - Biogeosciences and Forestry, 4*(2), 69–76. https://doi.org/10.3832/ifor0570-004

Khan, M. R., & Khan, M. W. (1999). Effects of intermittent ozone exposures on powdery mildew of cucumber. *Environmental and Experimental Botany, 42*(3), 163–171. https://doi.org/10.1016/S0098-8472(99)00029-5

Kim, M.-S., Yang, J.-Y., Yu, J.-K., Lee, Y., Park, Y.-J., Kang, K.-K., & Cho, Y.-G. (2021). Breeding of high cooking and eating quality in rice by marker-assisted backcrossing (MABc) using KASP markers. *Plants, 10*(4), 804. https://doi.org/10.3390/plants10040804

Kobayashi, A., Hori, K., Yamamoto, T., & Yano, M. (2018). Koshihikari: A premium short-grain rice cultivar—its expansion and breeding in Japan. *Rice, 11*, 15. https://doi.org/10.1186/s12284-018-0207-4

Kovach, M. J., Sweeney, M. T., & McCouch, S. R. (2007). New insights into the history of rice domestication. *Trends in Genetics, 23*(11), 578–587. https://doi.org/10.1016/j.tig.2007.08.012

Kang, J., Wang, J., Heal, M. R., Goulding, K., de Vries, W., Zhao, Y., Feng, S., Zhang, X., Gu, B., Niu, X., Zhang, H., Liu, X., Cui, Z., Zhang, F., & Xu, W. (2023). Ammonia mitigation

campaign with smallholder farmers improves air quality while ensuring high cereal production. *Nature Food, 4*, 751–761. https://doi.org/10.1038/s43016-023-00833-7

Kittipornkul, P., Treesubsuntorn, C., & Thiravetyan, P. (2020). Effect of exogenous catechin and salicylic acid on rice productivity under ozone stress: The role of chlorophyll contents, lipid peroxidation, and antioxidant enzymes. *Environmental Science and Pollution Research, 27*, 25774–25784. https://doi.org/10.1007/s11356-020-08962-3

Liu, Y., Pan, T., Tang, Y., Zhuang, Y., Liu, Z., Li, P., Li, H., Huang, W., Tu, S., Ren, G., Wang, T., & Wang, S. (2020). Proteomic analysis of rice subjected to low light stress and overexpression of *OsGAPB* increases the stress tolerance. *Rice, 13*, 30. https://doi.org/10.1186/s12284-020-00390-8

Liu, Z., Zhu, C., Jiang, Y., Tian, Y., Yu, J., An, H., Tang, W., Sun, J., Tang, J., Chen, G., Zhai, H., Wang, C., & Wan, J. (2016). Association mapping and genetic dissection of nitrogen use efficiency-related traits in rice (*Oryza sativa* L.). *Functional & Integrative Genomics, 16*, 323–333. https://doi.org/10.1007/s10142-016-0486-z

Lal, D. M., Ghude, S. D., Patil, S. D., Kulkarni, S. H., Jena, C., Tiwari, S., & Srivastava, M. (2012). Tropospheric ozone and aerosol long-term trends over the Indo-Gangetic Plain (IGP), India. *Atmospheric Research, 116*, 82–92. https://doi.org/10.1016/j.atmosres.2012.02.014

Larkin, D. L., Lozada, D. N., & Mason, R. E. (2019). Genomic selection—Considerations for successful implementation in wheat breeding programs. *Agronomy, 9*(9), 479. https://doi.org/10.3390/agronomy9090479

Li, P., Feng, Z., Catalayud, V., Yuan, X., Xu, Y., & Paoletti, E. (2017). A meta-analysis on growth, physiological, and biochemical responses of woody species to ground-level ozone highlights the role of plant functional types. *Plant, Cell & Environment, 40*(10), 2369–2380. https://doi.org/10.1111/pce.13043

Lichtenthaler, H. K., Lang, M., Sowinska, M., Heisel, F., & Miehé, J. A. (1996). Detection of vegetation stress via a new high resolution fluorescence imaging system. *Journal of Plant Physiology, 148*(5), 599–612. https://doi.org/10.1016/S0176-1617(96)80081-2

Liu, C., Liu, Y., Guo, K., Fan, D., Li, G., Zheng, Y., Yu, L., & Yang, R. (2011). Effect of drought on pigments, osmotic adjustment, and antioxidant enzymes in six woody plant species in karst habitats of southwestern China. *Environmental and Experimental Botany, 71*(2), 174–183. https://doi.org/10.1016/j.envexpbot.2010.11.012

López López, P., Wanders, N., Schellekens, J., Renzullo, L. J., Sutanudjaja, E. H., & Bierkens, M. F. P. (2016). Improved large-scale hydrological modelling through the assimilation of streamflow and downscaled satellite soil moisture observations. *Hydrology and Earth System Sciences*, 20(7), 3059–3076. https://doi.org/10.5194/hess-20-3059-2016

Ladha, J. K., Tirol, A. C., Daroy, M. L. G., Caldo, G., Ventura, W., & Watanabe, I. (1986). Plant-associated N_2 fixation (C_2H_2-reduction) by five rice varieties, and relationship with plant growth characters as affected by straw incorporation. *Soil Science and Plant Nutrition, 32*(1), 91–106. https://doi.org/10.1080/00380768.1986.10557484

Li, B., Liao, H., Li, K., Wang, Y., Zhang, L., Guo, Y., Liu, L., Li, J., Jin, J., Yang, Y., Gong, C., Wang, T., Shen, W., Wang, P., Dang, R., Liao, K., Zhu, Q., & Jacob, D. J. (2024). Unlocking nitrogen management potential via large-scale farming for air quality and substantial co-benefits. *National Science Review, 11*(10), Article nwae324. https://doi.org/10.1093/nsr/nwae324

Li, G., Jain, R., Chern, M., Pham, N. T., Martin, J. A., Wei, T., Schackwitz, W. S., Lipzen, A. M., Duong, P. Q., Jones, K. C., Jiang, L., Ruan, D., Bauer, D., Peng, Y., Barry, K. W., Schmutz, J., & Ronald, P. C. (2017). The sequences of 1,504 mutants in the model rice variety Kitaake facilitate rapid functional genomic studies. *The Plant Cell, 29*(6), 1218–1231. https://doi.org/10.1105/tpc.17.00154

Li, J., Zhang, F., Qian, X., Zhu, Y., & Shen, G. (2015). Quantification of rice canopy nitrogen balance index with digital imagery from unmanned aerial vehicle. *Remote Sensing Letters, 6*(3), 183–189. https://doi.org/10.1080/2150704X.2015.1021934

Li, L., Wang, J., Zhang, Z., Wang, Y., Liu, M., Jiang, H., Chai, R., Mao, X., Qiu, H., Liu, F., & Sun, G. (2014). *MoPex19*, which is essential for maintenance of peroxisomal structure and Woronin bodies, is required for metabolism and development in the rice blast fungus. *PLOS ONE, 9*(1), e85252. https://doi.org/10.1371/journal.pone.0085252

Li, S., Leakey, A. D. B., Moller, C. A., Montes, C. M., Sacks, E. J., Lee, D., & Ainsworth, E. A. (2023). Similar photosynthetic but different yield responses of C_3 and C_4 crops to elevated O_3. *Proceedings of the National Academy of Sciences, 120*(46), e2313591120. https://doi.org/10.1073/pnas.2313591120

Lichtenthaler, H. K., & Miehé, J. A. (1997). Fluorescence imaging as a diagnostic tool for plant stress. *Trends in Plant Science, 2*(8), 316–320. https://doi.org/10.1016/S1360-1385(97)89954-2

Lichtenthaler, H. K., Langsdorf, G., Lenk, S., & Buschmann, C. (2005). Chlorophyll fluorescence imaging of photosynthetic activity with the flash-lamp fluorescence imaging system. *Photosynthetica, 43*(3), 355–369. https://doi.org/10.1007/s11099-005-0060-8

Londo, J. P., Chiang, Y.-C., Hung, K.-H., Chiang, T.-Y., & Schaal, B. A. (2006). Phylogeography of Asian wild rice, *Oryza rufipogon*, reveals multiple independent domestications of cultivated rice, *Oryza sativa*. *Proceedings of the National Academy of Sciences, 103*(25), 9578–9583. https://doi.org/10.1073/pnas.0603152103

Luwe, M. W. F., Takahama, U., & Heber, U. (1993). Role of ascorbate in detoxifying ozone in the apoplast of spinach (*Spinacia oleracea* L.) leaves. *Plant Physiology, 101*(3), 969–976. https://doi.org/10.1104/pp.101.3.969

Mikkelsen, B. L., Olsen, C. E., & Lyngkjær, M. F. (2015). Accumulation of secondary metabolites in healthy and diseased barley, grown under future climate levels of CO_2, ozone and temperature. *Phytochemistry, 118*, 162–173. https://doi.org/10.1016/j.phytochem.2015.07.007

Mir, S. A., Bosco, S. J. D., Shah, M. A., Mir, M. M., & Sunooj, K. V. (2016). Variety difference in quality characteristics, antioxidant properties and mineral composition of brown rice. *Journal of Food Measurement and Characterization, 10*, 177–184. https://doi.org/10.1007/s11694-015-9291-y

Mashaheet, A. M., Burkey, K. O., Saitanis, C. J., Abdelrhim, A. S., Rafiullah, & Marshall, D. S. (2020). Differential ozone responses identified among key rust-susceptible wheat genotypes. *Agronomy, 10*(12), 1853. https://doi.org/10.3390/agronomy10121853

Mehta, S., Singh, B., Dhakate, P., Rahman, M., & Islam, M. A. (2019). Rice, marker-assisted breeding, and disease resistance. In S. H. Wani (Ed.), *Disease resistance in crop plants* (pp. 83–111). Springer. https://doi.org/10.1007/978-3-030-20728-1_5

Meroni, M., Rossini, M., Guanter, L., Alonso, L., Rascher, U., Colombo, R., & Moreno, J. (2009). Remote sensing of solar-induced chlorophyll fluorescence: Review of methods and applications. *Remote Sensing of Environment, 113*(10), 2037–2051. https://doi.org/10.1016/j.rse.2009.05.003

Miao, W., Huang, X., & Song, Y. (2017). An economic assessment of the health effects and crop yield losses caused by air pollution in mainland China. *Journal of Environmental Sciences, 56*, 102–113. https://doi.org/10.1016/j.jes.2016.08.024

Mills, G., Pleijel, H., Braun, S., Bueker, P., Bermejo, V., Calvo, E., Danielsson, H., Emberson, L., Gonzalez Fernandez, I., Gruenhage, L., Harmens, H., Hayes, F., Karlsson, P.-E., & Simpson, D. (2011). New stomatal flux-based critical levels for ozone effects on vegetation. *Atmospheric Environment, 45*(28), 5064–5068. https://doi.org/10.1016/j.atmosenv.2011.06.009

Mohidem, N. A., Hashim, N., Shamsudin, R., & Che Man, H. (2022). Rice for food security: Revisiting its production, diversity, rice milling process, and nutrient content. *Agriculture, 12*(6), 741. https://doi.org/10.3390/agriculture12060741

Moldau, H., Vahisalu, T., & Kollist, H. (2011). Rapid stomatal closure triggered by a short ozone pulse is followed by reopening to overshooting values. *Plant Signaling & Behavior, 6*(2), 311–313. https://doi.org/10.4161/psb.6.2.15044

Muthu, V., Abbai, R., Nallathambi, J., Rahman, H., Ramasamy, S., Kambale, R., Thulasinathan, T., Ayyenar, B., & Muthurajan, R. (2020). Pyramiding QTLs controlling tolerance against drought, salinity, and submergence in rice through marker assisted breeding. *PLOS ONE, 15*(1), e0227421. https://doi.org/10.1371/journal.pone.0227421

Mäenpää, M., Riikonen, J., Kontunen-Soppela, S., Rousi, M., & Oksanen, E. (2011). Vertical profiles reveal impact of ozone and temperature on carbon assimilation of *Betula pendula* and *Populus tremula*. *Tree Physiology, 31*(8), 808–818. https://doi.org/10.1093/treephys/tpr075

Mahmood, F., Khokhar, M. F., & Mahmood, Z. (2020). Examining the relationship of tropospheric ozone and climate change on crop productivity using the multivariate panel data techniques. *Journal of Environmental Management, 272*, 111024. https://doi.org/10.1016/j.jenvman.2020.111024

Mahmood-ur-Rahman, M., Ijaz, M., Qamar, S., Bukhari, S. A., & Malik, K. (2019). Abiotic stress signaling in rice crop. In M. Hasanuzzaman, M. Fujita, K. Nahar, & J. K. Biswas (Eds.), *Advances in rice research for abiotic stress tolerance* (pp. 559–576). Elsevier. https://doi.org/10.1016/B978-0-12-814332-2.00027-7

Manisalidis, I., Stavropoulou, E., Stavropoulos, A., & Bezirtzoglou, E. (2020). Environmental and health impacts of air pollution: A review. *Frontiers in Public Health, 8*, 14. https://doi.org/10.3389/fpubh.2020.00014

Manning, W. J., Paoletti, E., Sandermann, H. Jr., & Ernst, D. (2011). Ethylenediurea (EDU): A research tool for assessment and verification of the effects of ground level ozone on plants under natural conditions. *Environmental Pollution, 159*(12), 3283–3293. https://doi.org/10.1016/j.envpol.2011.07.005

McCouch, S. R., Wright, M. H., Tung, C.-W., Maron, L. G., McNally, K. L., Fitzgerald, M., Singh, N., DeClerck, G., Agosto-Perez, F., Korniliev, P., Greenberg, A. J., Naredo, M. E. B., Mercado, S. M. Q., Harrington, S. E., Shi, Y., Branchini, D. A., Kuser-Falcão, P. R., Leung, H., Ebana, K., Yano, M., Eizenga, G., McClung, A., & Mezey, J. (2016). Open access resources for genome-wide association mapping in rice. *Nature Communications, 7*, 10532. https://doi.org/10.1038/ncomms10532

McDowell, J. M., & Dangl, J. L. (2000). Signal transduction in the plant immune response. *Trends in Biochemical Sciences, 25*(2), 79–82. https://doi.org/10.1016/S0968-0004(99)01532-7

Middleton, J. T., Kendrick, J. B. J., & Schwalm, H. W. (1950). Injury to herbaceous plants by smog or air pollution. *Plant Disease Reporter, 32*, 245–252.

Mills, G., Sharps, K., Simpson, D., Pleijel, H., Broberg, M., Uddling, J., Jaramillo, F., Davies, W. J., Dentener, F., Van den Berg, M., Agrawal, M., Agrawal, S. B., Ainsworth, E. A., Büker, P., Emberson, L., Feng, Z., Harmens, H., Hayes, F., Kobayashi, K., Paoletti, E., & Van Dingenen, R. (2018a). Ozone pollution will compromise efforts to increase global wheat production. *Global Change Biology, 24*(8), 3560–3574. https://doi.org/10.1111/gcb.14157

Mills, G., Sharps, K., Simpson, D., Pleijel, H., Frei, M., Burkey, K., Emberson, L., Uddling, J., Broberg, M., Feng, Z., Kobayashi, K., & Agrawal, M. (2018b). Closing the global ozone yield gap: Quantification and co-benefits for multi-stress tolerance. *Global Change Biology, 24*(10), 4869–4893. https://doi.org/10.1111/gcb.14381

Moldau, H., Padu, E., & Bichele, I. (1997). Quantification of ozone decay and requirement for ascorbate in *Phaseolus vulgaris* L. mesophyll cell walls. *Phyton*, *37*, 175–180.

Monks, P. S., Archibald, A. T., Colette, A., Cooper, O., Coyle, M., Derwent, R., Fowler, D., Granier, C., Law, K. S., Mills, G. E., Stevenson, D. S., Tarasova, O., Thouret, V., von

Schneidemesser, E., Sommariva, R., Wild, O., & Williams, M. L. (2015). Tropospheric ozone and its precursors from the urban to the global scale: From air quality to short-lived climate forcer. *Atmospheric Chemistry and Physics, 15*(15), 8889–8973. https://doi.org/10.5194/acp-15-8889-2015

Norvienyeku, J., Lin, L., Waheed, A., Chen, X., Bao, J., Aliyu, S. R., Lin, L., Shabbir, A., Batool, W., Zhong, Z., Zhou, J., Lu, G., & Wang, Z. (2021). Bayogenin 3-O-cellobioside confers non-cultivar-specific defence against the rice blast fungus *Pyricularia* oryzae. *Plant Biotechnology Journal, 19*(3), 589–601. https://doi.org/10.1111/pbi.13488

Nowroz, F., Hasanuzzaman, M., Siddika, A., Parvin, K., Garcia Caparros, P., Nahar, K., & Prasad, P. V. V. (2024). Elevated tropospheric ozone and crop production: Potential negative effects and plant defense mechanisms. *Frontiers in Plant Science*, 14, 1244515. https://doi.org/10.3389/fpls.2023.1244515

Nadeem, M. A., Nawaz, M. A., Shahid, M. Q., Doğan, Y., Comertpay, G., Yıldız, M., Hatipoğlu, R., Ahmad, F., Alsaleh, A., Labhane, N., Özkan, H., Chung, G., & Baloch, F. S. (2018). DNA molecular markers in plant breeding: Current status and recent advancements in genomic selection and genome editing. *Biotechnology & Biotechnological Equipment, 32*(2), 261–285. https://doi.org/10.1080/13102818.2017.1400401

Nagatoshi, Y., Mitsuda, N., Hayashi, M., Inoue, S., Okuma, E., Kubo, A., Murata, Y., Seo, M., Saji, H., Kinoshita, T., & Ohme-Takagi, M. (2016). GOLDEN 2-LIKE transcription factors for chloroplast development affect ozone tolerance through the regulation of stomatal movement. *Proceedings of the National Academy of Sciences, 113*(15), 4218–4223. https://doi.org/10.1073/pnas.1521579113

Nouchi, I., Ito, O., Harazono, Y., & Kouchi, H. (1995). Acceleration of ^{13}C-labelled photosynthate partitioning from leaves to panicles in rice plants exposed to chronic ozone at the reproductive stage. *Environmental Pollution, 88*(3), 253–260. https://doi.org/10.1016/0269-7491(95)93437-5

Ohashi, Y., Nakayama, N., Saneoka, H., & Fujita, K. (2006). Effects of drought stress on photosynthetic gas exchange, chlorophyll fluorescence, and stem diameter of soybean plants. *Biologia Plantarum*, *50*, 138–141. https://doi.org/10.1007/s10535-005-0089-3

Orts, A., Navarro-Torre, S., Macías-Benítez, S., Orts, J. M., Naranjo, E., Castaño, A., & Parrado, J. (2024). A new biostimulant derived from soybean by-products enhances plant

tolerance to abiotic stress triggered by ozone. *BMC Plant Biology, 24*, 580. https://doi.org/10.1186/s12870-024-05290-3

Ogawa, D., Nakajima, N., Sano, T., Tamaoki, M., Aono, M., Kubo, A., Kamada, H., & Saji, H. (2005). Regulation of salicylic acid synthesis in ozone-exposed tobacco and Arabidopsis. *Phyton: Annales Rei Botanicae, 45*(4), 169–175.

Pang, Y., Chen, K., Wang, X., Wang, W., Xu, J., Ali, J., & Li, Z. (2017). Simultaneous improvement and genetic dissection of salt tolerance of rice (*Oryza sativa* L.) by designed QTL pyramiding. *Frontiers in Plant Science, 8*, Article 1275. https://doi.org/10.3389/fpls.2017.01275

Paoletti, E., & Grulke, N. E. (2005). Does living in elevated CO_2 ameliorate tree response to ozone? A review on stomatal responses. *Environmental Pollution, 137*(3), 483–493. https://doi.org/10.1016/j.envpol.2005.01.035

Paoletti, E., & Grulke, N. E. (2010). Ozone exposure and stomatal sluggishness in different plant physiognomic classes. *Environmental Pollution, 158*(8), 2664–2671. https://doi.org/10.1016/j.envpol.2010.04.024

Paoletti, E., Manning, W. J., Spaziani, F., & Tagliaferro, F. (2007). Gravitational infusion of ethylenediurea (EDU) into trunks protected adult European ash trees (*Fraxinus excelsior* L.) from foliar ozone injury. *Environmental Pollution, 145*(3), 869–873. https://doi.org/10.1016/j.envpol.2006.05.005

Park, J.-Y., Jin, J., Lee, Y.-W., Kang, S., & Lee, Y.-H. (2009). Rice blast fungus (*Magnaporthe oryzae*) infects Arabidopsis via a mechanism distinct from that required for the infection of rice. *Plant Physiology, 149*(1), 474–486. https://doi.org/10.1104/pp.108.129536

Pazarlar, S., Cetinkaya, N., Bor, M., & Ozdemir, F. (2017). Ozone triggers different defence mechanisms against powdery mildew (*Blumeria graminis* DC. Speer f. sp. *tritici*) in susceptible and resistant wheat genotypes. *Functional Plant Biology, 44*(10), 1016–1028. https://doi.org/10.1071/FP17038

Pettorelli, N., Vik, J. O., Mysterud, A., Gaillard, J.-M., Tucker, C. J., & Stenseth, N. C. (2005). Using the satellite-derived NDVI to assess ecological responses to environmental change. *Trends in Ecology & Evolution, 20*(9), 503–510. https://doi.org/10.1016/j.tree.2005.05.011

Pleijel, H., Danielsson, H., Karlsson, G. P., Gelang, J., Karlsson, P. E., & Selldén, G. (2000). An ozone flux–response relationship for wheat. *Environmental Pollution*, 109(3), 453–462. https://doi.org/10.1016/S0269-7491(00)00048-8

Poland, J., Endelman, J., Dawson, J., Rutkoski, J., Wu, S., Manes, Y., Dreisigacker, S., Crossa, J., Sánchez-Villeda, H., Sorrells, M., & Jannink, J.-L. (2012). Genomic selection in wheat breeding using genotyping-by-sequencing. *The Plant Genome*, 5(3), 103–113. https://doi.org/10.3835/plantgenome2012.06.0006

Padilla, F. M., Peña-Fleitas, M. T., Gallardo, M., & Thompson, R. B. (2016). Proximal optical sensing of cucumber crop N status using chlorophyll fluorescence indices. *European Journal of Agronomy, 73*, 83–97. https://doi.org/10.1016/j.eja.2015.11.001

Pennisi, E. (2010). Armed and dangerous. *Science, 327*(5967), 804–805. https://doi.org/10.1126/science.327.5967.804

Peñuelas, J., Baret, F., & Filella, I. (1995). Semi-empirical indices to assess carotenoids/chlorophyll a ratio from leaf spectral reflectance. *Photosynthetica, 31*(2), 221–230.

Periyasamy, Ramya, A., Maheswari, M., Jayabalakrishnan, R. M., Saraswathi, R., & Chandrasekhar, C. N. (2020). Assessment of physiological, biochemical and yield attributes of rice cultivars under elevated ozone stress. *Madras Agricultural Journal, 107*(10-12), 1–4. https://doi.org/10.29321/MAJ.10.000463

Phothi, R., Umponstira, C., Sarin, C., Siriwong, W., & Nabheerong, N. (2016). Combining effects of ozone and carbon dioxide application on photosynthesis of Thai jasmine rice (*Oryza sativa* L.) cultivar Khao Dawk Mali 105. *Australian Journal of Crop Science, 10*(4), 591–597. https://doi.org/10.21475/ajcs.2016.10.04.p7595x

R Core Team. (2018). *R: A language and environment for statistical computing*. R Foundation for Statistical Computing. https://www.R-project.org/

Rao, M. V., & Davis, K. R. (2001). The physiology of ozone induced cell death. *Planta, 213*, 682–690. https://doi.org/10.1007/s004250100618

Ravelombola, W., Shi, A., & Huynh, B.-L. (2021). Loci discovery, network-guided approach, and genomic prediction for drought tolerance index in a multi-parent advanced generation intercross (MAGIC) cowpea population. *Horticulture Research, 8*, 24. https://doi.org/10.1038/s41438-021-00462-w

Rahman, M. M., Mahamud, S., & Thurston, G. D. (2019). Recent spatial gradients and time trends in Dhaka, Bangladesh, air pollution and their human health implications. *Journal of the Air & Waste Management Association, 69*(4), 478–501. https://doi.org/10.1080/10962247.2018.1548388

Rai, R., & Agrawal, M. (2012). Impact of tropospheric ozone on crop plants. *Proceedings of the National Academy of Sciences, India Section B: Biological Sciences, 82*, 241–257. https://doi.org/10.1007/s40011-012-0032-2

Rao, M. V., & Davis, K. R. (1999). Ozone-induced cell death occurs via two distinct mechanisms in *Arabidopsis*: the role of salicylic acid. *The Plant Journal*, 17(6), 603–614. https://doi.org/10.1046/j.1365-313x.1999.00400.x

Rao, M. V., Lee, H., Creelman, R. A., Mullet, J. E., & Davis, K. R. (2000). Jasmonic acid signaling modulates ozone-induced hypersensitive cell death. *The Plant Cell*, 12(9), 1633–1646. https://doi.org/10.1105/tpc.12.9.1633

Rasheed, A., Wen, W., Gao, F., Zhai, S., Jin, H., Liu, J., Guo, Q., Zhang, Y., Dreisigacker, S., Xia, X., & He, Z. (2016). Development and validation of KASP assays for genes underpinning key economic traits in bread wheat. *Theoretical and Applied Genetics, 129*, 1843–1860. https://doi.org/10.1007/s00122-016-2743-x

Reguera, M., Peleg, Z., Abdel-Tawab, Y. M., Tumimbang, E. B., Delatorre, C. A., & Blumwald, E. (2013). Stress-induced cytokinin synthesis increases drought tolerance through the coordinated regulation of carbon and nitrogen assimilation in rice. *Plant Physiology, 163*(4), 1609–1622. https://doi.org/10.1104/pp.113.227702

Ribas, A., Peñuelas, J., Elvira, S., & Gimeno, B. S. (2005). Ozone exposure induces the activation of leaf senescence-related processes and morphological and growth changes in seedlings of Mediterranean tree species. *Environmental Pollution*, 134(2), 291–300. https://doi.org/10.1016/j.envpol.2004.07.026

Rouse, J. W., Haas, R. H., Schell, J. A., & Deering, D. W. (1973). Monitoring vegetation systems in the Great Plains with ERTS (Earth Resources Technology Satellite). *Proceedings of the 3rd Earth Resources Technology Satellite Symposium*, Greenbelt, MD, December 10–14, 1973 (SP-351, pp. 309–317). NASA.

Roy, S. D., Beig, G., & Ghude, S. D. (2009). Exposure-plant response of ambient ozone over the tropical Indian region. *Atmospheric Chemistry and Physics, 9*(14), 5253–5260. https://doi.org/10.5194/acp-9-5253-2009

Sakulkoo, W., Osés-Ruiz, M., Garcia, E. O., Soanes, D. M., Littlejohn, G. R., Hacker, C., Correia, A., Valent, B., & Talbot, N. J. (2018). A single fungal MAP kinase controls plant cell-to-cell invasion by the rice blast fungus. *Science, 359*(6382), 1399–1403. https://doi.org/10.1126/science.aaq0892

Sallaud, C., Lorieux, M., Roumen, E., Tharreau, D., Berruyer, R., Svestasrani, P., Garsmeur, O., Ghesquiere, A., & Notteghem, J.-L. (2003). Identification of five new blast resistance genes in the highly blast-resistant rice variety IR64 using a QTL mapping strategy. *Theoretical and Applied Genetics, 106*, 794–803. https://doi.org/10.1007/s00122-002-1088-9

Sandermann, H. (1996). Ozone and plant health. *Annual Review of Phytopathology, 34*(1), 347–366. https://doi.org/10.1146/annurev.phyto.34.1.347

Sandermann, H., Jr., Ernst, D., Heller, W., & Langebartels, C. (1998). Ozone: An abiotic elicitor of plant defence reactions. *Trends in Plant Science, 3*(2), 47–50. https://doi.org/10.1016/S1360-1385(97)01162-X

Sandhu, K. S., Shiv, A., Kaur, G., Meena, M. R., Raja, A. K., Vengavasi, K., Mall, A. K., Kumar, S., Singh, P. K., Singh, J., Hemaprabha, G., Pathak, A. D., Krishnappa, G., & Kumar, S. (2022). Integrated approach in genomic selection to accelerate genetic gain in sugarcane. *Plants, 11*(16), 2139. https://doi.org/10.3390/plants11162139

Sanmartin, M., Drogoudi, P. D., Lyons, T., Pateraki, I., Barnes, J., & Kanellis, A. K. (2003). Over-expression of ascorbate oxidase in the apoplast of transgenic tobacco results in altered ascorbate and glutathione redox states and increased sensitivity to ozone. *Planta, 216*, 918–928. https://doi.org/10.1007/s00425-002-0944-9

Sarkar, A., & Agrawal, S. B. (2010). Identification of ozone stress in Indian rice through foliar injury and differential protein profile. *Environmental Monitoring and Assessment, 161*(), 205–215. https://doi.org/10.1007/s10661-008-0738-z

Sarma, B., Kashtoh, H., Tamang, T. L., Bhattacharyya, P. N., Mohanta, Y. K., & Baek, K.-H. (2023). Abiotic stress in rice: visiting the physiological response and its tolerance mechanisms. *Plants, 12*(23), 3948. https://doi.org/10.3390/plants12233948

Sawada, H., & Kohno, Y. (2009). Differential ozone sensitivity of rice cultivars as indicated by visible injury and grain yield. *Plant Biology*, 11(S1), 70–75. https://doi.org/10.1111/j.1438-8677.2009.00233.x

Schubert, R., Fischer, R., Hain, R., Schreier, P. H., Bahnweg, G., Ernst, D., & Sandermann, H. Jr. (1997). An ozone-responsive region of the grapevine resveratrol synthase promoter differs from the basal pathogen-responsive sequence. *Plant Molecular Biology, 34*, 417–426. https://doi.org/10.1023/a:1005830714852

Shah, S. H., Houborg, R., & McCabe, M. F. (2017). Response of chlorophyll, carotenoid and SPAD-502 measurement to salinity and nutrient stress in wheat (*Triticum aestivum* L.). *Agronomy, 7*(3), 61. https://doi.org/10.3390/agronomy7030061

Shang, B., Deng, T., Chen, H., Xu, Y., & Feng, Z. (2024). Effects of elevated ozone on physiology, growth, yield and grain quality of rice (*Oryza sativa* L.): an ozone gradient experiment. *Agriculture, Ecosystems & Environment, 363*, 108858. https://doi.org/10.1016/j.agee.2023.108858

Sharif, M. K., Butt, M. S., Anjum, F. M., & Khan, S. H. (2014). Rice bran: A novel functional ingredient. *Critical Reviews in Food Science and Nutrition, 54*(6), 807–816. https://doi.org/10.1080/10408398.2011.608586

Sharma, Y. K., León, J., Raskin, I., & Davis, K. R. (1996). Ozone-induced responses in *Arabidopsis thaliana*: The role of salicylic acid in the accumulation of defense-related transcripts and induced resistance. *Proceedings of the National Academy of Sciences*, *93*(10), 5099–5104. https://doi.org/10.1073/pnas.93.10.5099

Shinada, H., Iwata, N., Sato, T., & Fujino, K. (2014). QTL pyramiding for improving of cold tolerance at fertilization stage in rice. *Breeding Science, 63*(5), 483–488. https://doi.org/10.1270/jsbbs.63.483

Sierla, M., Hõrak, H., Overmyer, K., Waszczak, C., Yarmolinsky, D., Maierhofer, T., Vainonen, J. P., Salojärvi, J., Denessiouk, K., Laanemets, K., Tõldsepp, K., Vahisalu, T., Gauthier, A., Puukko, T., Paulin, L., Auvinen, P., Geiger, D., Hedrich, R., Kollist, H., & Kangasjärvi, J. (2018). The receptor-like pseudokinase GHR1 is required for stomatal closure. *The Plant Cell*, 30(11), 2813–2837. https://doi.org/10.1105/tpc.18.00441

Sims, D. A., & Gamon, J. A. (2002). Relationships between leaf pigment content and spectral reflectance across a wide range of species, leaf structures and developmental stages. *Remote Sensing of Environment, 81*(2-3), 337–354. https://doi.org/10.1016/S0034-4257(02)00010-X

Sinclair, T. R. (1998). Historical changes in harvest index and crop nitrogen accumulation. *Crop Science, 38*(3), 638–643. https://doi.org/10.2135/cropsci1998.0011183X003800030002x

Sinclair, T. R. (2019). The biological yield and harvest index of cereals as agronomic and plant breeding criteria by C.M. Donald and J. Hamblin, Advances in Agronomy (1976) 28:361–405. *Crop Science, 59*(3), 850–852. https://doi.org/10.2135/cropsci2018.10.0645

Skärby, L., & Pell, E. J. (1979). Concentrations of coumestrol and 4',7-dihydroxyflavone in four alfalfa cultivars after exposure to ozone. *Journal of Environmental Quality, 8*(3), 285–286. https://doi.org/10.2134/jeq1979.00472425000800030004x

Sperdouli, I., Andreadis, S., Moustaka, J., Panteris, E., Tsaballa, A., & Moustakas, M. (2021). Changes in light energy utilization in photosystem II and reactive oxygen species generation in potato leaves by the pinworm *Tuta* absoluta. *Molecules, 26*(10), 2984. https://doi.org/10.3390/molecules26102984

Sun, G., McLaughlin, S. B., Porter, J. H., Uddling, J., Mulholland, P. J., Adams, M. B., & Pederson, N. (2012). Interactive influences of ozone and climate on streamflow of forested watersheds. *Global Change Biology, 18*(11), 3395–3409. https://doi.org/10.1111/j.1365-2486.2012.02787.x

Sakamoto, T., & Matsuoka, M. (2008). Identifying and exploiting grain yield genes in rice. *Current Opinion in Plant Biology, 11*(2), 209–214. https://doi.org/10.1016/j.pbi.2008.01.009

Shandilya, R., Shandilya, R., & Shandilya, R. (2024). Assessment of the statistical performance of chemical transport model studies in India. *ACS ES&T Air*, *1*(12), 1519–1530. https://doi.org/10.1021/acsestair.4c00072

Shang, B., Fu, R., Agathokleous, E., Dai, L., Zhang, G., Wu, R., & Feng, Z. (2022). Ethylenediurea offers moderate protection against ozone-induced rice yield loss under high ozone pollution. *Science of The Total Environment, 806*(Part 3), 151341. https://doi.org/10.1016/j.scitotenv.2021.151341

Sikirou, M., Saito, K., Achigan-Dako, E. G., Dramé, K. N., Ahanchédé, A., & Venuprasad, R. (2015). Genetic improvement of iron toxicity tolerance in rice—Progress, challenges and prospects in West Africa. *Plant Production Science, 18*(4), 423–434. https://doi.org/10.1626/pps.18.423

Simpson, D., Arneth, A., Mills, G., Solberg, S., & Uddling, J. (2014). Ozone—the persistent menace: Interactions with the N cycle and climate change. *Current Opinion in Environmental Sustainability, 9–10*, 9–19. https://doi.org/10.1016/j.cosust.2014.07.008

Singh, A. A., Chaurasia, M., Gupta, V., Agrawal, M., & Agrawal, S. B. (2018). Responses of *Zea mays* L. cultivars 'Buland' and 'Prakash' to an antiozonant ethylenediurea grown under ambient and elevated levels of ozone. *Acta Physiologiae Plantarum, 40*, 92. https://doi.org/10.1007/s11738-018-2666-z

Singh, J., Gupta, S. K., Devanna, B. N., Singh, S., Upadhyay, A., & Sharma, T. R. (2020). Blast resistance gene Pi54 over-expressed in rice to understand its cellular and sub-cellular localization and response to different pathogens. *Scientific Reports, 10*, 5243. https://doi.org/10.1038/s41598-020-59027-x

Siwach, P., Jain, S., Saini, N., Chowdhury, V. K., & Jain, R. K. (2004). Allelic diversity among Basmati and non-Basmati long-grain indica rice varieties using microsatellite markers. *Journal of Plant Biochemistry and Biotechnology, 13*, 25–32. https://doi.org/10.1007/BF03263186

Steele, K. A., Quinton-Tulloch, M. J., Amgai, R. B., Dhakal, R., Khatiwada, S. P., Vyas, D., Heine, M., & Witcombe, J. R. (2018). Accelerating public sector rice breeding with high-density KASP markers derived from whole genome sequencing of indica rice. *Molecular Breeding, 38*, 38. https://doi.org/10.1007/s11032-018-0777-2

Stevenson, D. S., Dentener, F. J., Schultz, M. G., Ellingsen, K., van Noije, T. P. C., Wild, O., Zeng, G., Amann, M., Atherton, C. S., Bell, N., Bergmann, D. J., Bey, I., Butler, T., Cofala, J., Collins, W. J., Derwent, R. G., Doherty, R. M., Drevet, J., Eskes, H. J., Fiore, A. M., Gauss, M., Hauglustaine, D. A., Horowitz, L. W., Isaksen, I. S. A., Krol, M. C., Lamarque, J.-F., Lawrence, M. G., Montanaro, V., Müller, J.-F., Pitari, G., Prather, M. J., Pyle, J. A., Rast, S., Rodriguez, J. M., Sanderson, M. G., Savage, N. H., Shindell, D. T., Strahan, S. E., Sudo, K., & Szopa, S. (2006). Multimodel ensemble simulations of present-day and near-future tropospheric ozone. *Journal of Geophysical Research: Atmospheres*, 111(D8), D08301. https://doi.org/10.1029/2005JD006338

Swamy, B. P. M., & Kumar, A. (2013). Genomics-based precision breeding approaches to improve drought tolerance in rice. *Biotechnology Advances, 31*(8), 1308–1318. https://doi.org/10.1016/j.biotechadv.2013.05.004

Tamaoki, M. (2008). The role of phytohormone signaling in ozone-induced cell death in plants. *Plant Signaling & Behavior, 3*(3), 166–174. https://doi.org/10.4161/psb.3.3.5538

Tcherkez, G., & Limami, A. M. (2019). Net photosynthetic CO_2 assimilation: More than just CO_2 and O_2 reduction cycles. *New Phytologist, 223*(2), 520–529. https://doi.org/10.1111/nph.15828

Tang, W., Lin, J., Wang, Y., An, H., Chen, H., Pan, G., Zhang, S., Guo, B., Yu, K., Li, H., Fang, X., & Zhang, Y. (2022). Selection and validation of 48 KASP markers for variety identification and breeding guidance in conventional and hybrid rice (*Oryza sativa* L.). *Rice, 15*, 48. https://doi.org/10.1186/s12284-022-00594-0

Telebanco-Yanoria, M.J., Koide, Y., Fukuta, Y., Imbe, T., Tsunematsu, H., Kato, H., Ebron, L. A., Nguyen, T. M. N., & Kobayashi, N. (2011). A set of near-isogenic lines of Indica-type rice variety CO 39 as differential varieties for blast resistance. *Molecular Breeding*, *27*, 357–373. https://doi.org/10.1007/s11032-010-9437-x

Tian, Y., Wang, Y., Han, Y., Che, H., Qi, X., Xu, Y., Chen, Y., Long, X., & Wei, C. (2023). Spatiotemporal characteristics of ozone pollution and resultant increased human health risks in Central China. *Atmosphere, 14*(10), 1591. https://doi.org/10.3390/atmos14101591

Tiwari, S., Rai, R., & Agrawal, M. (2008). Annual and seasonal variations in tropospheric ozone concentrations around Varanasi. *International Journal of Remote Sensing, 29*(15), 4499–4514. https://doi.org/10.1080/01431160801961391

Torres, M. A., Jones, J. D. G., & Dangl, J. L. (2006). Reactive oxygen species signaling in response to pathogens. *Plant Physiology, 141*(2), 373–378. https://doi.org/10.1104/pp.106.079467

Tsukahara, K., Sawada, H., Matsumura, H., Kohno, Y., & Tamaoki, M. (2013). Quantitative trait locus analyses of ozone-induced grain yield reduction in rice. *Environmental and Experimental Botany, 88*, 100–106. https://doi.org/10.1016/j.envexpbot.2011.12.012

Turcsányi, E., Lyons, T., Plöchl, M., & Barnes, J. (2000). Does ascorbate in the mesophyll cell walls form the first line of defence against ozone? Testing the concept using broad bean (*Vicia faba* L.). *Journal of Experimental Botany, 51*(346), 901–910. https://doi.org/10.1093/jexbot/51.346.901

Tagaris, E., Liao, K.-J., DeLucia, A. J., Deck, L., Amar, P., & Russell, A. G. (2010). Sensitivity of air pollution-induced premature mortality to precursor emissions under the influence of climate change. *International Journal of Environmental Research and Public Health, 7*(5), 2222–2237. https://doi.org/10.3390/ijerph7052222

Takehisa, H., Yasuda, M., Fukuta, Y., Kobayashi, N., Hayashi, N., Nakashita, H., Abe, T., & Sato, T. (2009). Genetic analysis of resistance genes in an Indica-type rice (*Oryza sativa* L.), Kasalath, using DNA markers. *Breeding Science, 59*(3), 253–260. https://doi.org/10.1270/jsbbs.59.253

Tan, J., Wang, M., Shi, Z., & Miao, X. (2018). *OsEXPA10* mediates the balance between growth and resistance to biotic stress in rice. *Plant Cell Reports, 37*, 993–1002. https://doi.org/10.1007/s00299-018-2284-7

Tang, H., Takigawa, M., Liu, G., Zhu, J., & Kobayashi, K. (2013). A projection of ozone-induced wheat production loss in China and India for the years 2000 and 2020 with exposure-based and flux-based approaches. *Global Change Biology, 19*(9), 2739–2752. https://doi.org/10.1111/gcb.12252

The Royal Society. (2008). *Ground-level ozone in the 21st century: Future trends, impacts and policy implications.* The Royal Society.

Tiedemann, A. V. (1992). Ozone effects on fungal leaf diseases of wheat in relation to epidemiology II. Biotrophic pathogens. *Journal of Phytopathology, 134*(3), 187–197.

Tsukahara, K., Sawada, H., Kohno, Y., Matsuura, T., Mori, I. C., Terao, T., Ioki, M., & Tamaoki, M. (2015). Ozone-induced rice grain yield loss is triggered via a change in panicle morphology that is controlled by *ABERRANT PANICLE ORGANIZATION 1* gene. *PLOS ONE, 10*(4), e0123308. https://doi.org/10.1371/journal.pone.0123308

U.S. Department of Agriculture. (2024). *Data and analysis of global production.* Retrieved January 2, 2025, from https://fas.usda.gov/data/production/commodity/0422110

Ueda, Y., Frimpong, F., Qi, Y., Matthus, E., Wu, L., Höller, S., Kraska, T., & Frei, M. (2015a). Genetic dissection of ozone tolerance in rice (*Oryza sativa* L.) by a genome-wide association study. *Journal of Experimental Botany, 66*(1), 293–306. https://doi.org/10.1093/jxb/eru419

Ueda, Y., Siddique, S., & Frei, M. (2015b). A novel gene, *OZONE-RESPONSIVE APOPLASTIC PROTEIN1*, enhances cell death in ozone stress in rice. *Plant Physiology, 169*(1), 873–889. https://doi.org/10.1104/pp.15.00956

Unger, N., Shindell, D. T., Koch, D. M., & Streets, D. G. (2008). Air pollution radiative forcing from specific emissions sectors at 2030. *Journal of Geophysical Research: Atmospheres*, 113(D2), D02306. https://doi.org/10.1029/2007JD008683

Ur Rehman, S., Ali Sher, M., Saddique, M. A. B., Ali, Z., Khan, M. A., Mao, X., Irshad, A., Sajjad, M., Ikram, R. M., Naeem, M., & Jing, R. (2021). Development and exploitation of KASP assays for genes underpinning drought tolerance among wheat cultivars from Pakistan. *Frontiers in Genetics, 12*, 684702. https://doi.org/10.3389/fgene.2021.684702

Vahisalu, T., Kollist, H., Wang, Y.-F., Nishimura, N., Chan, W.-Y., Valerio, G., Lamminmäki, A., Brosché, M., Moldau, H., Desikan, R., Schroeder, J. I., & Kangasjärvi, J. (2008). SLAC1 is required for plant guard cell S-type anion channel function in stomatal signalling. *Nature, 452*(7186), 487–491. https://doi.org/10.1038/nature06608

Vahisalu, T., Puzõrjova, I., Brosché, M., Valk, E., Lepiku, M., Moldau, H., Pechter, P., Wang, Y.-S., Lindgren, O., Salojärvi, J., Loog, M., Kangasjärvi, J., & Kollist, H. (2010). Ozone-triggered rapid stomatal response involves the production of reactive oxygen species, and is controlled by SLAC1 and OST1. *The Plant Journal, 62*(3), 442–453. https://doi.org/10.1111/j.1365-313X.2010.04159.x

Van Dingenen, R., Dentener, F. J., Raes, F., Krol, M. C., Emberson, L., & Cofala, J. (2009). The global impact of ozone on agricultural crop yields under current and future air quality legislation. *Atmospheric Environment, 43*(3), 604–618. https://doi.org/10.1016/j.atmosenv.2008.10.033

Varshney, R. K. (2010). Gene-based marker systems in plants: High throughput approaches for marker discovery and genotyping. In S. M. Jain & D. S. Brar (Eds.), *Molecular techniques in crop improvement* (2nd ed., pp. 119–142). Springer. https://doi.org/10.1007/978-90-481-2967-6_5

Violini, G. (1995). Ozone and plant pathogens: An overview. *Rivista di Patologia Vegetale, 5*(3), 113–130.

Wang, Y., Song, Q., Frei, M., Shao, Z., & Yang, L. (2014a). Effects of elevated ozone, carbon dioxide, and the combination of both on the grain quality of Chinese hybrid rice. *Environmental Pollution, 189*, 9–17. https://doi.org/10.1016/j.envpol.2014.02.016

Wang, Y., Yang, L., Höller, M., Zaisheng, S., Pariasca-Tanaka, J., Wissuwa, M., Frei, M., & Kohno, Y. (2014b). Pyramiding of ozone tolerance QTLs *OzT8* and *OzT9* confers

improved tolerance to season-long ozone exposure in rice. *Environmental and Experimental Botany, 104*, 26–33. https://doi.org/10.1016/j.envexpbot.2014.03.005

Werner, C. R., Voss-Fels, K. P., Miller, C. N., Qian, W., Hua, W., Guan, C.-Y., Snowdon, R. J., & Qian, L. (2018). Effective genomic selection in a narrow-genepool crop with low-density markers: Asian rapeseed as an example. *The Plant Genome, 11*(2), 170084. https://doi.org/10.3835/plantgenome2017.09.0084

West, J. J., Naik, V., Horowitz, L. W., & Fiore, A. M. (2009a). Effect of regional precursor emission controls on long-range ozone transport – Part 1: Short-term changes in ozone air quality. *Atmospheric Chemistry and Physics, 9*(16), 6077–6093. https://doi.org/10.5194/acp-9-6077-2009

West, J. J., Naik, V., Horowitz, L. W., & Fiore, A. M. (2009b). Effect of regional precursor emission controls on long-range ozone transport – Part 2: Steady-state changes in ozone air quality and impacts on human mortality. *Atmospheric Chemistry and Physics*, 9(16), 6095–6107. https://doi.org/10.5194/acp-9-6095-2009

Wang, L., Yang, X., Dong, J., Yang, Y., Ma, P., & Zhao, W. (2023). Evolution of surface ozone pollution pattern in eastern China and its relationship with different intensity heatwaves. *Environmental Pollution, 338*, 122725. https://doi.org/10.1016/j.envpol.2023.122725

Wang, M., Yu, Y., Haberer, G., Marri, P. R., Fan, C., Goicoechea, J. L., Zuccolo, A., Song, X., Kudrna, D., Ammiraju, J. S. S., Cossu, R. M., Maldonado, C., Chen, J., Lee, S., Sisneros, N., de Baynast, K., Golser, W., Wissotski, M., Kim, W., Sanchez, P., Ndjiondjop, M.-N., Sanni, K., Long, M., Carney, J., Panaud, O., Wicker, T., Machado, C. A., Chen, M., Mayer, K. F. X., Rounsley, S., & Wing, R. A. (2014). The genome sequence of African rice (*Oryza glaberrima*) and evidence for independent domestication. *Nature Genetics*, 46, 982–988. https://doi.org/10.1038/ng.3044

Wang, Q., Sude, B., Dong, M., Shi, Y., Geng, C., & Wang, X. (2014). Effect of ozone fumigation on morpho-physiology and yield of field-grown rice in the Pearl River Delta, China. *Scientific Research and Essays, 9*(9), 315-320. https://doi.org/10.5897/SRE2014.5909

Wang, X., Fu, T.-M., Zhang, L., Cao, H., Zhang, Q., Ma, H., Shen, L., Evans, M. J., Ivatt, P. D., Lu, X., Chen, Y., Zhang, L., Feng, X., Yang, X., Zhu, L., & Henze, D. K. (2021). Sensitivities of ozone air pollution in the Beijing-Tianjin-Hebei area to local and

upwind precursor emissions using adjoint modeling. *Environmental Science & Technology, 55*(9), 5752–5762. https://doi.org/10.1021/acs.est.1c00131

Wang, Y., & Frei, M. (2011). Stressed food – the impact of abiotic environmental stresses on crop quality. *Agriculture, Ecosystems & Environment, 141*(3-4), 271–286. https://doi.org/10.1016/j.agee.2011.03.017

Wang, Y., Gao, W., Wang, S., Song, T., Gong, Z., Ji, D., Wang, L., Liu, Z., Tang, G., Huo, Y., Tian, S., Li, J., Li, M., Yang, Y., Chu, B., Petäjä, T., Kerminen, V.-M., He, H., Hao, J., Kulmala, M., Wang, Y., & Zhang, Y. (2020). Contrasting trends of $PM_{2.5}$ and surface-ozone concentrations in China from 2013 to 2017. *National Science Review, 7*(8), 1331–1339. https://doi.org/10.1093/nsr/nwaa032

Weigel, H. J., Bergmann, E., & Bender, J. (2015). Plant-mediated ecosystem effects of tropospheric ozone. In U. Lüttge & W. Beyschlag (Eds.), *Progress in Botany* (Vol. 76, pp. 395–438). Springer. https://doi.org/10.1007/978-3-319-08807-5_15

Wilson, R. A., & Talbot, N. J. (2009). Under pressure: Investigating the biology of plant infection by *Magnaporthe oryzae*. *Nature Reviews Microbiology, 7*, 185–195. https://doi.org/10.1038/nrmicro2032

World Meteorological Organization. (2014). *Assessment for decision-makers: Scientific assessment of ozone depletion (Global Ozone Research and Monitoring Project—Report No. 56)*. Geneva, Switzerland.

Xiao, N., Wu, Y., Pan, C., Yu, L., Chen, Y., Liu, G., Li, Y., Zhang, X., Wang, Z., Dai, Z., Liang, C., & Li, A. (2017). Improving of rice blast resistances in Japonica by pyramiding major R genes. *Frontiers in Plant Science, 7*, 1918. https://doi.org/10.3389/fpls.2016.01918

Xing, J., Zhang, F., Zhou, Y., Wang, S., Ding, D., Jang, C., Zhu, Y., & Hao, J. (2019). Least-cost control strategy optimization for air quality attainment of Beijing-Tianjin-Hebei region in China. *Journal of Environmental Management, 245*, 95–104. https://doi.org/10.1016/j.jenvman.2019.05.022

Xu, H., Biswas, D. K., Li, W. D., Chen, S. B., Zhang, L., Jiang, G. M., & Li, Y. G. (2007). Photosynthesis and yield responses of ozone-polluted winter wheat to drought. *Photosynthetica, 45*(4), 582–588. https://doi.org/10.1007/s11099-007-0100-7

Xu, J., Henry, A., & Sreenivasulu, N. (2020). Rice yield formation under high day and night temperatures—A prerequisite to ensure future food security. *Plant, Cell & Environment*, 43(7), 1595–1608. https://doi.org/10.1111/pce.13748

Xu, Y., & Crouch, J. H. (2008). Marker-assisted selection in plant breeding: from publications to practice. *Crop Science, 48*(2), 391–407. https://doi.org/10.2135/cropsci2007.04.0191

Yamaguchi, M., Hoshino, D., Inada, H., Akhtar, N., Sumioka, C., Takeda, K., & Izuta, T. (2014). Evaluation of the effects of ozone on yield of Japanese rice (*Oryza sativa* L.) based on stomatal ozone uptake. *Environmental Pollution*, 184, 472–480. https://doi.org/10.1016/j.envpol.2013.09.024

Yang, C., Li, W., Cao, J., Meng, F., Yu, Y., Huang, J., Jiang, L., Liu, M., Zhang, Z., Chen, X., Miyamoto, K., Yamane, H., Zhang, J., Chen, S., & Liu, J. (2017). Activation of ethylene signaling pathways enhances disease resistance by regulating ROS and phytoalexin production in rice. *The Plant Journal, 89*(2), 338–353. https://doi.org/10.1111/tpj.13388

Yuan, X., Calatayud, V., Gao, F., Fares, S., Paoletti, E., Tian, Y., & Feng, Z. (2016). Interaction of drought and ozone exposure on isoprene emission from extensively cultivated poplar. *Plant, Cell & Environment*, 39(10), 2276–2287. https://doi.org/10.1111/pce.12798

Yadav, A. K., Kumar, A., Grover, N., Ellur, R. K., Krishnan, S. G., Bollinedi, H., Bhowmick, P. K., Vinod, K. K., Nagarajan, M., Krishnamurthy, S. L., & Singh, A. K. (2020). Marker aided introgression of *'Saltol'*, a major QTL for seedling stage salinity tolerance into an elite Basmati rice variety 'Pusa Basmati 1509'. *Scientific Reports, 10*, 13877. https://doi.org/10.1038/s41598-020-70664

Yalpani, N., Enyedi, A. J., León, J., & Raskin, I. (1994). Ultraviolet light and ozone stimulate accumulation of salicylic acid, pathogenesis-related proteins and virus resistance in tobacco. *Planta, 193*, 372–376. https://doi.org/10.1007/BF00201815

Yamaji, K., Ohara, T., Uno, I., Tanimoto, H., Kurokawa, J. I., & Akimoto, H. (2006). Analysis of the seasonal variation of ozone in the boundary layer in East Asia using the Community Multi-scale Air Quality model: What controls surface ozone levels over Japan? *Atmospheric Environment*, 40(10), 1856–1868. https://doi.org/10.1016/j.atmosenv.2005.10.067

Yendrek, C. R., Koester, R. P., & Ainsworth, E. A. (2015). A comparative analysis of transcriptomic, biochemical, and physiological responses to elevated ozone identifies

species-specific mechanisms of resilience in legume crops. *Journal of Experimental Botany, 66*(22), 7101–7112. https://doi.org/10.1093/jxb/erv404

Yoshida, S., Forno, D. A., Cock, J. H., & Gomez, K. A. (1976). *Laboratory manual for physiological studies of rice*. International Rice Research Institute.

Zhang, J., Wang, Y., Mao, Z., Liu, W., Ding, L., Zhang, X., Yang, Y., Wu, S., Chen, X., & Wang, Y. (2022). Transcription factor McWRKY71 induced by ozone stress regulates anthocyanin and proanthocyanidin biosynthesis in *Malus* crabapple. *Ecotoxicology and Environmental Safety, 232*, Article 113274. https://doi.org/10.1016/j.ecoenv.2022.113274

Zhang, S., Tao, F., & Zhang, Z. (2014). Rice reproductive growth duration increased despite of negative impacts of climate warming across China during 1981–2009. *European Journal of Agronomy, 54*, 70–83. https://doi.org/10.1016/j.eja.2013.12.001

Zhao, Z., Pearsall, D. M., Benfer, R. A., & Piperno, D. R. (1998). Distinguishing rice (*Oryza sativa* poaceae) from wild *Oryza* species through phytolith analysis, II: Finalized method. *Economic Botany, 52*, 134–145. https://doi.org/10.1007/BF0286120

Zeng, Y., Cao, Y., Qiao, X., Seyler, B. C., & Tang, Y. (2019). Air pollution reduction in China: Recent success but great challenge for the future. *Science of The Total Environment, 663*, 329–337. https://doi.org/10.1016/j.scitotenv.2019.01.262

Zhang, H., Wu, Z., Wang, C., Li, Y., & Xu, J.-R. (2014). Germination and infectivity of microconidia in the rice blast fungus *Magnaporthe oryzae*. *Nature Communications, 5*, 4518. https://doi.org/10.1038/ncomms5518

Zhang, T., Huang, Y., & Yang, X. (2013). Climate warming over the past three decades has shortened rice growth duration in China and cultivar shifts have further accelerated the process for late rice. *Global Change Biology, 19*(2), 563–570. https://doi.org/10.1111/gcb.12057

Zhao, M., Lin, Y., & Chen, H. (2020). Improving nutritional quality of rice for human health. *Theoretical and Applied Genetics, 133*(5), 1397–1413. https://doi.org/10.1007/s00122-019-03530-x

Zheng, F., Wang, X., Zhang, W., Hou, P., Lu, F., Du, K., & Sun, Z. (2013). Effects of elevated O_3 exposure on nutrient elements and quality of winter wheat and rice grain in Yangtze River Delta, China. *Environmental Pollution, 179*, 19–26. https://doi.org/10.1016/j.envpol.2013.03.051

Ziemke, J. R., Chandra, S., Duncan, B. N., Froidevaux, L., Bhartia, P. K., Levelt, P. F., & Waters, J. W. (2006). Tropospheric ozone determined from Aura OMI and MLS: Evaluation of measurements and comparison with the Global Modeling Initiative's Chemical Transport Model. *Journal of Geophysical Research: Atmospheres*, 111(D19), D19303. https://doi.org/10.1029/2006JD007089

Appendices

Supplementary Table 1 List of genotypes along with their corresponding results from Competitive allele-specific PCR (KASP) genotyping.

Sl	Background	Line	QTL's	KASP results (Foreground selection)								*OsORAP1*
				OzT8			*OzT9*					
				1Mb	QTL Start	QTL End	1Mb	1Mb	QTL Start	QTL End	1Mb	
1	Donor	Kasalath	*OzT8* + *OzT9*	C:C	G:G	G:G	T:T	A:A	C:C	T:T	T:T	KAS
2	Recipient	BRRI dhan28	-	A:A	C:C	A:A	G:G	G:G	T:T	A:A	C:C	NB
3	Recipient	Binadhan-11	-	A:A	G:G	A:A	G:G	G:G	T:T	A:A	C:C	NB
4	BRRI dhan28	MFOL-2090	*OzT8*	C:C	G:G	G:G	T:T	G:G	T:T	A:A	C:C	NB
5	BRRI dhan28	MFOL-2102	*OzT8*	C:C	G:G	G:G	T:T	G:G	T:T	A:A	C:C	NB
6	BRRI dhan28	MFOL-2109	*OzT8*	C:C	G:G	G:G	T:T	G:G	T:T	A:A	C:C	NB
7	BRRI dhan28	MFOL-2149	*OzT8*	C:C	G:G	G:G	T:T	G:G	T:T	A:A	C:C	NB
8	BRRI dhan28	MFOL-2163	*OzT8*	C:C	G:G	G:G	T:T	G:G	T:T	A:A	C:C	NB
9	BRRI dhan28	MFOL-2179	*OzT8*	C:C	G:G	G:G	T:T	G:G	T:T	A:A	C:C	NB
10	BRRI dhan28	MFOL-2181	*OzT8*	C:C	G:G	G:G	T:T	G:G	T:T	A:A	C:C	NB
11	BRRI dhan28	MFOL-2197	*OzT8*	C:C	G:G	G:G	T:T	G:G	T:T	A:A	C:C	NB
12	BRRI dhan28	MFOL-2204	*OzT8*	C:C	G:G	G:G	T:T	G:G	T:T	A:A	C:C	NB
13	BRRI dhan28	MFOL-2218	*OzT8*	C:C	G:G	G:G	T:T	G:G	T:T	A:A	C:C	NB
14	BRRI dhan28	MFOL-2236	*OzT8*	C:C	G:G	G:G	T:T	G:G	T:T	A:A	C:C	NB

15	Binadhan-11	MFOL-1121	*OzT8*	C:C	G:G	G:G	T:T	G:G	T:T	A:A	C:C	NB
16	Binadhan-11	MFOL-1131	*OzT8*	C:C	G:G	G:G	T:G	G:G	T:T	A:A	C:C	NB
17	Binadhan-11	MFOL-1133	*OzT8*	C:C	G:G	G:G	T:G	G:G	T:T	A:A	C:C	NB
18	Binadhan-11	MFOL-1135	*OzT8*	C:C	G:G	G:G	T:T	G:G	T:T	A:A	C:C	NB
19	Binadhan-11	MFOL-1154	*OzT8*	C:C	G:G	G:G	T:T	G:G	T:T	A:A	C:C	NB
20	BRRI dhan28	MFOL-2248	*OzT8*	C:C	G:G	G:G	G:G	G:G	T:T	A:A	C:C	NB
21	Binadhan-11	MFOL-1163	*OzT8*	C:C	G:G	G:G	G:G	G:G	T:T	A:A	C:C	NB
22	Binadhan-11	MFOL-1170	*OzT8*	C:C	G:G	G:G	G:G	G:G	T:T	A:A	C:C	NB
23	Binadhan-11	MFOL-1198	*OzT8*	C:C	G:G	G:G	G:G	G:G	T:T	A:A	C:C	NB
24	Binadhan-11	MFOL-1211	*OzT8*	C:C	G:G	G:G	G:G	G:G	T:T	A:A	C:C	NB
25	Binadhan-11	MFOL-1216	*OzT8*	A:A	G:G	G:G	T:T	G:G	T:T	A:A	C:C	NB
26	Binadhan-11	MFOL-1231	*OzT8*	A:A	G:G	G:G	T:T	G:G	T:T	A:A	C:C	NB
27	Binadhan-11	MFOL-1238	*OzT8*	A:A	G:G	G:G	G:G	G:G	T:T	A:A	C:C	NB
28	Binadhan-11	MFOL-1259	*OzT8*	C:C	G:G	A:A	G:G	G:G	T:T	A:A	C:C	NB
29	Binadhan-11	MFOL-1263	*OzT8*	C:C	G:G	A:A	G:G	G:G	T:T	A:A	C:C	NB
30	Binadhan-11	MFOL-1281	*OzT8*	A:A	G:G	G:G	T:T	G:G	T:T	A:A	C:C	NB
31	Binadhan-11	MFOL-471	*OzT8* + *OzT9*	C:C	G:G	G:G	T:T	A:A	C:C	T:T	T:T	KAS
32	Binadhan-11	MFOL-491	*OzT8* + *OzT9*	C:C	G:G	G:G	T:T	A:A	C:C	T:T	T:T	KAS
33	Binadhan-11	MFOL-518	*OzT8* + *OzT9*	C:A	G:G	G:G	T:T	A:A	C:C	T:T	T:T	KAS
34	Binadhan-11	MFOL-544	*OzT8* + *OzT9*	A:A	G:G	G:G	T:T	A:A	C:C	T:T	T:T	KAS

35	Binadhan-11	MFOL-579	*OzT8 + OzT9*	C:C	G:G	G:G	T:T	G:G	T:T	T:T	T:T	KAS
36	BRRI dhan28	MFOL-1325	*OzT8 + OzT9*	C:C	G:G	G:G	T:T	A:A	C:C	T:T	T:T	KAS
37	BRRI dhan28	MFOL-2301	*OzT8 + OzT9*	C:C	G:G	G:G	T:T	A:A	C:C	T:T	T:T	KAS
38	BRRI dhan28	MFOL-1378	*OzT8 + OzT9*	C:C	G:G	G:G	T:T	A:A	C:C	T:T	T:T	KAS
39	BRRI dhan28	MFOL-1474	*OzT8 + OzT9*	C:C	G:G	G:G	T:T	A:A	C:C	T:T	T:T	KAS
40	BRRI dhan28	MFOL-2349	*OzT8 + OzT9*	C:C	G:G	G:G	T:T	A:A	C:C	T:T	T:T	KAS
41	BRRI dhan28	MFOL-1488	*OzT8 + OzT9*	C:C	G:G	G:G	T:G	A:G	C:T	T:T	T:T	KAS
42	BRRI dhan28	MFOL-1491	*OzT8 + OzT9*	C:A	G:C	G:A	T:G	A:G	C:T	T:T	T:T	KAS
43	BRRI dhan28	MFOL-1547	*OzT8 + OzT9*	C:A	G:C	G:G	T:T	G:G	T:T	A:A	T:T	KAS
44	BRRI dhan28	MFOL-2388	*OzT8 + OzT9*	C:C	G:G	G:G	T:T	G:G	T:T	T:T	T:T	KAS
45	BRRI dhan28	MFOL-2395	*OzT8 + OzT9*	C:C	G:G	G:G	T:T	G:G	T:T	T:T	T:T	KAS
46	BRRI dhan28	MFOL-2406	*OzT8 + OzT9*	C:C	G:G	G:G	G:G	A:A	C:C	T:T	T:T	KAS
47	BRRI dhan28	MFOL-1720	*OzT8 + OzT9*	C:C	G:G	G:G	T:T	A:A	C:C	A:A	C:C	NB
48	Binadhan-11	MFOL-729	*OzT9*	A:A	G:G	A:A	G:G	A:A	C:C	T:T	T:T	KAS
49	Binadhan-11	MFOL-774	*OzT9*	A:A	G:G	A:A	G:G	A:A	C:C	T:T	T:T	KAS
50	Binadhan-11	MFOL-842	*OzT9*	A:A	G:G	A:A	G:G	A:A	C:C	T:T	T:T	KAS
51	Binadhan-11	MFOL-866	*OzT9*	A:A	G:G	A:A	G:G	A:A	C:C	T:T	T:T	KAS
52	Binadhan-11	MFOL-1001	*OzT9*	A:A	G:G	A:A	G:G	G:G	C:C	T:T	T:T	KAS
53	Binadhan-11	MFOL-1011	*OzT9*	A:A	G:G	A:A	G:G	G:G	C:C	T:T	T:T	KAS
54	Binadhan-11	MFOL-1031	*OzT9*	A:A	G:G	A:A	G:G	A:A	C:C	T:T	T:T	KAS

55	Binadhan-11	MFOL-1102	*OzT9*	A:A	G:G	A:A	G:G	G:G	T:T	A:A	T:T	KAS
56	Binadhan-11	MFOL-1289	*OzT9*	A:A	G:G	A:A	G:G	A:A	C:C	T:T	T:T	KAS
57	Binadhan-11	MFOL-1302	*OzT9*	A:A	G:G	A:A	G:G	A:A	C:C	T:T	T:T	KAS
58	BRRI dhan28	MFOL-1772	*OzT9*	A:A	C:C	A:A	G:G	A:A	C:C	T:T	T:T	KAS
59	BRRI dhan28	MFOL-1778	*OzT9*	A:A	C:C	A:A	G:G	A:A	C:C	T:T	T:T	KAS
60	BRRI dhan28	MFOL-1779	*OzT9*	A:A	C:C	A:A	G:G	A:A	C:C	T:T	T:T	KAS
61	BRRI dhan28	MFOL-1798	*OzT9*	A:A	C:C	A:A	G:G	A:A	C:C	T:T	T:T	KAS
62	BRRI dhan28	MFOL-1801	*OzT9*	A:A	C:C	A:A	G:G	A:A	C:C	T:T	T:T	KAS
63	BRRI dhan28	MFOL-1838	*OzT9*	A:A	C:C	A:A	G:G	A:A	C:C	T:T	T:T	KAS
64	BRRI dhan28	MFOL-1856	*OzT9*	A:A	C:C	A:A	G:G	A:A	C:C	T:T	T:T	KAS
65	BRRI dhan28	MFOL-1857	*OzT9*	A:A	C:C	A:A	G:G	A:A	C:C	T:T	T:T	KAS
66	BRRI dhan28	MFOL-1881	*OzT9*	A:A	C:C	A:A	G:G	A:A	C:C	T:T	T:T	KAS
67	BRRI dhan28	MFOL-1925	*OzT9*	A:A	C:C	A:A	G:G	A:A	C:C	T:T	T:T	KAS
68	BRRI dhan28	MFOL-1926	*OzT9*	A:A	C:C	A:A	G:G	A:A	C:C	T:T	T:T	KAS
69	BRRI dhan28	MFOL-1928	*OzT9*	A:A	C:C	A:A	G:G	A:A	C:C	T:T	T:T	KAS
70	BRRI dhan28	MFOL-1956	*OzT9*	A:A	C:C	A:A	G:G	G:G	C:C	T:T	T:T	KAS
71	BRRI dhan28	MFOL-1973	*OzT9*	A:A	C:C	A:A	G:G	G:G	T:T	T:T	T:T	KAS
72	BRRI dhan28	MFOL-2018	*OzT9*	A:A	C:C	A:A	G:G	A:A	C:C	A:A	C:C	NB
73	BRRI dhan28	MFOL-2026	*OzT9*	A:A	C:C	A:A	G:G	A:A	C:C	A:A	C:C	NB
74	BRRI dhan28	MFOL-96-325	*OzT9*	A:A	C:C	A:A	G:G	G:G	T:T	T:T	T:T	KAS

75	BRRI dhan28	MFOL-111-328	*OzT9*	A:A	C:C	A:A	G:G	G:G	T:T	T:T	T:T	KAS
76	BRRI dhan28	MFOL-328	*OzT9*	A:A	C:C	A:A	G:G	G:G	T:T	T:T	T:T	KAS
77	BRRI dhan28	MFOL-117-331	*OzT9*	A:A	C:C	A:A	G:G	G:G	T:T	T:T	T:T	KAS

Supplementary Table 2 List of parental lines and the selected breeding lines with their generation advancement stage.

SL	Background	Line	QTL	Breeding generations
1	Donor	Kasalath	*OzT8* + *OzT9*	-
2	Recipient	BRRI dhan28	-	-
3	BRRI dhan28	MFOL-2197	*OzT8*	BC_2F_4
4	BRRI dhan28	MFOL-2236	*OzT8*	BC_2F_4
5	BRRI dhan28	MFOL-1956	*OzT9*	BC_2F_4
6	BRRI dhan28	MFOL-328	*OzT9*	BC_2F_4
7	BRRI dhan28	MFOL-233	*OzT9*	BC_3F_3
8	BRRI dhan28	MFOL-1378	*OzT8* + *OzT9*	BC_2F_4
9	BRRI dhan28	MFOL-1547	*OzT8* + *OzT9*	BC_2F_4
10	BRRI dhan28	MFOL-1488	*OzT8* + *OzT9*	BC_2F_4
11	BRRI dhan28	MFOL-1491	*OzT8* + *OzT9*	BC_2F_4
12	BRRI dhan28	MFOL-230	*OzT8* + *OzT9*	BC_3F_3
13	Recipient	Binadhan-11	-	-
14	Binadhan-11	MFOL-1198	*OzT8*	BC_2F_4
15	Binadhan-11	MFOL-1135	*OzT8*	BC_2F_4
16	Binadhan-11	MFOL-1102	*OzT9*	BC_2F_4
17	Binadhan-11	MFOL-1011	*OzT9*	BC_2F_4
18	Binadhan-11	MFOL-1302	*OzT9*	BC_2F_4
19	Binadhan-11	MFOL-544	*OzT8* + *OzT9*	BC_2F_4
20	Binadhan-11	MFOL-60	*OzT8* + *OzT9*	BC_3F_3
21	Binadhan-11	MFOL-50	*OzT8* + *OzT9*	BC_3F_3
22	Binadhan-11	MFOL-471	*OzT8* + *OzT9*	BC_2F_4

Supplementary Table 3 KASP genotyping results for background, foreground, and recombinant selection in selected breeding lines with genome recovery percentages across 12 rice chromosomes.

Genotype		Kasalath	BRRI dhan28	MFOL-2197	MFOL-2236	MFOL-1956	MFOL-328	MFOL-233	MFOL-1378	MFOL-1488	MFOL-1491	MFOL-1547	MFOL-230	Binadhan-11	MFOL-1135	MFOL-1198	MFOL-1011	MFOL-1102	MFOL-1302	MFOL-471	MFOL-50	MFOL-544	MFOL-60
GenomeRecovery (%)		-	-	85.37	82.93	90.24	87.80	92.68	85.37	87.80	87.80	85.37	85.37	-	92.68	90.24	92.68	90.24	95.12	82.93	82.93	85.37	87.80
Chromosome 1	RIOZ_101	G:G	C:C	C:C	C:C	C:C	G:G	C:C	C:C	C:C	C:C	C:C	C:C	C:C	C:C	C:C	C:C	C:C	C:C	C:C	C:C	C:C	C:C
	RIOZ_102	A:A	G:G	G:G	G:G	G:G	G:G	G:G	G:G	G:G	G:G	G:G	G:G	G:G	G:G	G:G	A:A	G:G	G:G	G:G	G:G	A:A	G:G
	RIOZ_103	T:T	C:C	C:C	C:C	C:C	C:C	C:C	C:C	C:C	C:C	C:C	C:C	C:C	C:C	C:C	C:C	C:C	C:C	C:C	C:C	C:C	C:C
Chromosome 2	RIOZ_104	A:A	G:G	G:G	G:G	G:G	G:G	G:G	G:G	G:G	G:G	G:G	G:G	G:G	G:G	G:G	G:G	G:G	G:G	G:G	G:G	G:G	G:G
	RIOZ_105	A:A	C:C	C:C	C:C	C:C	C:C	C:C	C:C	C:C	C:C	C:C	C:C	C:C	C:C	C:C	C:C	C:C	C:C	C:C	C:C	C:C	C:C
	RIOZ_106	T:T	C:C	C:C	C:C	C:C	C:C	C:C	C:C	C:C	C:C	C:C	C:C	C:C	C:C	C:C	C:C	C:C	C:C	T:T	C:C	C:C	C:C
Chromosome 3	RIOZ_107	G:G	A:A	A:A	G:G	A:A	A:A	A:A	A:A	A:A	A:A	A:A	A:A	A:A	A:A	G:G	A:A	A:A	A:A	A:A	A:A	A:A	A:A
	RIOZ_108	C:C	T:T	T:T	T:T	T:T	T:T	T:T	C:C	T:T	T:T	T:T	T:T	T:T	T:T	T:T	T:T	T:T	T:T	T:T	T:T	T:T	T:T
	RIOZ_109	A:A	C:C	C:C	C:C	C:C	C:C	C:C	C:C	C:C	C:C	C:C	C:C	C:C	C:C	C:C	C:C	C:C	C:C	C:C	C:C	C:C	C:C
Chromosome 4	RIOZ_110	T:T	C:C	C:C	C:C	C:C	C:C	C:C	C:C	C:C	C:C	C:C	C:C	C:C	C:C	C:C	C:C	C:C	C:C	C:C	C:C	C:C	C:C
	RIOZ_111	G:G	A:A	A:A	A:A	A:A	A:A	A:A	A:A	A:A	A:A	A:A	A:A	A:A	A:A	A:A	A:A	A:A	A:A	A:A	A:A	A:A	A:A
	RIOZ_112	A:A	C:C	C:C	C:C	C:C	C:C	C:C	C:C	C:C	C:C	C:C	C:C	C:C	C:C	C:C	C:C	C:C	C:C	C:C	C:C	C:C	C:C
Chromosome 5	RIOZ_113	T:T	C:C	C:C	C:C	C:C	C:C	C:C	C:C	C:C	C:C	C:C	C:C	C:C	C:C	C:C	C:C	C:C	C:C	C:C	C:C	C:C	C:C
	RIOZ_114	A:A	C:C	C:C	C:C	C:C	C:C	C:C	C:C	C:C	C:C	C:C	C:C	C:C	C:C	C:C	C:C	C:C	C:C	C:C	C:C	C:C	C:C
	RIOZ_115	T:T	C:C	C:C	T:T	C:C	C:C	C:C	C:C	C:C	C:C	C:C	C:C	C:C	C:C	C:C	C:C	C:C	C:C	C:C	C:C	C:C	C:C
Chromosome 6	RIOZ_116	C:C	T:T	T:T	C:C	C:C	T:T	T:T	T:T	T:T	T:T	T:T	T:T	T:T	T:T	T:T	T:T	T:T	T:T	T:T	T:T	T:T	T:T
	RIOZ_117	C:C	A:A	A:A	A:A	A:A	A:A	A:A	A:A	A:A	A:A	A:A	A:A	A:A	A:A	A:A	A:A	A:A	A:A	C:C	A:A	A:A	A:A
	RIOZ_118	T:T	C:C	C:C	C:C	C:C	C:C	C:C	C:C	C:C	C:C	C:C	C:C	C:C	C:C	C:C	C:C	C:C	C:C	C:C	C:C	C:C	C:C
Chromosome 7	RIOZ_119	A:A	C:C	C:C	C:C	C:C	C:C	C:C	C:C	C:C	C:C	C:C	C:C	C:C	C:C	C:C	C:C	C:C	C:C	C:C	C:C	C:C	C:C
	RIOZ_120	T:T	C:C	C:C	C:C	C:C	C:C	C:C	C:C	C:C	C:C	T:T	C:C	C:C	C:C	C:C	C:C	C:C	C:C	C:C	C:C	C:C	C:C
	RIOZ_121	C:C	A:A	A:A	A:A	A:A	A:A	A:A	A:A	A:A	A:A	A:A	A:A	A:A	A:A	A:A	A:A	A:A	A:A	A:A	A:A	A:A	A:A
Chromosome 8	RIOZ_122	C:C	T:T	T:T	T:T	T:T	C:C	T:T	T:T	T:T	T:T	T:T	T:T	T:T	T:T	T:T	T:T	T:T	T:T	T:T	T:T	T:T	T:T
	RIOZ_123	C:C	G:G	C:C	C:C	G:G	G:G	G:G	G:G	C:C	G:G	G:G	G:G	G:G	G:G	C:C	G:G	G:G	G:G	G:G	G:G	G:G	G:G
	RIOZ_124	C:C	A:A	C:C	C:C	A:A	A:A	A:A	C:C	C:C	A:A	A:A	C:C	A:A	C:C	C:C	A:A	A:A	A:A	A:A	C:C	A:A	A:A
	RIOZ_125	T:T	C:C	T:T	T:T	C:C	C:C	C:C	T:T	T:T	T:T	C:C	T:T	C:C	T:T	T:T	C:C	C:C	C:C	T:T	T:T	T:T	T:T
	RIOZ_126	G:G	C:C	G:G	G:G	C:C	C:C	C:C	G:G	G:G	C:C	C:C	G:G	G:G	G:G	G:G	G:G	G:G	G:G	G:G	G:G	G:G	G:G
	RIOZ_127	T:T	C:C	T:T	T:T	T:T	T:T	T:T	T:T	T:T	T:T	C:C	T:T	C:C	T:T	T:T	C:C	C:C	C:C	T:T	T:T	T:T	T:T
	RIOZ_128	G:G	A:A	G:G	G:G	A:A	A:A	A:A	G:G	G:G	G:G	G:G	G:G	A:A	G:G	G:G	A:A	A:A	A:A	G:G	G:G	G:G	G:G
	RIOZ_129	T:T	G:G	T:T	T:T	G:G	G:G	G:G	G:G	G:G	T:T	T:T	T:T	G:G	T:T	G:G	G:G	G:G	G:G	T:T	T:T	T:T	T:T
	RIOZ_130	A:A	C:C	A:A	C:C	C:C	C:C	C:C	C:C	C:C	A:A	A:A	A:A	C:C	C:C	C:C	C:C	C:C	C:C	C:C	A:A	C:C	C:C
	RIOZ_131	G:G	A:A	G:G	A:A	G:G	A:A	A:A	A:A	A:A	A:A	G:G	A:A	A:A	A:A	A:A	A:A	A:A	A:A	A:A	A:A	A:A	A:A
Chromosome 9	RIOZ_132	A:A	G:G	G:G	G:G	G:G	G:G	G:G	G:G	G:G	G:G	G:G	G:G	G:G	G:G	G:G	G:G	G:G	G:G	G:G	G:G	G:G	G:G
	RIOZ_133	C:C	G:G	G:G	G:G	G:G	C:C	G:G	G:G	G:G	G:G	G:G	G:G	G:G	G:G	G:G	G:G	G:G	G:G	G:G	G:G	G:G	G:G
	RIOZ_134	A:A	G:G	G:G	G:G	G:G	G:G	A:A	A:A	G:G	G:G	G:G	A:A	G:G	G:G	G:G	G:G	G:G	G:G	A:A	A:A	A:A	A:A
	RIOZ_135	C:C	T:T	T:T	T:T	C:C	T:T	C:C	C:C	T:T	C:C	T:T	C:C	T:T	T:T	T:T	C:C	T:T	C:C	C:C	C:C	C:C	C:C
	RIOZ_136	A:A	G:G	G:G	G:G	A:A	G:G	A:A	A:A	G:G	A:A	G:G	A:A	G:G	G:G	G:G	G:G	G:G	A:A	A:A	A:A	A:A	A:A
	RIOZ_137	T:T	C:C	C:C	C:C	T:T	C:C	T:T	T:T	C:C	T:T	C:C	T:T	C:C	C:C	C:C	T:T	C:C	T:T	T:T	T:T	T:T	T:T
	RIOZ_138	T:T	A:A	A:A	A:A	T:T	T:T	T:T	T:T	T:T	T:T	A:A	T:T	A:A	A:A	A:A	T:T	A:A	T:T	T:T	T:T	T:T	T:T
	RIOZ_139	T:T	C:C	C:C	C:C	T:T	T:T	T:T	T:T	T:T	T:T	T:T	T:T	C:C	C:C	C:C	T:T	T:T	T:T	T:T	T:T	T:T	T:T
	RIOZ_140	G:G	A:A	A:A	A:A	G:G	A:A	G:G	G:G	G:G	G:G	G:G	G:G	A:A	A:A	A:A	G:G	G:G	G:G	G:G	G:G	G:G	G:G
	OsORAP1	KAS	NB	NB	NB	KAS	KAS	KAS	KAS	KAS	KAS	KAS	KAS	NB	NB	NB	KAS	KAS	KAS	KAS	KAS	KAS	KAS
	RIOZ_141	G:G	C:C	C:C	C:C	C:C	C:C	C:C	C:C	C:C	C:C	C:C	C:C	C:C	C:C	C:C	C:C	G:G	C:C	C:C	C:C	C:C	C:C
	RIOZ_142	C:C	T:T	T:T	T:T	T:T	T:T	T:T	T:T	T:T	T:T	T:T	T:T	T:T	T:T	T:T	T:T	C:C	T:T	T:T	T:T	T:T	T:T
Chromosome 10	RIOZ_143	T:T	C:C	C:C	C:C	C:C	C:C	C:C	C:C	C:C	C:C	C:C	C:C	C:C	C:C	C:C	C:C	C:C	C:C	C:C	C:C	C:C	C:C
	RIOZ_144	T:T	C:C	C:C	C:C	C:C	C:C	C:C	C:C	C:C	C:C	C:C	C:C	C:C	C:C	C:C	C:C	C:C	C:C	C:C	C:C	C:C	C:C
Chromosome 11	RIOZ_145	A:A	G:G	G:G	G:G	G:G	G:G	G:G	G:G	G:G	G:G	G:G	G:G	G:G	G:G	G:G	G:G	G:G	G:G	G:G	G:G	G:G	G:G
	RIOZ_146	G:G	A:A	A:A	A:A	A:A	A:A	A:A	A:A	A:A	A:A	A:A	A:A	A:A	A:A	A:A	A:A	A:A	A:A	A:A	A:A	A:A	A:A
Chromosome 12	RIOZ_147	G:G	A:A	A:A	A:A	A:A	A:A	A:A	A:A	A:A	A:A	A:A	A:A	A:A	A:A	A:A	A:A	A:A	A:A	A:A	A:A	A:A	A:A
	RIOZ_148	A:A	G:G	G:G	G:G	G:G	A:A	G:G	G:G	G:G	G:G	G:G	G:G	G:G	G:G	G:G	G:G	G:G	G:G	G:G	G:G	G:G	G:G

Supplementary Table 4 Categorizing genotypes based on average leaf bronzing score (LBS) and Blast severity score (BSS).

Genotypes	Leaf bronzing score (LBS)		Genotype	Blast severity score (BSS)	
	Ozone	Ozone & Blast		Blast	Ozone & Blast
CO 39	8.1	8.3	CO 39	8	5
Binadhan-11	7.5	8.1	Koshihikari	5	5
IR 64	7.3	7.0	L 81	3	1
BRRI dhan28	7.0	7.1	Nipponbare	3	3
Koshihikari	6.3	6.9	BRRI dhan28	1	1
Nipponbare	6.0	6.0	IR 64	1	1
Kitaake	4.4	4.5	Kasalath	1	1
Kasalath	2.8	2.6	Binadhan-11	0	0
L 81	2.5	3.0	Kitaake	0	0

Supplementary Figure 1 Differential visual injury by plant, (A) Control, (B) Blast, (C) Ozone, and (D) Ozone and Blast in combined ozone & Blast stress.

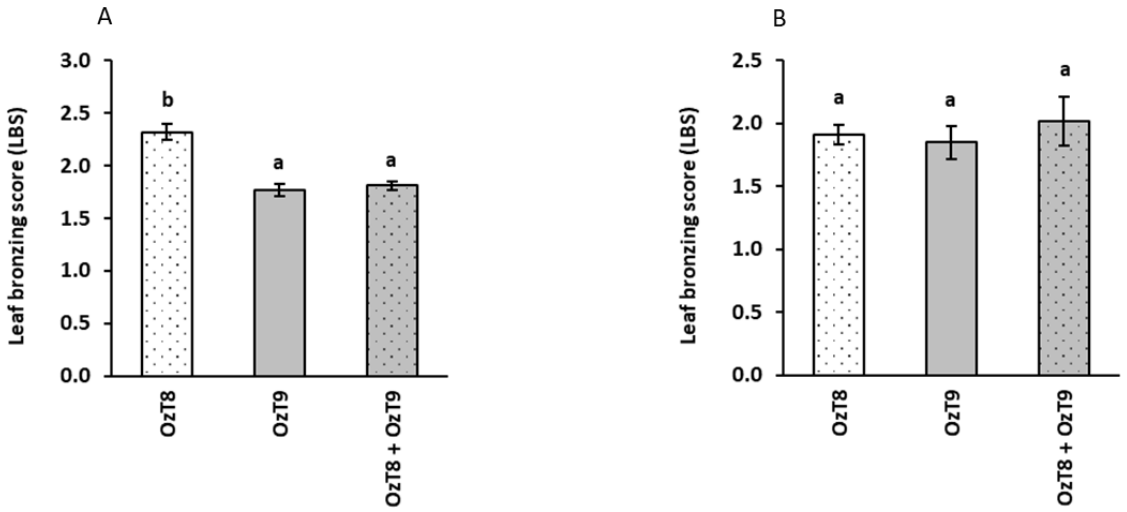

Supplementary Figure 2 Leaf bronzing score for different QTL combinations (*OzT8*, *OzT9*, and *OzT8* + *OzT9*) in response to ozone exposure in breeding lines derived from (A) BRRI dhan28 × Kasalath and (B) Binadhan-11 × Kasalath. Bars labeled with the same letter are not significantly different according to Tukey's HSD test ($p < 0.05$). Error bars represent the standard error of the mean.

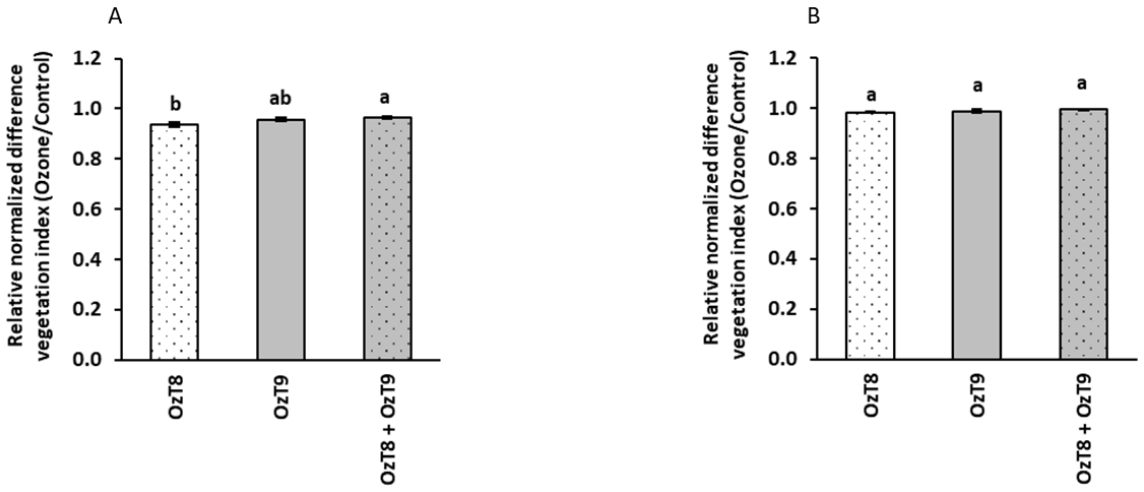

Supplementary Figure 3 Relative normalized difference vegetation index for different QTL combinations (*OzT8*, *OzT9*, and *OzT8* + *OzT9*) in response to ozone exposure in breeding lines derived from (A) BRRI dhan28 × Kasalath and (B) Binadhan-11 × Kasalath. Bars labeled with the same letter are not significantly different according to Tukey's HSD test ($p < 0.05$). Error bars represent the standard error of the mean.

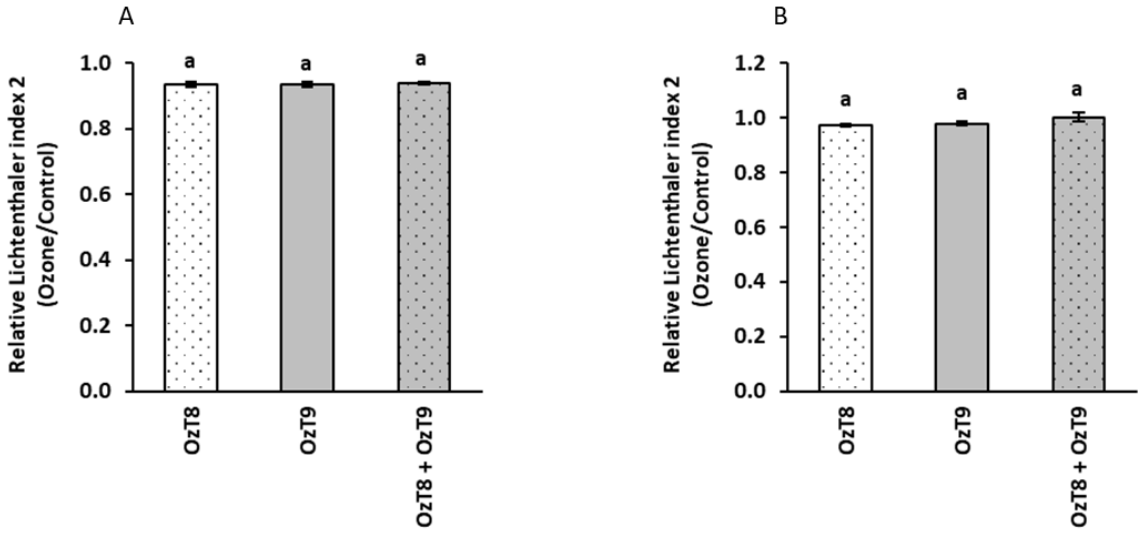

Supplementary Figure 4 Relative Lichtenthaler index 2 for different QTL combinations (*OzT8*, *OzT9*, and *OzT8* + *OzT9*) in response to ozone exposure in breeding lines derived from (A) BRRI dhan28 × Kasalath and (B) Binadhan-11 × Kasalath. Bars labeled with the same letter are not significantly different according to Tukey's HSD test ($p < 0.05$). Error bars represent the standard error of the mean.

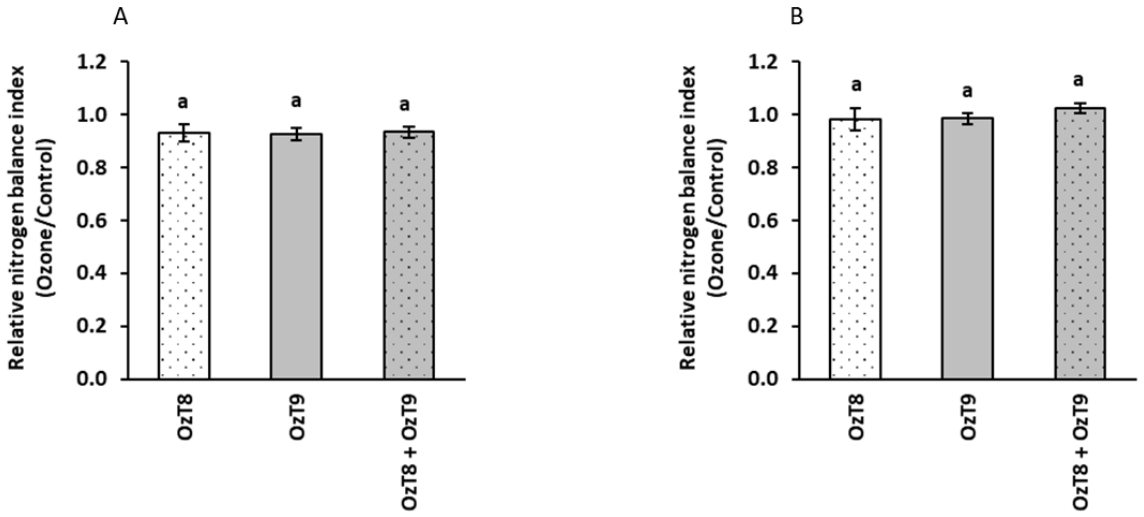

Supplementary Figure 5 Relative nitrogen balance index for different QTL combinations (*OzT8*, *OzT9*, and *OzT8* + *OzT9*) in response to ozone exposure in breeding lines derived from (A) BRRI dhan28 × Kasalath and (B) Binadhan-11 × Kasalath. Bars labeled with the same letter are not significantly different according to Tukey's HSD test ($p < 0.05$). Error bars represent the standard error of the mean.

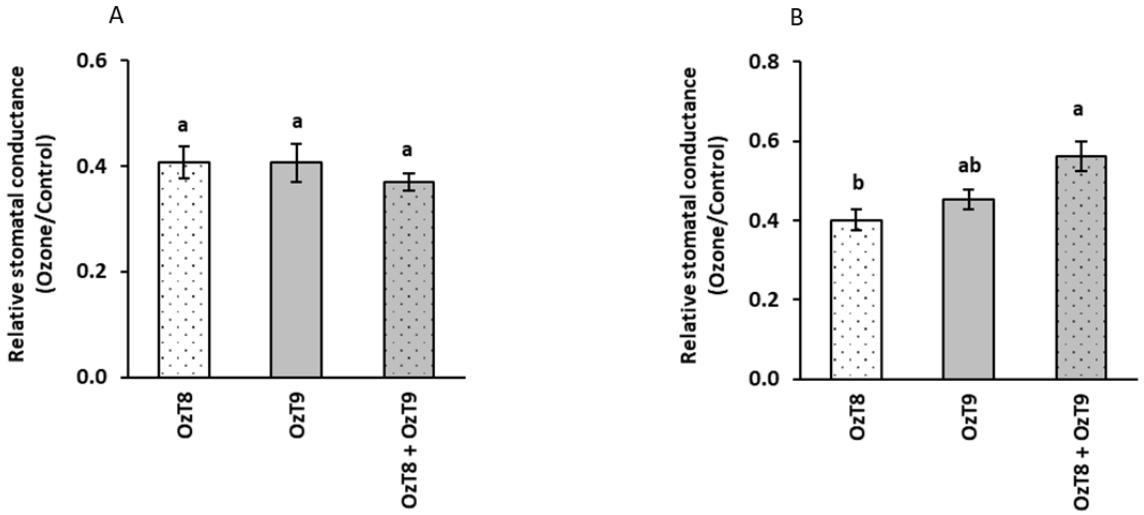

Supplementary Figure 6 Relative stomatal conductance for different QTL combinations (*OzT8*, *OzT9*, and *OzT8* + *OzT9*) in response to ozone exposure in breeding lines derived from (A) BRRI dhan28 × Kasalath and (B) Binadhan-11 × Kasalath. Bars labeled with the same letter are not significantly different according to Tukey's HSD test ($p < 0.05$). Error bars represent the standard error of the mean.

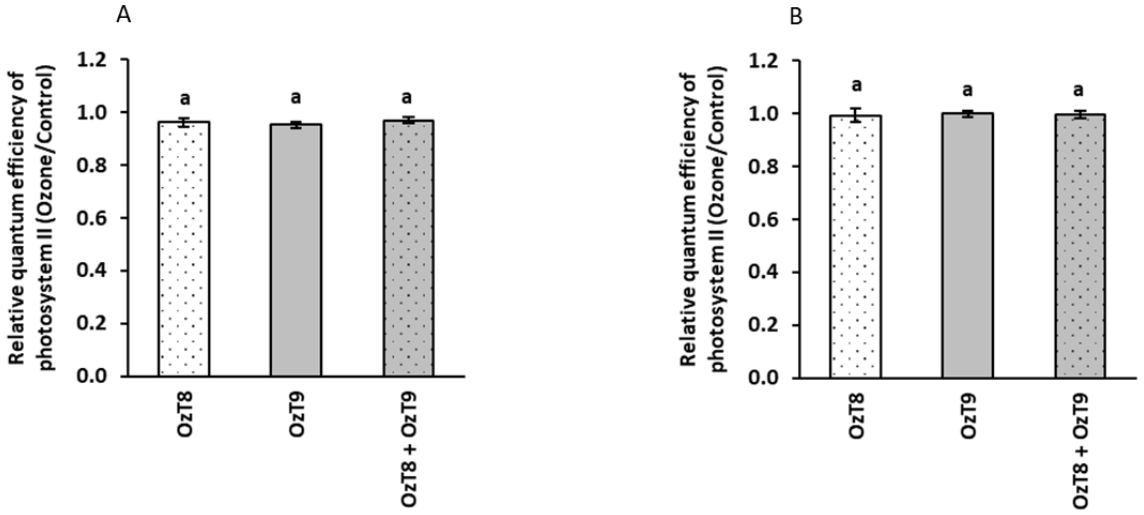

Supplementary Figure 7 Relative quantum efficiency of photosystem II for different QTL combinations (*OzT8*, *OzT9*, and *OzT8* + *OzT9*) in response to ozone exposure in breeding lines derived from (A) BRRI dhan28 × Kasalath and (B) Binadhan-11 × Kasalath. Bars labeled with the same letter are not significantly different according to Tukey's HSD test ($p < 0.05$). Error bars represent the standard error of the mean.

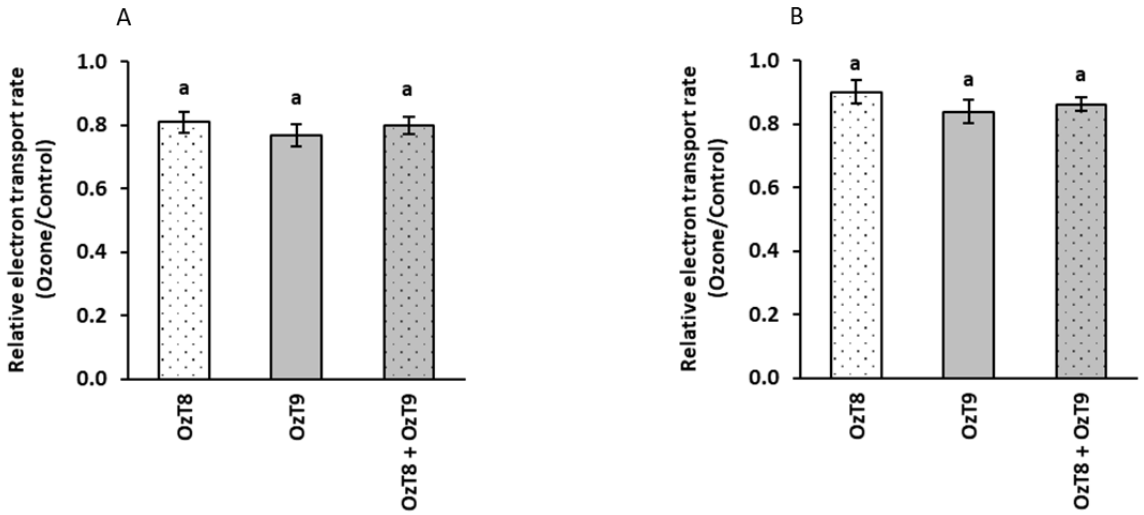

Supplementary Figure 8 Relative electron transport rate for different QTL combinations (*OzT8*, *OzT9*, and *OzT8* + *OzT9*) in response to ozone exposure in breeding lines derived from (A) BRRI dhan28 × Kasalath and (B) Binadhan-11 × Kasalath. Bars labeled with the same letter are not significantly different according to Tukey's HSD test ($p < 0.05$). Error bars represent the standard error of the mean.

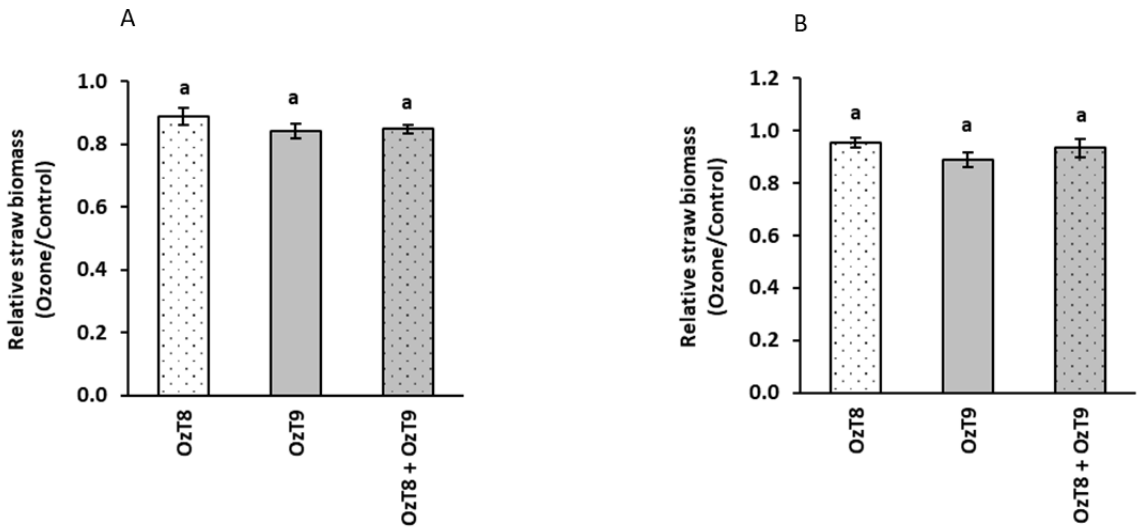

Supplementary Figure 9 Relative straw biomass for different QTL combinations (*OzT8*, *OzT9*, and *OzT8* + *OzT9*) in response to ozone exposure (greenhouse condition) in breeding lines derived from (A) BRRI dhan28 × Kasalath and (B) Binadhan-11 × Kasalath. Bars labeled with the same letter are not significantly different according to Tukey's HSD test ($p < 0.05$). Error bars represent the standard error of the mean.

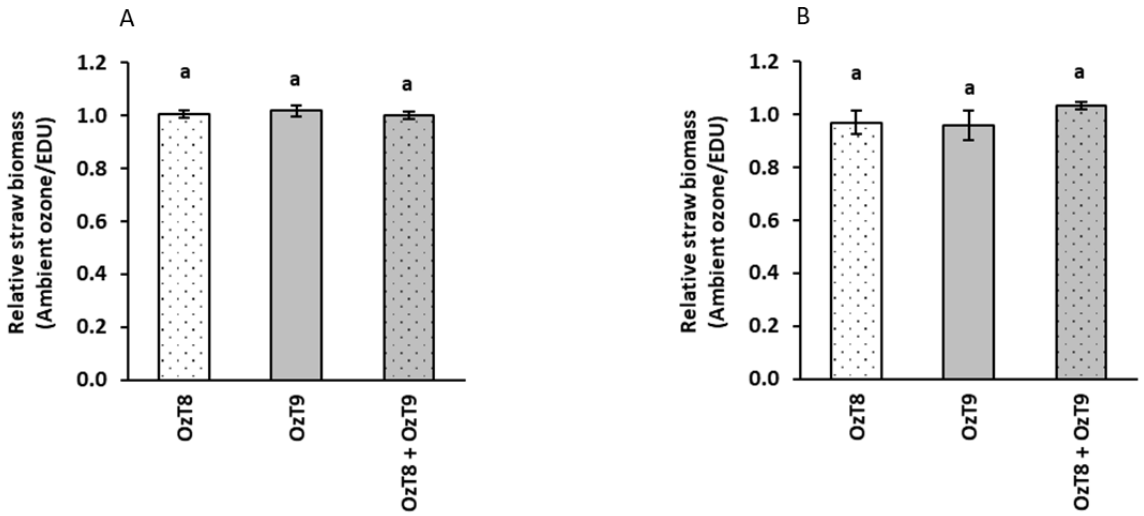

Supplementary Figure 10 Relative straw biomass for different QTL combinations (*OzT8*, *OzT9*, and *OzT8* + *OzT9*) in response to ozone exposure (field trial) in breeding lines derived from (A) BRRI dhan28 × Kasalath and (B) Binadhan-11 × Kasalath. Bars labeled with the same letter are not significantly different according to Tukey's HSD test ($p < 0.05$). Error bars represent the standard error of the mean.

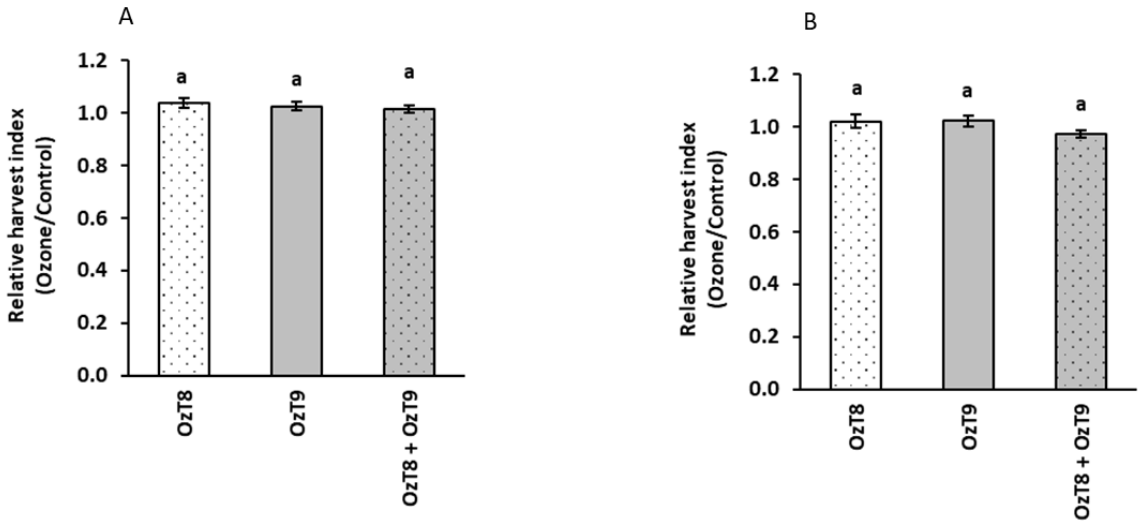

Supplementary Figure 11 Relative harvest index for different QTL combinations (*OzT8*, *OzT9*, and *OzT8* + *OzT9*) in response to ozone exposure (greenhouse condition) in breeding lines derived from (A) BRRI dhan28 × Kasalath and (B) Binadhan-11 × Kasalath. Bars labeled with the same letter are not significantly different according to Tukey's HSD test ($p < 0.05$). Error bars represent the standard error of the mean.

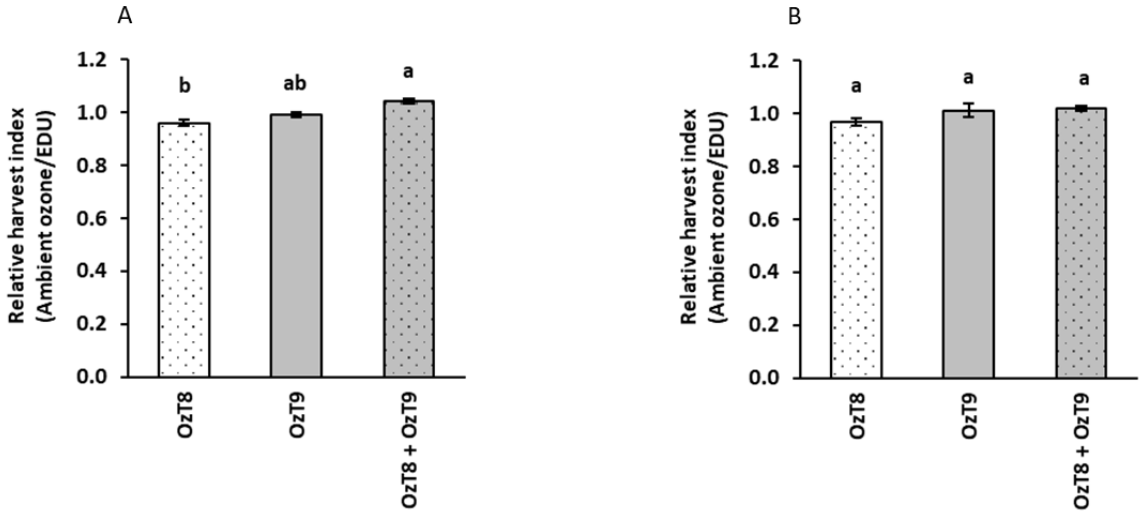

Supplementary Figure 12 Relative harvest index for different QTL combinations (*OzT8*, *OzT9*, and *OzT8* + *OzT9*) in response to ozone exposure (field trial) in breeding lines derived from (A) BRRI dhan28 × Kasalath and (B) Binadhan-11 × Kasalath. Bars labeled with the same letter are not significantly different according to Tukey's HSD test ($p < 0.05$). Error bars represent the standard error of the mean.

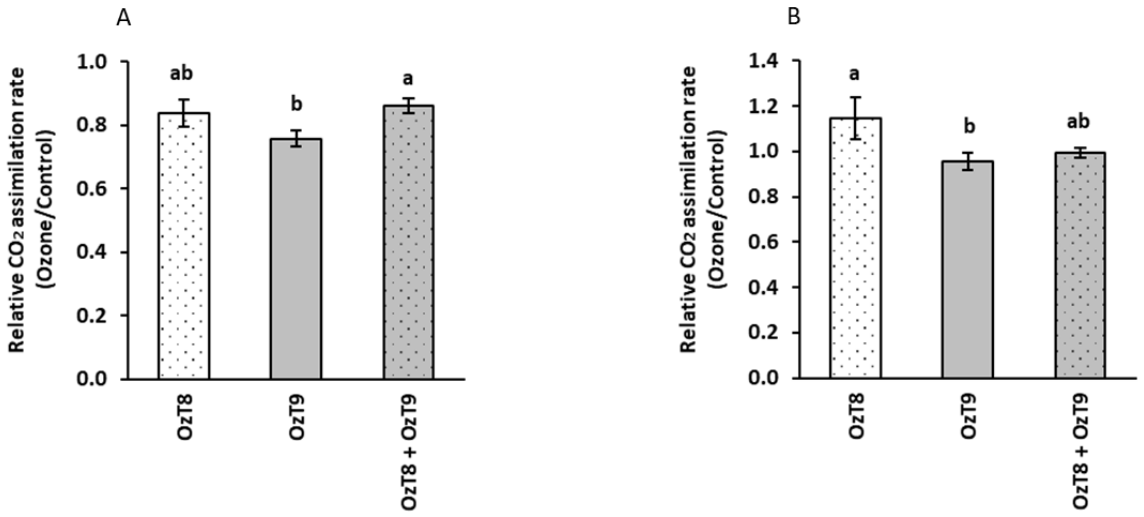

Supplementary Figure 13 Relative CO_2 assimilation rate for different QTL combinations (*OzT8*, *OzT9*, and *OzT8* + *OzT9*) in response to ozone exposure in breeding lines derived from (A) BRRI dhan28 × Kasalath and (B) Binadhan-11 × Kasalath. Bars labeled with the same letter are not significantly different according to Tukey's HSD test ($p < 0.05$). Error bars represent the standard error of the mean.

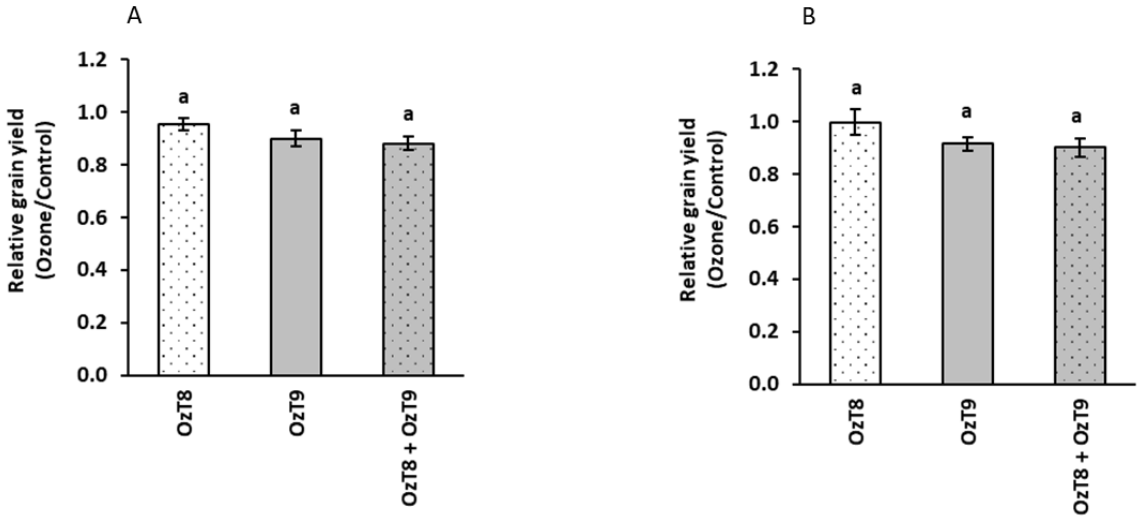

Supplementary Figure 14 Relative grain yield for different QTL combinations (*OzT8*, *OzT9*, and *OzT8* + *OzT9*) in response to ozone exposure (greenhouse condition) in breeding lines derived from (A) BRRI dhan28 × Kasalath and (B) Binadhan-11 × Kasalath. Bars labeled with the same letter are not significantly different according to Tukey's HSD test ($p < 0.05$). Error bars represent the standard error of the mean.

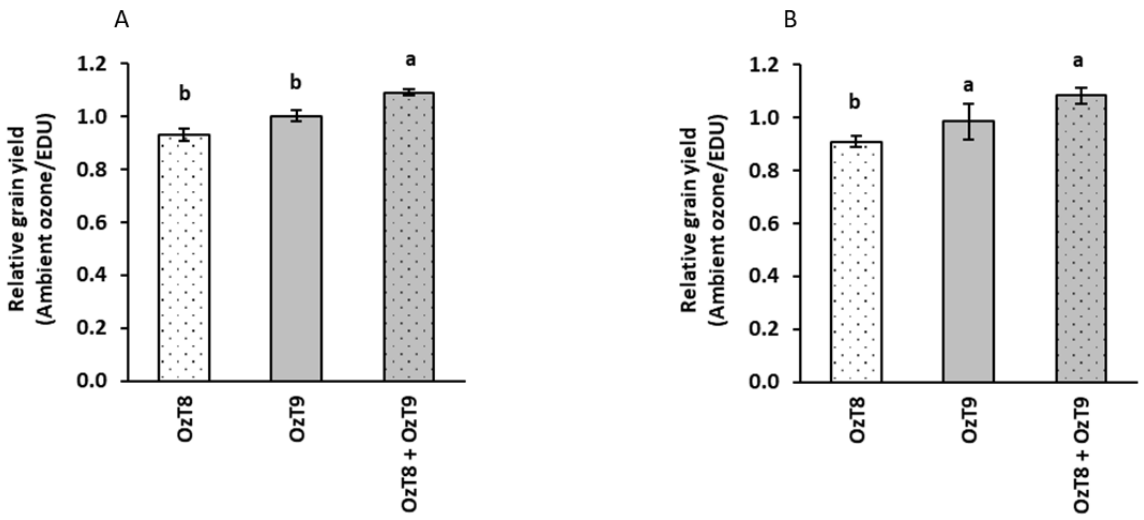

Supplementary Figure 15 Relative grain yield for different QTL combinations (*OzT8*, *OzT9*, and *OzT8* + *OzT9*) in response to ozone exposure (field trial) in breeding lines derived from (A) BRRI dhan28 × Kasalath and (B) Binadhan-11 × Kasalath. Bars labeled with the same letter are not significantly different according to Tukey's HSD test ($p < 0.05$). Error bars represent the standard error of the mean.

Supplementary Table 5 Breeding lines with recombination at the QTL *OzT9* region derived from (A) BRRI dhan28 × Kasalath and (b) Binadhan-11 × Kasalath crosses, based on KASP marker analysis. Light blue indicates alleles identical to the recipient parent (BRRI dhan28 or Binadhan-11), while light orange represents introgression from the donor parent (Kasalath).

KASP	Position (Mb)	MFOL-1956	MFOL-328	MFOL-233	MFOL-1488	MFOL-1547	MFOL-1011	MFOL-1102	MFOL-1302
RIOZ_134	9.35	G:G	G:G	A:A	G:G	G:G	G:G	G:G	G:G
RIOZ_135	9.68	C:C	T:T	C:C	T:T	T:T	C:C	T:T	C:C
RIOZ_136	10.28	A:A	G:G	A:A	G:G	G:G	G:G	G:G	A:A
RIOZ_137	10.36	T:T	C:C	T:T	C:C	C:C	T:T	C:C	T:T
RIOZ_138	10.50	T:T	T:T	T:T	T:T	A:A	T:T	A:A	T:T
RIOZ_139	11.25	T:T	T:T	T:T	T:T	T:T	T:T	T:T	T:T
RIOZ_140	11.84	G:G	A:A	G:G	G:G	G:G	G:G	G:G	G:G
OsORAP1	12.04	KAS	KAS	KAS	KAS	KAS	KAS	KAS	KAS
RIOZ_141	12.08	C:C	C:C	C:C	C:C	C:C	C:C	G:G	C:C
RIOZ_142	20.21	T:T	T:T	T:T	T:T	T:T	T:T	C:C	T:T

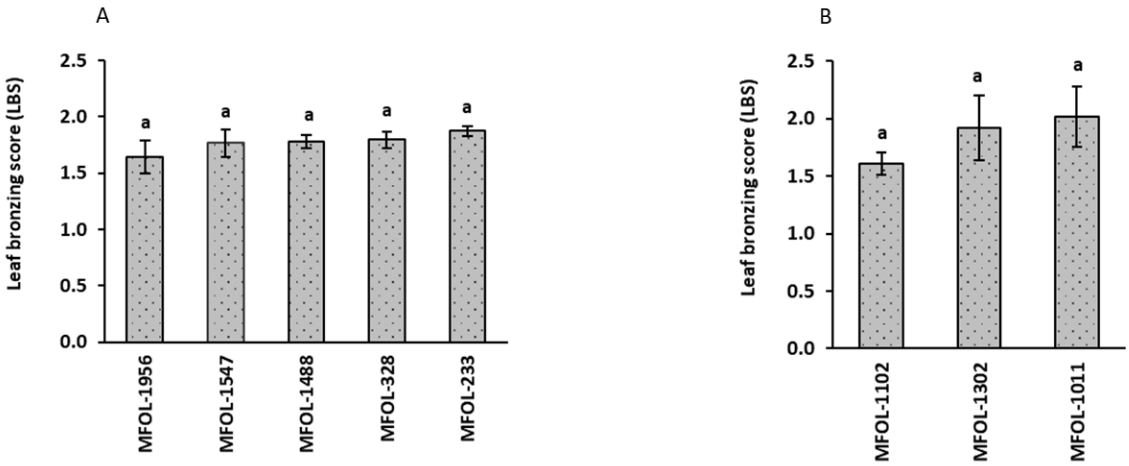

Supplementary Figure 16 Leaf bronzing scores of selected breeding lines with recombination at the QTL *OzT9* region derived from (A) BRRI dhan28 × Kasalath and (B) Binadhan-11 × Kasalath crosses under ozone stress. Bars sharing the same letter are not significantly different (tukey's hsd, $p < 0.05$). Error bars represent the standard error of the mean.